Computational Methods for Identification and Modelling of Complex Biological Systems

Lead Guest Editor: Alejandro F. Villaverde
Guest Editors: Carlo Cosentino, Attila Gabor, and Gábor Szederkényi

Computational Methods for Identification and Modelling of Complex Biological Systems

Computational Methods for Identification and Modelling of Complex Biological Systems

Lead Guest Editor: Alejandro F. Villaverde
Guest Editors: Carlo Cosentino, Attila Gabor,
and Gábor Szederkényi

Editorial Board

Contents

Editorial

Computational Methods for Identification and Modelling of Complex Biological Systems

Alejandro F. Villaverde [ID],[1] **Carlo Cosentino** [ID],[2] **Attila Gábor** [ID],[3] and **Gábor Szederkényi**[4,5]

[1]*Bioprocess Engineering Group, IIM-CSIC, Vigo 36208, Galicia, Spain*
[2]*School of Computer and Biomedical Engineering, Department of Experimental and Clinical Medicine,*
 Università degli Studi Magna Graecia di Catanzaro, 88100 Catanzaro, Italy
[3]*Joint Research Center for Computation Biomedicine, RWTH-Aachen, 52074 Aachen, Germany*
[4]*Process Control Research Group, Computer and Automation Research Institute, Hungarian Academy of Sciences,*
 1518 Budapest, Hungary
[5]*Faculty of Information Technology and Bionics, Pázmány Péter Catholic University, 1083 Budapest, Hungary*

Correspondence should be addressed to Alejandro F. Villaverde; afvillaverde@iim.csic.es

Mathematical and computational models are key tools for understanding biological phenomena. In the last decades, scientific and technological advances have facilitated their evergrowing adoption in biologically oriented research. The strongly interdisciplinary character of these areas, in which biologists work along with researchers from physical sciences, engineering, and medicine, fosters the cross-fertilization between scientific fields. However, the large degree of structural and parametric uncertainty typically associated with biological processes makes it nontrivial to analyze them using techniques imported from fields in which these issues are less prevalent. Thus, there is a need for new methodological developments that fill this gap. The present special issue addresses this need by providing an overview of current open problems and presenting recent results regarding mathematical inference and modelling of biological systems.

A total of 18 submissions were received for this special issue. Six of them, contributed by research groups from Africa, America, Asia, and Europe, were finally accepted for publication. Among the published papers there is a clear distinction between methodological and application papers: there are three methodological papers that address model analysis from a structural viewpoint and three papers that present recent applications. Admittedly, there is a certain overlap between both categories, since some application papers incorporate new methodological developments, while the methodological papers include biological applications as case studies.

The application papers deal with three different types of diseases: cancer, diabetes, and viral infections. One paper addresses the modeling of one of the hallmarks of cancer: angiogenesis, the formation of new blood vessels that is both driven by and needed for the development of tumors. In "Dynamic Modeling of the Angiogenic Switch and Its Inhibition by Bevacizumab", D. Csercsik and L. Kovács present a model that describes the effect of a therapeutic drug, Bevacizumab, in the inhibition of vascularization. The model is built on previous work by the authors, incorporating a description of vasculature dynamics while keeping the number of states and parameters as low as possible. The paper reports results of its fit to tumor volume data resulting from two therapies and discusses identifiability issues and other aspects. The model is part of ongoing work currently being carried out in the ERC project Tamed Cancer. In this framework, the model is expected to be refined and validated in the near future and eventually to be used for therapy optimization in open-loop and closed-loop.

H.-C. Wei et al. give a novel method to evaluate the neurological damage associated with diabetes (in "Assessment of Diabetic Autonomic Nervous Dysfunction with

a Novel Percussion Entropy Approach"). The approach is based on computing the so-called percussion entropy index (PEI) to obtain information on the similarity in the pattern of changes of two noninvasively measured digital volume pulse signals. Using data taken from 114 individuals, the authors show that two-dimensional PEI is safely applicable to differentiate between healthy subjects, those with well-controlled diabetes, and subjects with poor blood sugar control. The advantageous properties of the proposed method are also shown by comparing it to other possible approaches such as multiscale entropy index and low- to high-frequency power ratio computing.

A. A. M. Arafa et al. ("A Non-Integer Variable Order Mathematical Model of Human Immunodeficiency Virus and Malaria Coinfection with Time Delay") propose a novel mathematical model to investigate the spreading of HIV and malaria infection and the mutual interactions between the dynamics of the two infections. This is an important application of mathematical modeling, since the coinfection of HIV and malaria has become endemic in several developing countries. Thus, there is an urgent need for a better understanding of the dynamics of this coinfection, in order to design effective vaccination strategies. A feature of the modeling approach exploited by the authors is the use of variable (instead of constant) fractional order derivatives with time delay. This feature is utilized to effectively describe the variable memory of the infection progression in distinct patients, taking also into account the important effect of time delay after contagion, required for the individuals and mosquitoes to become infectious.

The three methodological papers address topics such as reachability, observability, identifiability, and model discrimination of nonlinear models, using structural approaches.

The review by A. F. Villaverde ("Observability and Structural Identifiability of Nonlinear Biological Systems") focuses on two properties that characterize the ability to infer model unknowns by measuring the model output. The first one, observability, describes the possibility of reconstructing the state vector, while the second one, structural identifiability, refers to the parameter vector. The latter can be considered as a special case of the former, and both properties can be studied locally for nonlinear models using the differential geometry approach. The paper by A. F. Villaverde provides a brief tutorial of this approach, surveys the recent literature, and discusses the relationship between these properties and other concepts. Finally, it suggests some possible directions for future research.

H. A. Harrington et al. ("A Parameter-Free Model Comparison Test Using Differential Algebra") propose a model discrimination procedure that is applicable for noisy measurements without performing parameter estimation. The candidate models are given in the form of parameterized polynomial ordinary differential equations. Using differential algebra, invariants can be written from the system models which are polynomial in the inputs, outputs, and their derivatives, and the coefficients of monomials are rational in the parameters. By substituting the measured and computed values of the inputs, outputs, and their derivatives into the invariants at different time-instants, a set of linear equations can be obtained which is uniquely solvable for the true model in the noise-free case, but not solvable for others. For the realistic noisy case, probability bounds can be computed for the rejection of models, and the derivatives can be estimated using Gaussian Process Regression.

G. Szlobodnyik and G. Szederkényi study the reachability properties of a special class of discrete reaction networks having at most one input and one output species beyond the possible catalyzers from a computational point of view ("Reachability Analysis of Low-Order Discrete State Reaction Networks Obeying Conservation Laws"). The subconservativity of a discrete reaction network ensures the boundedness of its state-space. The authors show that the reachability problem can be rewritten as an Integer Linear Programming feasibility problem. This computational framework allows deciding the reachability problem and counting the number of feasible discrete trajectories in polynomial time in the number of species and in the distance of initial and target states, if the number of reactions is fixed.

Overall, the aforementioned contributions show that (1) biological problems pose challenges that are different to those of physical and engineered systems; (2) for this reason, they are an important driver of innovation in mathematical and computational techniques for dynamic modelling; (3) as a result of recent developments, these methodologies are already capable of providing key information in biomedical applications; (4) however, the identification of open challenges also highlights the need for further advances.

As a final remark, we would like to note that another special issue dealing with biological modeling has been recently published in Complexity: "Mathematical Modeling and Dynamic Analysis of Complex Biological Systems" (MMDACBS, https://www.hindawi.com/journals/complexity/si/860912/). There are similarities and differences between the MMDACBS special issue and the present one, which can thus be seen as complementary collections. While the present special issue has an emphasis on biomedicine, the MMDACBS is more oriented towards biotechnological applications. The methodologies considered in the MMDACBS special issue include different types of flux analysis and statistical techniques for black-box modelling, while the present special issue focuses on the reverse engineering, modelling, and identification of kinetic models. Furthermore, as of writing this editorial, submissions are being accepted for another related special issue: "Dynamical Analysis of Biological Systems", edited by Popescu, Voit, and Udriste (https://www.hindawi.com/journals/complexity/si/394076/cfp/). The proliferation of special issues on this topic, which can also be noticed in other multidisciplinary journals, is an indication of the strong interest among the scientific community in the development and application of dynamical modelling tools for unravelling the complexity of biological systems.

Conflicts of Interest

The authors declare that there are no conflicts of interest regarding the publication of this paper.

Acknowledgments

Research Article

Reachability Analysis of Low-Order Discrete State Reaction Networks Obeying Conservation Laws

Gergely Szlobodnyik [iD] [1] and **Gábor Szederkényi**[1,2]

[1]*Faculty of Information Technology and Bionics, Pázmány Péter Catholic University, Práter u. 50/a, H-1083 Budapest, Hungary*
[2]*Systems and Control Laboratory, Institute for Computer Science and Control (MTA SZTAKI) of the Hungarian Academy of Sciences, Kende u. 13-17, H-1111 Budapest, Hungary*

Correspondence should be addressed to Gergely Szlobodnyik; szlger91@gmail.com

In this paper we study the reachability problem of sub- and superconservative discrete state chemical reaction networks (d-CRNs). It is known that a subconservative network has bounded reachable state space, while that of a superconservative one is unbounded. The reachability problem of superconservative reaction networks is traced back to the reachability of subconservative ones. We consider network structures composed of reactions having at most one input and one output species beyond the possible catalyzers. We give a proof that, assuming all the reactions are charged in the initial and target states, the reachability problems of sub- and superconservative reaction networks are equivalent to the existence of nonnegative integer solution of the corresponding d-CRN state equations. Using this result, the reachability problem is reformulated as an Integer Linear Programming (ILP) feasibility problem. Therefore, the number of feasible trajectories satisfying the reachability relation can be counted in polynomial time in the number of species and in the distance of initial and target states, assuming fixed number of reactions in the system.

1. Introduction

Employing deterministic ordinary differential equation systems to characterize the dynamical behavior of complex networks of chemically interacting components (species) is a widely used approach in mathematical and computational systems biology [1–3]. Such a continuous state modeling approach assumes high molecular count of species and their homogeneous (well-mixed) distribution in the surrounding media [4]. However, in several (bio)chemically interesting systems, such as some enzymatic and genetic networks, the molecular count of different species is relatively low (e.g., < 100 molecules) [4–6] implying that the assumption of homogeneous species distribution does not hold [7, 8]. Hence it is necessary to introduce a discrete state model capable of keeping track of the individual molecular counts in order to properly characterize the qualitative dynamical behavior of (bio)chemical networks of species with low number of

molecules [9, 10]. There exist several mathematical models describing the state evolution of discrete state chemical reactions networks, such as Markov chain models [8, 10] and stochastic Petri nets [11].

In the context of chemical reaction networks of several interacting components, in order to completely characterize the system it is needed to simultaneously study the dynamical behavior and the underlying network structure as well. Moreover, it is also important to examine how the dynamical behavior and the network structure are related to each other, and how we can predict the dynamical behavior (e.g., in the form of possible state space trajectories) and be aware of the underlying network structure. For continuous state reaction networks obeying the law of mass action, it is recognized that the network structure (i.e., topology) is not necessarily unique; i.e., the same system of differential equations can be generated by different network topologies (different sets of interactions among the given species) [12–15].

TABLE 1: Notations.

$\mathbb{R}$	the set of real numbers
$\mathbb{Z}$	the set of integer numbers
$\mathbb{Z}_{\geq 0}$	the set of non-negative integer numbers
$\mathbb{T}^{n \times m}$	the set of $(n \times m)$-dimensional vectors over the set $\mathbb{T}$
$0^{n \times m}$	a zero matrix of dimension $n \times m$
$1^{n \times m}$	a matrix of dimension $n \times m$ for which all the entries are equal to 1
$\{0, 1\}^{n \times m}$	the set of $(n \times m)$-dimensional binary vectors (all the entries are equal to 0 or 1)
$\{-1, 0, 1\}^{n \times m}$	the set of $(n \times m)$-dimensional vectors composed of the entries $-1, 0, 1$
$[A]_{i,:}$	the ith row of the matrix A
$a \prec b$	for $a, b \in \mathbb{R}^n$, $a_i < b_i$ for $i = 1, \ldots, n$
$a \preceq b$	for $a, b \in \mathbb{R}^n$, $a_i \leq b_i$ for $i = 1, \ldots, n$
σ_X	an ordered sequence of states
σ_r	an ordered sequence of reaction vectors
σ_S	an ordered sequence of species
σ_C	an ordered sequence of complexes

In the case of discrete state reaction networks the so-called reachability is a strictly related problem to the dynamical behavior; namely, is it possible to reach a prescribed target state from a given initial one through a finite sequence of transition (reactions)? It is known that the reachability relation between any pair of nonnegative initial and target states is determined by the network structure itself. Through the reachability analysis several problems of great importance can be analyzed; one of them having high interest is the existence of so-called extinction events: the existence of trajectories resulting in the irreversible extinction of some species from the system. It has been shown that under some conditions on the network structure a discrete state chemical reaction network exhibits an extinction event from any point of its state space [9, 16, 17]. The properties of recurrence (the ability of returning to any initial state) and irreducibility (the ability of reaching any state from any other one) are also examined in the context of discrete state reaction networks [18, 19].

The mathematical model of discrete state chemical reaction networks is equivalent to an important model of theoretical computer science, namely, the so-called vector addition systems with states (VASS) or equivalently Petri nets [20, 21]. Hence the discrete chemical reaction network reachability problem is equivalent to the extensively studied problem of vector addition system (VAS) reachability. The VAS reachability problem is known to be decidable [22–25], and for the space complexity we have EXSPACE lower bound [26]. Unfortunately, contrary to the proven polynomial time complexity of reachability of rate independent continuous state chemical reaction networks [21], in the case of discrete state reaction networks it is not known whether there exists an algorithm of primitive-recursive time complexity deciding this problem [27].

The aim of this paper is to study of the reachability problem of sub- and superconservative d-CRNs. We make use of the relation between the sub- and superconservative properties. In Propositions 15 and 17, we give necessary and sufficient conditions on the network structure and the initial and target states under which the reachability is equivalent to the nonnegative integer solution of the d-CRN state equation. Then these results in Corollaries 16 and 18 are extended to a subclass of superconservative d-CRNs.

The paper is organized as follows. In Section 2 the necessary mathematical notations and concepts of Chemical Reaction Network Theory (CRNT) are introduced. Section 3 discusses the classes of sub- and superconservative d-CRNs and their duality as well. In Section 4 the reachability problem of sub- and superconservative d-CRNs is examined. Firstly the case of low state space-dimensional d-CRNs is discussed, followed by the extension to the general case when the dimension of the state space is arbitrarily high. In Section 5 our findings are illustrated in a representative example.

2. Notations and Mathematical Background

In Table 1 we summarize the notations and concepts of discrete chemical reaction networks which will be extensively used later.

2.1. Discrete State Chemical Reaction Networks. A discrete state Chemical Reaction Network (d-CRN) with *n species*, *m complexes*, and *l reactions* is a triple $\mathcal{N} = (\mathcal{S}, \mathcal{C}, \mathcal{R})$ so that

$$\mathcal{S} = \{s_i \mid i = 1, \ldots, n\}$$

$$\mathcal{C} = \left\{ y_j = \sum_{i=1}^{n} \alpha_{ji} s_i \mid s_i \in \mathcal{S}, \ \alpha_{ji} \in \mathbb{Z}_{\geq 0}, \ i = 1, \ldots, n, \ j \right.$$

$$\left. = 1, \ldots, m \right\} \tag{1}$$

$$\mathcal{R} = \left\{ r_v = y_{source(r_v)} \right.$$

$$\longrightarrow y_{product(r_v)} \mid y_{source(r_v)}, y_{product(r_v)} \in \mathcal{C}, v$$

$$= 1, \ldots, l \right\}$$
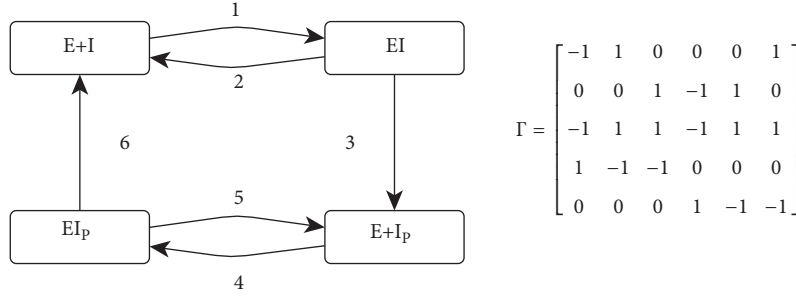
FIGURE 1: A discrete state chemical reaction network. *Left:* reaction network structure. The nodes and directed edges represent the complexes and the reactions, respectively. The numbers on the edges denote a fixed ordering of the reactions. *Right:* the stoichiometric matrix associated with the system, i.e. $[\Gamma]_{ij}$ is the net change in the number of the i'th species upon occurring the j'th reaction.

where s_i is the i'th *species*, y_j is the j'th *complex*, and r_v is the v'th *reaction* of the network. Moreover, α_{ji} is the *stoichiometric coefficient* of the i'th species in the j'th complex. For a *reaction* $r_v = y_{source(r_v)} \longrightarrow y_{product(r_v)}$ of $\mathscr{R}$, $y_{source(r_v)}$ and $y_{product(r_v)}$ are the source complex and the product complex, respectively.

For each complex $y_j \in \mathscr{C}$, $j \in \{1, \ldots, m\}$, the stoichiometric coefficients of the species can be represented as a vector of the following form:

$$\overline{y}_j = [\alpha_{j1} \ \alpha_{j2} \ \ldots \ \alpha_{jn}]^{\top} \tag{2}$$

For each $r \in \mathscr{R}$, a reaction vector $r_{ij} \in \mathbb{Z}^n$ can be associated with the track of the net molecular count changes of the species upon firing the reaction:

$$r_{ij} = \overline{y}_j - \overline{y}_i \tag{3}$$

so that y_j and y_i are the corresponding source and product complexes of r. In the sequel the notation r_i will be used for denoting both the i'th reaction of the d-CRN and the associated reaction vector as well. We will also assume that for all the examined d-CRNs a fixed order of the reaction vectors is given; i.e., an order $r_1, r_2, \ldots, r_l$ is fixed and $l = |\mathscr{R}|$.

A d-CRN can also be represented by a directed graph $G = G(V, E)$ such that the vertices and edges correspond to the complexes and the reactions, respectively, i.e.,

$$V = \mathscr{C} \tag{4}$$

$$E = \mathscr{R}. \tag{5}$$

The direction of the edges is determined by the reactions of $\mathscr{R}$, so that if $y_i \longrightarrow y_j \in \mathscr{R}$, then there exists an edge $e \in E$ from the vertex representing y_i to the vertex of y_j. For each edge a weight corresponding to the reaction rate constant (also called intensity or propensity) corresponding to the respective reaction can also be associated.

Beyond the above representations it is also possible to describe a d-CRN in an algebraic way by means of its unique stoichiometric matrix.

Definition 1. Let us consider a d-CRN $\mathscr{N} = (\mathscr{S}, \mathscr{C}, \mathscr{R})$. The *stoichiometric matrix* $\Gamma \in \mathbb{Z}^{n \times l}$ of $\mathscr{N}$ is defined as follows:

$$\Gamma = [r_1 \ldots r_l] \tag{6}$$

Note that $[\Gamma]_{ij}$ encodes the net molecule count change on species s_i upon the occurrence of reaction r_j. Besides Γ we also define the following matrices:

$$\Gamma^+ = \left[\overline{y}_{r_1}^+ \ldots \overline{y}_{r_l}^+\right]^{\top} \tag{7}$$

$$\Gamma^- = \left[\overline{y}_{r_1}^- \ldots \overline{y}_{r_l}^-\right]^{\top} \tag{8}$$

where $\overline{y}_{r_i}^+$ denotes the vector form of the product complex belonging to reaction r_i while $\overline{y}_{r_j}^-$ represents the vector of the source complex associated with reaction r_j. The relation among the above defined matrices is as follows:

$$\Gamma = \Gamma^+ - \Gamma^- \tag{9}$$

Example 2. Let us consider the d-CRN $\mathscr{N} = (\mathscr{S}, \mathscr{C}, \mathscr{R})$ depicted in Figure 1. $\mathscr{N}$ characterizes a simple network of a bifunctional enzyme E having both phosphorylation and dephosphorylation activities on species I and I_p, respectively. This network is characterized by the following sets.

$$\mathscr{S} = \left\{I, \ I_p, \ E, \ EI, \ EI_p\right\}$$

$$\mathscr{C} = \left\{I + E, \ EI, \ I_p + E, \ EI_p\right\}$$

$$\mathscr{R} = \left\{E + I \longrightarrow EI, \ IE \longrightarrow E + I, \ EI \longrightarrow I_p + E, \ E \right.$$

$$\left. + I_p \longrightarrow EI_p, \ EI_p \longrightarrow E + I_p, \ EI_p \longrightarrow E + I\right\} \tag{10}$$

We fix the order of species and reactions as they are listed in the above sets.

$\mathscr{N}$ has no information on the probabilities of the reactions, but at any given time instant at most one reaction can occur.

The molecular count of each species of a d-CRN at any time $t \geq 0$ is given by its state vector $X(t) \in \mathbb{Z}_{\geq 0}^n$ and the time evolution of the system is characterized by the following *discrete state equation*:

$$X(t) = X(0) + \Gamma N(t) \tag{11}$$

where $X(0)$ is the state vector belonging to the initial time instant and $N(t) = [N_1(t), N_2(t), \ldots, N_m(t)]^{\top} \in \mathbb{Z}_{\geq 0}^l$ such

that $N_k(t) \in \mathbb{Z}_{\geq 0}$ stores the number of occurrences of the k'th reaction up to time t. We note that $N(t)$ is typically modeled as some point process [8, 10].

For our further analysis the time instants when the reactions have occurred are not of interest, but only the order of reactions; therefore we abandon the notation of time t in the formulas.

Definition 3. Let us consider a d-CRN $\mathcal{N} = (\mathcal{S}, \mathcal{C}, \mathcal{R})$. It is said that:

(1) a species $s \in \mathcal{S}$ is a *catalyzer* of a reaction $r \in \mathcal{R}$ if it has the form of $r = s + s_1 \longrightarrow s + s_2$ with $s_1, s_2 \in \mathcal{S}$,

(2) a complex $y \in \mathcal{C}$ is *charged* at state $X \in \mathbb{Z}_{\geq 0}^n$ if $X \succeq y$,

(3) a reaction $r \in \mathcal{R}$ is charged if its respective source complex is charged,

(4) a state $X \in \mathbb{Z}_{\geq 0}^n$ *reacts* to a state $X' \in \mathbb{Z}_{\geq 0}^n$ (denoted by $X \longrightarrow X'$) if there exists a reaction $r \in \mathcal{R}$ such that r is charged at state X and $X + r = X'$,

(5) a *reaction (vector) sequence* σ_r is an ordered set of reaction vectors $\sigma_r = r_1 \ldots r_\nu$ where $r_i \in \mathcal{R}, i = 1, \ldots, \nu$,

(6) a *state transition sequence* σ_X is an ordered set states $X_0, X_1, \ldots, X_p$ so that $X_1 \longrightarrow X_2 \longrightarrow \cdots \longrightarrow X_{p-1} \longrightarrow X_p$,

(7) a state $X' \in \mathbb{Z}_{\geq 0}^n$ is *reachable* from a state $X \in \mathbb{Z}_{\geq 0}^n$ (denoted by $X \rightsquigarrow_{\mathcal{N}} X'$) if there exists a directed path in the state space so that $X = X_{\nu(1)} \longrightarrow X_{\nu(2)} \longrightarrow \cdots \longrightarrow X_{\nu(\nu)} = X'$.

Considering a state transition sequence $\sigma_X = X_0 X_1 \ldots X_{p-1} X_p$, we call X_0 and X_p the initial and target states, respectively, while X_i for $i \in \{1, \ldots, p - 1\}$ are called transition states of σ_X.

The condition that a reaction $r \in \mathcal{R}$ is charged at state $X \in \mathbb{Z}_{\geq 0}^n$ can be expressed by the inequality $X \succeq \overline{y_r}$. For a reaction sequence σ_r a state transition sequence $\sigma_X = X_0 X_1 \ldots X_\nu$ can be uniquely associated so that

$$X_j = X_{j-1} + r_j, \quad j \in \{1, \ldots, \nu\} \tag{12}$$

where the initial state X_0 is assumed to be given. A state transition sequence σ_X is said to be *admissible* if $X_i \succeq r_{i+1}$ for $X_i \in \sigma_X, i \in \{0, \ldots, \nu - 1\}$; moreover, we say that a reaction sequence σ_r is admissible if the corresponding state transition sequence is admissible.

From the reachability of a state $X' \in \mathbb{Z}_{\geq 0}^n$ from an initial state $X_0 \in \mathbb{Z}_{\geq 0}^n$, it follows that the following equation has a nonnegative integer solution $c \in \mathbb{Z}_{\geq 0}^l$:

$$X' = X_0 + \Gamma c \tag{13}$$

where $[c]_i$ encodes the number of occurrences for reaction $r_i \in \mathcal{R}$ for $i \in \{1, \ldots, l\}$. However, it is important to note that from the existence of a nonnegative integer solution c of (13), the reachability relation $X_0 \rightsquigarrow_{\mathcal{N}} X'$ does not necessary follow.

We note that c of (13) corresponds to $N(t)$ of (11). Since a solution $c \in \mathbb{Z}_{\geq 0}^l$ of (13) encodes the number of occurrences for each reaction in a fixed order, the following equality is fulfilled:

$$\Gamma c = \sum_{i=1}^h r_i \tag{14}$$

where $h = \sum_{i=1}^l [c]_i$ and $r_i \in \mathcal{R}$ for $i \in \{1, \ldots, h\}$. When we want to emphasize that a reaction vector sequence is encoded by a particular $c \in \mathbb{Z}_{\geq 0}^l$, we will use the notation $\sigma_r^c = r_1, \ldots, r_h$ and the state transition sequence determined by σ_r^c will be denoted by σ_X^c.

Definition 4. Let us consider a d-CRN $\mathcal{N}$ with stoichiometric matrix $\Gamma \in \mathbb{Z}^{n \times l}$ and an initial state $X_0 \in \mathbb{Z}_{\geq 0}^n$. The *reachable state space Reach$(\mathcal{N}, X_0)$* of $\mathcal{N}$ with initial state X_0 is the set of nonnegative discrete states reachable from X_0.

$$Reach(\mathcal{N}, X_0) = \{X \mid X \in \mathbb{Z}_{\geq 0}^n, \ X_0 \rightsquigarrow_{\mathcal{N}} X\} \tag{15}$$

3. Integer Linear Programming

In this section some relevant concepts of mathematical programming that will be extensively employed later are briefly reviewed. An Integer Linear Programming (ILP) instance can be formulated as follows:

$$ILP \begin{cases} \min_x \{a^\top x\} \\ subject\ to \\ Ax \leq b \\ x \in \mathbb{Z}^n \end{cases} \tag{16}$$

where x is the n-dimensional vector of decision variables while $a \in \mathbb{Z}^n$, $A \in \mathbb{Z}^{m \times n}$, and $b \in \mathbb{Z}^m$ are fixed coefficients. Generally, the above ILP computational problem is known to be NP-hard, which may highly confine our ability to efficiently solve problems of integers in high dimension.

However, if the value of the decision vector that minimizes (or maximizes) the prescribed objective function is not important for us, but only the existence of a $x \in \mathbb{Z}^n$ vector satisfying the set of specified constraints, then the problem is called ILP feasibility problem.

$$FP \begin{cases} P = \{x \mid Ax \leq b, \ A \in \mathbb{Z}^{m \times n}, \ b \in \mathbb{Z}^m, \ x \in \mathbb{R}^n\} \\ P \cap \mathbb{Z}^n \overset{?}{=} \emptyset \end{cases} \tag{17}$$

An ILP feasibility problem, as a decision problem, addresses the question of whether the polytope P contains an integer lattice point, formally $P \cap \mathbb{Z}^n \overset{?}{=} \emptyset$. While a FP is also known to be NP-hard, it has well-decoupled time complexity with respect to the number of variables, the number of constraints, and the maximum of the absolute values of the entries of A and b. Therefore, a feasibility problem of the form (17), assuming fixed dimension n, can be decided in polynomial time in the number of constraints m and the maximum of

the absolute values of the coefficients A and b by means of the Lenstra algorithm [28, 29]. Moreover, the number of integer lattice points in P can also be numerated in polynomial time in m and the maximum of the absolute value of the coefficients using Barvinok's integer lattice point counting algorithm [30–33]. We note that for the Barvinok algorithm there exists an effective implementation called LattE [34].

4. Sub- and Superconservative d-CRNs

We define conservativity and subconservativity in the same way as they were introduced, e.g. in [4, 16].

Definition 5. A d-CRN $\mathcal{N} = (\mathcal{S}, \mathcal{C}, \mathcal{R})$ having stoichiometric matrix $\Gamma \in \mathbb{Z}^{n \times l}$ is called *subconservative* (*superconservative*) if there exists a strictly positive vector $z \in \mathbb{R}^n_{>0}$ for which $z^\top \Gamma \leq 0^{1 \times l}$ ($z^\top \Gamma \geq 0^{1 \times l}$) holds. The vector z is called a *conservation vector*.

An important property related to subconservativity is the strong boundedness which is defined as follows.

Definition 6. A d-CRN $\mathcal{N}$ is said to be *strongly bounded* if, for any $X_0 \in \mathbb{Z}^n_{\geq 0}$ initial state, the reachable state space $Reach(\mathcal{N}, X_0)$ is bounded.

The subconservative property of the reaction network structure is a necessary and sufficient condition of strong boundedness [16, 35].

Proposition 7 (see [35]). *Let us consider a d-CRN $\mathcal{N}$. The following propositions are equivalent:*

(1) *$\mathcal{N}$ is subconservative,*

(2) *$\mathcal{N}$ is strongly bounded.*

As a special case covered by the intersection of sub- and superconservativity, we can define the conservative property as well.

Definition 8. Let us consider a d-CRN $\mathcal{N} = (\mathcal{S}, \mathcal{C}, \mathcal{R})$ with stoichiometric matrix $\Gamma \in \mathbb{Z}^{n \times l}$. The d-CRN $\mathcal{N}$ is said to be *conservative* if there exists a vector $z \in \mathbb{R}^n_{>0}$ satisfying the matrix equation $z^\top \Gamma = 0^{1 \times l}$.

We note that the above structural properties can be easily decided in polynomial time by means of an LP of the following form:

$$\min \quad \sum_{j=1}^{n} z_j$$

$$s.t. \tag{18}$$

$$z^\top \Gamma \leq 0^{1 \times l} \quad \left(or \ z^\top \Gamma \geq 0^{1 \times l} \right)$$

$$z \geq 0^{n \times 1} + \varepsilon^{n \times 1}, \quad \varepsilon \succ 0^{n \times 1}$$

The relationship between sub- and superconservativity can be expressed by the following proposition.

Proposition 9. *A d-CRN $\mathcal{N}$ with stoichiometric matrix $\Gamma_\mathcal{N} \in \mathbb{Z}^{n \times l}$ is subconservative if and only if the d-CRN $\mathcal{N}'$ with stoichiometric matrix $\Gamma_{\mathcal{N}'} = -\Gamma_\mathcal{N}$ is superconservative.*

Proof.

$$z^\top \Gamma \leq 0^{1 \times m} \iff z^\top (-\Gamma) \geq 0^{1 \times l} \tag{19}$$

□

We note that $-\Gamma_\mathcal{N}$ means the change of the direction of each reaction in the d-CRN $\mathcal{N}$ of stoichiometric matrix $\Gamma_\mathcal{N}$.

Example 10. Figure 2 depicts two d-CRNs: a subconservative and a superconservative reaction network structure. Indeed, these networks are counterparts that can be easily transformed to each other by changing the sign of the entries in the stoichiometric matrices. Such a transformation results in the change of the direction of the edges in the reaction network.

From Proposition 9 it follows that, instead of the reachability problem of a superconservative network structure, one can consider an equivalent subconservative d-CRN reachability problem as is discussed in Proposition 11.

Proposition 11. *Let us consider a subconservative d-CRN $\mathcal{N}$ characterized by the matrices $\Gamma_\mathcal{N} = \Gamma$, $\Gamma_\mathcal{N}^+ = \Gamma^+$ and a superconservative d-CRN $\mathcal{N}'$ with matrices $\Gamma_{\mathcal{N}'} = -\Gamma$, $\Gamma_{\mathcal{N}'}^- = \Gamma^+$. Let us take an initial state $X_0 \in \mathbb{Z}^n_{\geq 0}$ and a target state $X' \in \mathbb{Z}^n_{\geq 0}$. Then the reachability $X_0 \rightsquigarrow_\mathcal{N} X'$ holds if and only if $X' \rightsquigarrow_{\mathcal{N}'} X_0$ also holds.*

Proof.

(1) $X_0 \rightsquigarrow_\mathcal{N} X' \implies \exists c \in \mathbb{Z}^l_{\geq 0}$ such that $X_0 + \Gamma c = X'$ which is equivalent to $X' + (-\Gamma)c = X_0$.

From $X_0 \rightsquigarrow_\mathcal{N} X'$ it follows that the solution $c \in \mathbb{Z}^l_{\geq 0}$ can be decomposed to an admissible reaction vector sequence $\sigma_r^c = r_1^c \ldots r_h^c$, $h = \sum_{i=1}^l [c]_i$; i.e., all the states of σ_X^c determined by σ_r^c are composed of nonnegative entries. Then, by reversing σ_X^c, we obtain a nonnegative state transition sequence $\hat{\sigma}_X^c$ from X' to X_0 which is uniquely determined by means of the reaction vector sequence $\hat{\sigma}_r^c = -r_h^c \ldots - r_1^c$.

It is also needed to show that $\hat{\sigma}_r^c$ is an admissible reaction sequence. This can be done as follows: for each state $X \in \sigma_X^c \backslash X_0$ there exists a reaction $r \in \sigma_r^c$ so that upon firing r the resulting state is X, from which it follows that $X \geq \overline{y}_r^+$; moreover, considering the reversed reaction sequence $\hat{\sigma}_r^c$, the reaction vector that will occur at state X is $-r \in \hat{\sigma}_r^c$ which is charged at X even if $X \geq \overline{y}_r^+$.

Then the admissibility of $\hat{\sigma}_r^c$ follows.

(2) The proof for the other direction $X' \rightsquigarrow_{\mathcal{N}'} X_0$ works analogously as above.

□

The importance of Proposition 11 is that the reachability problem of a superconservative d-CRN of unbounded reachable state space can be easily traced back to the reachability

(a)

(b)
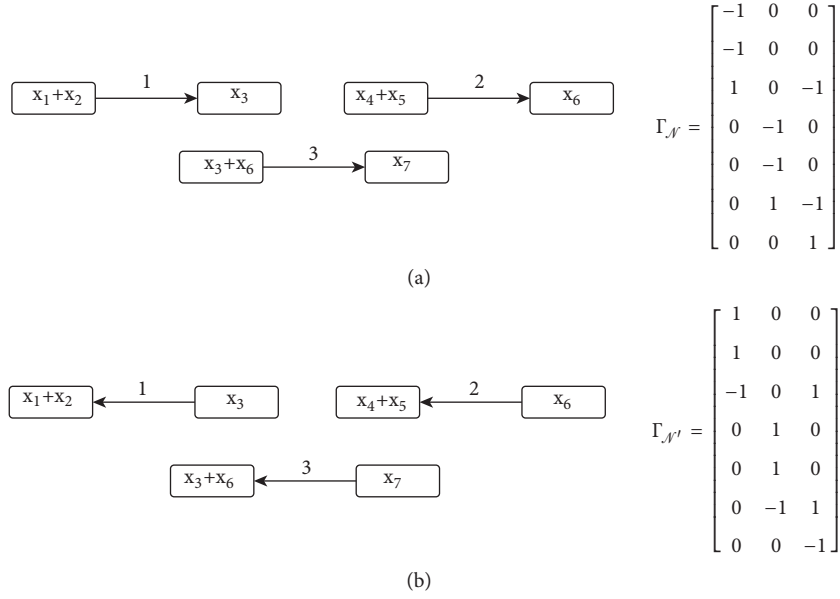
Figure 2: A pair of sub- and superconservative reaction network structures denoted by $\mathcal{N}$ and $\mathcal{N}'$, respectively. The ordering of the reactions are denoted by the numbers on the edges of the graphs. The two networks can be transformed to each other by changing the sign of the entries in their stoichiometric matrices. (a) Subconservative d-CRN. (b) Superconservative d-CRN.

problem of a d-CRN of bounded reachable state space which can make the original decision problem computationally tractable.

5. Reachability Analysis

5.1. Low-Dimensional Case. In this section the case of low-dimensional ($\mathrm{rank}(\Gamma) \leq 2$) subconservative d-CRNs is considered. We state a modified version of Proposition 5 of [36] where the conditions on the initial and target states are less strict. Then we extend the result to superconservative d-CRNs.

In order to discuss low-dimensional reachability problems, we introduce a distinguished state $M = M(\Gamma^-)$ as follows:

$$[M(\Gamma^-)]_i = \max\left\{[\Gamma^-]_{ij} : j = 1, \ldots, l\right\} \quad i = 1, \ldots, n. \quad (20)$$

Here Γ^- is defined by (8). Note that the set $\{X \mid X \in \mathbb{Z}^n_{\geq 0}, \; X \succeq M\}$ contains all the states where each reaction is charged.

Proposition 12. *Let us consider a subconservative d-CRN $\mathcal{N}$ with stoichiometric matrix $\Gamma \in \{-1, 0, 1\}^{n \times l}$ and $\Gamma^- \in \{0, 1\}^{n \times l}$. Assume that $\mathrm{rank}(\Gamma) \leq 2$. We consider an initial state $X_0 \in \mathbb{Z}^n_{\geq 0}$ and a target state $X' \in \mathbb{Z}^n_{\geq 0}$ such that $X_0 \succeq M$ and $X' \succeq M$ hold where $M = M(\Gamma^-)$ is defined by (20). Then the state X' is reachable from X_0 through a state transition sequence $\sigma_X = X_0 X_1 \ldots X'$ for which, $\forall X \in \sigma_X, \; X \succeq M$ if and only if the equation*

$$\Gamma c = X' - X_0 \quad (21)$$

has a nonnegative integer solution c.

Proof.

(1) If X' is reachable from X_0 through an admissible state transition sequence σ_X, then it follows that a solution $c \in \mathbb{Z}^l_{\geq 0}$ exists.

(2) Assume that there exists $c \in \mathbb{Z}^n_{\geq 0}$ such that $X_0 + \Gamma c = X'$ holds. Let us consider any reaction vector decomposition $\sigma_r = r_{\nu(1)} \ldots r_{\nu(h)}$ of c where $\sum_{j=1}^h r_{\nu(j)} = c$ and $\sum_{j=1}^l [c]_j = h$. We show that Algorithm 1 returns a permutation of σ_r so that for all the transition states X the inequality $X \succeq M$ holds.

Let us assume that there exists a transition state $X_i, X_i \succeq M$, so that the forthcoming state X_{i+1} satisfies the inequality $[X_{i+1}]_d < [M]_d$ for some $d \in \{1, 2\}$. For the target state X' to be reached the inequality $X' \succeq M$ holds; hence there exists a reaction increasing the state variable along the coordinate d. Let us assume that all the reactions increasing the state variable along X_i decrease the other coordinate d' so that the resulting forthcoming state X_{i+1} satisfies the inequality $[X_{i+1}]_{d'} < [M]_{d'}$. Then $X_i = M$ holds. Now there are two different cases:

(P_1) If $X' = M$, then Algorithm 1 terminates, and the correctness follows.

(P_2) If $X' \neq M$, then the subconservativity of $\mathcal{N}$ implies that it is not possible to reach a state $X, X \succeq M, X \neq M$; i.e., X' is not reachable from X_i. This is contradiction, since arbitrary permutation of the initial ordering σ_r results in the same target state X', given the initial state X_0. Then the correctness of Algorithm 1 follows.

□

```
1: procedure REORDER($X_0 [r_{\nu(1)}\ r_{\nu(2)}\ \dots\ r_{\nu(h)}], M$)
2:     $X_{current} \longleftarrow X_0$
3:     for $i = 1$ to $h$ do
4:         if $X_{current} = X'$ then
5:             return $[r_{\nu(1)}\ r_{\nu(2)}\ \dots\ r_{\nu(h)}]$
6:         end if
7:         if$[X_{current} + r_{\nu(i)}]_l < [M]_l$ for some $l \in \{1,\dots,n\}$ then
8:             Choose a transition vector $r_{\nu(j)}$, $i < j \le h$ so that
                 $X_{current} + r_{\nu(j)} \succeq M$
9:             $r' \longleftarrow r_{\nu(i)}$
10:            $r_{\nu(i)} \longleftarrow r_{\nu(j)}$
11:            $r_{\nu(j)} \longleftarrow r'$
12:        end if
13:        $X_{current} \longleftarrow X_{current} + r_{\nu(i)}$
14:    end for
15:    return $[r_{\nu(1)}\ r_{\nu(2)}\ \dots\ r_{\nu(h)}]$
16: end procedure
```

ALGORITHM 1

Algorithm 1 can be easily extended to the class of superconservative reaction networks.

Corollary 13. *Let us consider a superconservative d-CRN $\mathcal{N}$ with stoichiometric matrix $\Gamma \in \{-1, 0, 1\}^{n \times l}$ and $\Gamma^- \in {0, 1}^{n \times l}$. Assume that* rank$(\Gamma) \le 2$ *holds and consider an initial state $X_0 \in \mathbb{Z}_{\ge 0}^n$ and a target state $X' \in \mathbb{Z}_{\ge 0}^n$ for which $X_0 \succeq M$ and $X' \succeq M$ hold where M is defined by (20). Then the state $X' \in \mathbb{Z}_{\ge 0}^n$ is reachable from X_0 if and only if the equation*

$$\Gamma c = X' - X_0 \tag{22}$$

has a nonnegative integer solution c.

Proof. According to Proposition 11 we can consider a subconservative d-CRN $\mathcal{N}'$ of stoichiometric matrix $-\Gamma$ and take the reachability problem $X' \overset{?}{\leadsto}_{\mathcal{N}'} X_0$. Then Proposition 7 can be applied. □

5.2. Sub- and Superconservative d-CRNs of Arbitrary High State Space Dimension. In this section the reachability problem of arbitrary high-dimensional sub- and superconservative d-CRNs is considered. Firstly we examine network structures composed of reactions having at most one input and one output species. It is shown by an inductive proof that, under some auxiliary condition, the reachability relation $X_0 \leadsto_{\mathcal{N}} X'$ is equivalent to the existence of a $c \in \mathbb{Z}_{\ge 0}^l$ solution of the d-CRN state equation $X_0 + \Gamma c = X'$. Then, according to the relation between sub- and superconservative reaction network structures, this result is generalized to a subclass of superconservative d-CRNs as well. We also extend the results to d-CRNs containing second-order reactions by allowing catalyzer species.

Firstly, we adopt the following necessary and sufficient condition of reachability from the theory of Petri nets (see Theorem 16, [37]) which will be extensively used in the sequel.

Lemma 14. *Let us consider a d-CRN $\mathcal{N}$ with stoichiometric matrix $\Gamma \in \{-1, 0, 1\}^{n \times l}$ such that for all $r \in \mathcal{R}$ reactions $\sum_{i=1}^n [\overline{y}^+]_i \le 1$ and $\sum_{i=1}^n [\overline{y}^-]_i = 1$ holds. Assume that the reaction network of $\mathcal{N}$ does not contain directed cycle (i.e., $\mathcal{N}$ has an acyclic network structure). Consider two states $X_0, X' \in \mathbb{Z}_{\ge 0}^n$. Then the reachability relation $X_0 \leadsto_{\mathcal{N}} X'$ holds if and only if there exists $c \in \mathbb{Z}_{\ge 0}^l$ vector satisfying the state equation $X_0 + \Gamma c = X'$.*

Now we can state the result on the reachability of subconservative d-CRNs composed of reaction having at most one input and one output species.

Proposition 15. *Let us consider a subconservative d-CRN $\mathcal{N} = (\mathcal{S}, \mathcal{C}, \mathcal{R})$ of stoichiometric matrix $\Gamma \in \{-1, 0, 1\}^{n \times l}$ and $\Gamma^- \in \{0, 1\}^{n \times l}$ for which $\mathcal{C} = \mathcal{S} \cup \{0\}$. Assume that for all $r \in \mathcal{R}$ reactions $\sum_{i=1}^n [\overline{y}^+]_i \le 1$ and $\sum_{i=1}^n [\overline{y}^-]_i = 1$ hold. Let us consider two states $X_0, X' \in \mathbb{Z}_{\ge 0}^n$ so that $X_0 \succeq M$ and $X' \succeq M$ hold where $M = M(\Gamma^-)$ is defined by (20). Then the reachability relation $X_0 \leadsto_{\mathcal{N}} X'$ holds if and only if there exists a vector $c \in \mathbb{Z}_{\ge 0}^l$ satisfying the state equation $X_0 + \Gamma c = X'$.*

Proof.

(1) $X_0 \leadsto_{\mathcal{N}} X' \Longrightarrow \exists c \in \mathbb{Z}_{\ge 0}^l : X_0 + \Gamma c = X'$

By the definition of reachability it is guaranteed that the state equation is satisfied with some $c \in \mathbb{Z}_{\ge 0}^l$.

(2) $X_0 \leadsto_{\mathcal{N}} X' \Longleftarrow \exists c \in \mathbb{Z}_{\ge 0}^l : X_0 + \Gamma c = X'$

For this side an inductive proof is employed.

(a) $k = 2$

If a d-CRN is 2-dimensional, according to Proposition 12, the existence of a solution $c \in \mathbb{Z}_{\ge 0}^l$ of the state equation implies that the reachability relation holds.

(b) Inductive assumption

(a)   (b)
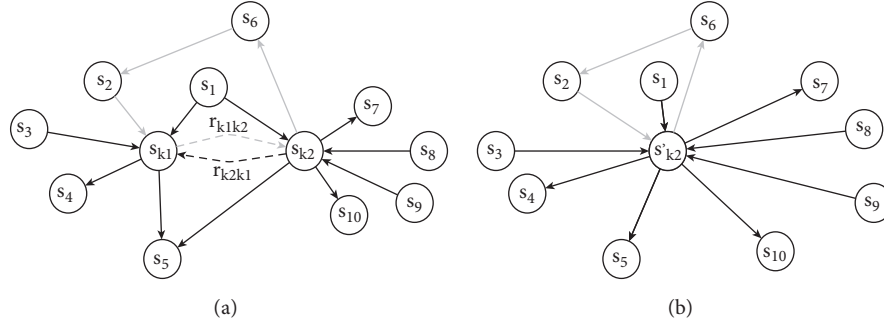
Figure 3: Graphical explanation of how the reaction network structure of $\mathcal{N}'$ in the proof of Proposition 15 is constructed. (a) Reaction network structure of an n-dimensional d-CRN $\mathcal{N}$. (b) Reaction network structure of $\mathcal{N}'$ resulting from merging the species s_{k_1} and s_{k_2} of $\mathcal{N}$ along their shared reaction $r_{k_1 k_2}$ (and reverse counterpart reaction $r_{k_2 k_1}$). Note that by merging s_{k_1} and s_{k_2} we obtain a stoichiometric matrix Γ' having redundant reactions (e.g., (s_1, s_{k_1}), (s_1, s_{k_2}) resulting in (s_1, s'_{k_1}), (s_1, s'_{k_1})) and zero reaction vectors (i.e., self-loops on s'_{k_1}), but they are omitted in (b). A directed cycle on which the chosen reaction $r_{k_1 k_2}$ lies is depicted in gray.

For $k = n - 1$ we assume that the reachability relation $X_0 \rightsquigarrow_{\mathcal{N}} X'$ holds.

(c) $k = n$

We have two different cases with respect to the existence of directed cycles.

If the reaction network has no directed cycle, then the reachability relation $X_0 \rightsquigarrow_{\mathcal{N}} X'$ is guaranteed by Lemma 14.

Assume that the reaction network contains at least one directed cycle

$$\sigma_S = s_{\nu(1)} \ldots s_{\nu(h)} \qquad (23)$$

where $h \le n$, $s_{\nu(1)} = s_{\nu(h)}$ and $s_{\nu(i)} \ne s_{\nu(j)}$ for $i, j \in \{1, \ldots, h\}$, $i \ne j$. Note again that $\mathscr{C} = \mathscr{S} \cup \{0\}$, and hence σ_S can be considered as a directed cycle of complexes in the reaction network (i.e., $\sigma_S = \sigma_C = s_{\nu(1)} \ldots s_{\nu(h)}$). Let us consider an arbitrary $r_{k_1 k_2} \in \mathscr{R}$ reaction defined between some $s_{k_1}, s_{k_2} \in \sigma_S$, i.e. $r_{k_1 k_2} = s_{k_1} \longrightarrow s_{k_2}$.

Now we construct a d-CRN $\mathcal{N}' = (\mathscr{S}', \mathscr{C}', \mathscr{R}')$ from the stoichiometric matrix $\Gamma \in \{-1, 0, 1\}^{(n-1) \times l}$ and $\Gamma^- \in \{0, 1\}^{(n-1) \times l}$ as follows:

$$[\Gamma']_{i,:} = \begin{cases} [\Gamma]_{i,:}, & i < k_{max}, \ i \ne k_{min}, \\ [\Gamma]_{k_{min},:} + [\Gamma]_{k_{max},:}, & i = k_{min}, \\ [\Gamma]_{i+1,:}, & k_{max} \le i \le n - 1, \end{cases} \qquad (24)$$

and

$$[\Gamma^{-'}]_{i,:}$$

$$= \begin{cases} [\Gamma^-]_{i,:}, & i < k_{max}, \ i \ne k_{min}, \\ [\Gamma^-]_{k_{min},:} + [\Gamma^-]_{k_{max},:}, & i = k_{min}, \quad (25) \\ [\Gamma^-]_{i+1,:}, & k_{max} \le i \le n - 1. \end{cases}$$

Here $k_{min} = \min\{k_1, k_2\}$ and $k_{max} = \max\{k_1, k_2\}$. This way we obtained a d-CRN $\mathcal{N}'$ satisfying the assumptions of the proposition. Figure 3 gives an illustrative example of how $\mathcal{N}'$ is constructed. Now we assign to each $r' \in \mathscr{R}'$ the ordered pair of source complex and product complex of $r \in \mathscr{R}$ from which it is obtained. In such a way every reaction of $\mathcal{N}'$ is uniquely described by an ordered pair $(r', r) \in \mathscr{R}' \times \mathscr{R}$. Then by the mapping $P((r', r)) = r$ one can uniquely determine the reaction $r \in \mathscr{R}$ from which $r' \in \mathscr{R}'$ is derived.

Let us construct the states $X_0^m \in \mathbb{Z}_{\ge 0}^{n-1}$ and $X^{m\prime} \in \mathbb{Z}_{\ge 0}^{n-1}$ as follows:

$$[X_0^m]_i = \begin{cases} [X_0]_i, & i < k_{max}, \ i \ne k_{min}, \\ [X_0]_{k_{min}} + [X_0]_{k_{max}}, & i = k_{min}, \quad (26) \\ [X_0]_{i+1}, & k_{max} \le i \le n - 1. \end{cases}$$

$$[X'^m]_i$$

$$= \begin{cases} [X']_i, & i < k_{max}, \ i \ne k_{min}, \\ [X']_{k_{min}} + [X']_{k_{max}}, & i = k_{min}, \quad (27) \\ [X']_{i+1}, & k_{max} \le i \le n - 1. \end{cases}$$

Then we have that $X_0^m \ge M(\Gamma^{-'})$ and $X'^m \ge M(\Gamma^{-'})$, and hence the $(n-1)$-dimensional d-CRN $\mathcal{N}'$ with the initial and final states X_0^m and X'^m satisfies the assumptions of the proposition. From $X_0 + \Gamma c = X'$ we have that $X_0^m + \Gamma' c = X'^m$ holds; hence, according to the $(n-1)$-dimensional inductive assumption, the reachability relation

$$X_0^m \rightsquigarrow_{\mathcal{N}'} X'^m \qquad (28)$$

follows.

Let us consider an admissible reaction vector sequence σ'_r associated with relation (28). Since for each $r' \in \mathcal{R}'$ we associated the reaction $r \in \mathcal{R}$ from which r' is obtained, making use of the mapping $P : \mathcal{R}' \times \mathcal{R} \longrightarrow \mathcal{R}$, we can consider the reaction vector sequence σ_r ($r \in \mathcal{R} \ \forall r \in \sigma_r$) uniquely determined by σ'_r. We start from X_0 and modify the state variable $X \in \mathbb{Z}^n_{\geq 0}$ according to the reaction vector sequence σ_r. We may get to two invalid cases:

(C_1) $[X]_{k_2} = 0$, but the source complex of the forthcoming reaction $r_{current} \in \sigma_r$ is s_{k_2}. Then, according to the $(n-1)$-dimensional reachability, it is guaranteed that s_{k_1} is charged at the current state X. Let us insert $r_{k_1 k_2}$ into σ_r before the current reaction $r_{current}$.

(C_2) $[X]_{k_1} = 0$, but the source complex of the forthcoming reaction $r_{current} \in \sigma_r$ is s_{k_1}. Then, according to the $(n-1)$-dimensional reachability, it is guaranteed that s_{k_2} is charged at the current state X. It is known that s_{k_1} can be reached from s_{k_2} along a reaction vector sequence σ^*_r in the reaction network of $\mathcal{N}$. Let us insert σ^*_r into σ_r before the current reaction $r_{current}$.

By modifying σ_r according to the above discussed cases (C_1) and (C_2), we obtain an admissible reaction vector sequence $\sigma_{r_{mod}}$ with respect to the reachability relation

$$X_0 \leadsto_{\mathcal{N}'} X^* \qquad (29)$$

where $X^* \succeq 0^n$, $[X^*]_i = [X']_i$ for $i \in \{1, \ldots n\}$, $i \neq k_1$ and $i \neq k_2$; moreover, $[X^*]_{k_1} + [X^*]_{k_2} = X'$. According to the assumptions $\mathcal{N}$ contains directed paths both from s_{k_1} to s_{k_2} and from s_{k_2} to s_{k_1}; hence the reachability relation $X^* \leadsto_{\mathcal{N}} X'$ follows. Then, due to the transitivity of the relation $\leadsto_{\mathcal{N}}$, we have that $X_0 \leadsto_{\mathcal{N}} X'$ also holds.

$\square$

Proposition 15 can be extended to the case of superconservative d-CRNs.

Corollary 16. *Let us consider a superconservative d-CRN $\mathcal{N} = (\mathcal{S}, \mathcal{C}, \mathcal{R})$ with stoichiometric matrix $\Gamma \in \{-1, 0, 1\}^{n \times l}$ and $\Gamma^- \in \{0, 1\}^{n \times l}$ for which $\mathcal{C} = \mathcal{S}$. Assume that for all $r \in \mathcal{R}$ reactions $\sum_{i=1}^n [\overline{y}^+]_i = 1$ and $\sum_{i=1}^n [\overline{y}^-]_i \leq 1$ hold. Let us consider two states $X_0, X' \in \mathbb{Z}^n_{\geq 0}$ so that $X_0 \succeq M$ and $X' \succeq M$ hold where $M = M(\Gamma^-)$ is defined by (20). Then the reachability relation $X_0 \leadsto_{\mathcal{N}} X'$ holds if and only if there exists a vector $c \in \mathbb{Z}^l_{\geq 0}$ satisfying the state equation $X_0 + \Gamma c = X'$.*

Proof. By changing the sign of the entries in the stoichiometric matrix Γ, we get a subconservative d-CRN $\mathcal{N}'$ of stoichiometric matrix $-\Gamma$. Then we can consider the reachability problem $X' \overset{?}{\leadsto}_{\mathcal{N}'} X_0$. $\square$

We can extend Proposition 15 by allowing the restricted application of catalyzer species as follows.

Proposition 17. *Let us consider a subconservative d-CRN $\mathcal{N} = (\mathcal{S}, \mathcal{C}, \mathcal{R})$ of stoichiometric matrix $\Gamma \in \{-1, 0, 1\}^{n \times l}$ and $\Gamma^- \in \{0, 1\}^{n \times l}$. Assume that for each reaction r:*

(1) $r = s_1 \longrightarrow s_2$ for some $s_1, s_2 \in \mathcal{S}$, $s_1 \neq s_2$, $s_1 \neq \mathbf{0}$, OR

(2) $r = s + s_1 \longrightarrow s + s_2$ where $s, s_1, s_2 \in \mathcal{S}$, $s \neq s_1 \neq s_2$, $s \neq \mathbf{0}$, $s_1 \neq \mathbf{0}$ and $\forall r' \in \mathcal{R} r'$ does not consume s.

Let us consider two states $X_0, X' \in \mathbb{Z}^n_{\geq 0}$ for which $X_0 \succeq M$ and $X' \succeq M$ where $M = M(\Gamma^-)$ is defined by (20). Then the reachability relation $X_0 \leadsto_{\mathcal{N}} X'$ holds if and only if there exists a vector $c \in \mathbb{Z}^l_{\geq 0}$ satisfying the state equation $X_0 + \Gamma c = X'$.

Proof.

(1) $X_0 \leadsto_{\mathcal{N}} X' \Longrightarrow X_0 + \Gamma c = X'$

It follows from the definition of reachability.

(2) $X_0 + \Gamma c = X' \Longrightarrow X_0 \leadsto_{\mathcal{N}} X'$

Since in the initial state X_0 the number of each catalyzer molecule is higher than or equal to 1 and there is no reaction in $\mathcal{N}$ consuming a catalyzer species, it follows that for each state reachable from X_0 the number of each catalyzer molecule is higher than or equal to 1. Let us remove all the catalyzer species of $\mathcal{N}$ from the reactions where they act as a catalyzer; i.e., for each $r \in \mathcal{R}$ of the form $r = s + s_1 \longrightarrow s + s_2$ we erase the catalyzer s to obtain $r' = s_1 \longrightarrow s_2$. In such a way a d-CRN $\mathcal{N}'$ is obtained so that for each $X \succeq M$, $X_0 \leadsto_{\mathcal{N}'} X$ iff $X_0 \leadsto_{\mathcal{N}} X$. $\mathcal{N}'$ satisfies the conditions of Proposition 15; hence the reachability relation $X_0 \leadsto_{\mathcal{N}'} X'$ holds implying that $X_0 \leadsto_{\mathcal{N}} X'$ also holds.

$\square$

According to the duality of the sub- and superconservativity properties, we can extend Proposition 17 to the case of superconservative d-CRNs.

Corollary 18. *Let us consider a superconservative d-CRN $\mathcal{N} = (\mathcal{S}, \mathcal{C}, \mathcal{R})$ of stoichiometric matrix $\Gamma \in \{-1, 0, 1\}^{n \times l}$ and $\Gamma^- \in \{0, 1\}^{n \times l}$. Assume that for each reaction r*

(1) $r = s_1 \longrightarrow s_2$ for some $s_1, s_2 \in \mathcal{S}$, $s_1 \neq s_2$, $s_2 \neq \mathbf{0}$, OR

(2) $r = s + s_1 \longrightarrow s + s_2$ where $s, s_1, s_2 \in \mathcal{S}$, $s \neq s_1 \neq s_2$, $s \neq \mathbf{0}$, $s_2 \neq \mathbf{0}$ and $\forall r' \in \mathcal{R} r'$ does not produce s.

Let us consider two states $X_0, X' \in \mathbb{Z}^n_{\geq 0}$ for which $X_0 \succeq M$ and $X' \succeq M$ where $M = M(\Gamma^-)$ is defined by (20). Then the reachability relation $X_0 \leadsto_{\mathcal{N}} X'$ holds if and only if there exists a vector $c \in \mathbb{Z}^l_{\geq 0}$ satisfying the state equation $X_0 + \Gamma c = X'$.

Proof. By changing the sign of the entries in the stoichiometric matrix Γ, we obtain a subconservative d-CRN $\mathcal{N}'$ of stoichiometric matrix $-\Gamma$ satisfying the conditions of Proposition 17. We can consider the reachability problem $X' \overset{?}{\leadsto}_{\mathcal{N}'} X_0$. $\square$
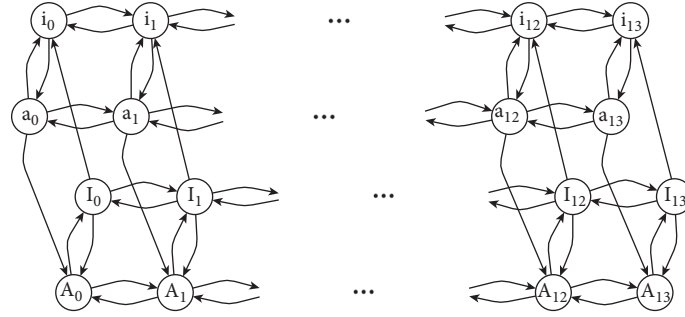
Figure 4: Conformational switch model of NFAT1 [38]. Lower case letters denote the protein located in the cytoplasm while upper case letters refer to the protein in the nucleus. a_j, A_j and i_j, I_j for $j = 0, \ldots 13$ denote the active and inactive proteins, respectively. Lower indices denote the number of phosphorylated residues.

By the above corollary, any reachability problem on a superconservative d-CRN satisfying the conditions of Corollary 18 can be easily traced back to that of a subconservative network; hence the problem is equivalent to finding a $c \in \mathbb{Z}_{\geq 0}^l$ solution for the respective d-CRN state equation.

The reaction network class covered by the above statements might be beneficial in modeling first- and second-order (bio)chemical reaction networks. For a representative example, see Example 19 below. We also note that any mass action type chemical reaction network can be dynamically described by an appropriately constructed reaction network containing at most second-order reactions [39]. Moreover, the hypergraph representation of chemical reaction networks (see, e.g., [40]) is helpful for checking the conditions of Proposition 17.

Example 19. Nuclear factors of activated T-cells (NFAT) are proteins that can exist in highly phosphorylated states [38]. They act as transcription factors; i.e., they have regulatory role in transcription. NFAT1, which is a member of the NFAT family, has 13 residues that can be dephosphorylated upon stimulation. NFAT1 has two different states: active and inactive. The transition between active and inactive states of the protein is regulated by the level of phosphorylation such that the higher the level of phosphorylation is, the lower the rate of transition becomes from inactive state to the active one and vice versa. Phosphorylation and dephosphorylation are achieved by a kinase and calcineurin, respectively. In the mathematical model the activities of kinase and calcineurin are modeled as rate constants; hence the respective reactions can be considered as first-order ones. The protein might be located in the cytoplasm or the nucleus of the cell. Cytoplasmic active NFAT1 is imported to the nucleus, while inactive NFAT1 of the nucleus is exported back to the cytoplasm.

The reaction network structure is depicted in Figure 4. It is visible that each reaction is of first order and there is no degradation and synthesis; hence the reaction network structure is conservative with a particular conservativity vector $z = 1^{56}$ and Proposition 15 can be applied.

We note that a reachability problem of the discussed reaction network class without additional constraints may be determined in polynomial time [41]. However, by using an ILP feasibility approach, the number of all distinct trajectories satisfying a prescribed reachability relation can be determined efficiently (see Remark 20), assuming the fixed number of reactions in the network. In addition, the ILP formulation can also be equipped with further linear constraints.

Remark 20. Let us consider a subconservative (superconservative) d-CRN $\mathcal{N} = (\mathcal{S}, \mathcal{C}, \mathcal{R})$ of n species, m complexes, and l reactions. Assume that $\mathcal{N}$ satisfies the conditions of Proposition 17 (Corollary 18). Then for any $X_0, X' \in \mathbb{Z}_{\geq 0}^n$ initial and target states for which $X_0 \succeq M(\Gamma^-)$, $X' \succeq M(\Gamma^-)$ hold we have that the number of distinct trajectories σ_X satisfying the reachability relation $X_0 \overset{?}{\rightsquigarrow}_{\mathcal{N}} X'$ can be determined in polynomial time in the distance of X_0 and X', given the fixed number of reactions l in the d-CRN. The explanation of this is the following. According to Proposition 17 (Corollary 18) the reachability problem $X_0 \overset{?}{\rightsquigarrow}_{\mathcal{N}} X'$ is equivalent to the existence of a nonnegative integer solution $c \in \mathbb{Z}_{\geq 0}^l$ of the state equation $X_0 + \Gamma c = X'$. In this way the reachability problem can be reformulated as an ILP feasibility problem in terms of c, and the Barvinok algorithm can be applied. Using the Barvinok algorithm in this particular case, the following complexity bounds are obtained:

(1) exponential in the dimension of the decision variables, that is, in the number of different reactions l,

(2) polynomial in the number of constraints, that is, in the number of species n,

(3) polynomial in the maximum of the absolute values of the coefficients Γ, $X' - X_0$.

The particular importance of Remark 20 is that the time complexity of the trajectory counting problem between a prescribed pair of states is polynomial in the number of constraints and in the distance of the initial and target states even in the case of superconservative d-CRNs for which the associated reachable state space can be unbounded for any X_0 initial state.
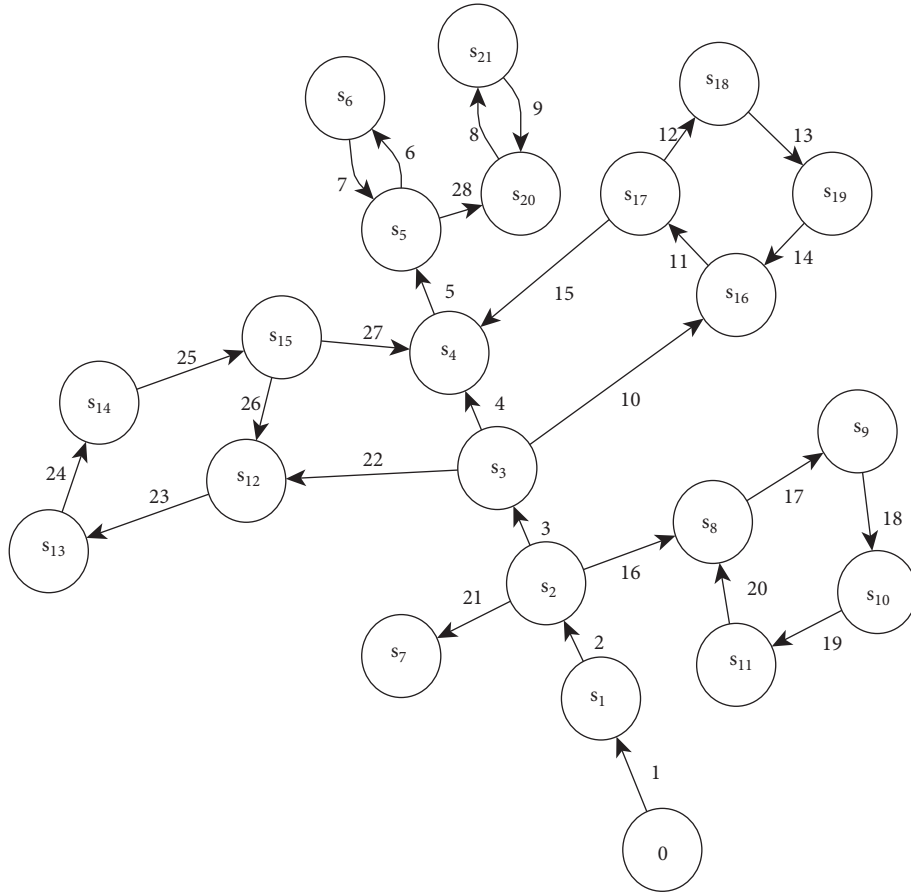
FIGURE 5: A superconservative d-CRN. **0** indicates the zero complex and the numbers denote the indices of the reactions on which they are located. Due to the superconservativity of the network structure, the above d-CRN is unbounded for any initial state $X_0 \in \mathbb{Z}_{\geq 0}^n$.

6. Computational Example: A Superconservative d-CRN of First-Order Reactions

Let us consider the d-CRN depicted in Figure 5. This system is superconservative with a particular conservation vector $z = 1^{21 \times 1}$ implying the unboundedness of its reachable state space regardless of the initial state X_0. Making use of the above results, the reachability problem of $X_0 \overset{?}{\leadsto} X'$ for any $X_0, X' \in \mathbb{Z}_{\geq 0}^{21}$ can be reformulated as a subconservative d-CRN reachability problem for which the boundedness of the reachable state space, i.e. structural boundedness, is guaranteed and is equivalent to the existence of a nonnegative integer solution of the respective subconservative d-CRN state equation.

As initial state we consider X_0 given by (31) that was randomly generated from $[10, 100]^{21}$. In order to find a target state X' satisfying the reachability relation $X_0 \leadsto X'$ we

randomly generated target states so that the number of each species was uniformly sampled from the interval $[40, 100]$. In the choice of the intervals from which we sample, it was taken into consideration that the discrete state model of reaction networks is typically employed in the case of low molecular counts [4, 5]. In order to decide the reachability relation between a pair of particular states X_0 and X', we need to solve the following decision problem.

$$\Gamma c = X' - X_0$$
$$c \in \mathbb{Z}_{\geq 0}^{28}$$
(30)

Clearly, Corollary 18 guarantees that $\Gamma c = X' - X_0$ is satisfied with some $c \in \mathbb{Z}_{\geq 0}^{28}$ if and only if the reachability relation $X_0 \leadsto X'$ holds. Let us consider the following initial and final states.

$$X_0 = \begin{bmatrix} 56 & 10 & 35 & 87 & 66 & 75 & 87 & 60 & 60 & 55 & 50 & 89 & 58 & 72 & 52 & 71 & 48 & 71 & 57 & 47 & 68 \end{bmatrix}^\top \tag{31}$$

$$X' = \begin{bmatrix} 50 & 46 & 65 & 77 & 88 & 95 & 71 & 56 & 59 & 54 & 43 & 76 & 55 & 78 & 40 & 62 & 51 & 71 & 53 & 64 & 91 \end{bmatrix}^\top \tag{32}$$

We found that for the target state X' given by (32) the reachability relation holds. To solve the decision problems of the form (30) the LattE [34] software was used.

Now, let us examine the reachability from X_0 to X' with additional constraints. One can observe that X' results in a significant increase in the number of molecules in the species s_5, s_6, s_{20}, and s_{21} and any trajectory from X_0 to X' results in a net increase in the number of molecules. These together imply the flow of molecules from the zero complex (environment). The flow of molecules over the network from the zero complex to s_5, s_6, s_{20}, and s_{21} can take place through different paths. We assume that the directed paths

$$\sigma_{S1} = s_3 \; s_{12} \; s_{13} \; s_{14} \; s_{15} \; s_4, \tag{33}$$

$$\sigma_{S2} = s_3 \; s_{16} \; s_{17} \; s_4 \tag{34}$$

are slow compared to the other ones; hence we wish to minimize the flow through them in order to lower their effect in c. This can be easily expressed by posing addition linear constraints on c as is done in the decision problem (35).

$$\Gamma c = X' - X_0$$
$$c \in \mathbb{Z}_{\geq 0}^{28}$$
$$[c]_{15} \leq 10 \tag{35}$$
$$[c]_{27} \leq 10$$

We also determined a particular solution c by equipping (35) with the objective function $\sum_{i=1}^{28} [c]_i$ to be minimized.

$$c = \begin{bmatrix} 112 & 106 & 112 & 111 & 118 & 48 & 8 & 29 & 12 & 18 & 16 & 11 & 11 & 7 & 8 & 13 & 17 & 16 & 15 & 8 & 17 & 13 & 16 & 13 & 19 & 16 & 9 & 51 \end{bmatrix}^{\top} \tag{36}$$

For implementation purposes we employed Python 2.7 programming language and the Gurobi mathematical optimization solver [42]. A Lenovo P51s workstation with two 2.70 GHz i7-7500U CPUs and 32GB RAM (DDR4 2133 MHz) was used for all the computations.

7. Conclusion

In this paper the reachability problems of sub- and super-conservative discrete state chemical reaction networks are considered. It is shown that the reachability problem of a superconservative reaction network of unbounded reachable state space can be transformed to that of a subconservative network for which the boundedness of the reachable state space is always guaranteed. Using an inductive proof we provided a set of necessary and sufficient conditions under which the equivalence between a d-CRN reachability problem and existence of nonnegative integer solution of the corresponding state equations is guaranteed. In such a way the reachability problem can be traced back to an IP-feasibility (decision) problem for which the number of decision variables is significantly lower than that employed in the literature [36]. Moreover the number of trajectories satisfying the reachability relation can also be enumerated efficiently, assuming a fixed reaction network structure. The applicability of our approach is illustrated on a high-dimensional superconservative d-CRN.

Data Availability

No data were used to support this study.

Conflicts of Interest

The authors declare that there are no conflicts of interest regarding the publication of this paper.

References

[1] U. Alon, *An Introduction to Systems Biology: Design Principles of Biological Circuits*, Chapman & Hall, 2007.

[2] W. Liu, *Introduction to Modeling Biological Cellular Control Systems*, Springer Science & Business Media, 2012.

[3] D. Angeli, "A tutorial on chemical reaction network dynamics," *European Journal of Control*, vol. 15, no. 3-4, pp. 398–406, 2009.

[4] P. érdi and J. Tóth, *Mathematical Models of Chemical Reactions. Theory and Applications of Deterministic and Stochastic Models*, Manchester Univ. Press, 1989.

[5] M. B. Elowitz, A. J. Levine, E. D. Siggia, and P. S. Swain, "Stochastic gene expression in a single cell," *Science*, vol. 297, no. 5584, pp. 1183–1186, 2002.

[6] S. Smith and R. Grima, "Single-cell variability in multicellular organisms," *Nature Communications*, vol. 9, no. 1, 2018.

[7] T. G. Kurtz, "The relationship between stochastic and deterministic models for chemical reactions," *The Journal of Chemical Physics*, vol. 57, no. 7, pp. 2976–2978, 1972.

[8] D. F. Anderson and T. G. Kurtz, *Stochastic Analysis of Biochemical Systems*, Springer, Berlin, Germany, 2015.

[9] D. F. Anderson, G. A. Enciso, and M. D. Johnston, "Stochastic analysis of chemical reaction networks with absolute concentration robustness," *Journal of the Royal Society Interface*, vol. 11, no. 90, Article ID 20130505, 2014.

[10] D. F. Anderson and T. G. Kurtz, "Continuous time Markov chain models for chemical reaction networks," in *Design and Analysis*

of Biomolecular Circuits: Engineering Approaches to Systems and Synthetic Biology, H. Koeppl, Ed., pp. 3–42, Springer, Berlin, Germany, 2011.

[11] F. Bause and P. S. Kritzinger, Stochastic Petri Nets: An Introduction to the Theory, Vieweg Verlag, 2002.

[12] G. Szederkenyi, K. M. Hangos, and T. Péni, "Maximal and minimal realizations of reaction kinetic systems: computation and properties," MATCH - Communications in Mathematical and in Computer Chemistry, vol. 65, no. 2, pp. 309–332, 2011.

[13] G. Szederkényi, "Computing sparse and dense realizations of reaction kinetic systems," Journal of Mathematical Chemistry, vol. 47, no. 2, pp. 551–568, 2010.

[14] B. Ács, G. Szederkényi, Z. Tuza, and Z. A. Tuza, "Computing all possible graph structures describing linearly conjugate realizations of kinetic systems," Computer Physics Communications, vol. 204, pp. 11–20, 2016.

[15] B. Ács, G. Szlobodnyik, and G. Szederkényi, "A computational approach to the structural analysis of uncertain kinetic systems," Computer Physics Communications, vol. 228, pp. 83–95, 2018.

[16] M. D. Johnston, "Conditions for extinction events in chemical reaction networks with discrete state spaces," Mathematical Biosciences, vol. 294, pp. 130–142, 2017.

[17] M. D. Johnston, "A computational approach to extinction events in chemical reaction networks with discrete state spaces," Mathematical Biosciences, vol. 294, pp. 130–142, 2017.

[18] L. Paulevé, G. Craciun, and H. Koeppl, "Dynamical properties of discrete reaction networks," Journal of Mathematical Biology, vol. 69, no. 1, pp. 55–72, 2014.

[19] R. Brijder, "Dominance and deficiency for Petri nets and chemical reaction networks," Natural Computing, vol. 16, no. 2, pp. 285–294, 2017.

[20] M. Cook, D. Soloveichik, E. Winfree, and J. Bruck, "Programmability of chemical reaction networks," in Algorithmic bioprocesses, Nat. Comput. Ser., pp. 543–584, Springer, Berlin, 2009.

[21] A. Case, J. H. Lutz, and D. M. Stull, "Reachability problems for continuous chemical reaction networks," Natural Computing, vol. 17, no. 2, pp. 223–230, 2018.

[22] E. W. Mayr, "An algorithm for the general petri net reachability problem," in Proceedings of the the thirteenth annual ACM symposium, pp. 238–246, Milwaukee, Wisconsin, USA, May 1981.

[23] S. R. Kosaraju, "Decidability of reachability in vector addition systems," in STOC, pp. 267-28, ACM, 1982.

[24] J.-L. Lambert, "A structure to decide reachability in Petri nets," Theoretical Computer Science, vol. 99, no. 1, pp. 79–104, 1992.

[25] J. Leroux, "Vector addition reachability problem (a simpler solution)," in The Alan Turing Centenary Conference, vol. 10, pp. 214–228, EPiC series, 2012.

[26] R. J. Lipton, "The reachability problem requires exponential space," Tech. Rep 62, Department of Computer Science, Yale University, 1976.

[27] S. Schmitz, "Complexity hierarchies beyond elementary," ACM Transactions on Computation Theory, vol. 8, no. 1, pp. 1–36, 2016.

[28] J. Lenstra, "Integer programming with a fixed number of variables," Mathematics of Operations Research, vol. 8, no. 4, pp. 538–548, 1983.

[29] M. Grötschel, L. Lovász, and A. Schrijver, Geometric Algorithms and Combinatorial Optimization, vol. 2 of Algorithms and Combinatorics: Study and Research Texts, Springer, Berlin, Germany, 1988.

[30] A. I. Barvinok, "A polynomial time algorithm for counting integral points in polyhedra when the dimension is fixed," Mathematics of Operations Research, vol. 19, no. 4, pp. 769–779, 1994.

[31] M. Köppe, "A primal Barvinok algorithm based on irrational decompositions," SIAM Journal on Discrete Mathematics, vol. 21, no. 1, pp. 220–236, 2007.

[32] S. Verdoolaege, R. Seghir, K. Beyls, V. Loechner, and M. Bruynooghe, "Counting integer points in parametric polytopes using Barvinok's rational functions," Algorithmica. An International Journal in Computer Science, vol. 48, no. 1, pp. 37–66, 2007.

[33] J. B. Lasserre, "Integer programming, Barvinok's counting algorithm and Gomory relaxations," Operations Research Letters, vol. 32, no. 2, pp. 133–137, 2004.

[34] J. A. De Loera, R. Hemmecke, J. Tauzer, and R. Yoshida, "Effective lattice point counting in rational convex polytopes," Journal of Symbolic Computation, vol. 38, no. 4, pp. 1273–1302, 2004.

[35] G. Memmi and G. Roucairol, "Linear algebra in net theory," in Net Theory and Applications, W. Brauer, Ed., vol. 84 of Lecture Notes in Comput. Sci., pp. 213–223, Springer, Berlin-New York, 1975.

[36] G. Szlobodnyik, G. Szederkenyi, and M. D. Johnston, "Reachability analaysis of subconservative discrete chemical reaction networks," MATCH Communications in Mathematical and in Computer Chemistry, vol. 81, no. 3, pp. 705–736, 2019.

[37] T. Murata, "Petri nets: properties, analysis and applications," Proceedings of the IEEE, vol. 77, no. 4, pp. 541–580, 1989.

[38] C. Salazar and T. Höfer, "Allosteric regulation of the transcription factor NFAT1 by multiple phosphorylation sites: a mathematical analysis," Journal of Molecular Biology, vol. 327, no. 1, pp. 31–45, 2003.

[39] T. Wilhelm, "Chemical systems consisting only of elementary steps –a paradigma for nonlinear behavior," Journal of Mathematical Chemistry, vol. 27, no. 1-2, pp. 71–88, 2000.

[40] R. Fagerberg, C. Flamm, D. Merkle, P. Peters, and P. F. Stadler, "On the complexity of reconstructing chemical reaction networks," Mathematics in Computer Science, vol. 7, no. 3, pp. 275–292, 2013.

[41] P. Alimonti, E. Feuerstein, L. Laura, and U. Nanni, "Linear time analysis of properties of conflict-free and general Petri nets," Theoretical Computer Science, vol. 412, no. 4-5, pp. 320–338, 2011.

[42] Gurobi Optimization, "Gurobi optimizer reference manual," 2016, http://www.gurobi.com.

Research Article

A Non-Integer Variable Order Mathematical Model of Human Immunodeficiency Virus and Malaria Coinfection with Time Delay

A. A. M. Arafa,[1] **M. Khalil** ⓘ**,**[2] **and A. Sayed** ⓘ[1]

[1]*Department of Mathematics and Computer Science, Faculty of Science, Port Said University, Port Said, Egypt*
[2]*Department of Mathematics, Faculty of Engineering, October University for Modern Sciences and Arts (MSA), Giza, Egypt*

Correspondence should be addressed to A. Sayed; amal_wa84@yahoo.com

The purpose of this paper is to propose a variable fractional-order model with a constant time delay of the coinfection of HIV/AIDS and malaria. The proposed model describes the interaction between HIV/AIDS and malaria. This model is presented by using variable fractional-order derivative which is an extension of the constant fractional-order derivative to explain a certain pattern in the development of infection of several patients. The presented model has been solved numerically via the predictor-corrector scheme. The local and global stability conditions of the disease-free equilibrium are investigated. Also, numerical simulations are presented for different variable fractional-order derivatives in Caputo sense.

1. Introduction

The human immunodeficiency virus (HIV) and malaria are considered among the most challenging global public health issues in the last few decades. HIV and malaria are life-threatening diseases which have similar geographic distributions [1]. They cause millions of deaths every year in several areas especially in Africa, Asia, and Latin America. In 2017, HIV killed about one million people [2] while malaria killed roughly 435 000 people worldwide [3]. HIV can be transmitted through certain body fluids while malaria is transmitted through bites of infected mosquitoes.

HIV is considered as one of the most deadly infectious diseases which strikes the human immune system and destroy the CD4+ cells. AIDS is the last stage of HIV which occurs when the CD4+ cells of the human body count drops below 200 cells/mm [4]. In this stage, the immune system cannot defend the body against the attacks by several opportunistic diseases. On the other hand, if malaria parasite invades the bloodstream, then, it destroys red blood cells. So, malaria infection may be developed to anemia or cerebral malaria, which can cause disabilities and death [5].

The coinfection of HIV and malaria has become endemic in several developing countries. World health organization (WHO) reports indicating that more than two million people die every year because of the malaria/AIDS coinfection [6]. The interaction between HIV and malaria in Sub-Saharan Africa has become among the major public health problems [7] and has resulted in many economic disasters [1] by negatively affecting the contribution of the labor force to the national economy.

Recently, increasing research efforts have been made to obtain an effective vaccine to halt the progression and transmission of malaria. Vaccination target is to reduce the rate of human infection, the severity of the disease [8–10], and the parasite's transmission to mosquitoes. Clinical trials in Africa proved that a malaria vaccine is partially protective [11].

From mathematicians' perspective, mathematical models are significant tools that help us to understand the current state and the future progress of infectious diseases in human networks in order to control and prevent such diseases. Several mathematical models have been presented to study the prevalence and the coinfection of HIV and malaria, but most

of such models are integer or constant fractional-order models [12–22]. This paper is devoted to propose a delay variable fractional-order model for the coinfection of HIV/AIDS and malaria. In this model, a discrete time delay τ_h is incorporated in the variables of active humans who are infected by malaria and the coinfected humans while a discrete time delay τ_m is incorporated in the variable of the infectious mosquitoes. After a time τ_h, susceptible people become infected by malaria while exposed individuals become infectious after the same time. On the other hand, mosquitoes become infectious after time τ_m. Introducing such a time delay to the proposed model is essential to characterize the time needed to start in vaccination and treatments processes. The merits of the proposed model are clear from putting in the time delay with the variable fractional-order derivative which is an extension of the constant fractional-order in the same model. Hence, using the proposed variable fractional-order model with time delay gives a better understanding of the interaction between malaria and HIV. To the best of our knowledge, the presented model is the first variable fractional-order model with a time delay which describes the prevalence and interactions between HIV and malaria. In this model, the integer order derivative is used to distinguish the short memory of systems, while the variable fractional-order derivative is utilized to characterize the variable memory of systems.

This paper is organized as follows. In Section 2, some preliminaries of fractional calculus and the algorithm of the predictor-corrector method are presented while Section 3 describes the proposed model. In Section 4, the disease-free equilibrium and stability are presented. The basic reproduction number is computed in Section 5. Section 6 is devoted to the numerical results and discussions. Our conclusion is illustrated in Section 7.

2. Preliminaries

2.1. Fractional Calculus. The fractional calculus is considered as a mathematical tool for characterizing memory of biological and epidemiological systems. The classical integer order derivative can be used to describe the short memory of the dynamical systems, while fractional-order derivative has the merit of describing the long memory of dynamical systems. The variable fractional-order derivative is an extension of the constant fractional-order derivative and has been introduced in several scientific fields [23–25]. Also, it is a powerful tool to characterize memory that varies from point to point. Furthermore, the variable fractional-order derivative can be applied to describe the variable memory of dynamical systems [26].

In this section, we present some basic definitions of constant/variable fractional-order derivatives as follows.

Definition 1 (Riemann–Liouville derivatives of fractional-order α). Let α be a bounded and continuous function; then Riemann–Liouville fractional-order derivative of $f(t)$: $[a, b] \longrightarrow \mathbb{R}$ is defined as follows [27].

(i) Left Riemann–Liouville derivative of fractional-order α is defined by

$$^{RL}_{a}D^{\alpha}_{t} f(t) = \frac{1}{\Gamma(1-\alpha)} \frac{d}{dt} \int_{a}^{t} (t-\omega)^{-\alpha} f(\omega) \, d\omega, \tag{1}$$

$$0 < \alpha \leq 1$$

(ii) Right Riemann–Liouville derivative of fractional-order α is defined by

$$^{RL}_{t}D^{\alpha}_{b} f(t) = \frac{1}{\Gamma(1-\alpha)} \frac{d}{dt} \int_{t}^{b} (t-\omega)^{-\alpha} f(\omega) \, d\omega, \tag{2}$$

$$0 < \alpha \leq 1$$

Definition 2 (Caputo derivatives of fractional-order α). Let α be a bounded and continuous function; then the Caputo fractional-order derivative of $f(t)$: $[a, b] \longrightarrow \mathbb{R}$ is defined as follows [27].

(i) Left Caputo derivative of fractional-order α is defined by

$$^{C}_{a}D^{\alpha}_{t} f(t) = \frac{1}{\Gamma(1-\alpha)} \int_{a}^{t} (t-\omega)^{-\alpha} f'(\omega) \, d\omega, \tag{3}$$

$$0 < \alpha \leq 1$$

(ii) Right Caputo derivative of fractional-order α is defined by

$$^{C}_{t}D^{\alpha}_{b} f(t) = \frac{-1}{\Gamma(1-\alpha)} \int_{t}^{b} (t-\omega)^{-\alpha} f'(\omega) \, d\omega, \tag{4}$$

$$0 < \alpha \leq 1$$

Definition 3 (Riemann–Liouville derivatives of variable fractional-order $\alpha(t)$). Let $\alpha(t)$ be a bounded and continuous function; then Riemann–Liouville fractional-order derivative of $f(t)$: $[a, b] \longrightarrow \mathbb{R}$ is defined as follows [27].

(i) Left Riemann–Liouville derivative of variable fractional-order $\alpha(t)$ is defined by

$$^{RL}_{a}D^{\alpha(t)}_{t} f(t) = \frac{1}{\Gamma(1-\alpha(t))} \frac{d}{dt} \int_{a}^{t} (t-\omega)^{-\alpha(t)} f(\omega) \, d\omega, \tag{5}$$

$$0 < \alpha(t) \leq 1$$

(ii) Right Riemann–Liouville derivative of fractional-order α is defined by

$$^{RL}_{t}D^{\alpha(t)}_{b} = \frac{1}{\Gamma(1-\alpha(t))} \frac{d}{dt} \int_{t}^{b} (t-\omega)^{-\alpha(t)} f(\omega) \, d\omega, \tag{6}$$

$$0 < \alpha(t) \leq 1$$

Definition 4 (Caputo derivatives of variable fractional-order $\alpha(t)$). Let $\alpha(t)$ be a bounded and continuous function; then the Caputo fractional-order derivative of $f(t)$: $[a, b] \longrightarrow \mathbb{R}$ is defined as follows [27].
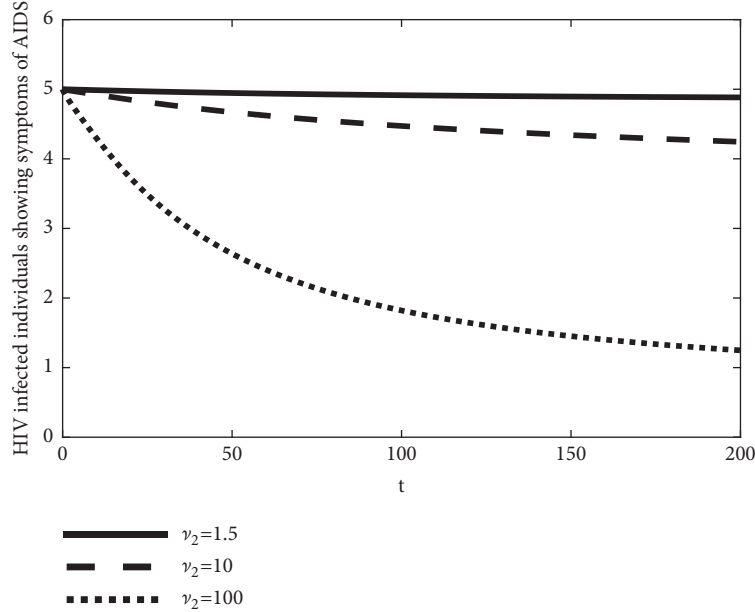
FIGURE 1: HIV infected individuals showing symptoms of AIDS at $\alpha(t) = 0.8$ with $\nu_2 = 1.5$ (solid line), $\nu_2 = 10$ (dashed line), and $\nu_2 = 100$ (dotted line). Parameters values are in Table 1 with $\beta_h = 0.01$.

(i) Left Caputo derivative of fractional-order $\alpha(t)$ is defined by

$$
{}^{C}_{a}D^{\alpha(t)}_{t}f(t) = \frac{1}{\Gamma(1 - \alpha(t))} \int_{a}^{t} (t - \omega)^{-\alpha(t)} f'(\omega)\, d\omega, \tag{7}
$$

$$
0 < \alpha(t) \le 1
$$

(ii) Right Caputo derivative of fractional-order $\alpha(t)$ is defined by

$$
{}^{C}_{t}D^{\alpha(t)}_{b}f(t) = \frac{-1}{\Gamma(1 - \alpha(t))} \int_{t}^{b} (t - \omega)^{-\alpha(t)} f'(\omega)\, d\omega, \tag{8}
$$

$$
0 < \alpha(t) \le 1
$$

2.2. Predictor-Corrector Method. There are many techniques for solving a delay variable fractional-order models such as finite difference [28], Hermite wavelet [29], and Adams-Bashforth-Morton [30] methods. In this section, we state a predictor-corrector method for solving a delay variable fractional-order model [31].

Let

$$
{}^{C}D^{\alpha(t)}y(t) = f(t, y(t), y(t - \varsigma)), \quad 0 \le t \le T, \tag{9}
$$

$$
y(t) = g(t), \quad -\varsigma \le t \le 0
$$

where $0 < \alpha(t) \le 1$, $T \in \mathbb{R}^{+}$, and $g(t)$ is a smooth function. Suppose a uniform grid $\{t_j = jh : j = -q, q+1, \ldots, -1, 0, 1, \ldots, n\}$, where n and q are integers such that $n = T/h$ and $q = \varsigma/h$.

The predictor approximation y^{p}_{n+1} is defined by

$$
y^{p}_{n+1} = y(0) + \frac{1}{\Gamma(\alpha(t_{n+1}))} \sum_{j=0}^{n} B_{j,n+1} f(t_j, y_j, y_{j-q}), \tag{10}
$$

where

$$
B_{j,n+1} = \frac{h^{\alpha(t_{n+1})}}{\alpha(t_{n+1})} \left[(n - j + 1)^{\alpha(t_{n+1})} - (n - j)^{\alpha(t_{n+1})} \right], \tag{11}
$$

$$
0 \le j \le n.
$$

The corrector approximation y_{n+1} is defined by

$$
y_{n+1} = y(0) + \frac{h^{\alpha(t_{n+1})}}{\Gamma(\alpha(t_{n+1}) + 2)} f\left(t_{n+1}, y^{p}_{n+1}, y_{n+1-q}\right)
$$

$$
+ \frac{h^{\alpha(t_{n+1})}}{\Gamma(\alpha(t_{n+1}) + 2)} \sum_{j=0}^{n} A_{j,n+1} f(t_j, y_j, y_{j-q}) \tag{12}
$$

where

$$
A_{j,n+1} = \begin{cases} n^{\alpha(t_{n+1})+1} - \left[n - \alpha(t_{n+1})\right](n + 1)^{\alpha(t_{n+1})}, & j = 0, \\ (n - j + 2)^{\alpha(t_{n+1})+1} - 2(n - j + 1)^{\alpha(t_{n+1})+1} + (n - j)^{\alpha(t_{n+1})+1}, & 1 \le j \le n, \\ 1, & j = n + 1. \end{cases} \tag{13}
$$

(a)

(b)
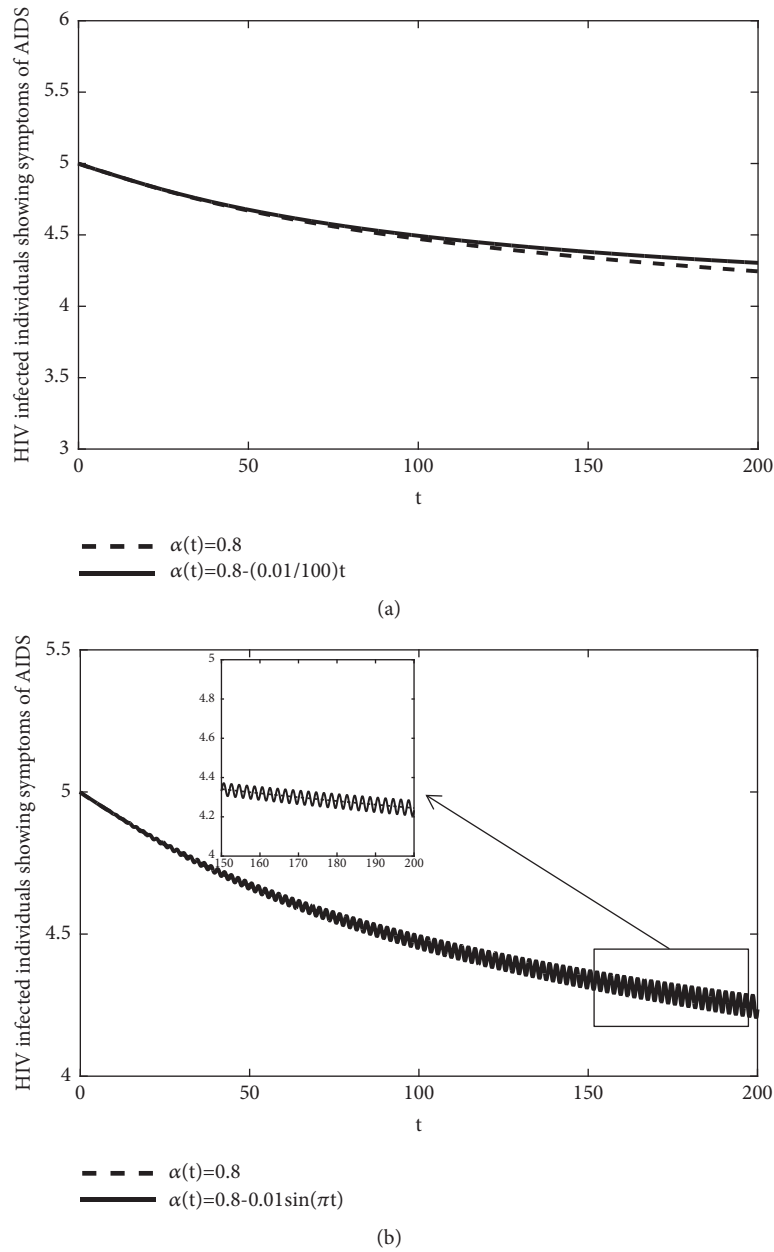
FIGURE 2: HIV infected individuals showing symptoms of AIDS with $\nu_2 = 10$. Parameters values are in Table 1 with $\beta_h = 0.01$. (a) $\alpha(t) = 0.8$ comparing with $\alpha(t) = 0.8 - (0.01/100)t$; (b) $\alpha(t) = 0.8$ comparing with $\alpha(t) = 0.8 - 0.01\sin(\pi t)$.

3. The Model

The proposed variable fractional-order model with a constant delay in this paper is based on the constant fractional delay model proposed in [32]. This model consists of 12 compartments, as follows:

$$^CD^{\alpha(t)}N_h(t)$$
$$= A_h - a_{h1}\left[I_h(t) + (1 - \theta_2)Y_h(t)\right] - \tau a_{h1}I_{mhiv}(t)$$
$$- \left[\tau a_{h1} + \psi\delta_H\right]A_{mhiv}(t) - \delta_H A_{hiv}(t)$$

$$- \mu_h N_h(t),$$

$$^CD^{\alpha(t)}S_h(t)$$
$$= (1 - p)A_h - f_h(t)S_h(t) - \beta_{hiv}(t)S_h(t)$$
$$+ r_h\left[I_h(t) + \theta_1 Y_h(t)\right] + \sigma V_h(t) - \mu_h S_h(t),$$

$$^CD^{\alpha(t)}V_h(t)$$
$$= pA_h - f_h(t)(1 - \gamma)V_h(t) - \left[\sigma + \mu_h\right]V_h(t),$$
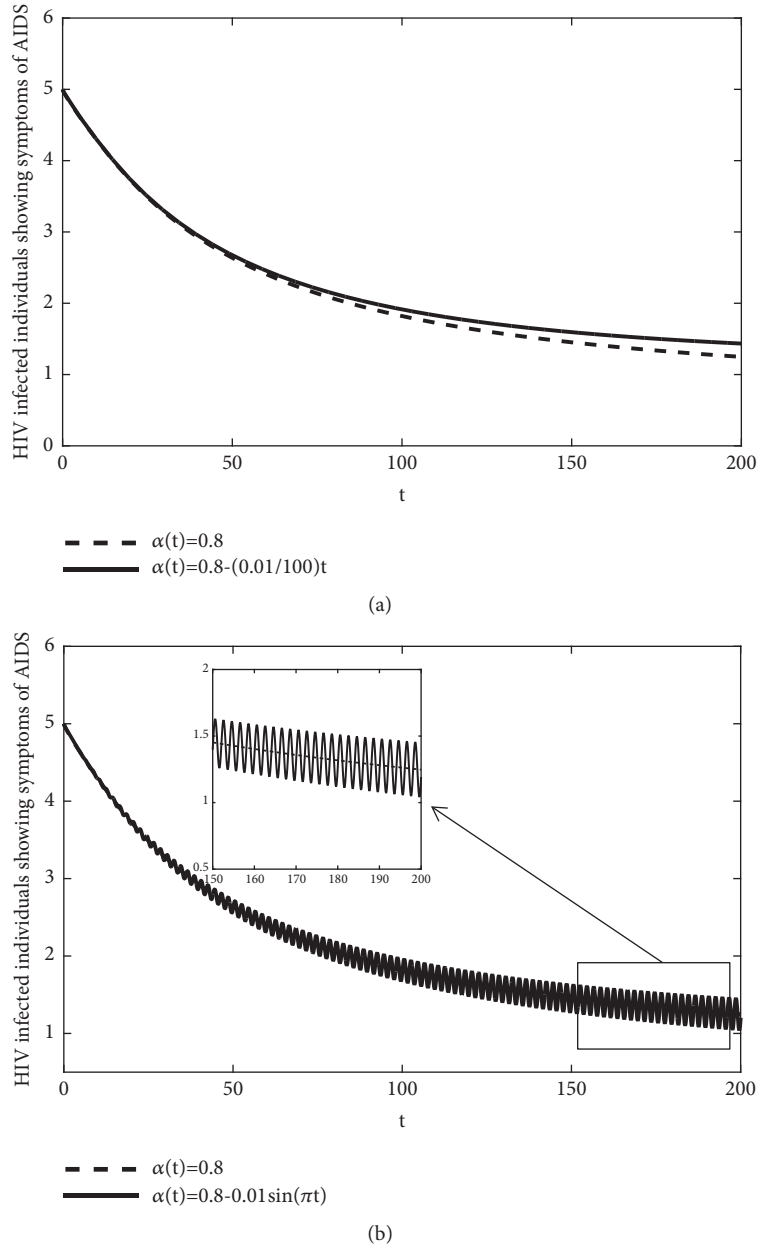
$$^CD^{\alpha(t)}I_h(t)$$

FIGURE 3: HIV infected individuals showing symptoms of AIDS with $v_2 = 100$. Parameters values are in Table 1 with $\beta_h = 0.01$. (a) $\alpha(t) = 0.8$ comparing with $\alpha(t) = 0.8 - (0.01/100)t$; (b) $\alpha(t) = 0.8$ comparing with $\alpha(t) = 0.8 - 0.01 \sin(\pi t)$.

$$= f_h\left(t - \tau_h\right) S_h\left(t - \tau_h\right) e^{-\mu_h \tau_h} - \varepsilon_2 \beta_{hiv}\left(t\right) I_h\left(t\right)$$

$$- \left[r_h + a_{h1} + \mu_h\right] I_h\left(t\right),$$

$${}^C D^{\alpha(t)} I_{mhiv}\left(t\right)$$

$$= v_1 f_h\left(t - \tau_h\right) I_{hiv}\left(t - \tau_h\right) e^{-\mu_h \tau_h} + \varepsilon_2 \beta_{hiv}\left(t\right) I_h\left(t\right)$$

$$- \left[\zeta a_{h2} + \phi_2 + \tau a_{h1} + \mu_h\right] I_{mhiv}\left(t\right),$$

$${}^C D^{\alpha(t)} I_{hiv}\left(t\right)$$

$$= \beta_{hiv}\left(t\right) S_h\left(t\right) + \phi_2 I_{mhiv}\left(t\right) - v_1 f_h\left(t\right) I_{hiv}\left(t\right)$$

$$- \left[a_{h2} + \mu_h\right] I_{hiv}\left(t\right),$$

$${}^C D^{\alpha(t)} Y_h\left(t\right)$$

$$= f_h\left(t - \tau_h\right) \left(1 - \gamma\right) V_h\left(t - \tau_h\right) e^{-\mu_h \tau_h}$$

$$- \left[\theta_1 r_h + \left(1 - \theta_2\right) a_{h1} + \mu_h\right] Y_h\left(t\right),$$

$${}^C D^{\alpha(t)} A_{mhiv}\left(t\right)$$

$$= \zeta a_{h2} I_{mhiv}\left(t\right) + v_2 f_h\left(t - \tau_h\right) A_{hiv}\left(t - \tau_h\right) e^{-\mu_h \tau_h}$$

$$- \left[\mu_h + \phi_3 + \tau a_{h1} + \psi \delta_H\right] A_{mhiv}\left(t\right),$$
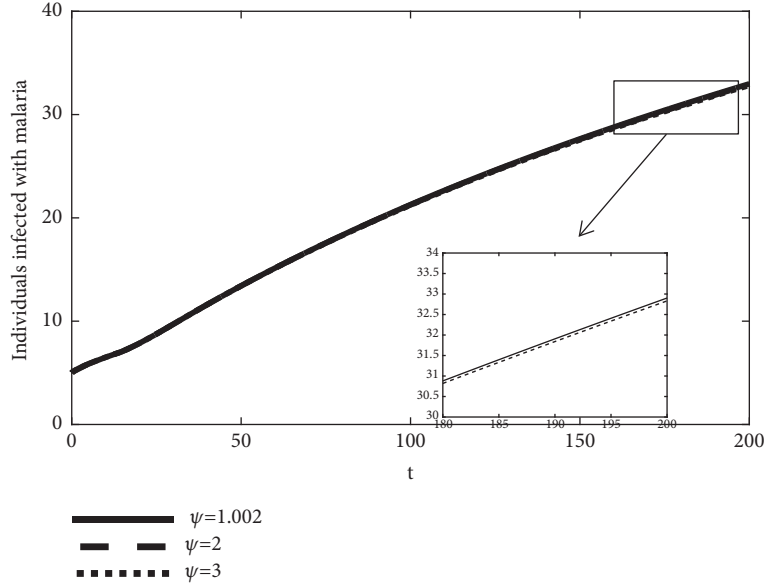
FIGURE 4: Individuals infected with malaria at $\alpha(t) = 0.8$ with $\psi = 1.002$ (solid line), $\psi = 2$ (dashed line), and $\psi = 3$ (dotted line). Parameters values are in Table 1 with $\beta_h = 0.05$.

$$^{C}D^{\alpha(t)}A_{hiv}(t)$$

$$= a_{h2}I_{hiv}(t) + \phi_3 A_{mhiv}(t) - \upsilon_2 f_h(t) A_{hiv}(t)$$

$$- [\mu_h + \delta_H] A_{hiv}(t),$$

$$^{C}D^{\alpha(t)}N_m(t) = A_m - a_m I_m(t) - \mu_m N_m(t),$$

$$^{C}D^{\alpha(t)}S_m(t) = A_m - f_m(t) S_m(t) - \mu_m S_m(t),$$

$$^{C}D^{\alpha(t)}I_m(t)$$

$$= f_m(t - \tau_m) S_m(t - \tau_m) e^{-\mu_m \tau_m}$$

$$- [\mu_m + a_m] I_m(t). \tag{14}$$

where the population of mosquitoes as follows:

$$N_m(t) = I_m(t) + S_m(t), \tag{15}$$

where $I_m(t)$ are the infectious mosquitoes and $S_m(t)$ are the susceptible mosquitoes.

And the population of human $N_h(t)$ is divided into the following classes:

S_h are the susceptible individuals

V_h are the individuals vaccinated against malaria

I_h are the individuals infected with malaria

Y_h are individuals infected and vaccinated against malaria

I_{mhiv} are the coinfected individuals showing no symptoms of AIDS

I_{hiv} are the individuals asymptomatically infected with HIV/AIDS

A_{hiv} are the HIV infected individuals showing symptoms of AIDS

A_{mhiv} are the coinfected individuals showing symptoms of AIDS

Besides, all human are subject to natural death, occurring at a rate μ_h. Susceptible individuals get in the human population at a rate A_h. The parameter p is the proportion of individuals successfully vaccinated, where $(1 - p)A_h$ is the proportion getting in the class $S_h(t)$ and pA_h is the proportion getting in the class $V_h(t)$. Susceptible individuals enter the class $I_h(t)$ after some time τ_h. The rate of infection by malaria parasite of susceptible individuals $f_h(t)$ is given by

$$f_h(t) = \beta_h c(1 - bz) \frac{I_m(t)}{N_h(t)} \tag{16}$$

where $0 < b \le 1$ is the proportion of individuals in the community and $0 < z \le 1$ models the efficacy of adopted strategies for individuals protection. c is the rate of female mosquitoes' bites. The value of the probability that a bite of an infectious mosquito leads to the infection of a susceptible human is β_h. The efficacy of the preerythrocytic vaccine is given by $0 < \gamma \le 1$. Vaccinated individuals may become susceptible at a rate σ. The rate of infection with HIV/AIDS of susceptible individuals is $\beta_{hiv}(t)$:

$$\beta_{hiv}(t)$$

$$= \frac{\beta_H [I_{hiv}(t) + \eta_{HM} I_{mhiv}(t) + \eta_A [A_{hiv}(t) + \eta_{HM} A_{mhiv}(t)]]}{N_h(t)} \tag{17}$$

where $\eta_A > 1$ is the infectiousness of individuals in the AIDS stage of HIV infection. β_H is the effective contact rate for HIV infection. Infectiousness to malaria of coinfected individuals showing symptoms of AIDS is $\eta_{HM} > 1$.

(a)

(b)
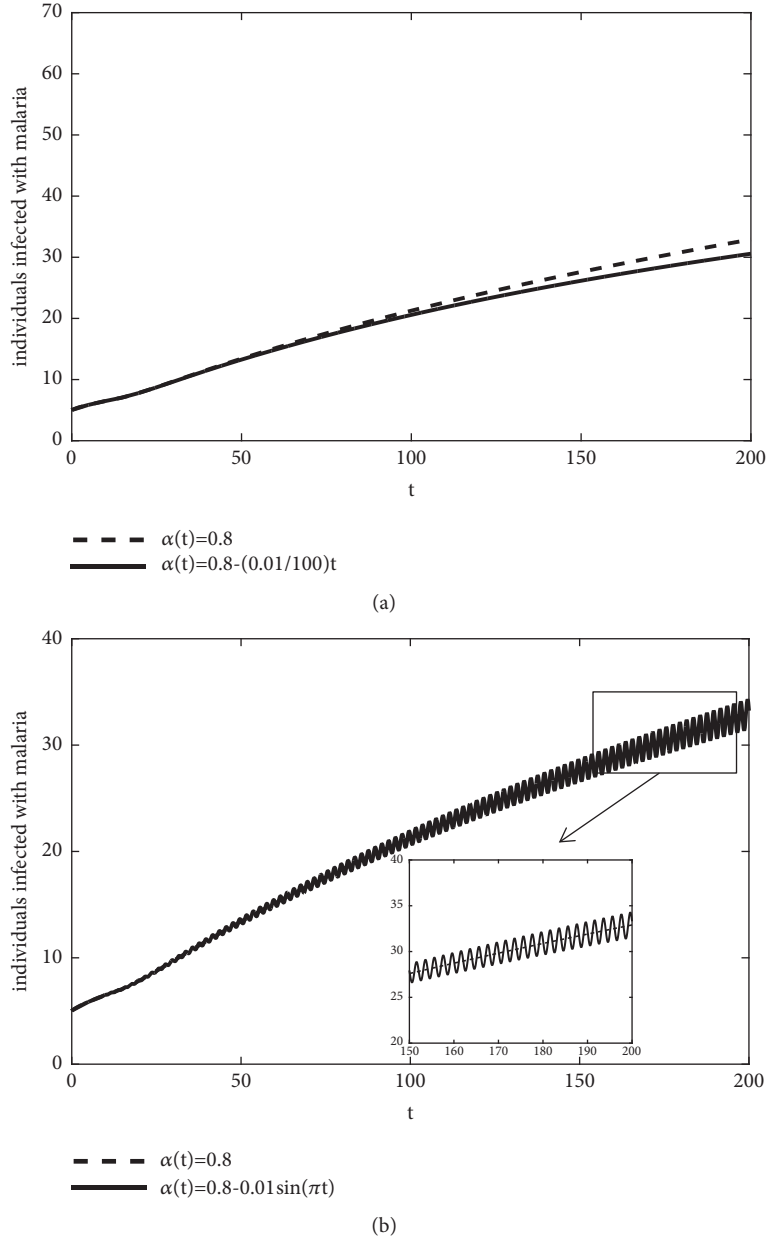
FIGURE 5: Individuals infected with malaria with $\psi = 2$. Parameters values are in Table 1 with $\beta_h = 0.05$. (a) $\alpha(t) = 0.8$ comparing with $\alpha(t) = 0.8 - (0.01/100)t$; (b) $\alpha(t) = 0.8$ comparing with $\alpha(t) = 0.8 - 0.01 \sin(\pi t)$.

Parameter $0 < \theta_2 \leq 1$ models the effect of the preerythrocytic vaccine in the raising of the recovery. Parameter $\theta_1 \geq 1$ models the effect of the preerythrocytic vaccine in the decreasing of mortality due to disease. The rate of recovery of individuals infected with malaria and going to the susceptible class is r_h. The rate of death of individuals infected with malaria is a_{h1}. $\varepsilon_2 < 1$ models the decrease in sexual activity due to malaria disease. ϕ_2 is the rate of recovery of the coinfected individuals showing no symptoms of AIDS from malaria. τ refers to the increased malaria mortality of individuals coinfected with HIV. ψ indicates the rise in HIV mortality due to the coinfection with malaria. a_{h2} is the rate of development of $I_{hiv}(t)$ to AIDS. The rate of death from

AIDS is δ_H. The rate of natural death of $I_{hiv}(t)$ is μ_h. υ_1 is the assumed rise in susceptibility to malaria as a result of HIV infection. The rate of recovery of $A_{mhiv}(t)$ from malaria is ϕ_3. υ_2 is the rise in susceptibility to malaria of individuals of $A_{hiv}(t)$. $\zeta > 1$ defines those coinfected individuals develop to AIDS faster than those infected only with HIV.

The rate of natural death of mosquitoes is μ_m. The rate of infection by the Anopheles parasite of susceptible mosquitoes $f_m(t)$ is given by

$$f_m(t) = \beta_m c (1 - bz)$$
$$\cdot \frac{I_h(t) + I_{mhiv}(t) + (1 - \varepsilon) Y_h(t) + A_{mhiv}(t)}{N_h(t)} \tag{18}$$

where $\varepsilon \in [0, 1]$ defines the decreasing of transmission from vaccinated humans to susceptible mosquitoes. The probability that a mosquito's bite in a malaria infective human tends to infection of the mosquito is β_m. The exposed mosquitoes turn infectious after time τ_m. The rate of increasing mortality due to the presence of the parasite in the body is a_m. In other words, all mosquitoes are subjected to a natural death, at a rate of μ_m. It is assumed that the infectious mosquitoes are subjected to death rate because of the presence of the parasite in their bodies at a rate a_m and that they do not recover before they die [32].

4. The Disease-Free Equilibrium and Stability

The equilibrium point of a dynamical system is a solution that does not change with time.

To obtain the disease-free equilibrium of model (14), let

$$
{}^C D^{\alpha(t)} N_h(t) = {}^C D^{\alpha(t)} S_h(t) = {}^C D^{\alpha(t)} V_h(t)
$$

$$
= {}^C D^{\alpha(t)} I_h(t) = {}^C D^{\alpha(t)} I_{mhiv}(t)
$$

$$
= {}^C D^{\alpha(t)} I_{hiv}(t) = {}^C D^{\alpha(t)} Y_h(t)
$$

$$
= {}^C D^{\alpha(t)} A_{mhiv}(t) \, {}^C D^{\alpha(t)} A_{hiv}(t)
$$

$$
= {}^C D^{\alpha(t)} N_m(t) = {}^C D^{\alpha(t)} S_m(t)
$$

$$
= {}^C D^{\alpha(t)} I_m(t) = 0
\tag{19}
$$

Then the disease-free equilibrium E_0 is

$$
E_0 = \left(\frac{A_h}{\mu_h}, \frac{(1-p) A_h (\sigma + \mu_h) + \sigma p A_h}{\mu_h (\sigma + \mu_h)}, \frac{p A_h}{\sigma + \mu_h}, 0, 0, \right.
$$
$$
\left. 0, 0, 0, 0, \frac{A_m}{\mu_m}, \frac{A_m}{\mu_m}, 0 \right)
\tag{20}
$$

The stability of disease-free equilibrium is defined by a sign of real part of eigenvalues of the Jacobian matrix evaluated at disease-free equilibrium. The Jacobian matrix is the matrix of partial derivatives of the right-hand side with respect to state variables.

The Jacobian matrix of model (14) around the disease-free equilibrium E_0 is

$$
J(E_0)
$$

$$
= \begin{bmatrix}
-\mu_h & 0 & 0 & -a_{h1} & -\tau a_{h1} & 0 & -a_{h1}(1-\theta_2) & -\tau a_{h1} - \psi\delta_H & -\delta_H & 0 & 0 & 0 \\
0 & -\mu_h & \sigma & r_h & -\eta_{HM}G_3 & G_3 & r_h\theta_1 & \eta_A\eta_{HM}G_3 & \eta_A G_3 & 0 & 0 & G_4 \\
0 & 0 & -(\sigma+\mu_h) & 0 & 0 & 0 & 0 & 0 & 0 & 0 & 0 & G_5 \\
0 & 0 & 0 & -(r_h+a_{h1}+\mu_h) & 0 & 0 & 0 & 0 & 0 & 0 & 0 & -e^{-\mu_h\tau_h}G_4 \\
0 & 0 & 0 & 0 & -(\zeta a_{h2}+\phi_2+\tau a_{h1}+\mu_h) & 0 & 0 & 0 & 0 & 0 & 0 & 0 \\
0 & 0 & 0 & 0 & \phi_2-\eta_{HM}G_3 & -G_3-(a_{h2}+\mu_h) & 0 & -\eta_A\eta_{HM}G_3 & -\eta_A G_3 & 0 & 0 & 0 \\
0 & 0 & 0 & 0 & 0 & 0 & -(\theta_1 r_h+(1-\theta_2)a_{h1}+\mu_h) & 0 & 0 & 0 & 0 & -e^{-\mu_h\tau_h}G_5 \\
0 & 0 & 0 & 0 & 0 & 0 & 0 & -(\mu_h+\phi_3+\tau a_{h1}+\psi\delta_H) & 0 & 0 & 0 & 0 \\
0 & 0 & 0 & 0 & 0 & a_{h2} & 0 & \phi_3 & -(\mu_h+\delta_H) & 0 & 0 & 0 \\
0 & 0 & 0 & 0 & 0 & 0 & 0 & 0 & 0 & -\mu_m & 0 & -a_m \\
0 & 0 & 0 & G_1 & G_1 & 0 & (1-\varepsilon)G_1 & G_1 & 0 & 0 & -\mu_m & 0 \\
0 & 0 & 0 & G_2 & G_2 & 0 & (1-\varepsilon)G_2 & G_2 & 0 & 0 & 0 & -(\mu_m+a_m)
\end{bmatrix}
\tag{21}
$$

where

$$
G_1 = -\beta_m c (1-bz) \frac{\mu_h A_m}{\mu_m A_h},
$$

$$
G_2 = \beta_m c (1-bz) \frac{\mu_h A_m}{\mu_m A_h} e^{-\tau_m(\lambda+\mu_m)},
$$

$$
G_3 = -\beta_H \left(\frac{\sigma + \mu_h(1-p)}{\sigma + \mu_h} \right),
\tag{22}
$$

$$
G_4 = -\beta_h c (1-bz) \frac{\sigma + \mu_h(1-p)}{\sigma + \mu_h},
$$

$$
G_5 = -\beta_h c (1-bz)(1-\gamma) \frac{p\mu_h}{\sigma + \mu_h}.
$$

The eigenvalues of the Jacobian matrix are

$$
\lambda_{1,2} = -\mu_h,
$$

$$
\lambda_{3,4} = -\mu_m,
$$

$$
\lambda_5 = -(\sigma + \mu_h),
$$

$$
\lambda_6 = -(\zeta a_{h2} + \phi_2 + \tau a_{h1} + \mu_h),
$$

$$
\lambda_7 = -(\mu_h + \phi_3 + \tau a_{h1} + \psi\delta_H)
\tag{23}
$$

The remaining five eigenvalues are obtained from the following matrix:

$$
M = \begin{bmatrix}
F_1 & 0 & 0 & 0 & F_2 \\
0 & F_3 & 0 & F_4 & 0 \\
0 & 0 & F_5 & 0 & F_6 \\
0 & F_7 & 0 & F_8 & 0 \\
F_9 & 0 & F_{10} & 0 & F_{11}
\end{bmatrix}
\tag{24}
$$

where

$$F_1 = -(r_h + a_{h1} + \mu_h),$$

$$F_2 = \beta_h c (1 - bz) \frac{\sigma + \mu_h (1 - p)}{\sigma + \mu_h} e^{-\tau_h(\lambda + \mu_h)}$$

$$F_3 = \beta_H \frac{\sigma + \mu_h (1 - p)}{\sigma + \mu_h} - (a_{h2} + \mu_h),$$

$$F_4 = \beta_H \eta_h \frac{\sigma + \mu_h (1 - p)}{\sigma + \mu_h}$$

$$F_5 = -(\theta_1 r_h + (1 - \theta_2) a_{h1} + \mu_h),$$

$$F_6 = \beta_h c (1 - bz) (1 - \gamma) \frac{p \mu_h}{\sigma + \mu_h} e^{-\tau_h(\lambda + \mu_h)} \quad (25)$$

$$F_7 = a_{h2},$$

$$F_8 = -(\mu_h + \delta_H),$$

$$F_9 = \beta_m c (1 - bz) \frac{\mu_h A_m}{\mu_m A_h} e^{-\tau_m(\lambda + \mu_m)}$$

$$F_{10} = \beta_m c (1 - bz) (1 - \varepsilon) \frac{\mu_h A_m}{\mu_m A_h} e^{-\tau_m(\lambda + \mu_m)},$$

$$F_{11} = -(\mu_m + a_m)$$

That matrix M has the characteristic equation

$$\lambda^5 + M_1 \lambda^4 + M_2 \lambda^3 + M_3 \lambda^2 + M_4 \lambda + M_5 = 0 \quad (26)$$

where

$$M_1 = -(F_1 + F_3 + F_5 + F_8 + F_{11}) \quad (27)$$

$$M_2 = F_{11} (F_1 + F_3 + F_5 + F_8) + F_5 F_8 - F_{10} F_6$$
$$\quad + (F_1 + F_3)(F_5 + F_8) + F_1 F_3 - F_7 F_4 - F_2 F_9 \quad (28)$$

$$M_3 = -F_5 F_8 (F_1 + F_3 + F_{11}) + F_{10} F_6 (F_1 + F_3 + F_8)$$
$$\quad - (F_1 + F_3)(F_5 + F_8) F_{11}$$
$$\quad - F_1 F_3 (F_5 + F_8 + F_{11})$$
$$\quad + F_7 F_4 (F_1 + F_5 + F_{11}) \quad (29)$$
$$\quad + F_2 F_9 (F_3 + F_5 + F_8)$$

$$M_4 = F_3 F_5 F_{11} (F_1 + F_3) + F_1 F_3 F_{11} (F_5 + F_8)$$
$$\quad + F_1 F_3 F_5 F_8 - F_7 F_4 (F_1 F_{11} + F_1 F_5 + F_5 F_{11})$$
$$\quad - F_6 F_{10} (F_1 F_8 + F_3 F_8 + F_1 F_3 - F_4 F_7) \quad (30)$$
$$\quad - F_2 F_9 (F_5 F_8 + F_3 F_5 + F_3 F_8 - F_4 F_7$$

$$M_5 = -F_1 F_5 F_{11} (F_3 F_8 - F_4 F_7)$$
$$\quad + F_6 F_{10} (F_1 F_3 F_8 - F_1 F_4 F_7) \quad (31)$$
$$\quad + F_2 F_9 (F_3 F_5 F_8 - F_4 F_5 F_7)$$

Using the results in [33], the disease-free equilibrium E_0 is locally asymptotically stable if the Routh-Hurwitz determinants $\Delta_1, \Delta_2, \Delta_3, \Delta_4, \Delta_5$ are

$$\Delta_1 = M_1,$$

$$\Delta_2 = \begin{vmatrix} M_1 & 1 \\ M_3 & M_2 \end{vmatrix},$$

$$\Delta_3 = \begin{vmatrix} M_1 & 1 & 0 \\ M_3 & M_2 & M_1 \\ M_5 & M_4 & M_3 \end{vmatrix},$$

$$\Delta_4 = \begin{vmatrix} M_1 & 1 & 0 & 0 \\ M_3 & M_2 & M_1 & 1 \\ M_5 & M_4 & M_3 & M_2 \\ 0 & 0 & M_5 & M_4 \end{vmatrix}, \quad (32)$$

$$\Delta_5 = \begin{vmatrix} M_1 & 1 & 0 & 0 & 0 \\ M_3 & M_2 & M_1 & 1 & 0 \\ M_5 & M_4 & M_3 & M_2 & M_1 \\ 0 & 0 & M_5 & M_4 & M_3 \\ 0 & 0 & 0 & 0 & M_5 \end{vmatrix}$$

satisfying $\Delta_i > 0$, $i = 1, 2, 3$, $\Delta_4 = 0$, and $M_5 > 0$. These conditions are the needed sufficient conditions to verify $|\arg(\lambda)| > \alpha(t)\pi/2$ for $\alpha(t) \in [0, 1)$.

We can put system (14) in the following form:

$$^C D^{\alpha(t)} y_i(t) = f(t, y_i(t), y_i(t - \tau_h), y_i(t - \tau_m)),$$
$$0 \leq t \leq T, \quad (33)$$
$$y_i(t) = g(t), \quad -\tau \leq t \leq 0, \; i = 1, 2, \ldots, 12$$

Let $y_i(t) = u_i$, $y_i(t - \tau_h) = w_i$, $y_i(t - \tau_m) = z_i$; then $f(t, u_i, w_i, z_i) \in C([0, T] \times \mathbb{R}^{12})$ is continuous with respect to t and globally Lipschitz continuous with respect to u_i, w_i, and z_i in the following norm: that is,

$$\|f(t, u_1, w_1, z_1) - f(t, u_2, w_2, z_2)\|$$
$$\leq L_1 \|u_1 - u_2\| + L_2 \|w_1 - w_2\| + L_3 \|z_1 - z_2\| \quad (34)$$

for some Lipschitz constants $L_1 > 0$, $L_2 > 0$, and $L_3 > 0$, and $t \in [0, T]$, $u_1, u_2, w_1, w_2, z_1, z_2 \in \mathbb{R}^{12}$. So $f(t, u_i, w_i, z_i)$ satisfies the standard conditions for the existence and uniqueness of solutions [34].

Also, let y^* be an equilibrium point of system (33). To determine the local stability of the system (33) we can use the indirect method of Lyapunov which uses the linearization of a system [35].

The linearization of the system (33) is

$$^C D^{\alpha(t)} y_i(t) = B_0 u_i + B_1 w_i + B_2 z_i \quad (35)$$

where $B_0 = \partial f(t, u_i, w_i, z_i)/\partial u_i$, $B_1 = \partial f(t, u_i, w_i, z_i)/\partial w_i$, and $B_2 = \partial f(t, u_i, w_i, z_i)/\partial z_i$ are 12×12 matrices evaluated at

the disease-free equilibrium (essentially a Jacobian matrix for each time delay) [36].

It follows that, for each fixed t, the remainder is

$$f_1\left(t, u_i, w_i, z_i\right) = f\left(t, u_i, w_i, z_i\right) - B_0 u_i - B_1 w_i \\ - B_2 z_i \tag{36}$$

And the remainder tends to zero as u_i, w_i, z_i tend to zero. But, the remainder may not tend to zero uniformly. So we need a stronger condition which is

$$\lim_{\|u_i\| \longrightarrow 0} \sup_{t \geq 0} \frac{\|f_1\left(t, u_i, w_i, z_i\right)\|}{\|u_i\|} = 0,$$

$$\lim_{\|w_i\| \longrightarrow 0} \sup_{t \geq 0} \frac{\|f_1\left(t, u_i, w_i, z_i\right)\|}{\|w_i\|} = 0, \tag{37}$$

$$\lim_{\|z_i\| \longrightarrow 0} \sup_{t \geq 0} \frac{\|f_1\left(t, u_i, w_i, z_i\right)\|}{\|z_i\|} = 0$$

If (37) holds, then system (35) is the linearization of the system (33). Once the linearization exits, its stability defines the local stability of the original nonlinear system.

Let B_0, B_1, B_2 be bounded. If y^* is a uniformly asymptotically stable equilibrium point of system (35) then y^* is a locally uniformly asymptotically stable equilibrium point of system (33).

5. The Basic Reproduction Number R_0

In epidemiology, the basic reproduction number is defined as the number of secondary infections due to a single infection in a totally susceptible population. It is useful since it decides if or not an infectious disease can spread through a population. When $R_0 > 1$, the infection will be able to spread in a population. But if $R_0 < 1$, the infection will disappear. For $R_0 > 1$, there was, at least, one stable endemic equilibrium [32]. In some cases, the basic reproduction number is not enough to predict the spread of epidemics because bifurcation may occur.

The basic reproduction number of the model (14) is shown in [32]

$$R_0 = \max\left(R_m, R_{hiv}\right) \tag{38}$$

where R_m is the basic reproduction number of malaria model and R_{hiv} is the basic reproduction of HIV model as follows:

$$R_m = \left(\frac{\mu_h \beta_h \beta_m A_m e^{-\mu_h \tau_h} e^{-\mu_m \tau_m} c^2 \left(1 - bz\right)^2}{\left(a_m + \mu_m\right) \mu_m A_h \left(\sigma + \mu_h\right)} \right) \\ \cdot \left(\frac{\sigma + \mu_h \left(1 - p\right)}{r_h + \mu_h + a_{h1}} + \frac{\left(1 - \gamma\right)\left(1 - \varepsilon\right)\mu_h p}{\theta_1 r_h + \left(1 - \theta_2\right) a_{h1} + \mu_h} \right) \tag{39}$$

$$R_{hiv} = \frac{\beta_H \left(\mu_h + \delta_H + \eta_A a_{h2}\right)\left(1 - p\right)}{\left(a_{h2} + \mu_h\right)\left(\mu_h + \delta_H\right)} \tag{40}$$

Theorem 5 (see [43]). *If $R_0 < 1$, then the disease-free equilibrium E_0 is globally asymptotically stable in Ω.*

$\Omega = (A_h, p, \sigma, \eta_{HM}, c, A_m, \phi_2, \phi_3, b, z, r_h, a_{h1}, a_{h2}, \beta_m, \beta_h, \varepsilon_2, \delta_H, \mu_h, \gamma, \varepsilon, \mu_m, \tau, \psi, \theta_1, \theta_2, \upsilon_1, \upsilon_2, \eta_A, a_m, \tau_h, \tau_m, \zeta, \beta_H$ *such that the solution of the system (14) is positive.*

Proof. From the previous section according to Routh-Hurwitz conditions M_5 defined by (31) must be greater than zero so we will rewrite M_5 in terms of R_{hiv} and R_m after some manipulation as follows:

$$M_5 = \left(r_h + a_{h1} + \mu_h\right)\left(\theta_1 r_h + \left(1 - \theta_2\right) a_{h1} + \mu_h\right) \\ \cdot \left(\mu_m + a_m\right)\left(a_{h2} + \mu_h\right)\left(\mu_h + \delta_H\right)\left(1 - R_{hiv}\right)\left(1 - R_m\right) \tag{41} \\ > 0.$$

Thus $M_5 > 0$ if $R_{hiv} < 1$ and $R_m < 1$ so the disease-free equilibrium E_0 is globally asymptotically stable in Ω. □

6. Numerical Results and Discussions

Applying the predictor-corrector method to solve model (14) with initial conditions,

$$N_h(0) = 430,$$
$$S_h(0) = 300,$$
$$V_h(0) = 100,$$
$$I_h(0) = 5,$$
$$I_{mhiv}(0) = 5,$$
$$I_{hiv}(0) = 5,$$
$$Y_h(0) = 5, \tag{42}$$
$$A_{mhiv}(0) = 5,$$
$$A_{hiv}(0) = 5,$$
$$N_m(0) = 450,$$
$$S_m(0) = 430,$$
$$I_m(0) = 20$$

And the values of parameters are shown in Table 1

We investigate the model behavior in two cases. Firstly, the variable fractional-order is $\alpha(t) = 0.8 - (0.01/100)t$. Secondly, the variable fractional-order is a periodic function $\alpha(t) = 0.8 - 0.01 \sin(\pi t)$.

In Figure 1, we show the effect of the parameter υ_2 which is the susceptibility to malaria of individuals showing symptoms of AIDS. It is shown that when υ_2 increases; the number of HIV infected individuals showing symptoms of AIDS decreases. Besides, when we use the variable fractional-order $\alpha(t) = 0.8 - 0.01 \sin(\pi t)$ means the memory of the model is described as a periodic function; hence the behavior of the model is also periodic. Also, when we use the variable fractional-order $\alpha(t) = 0.8 - (0.01/100)t$ means the memory
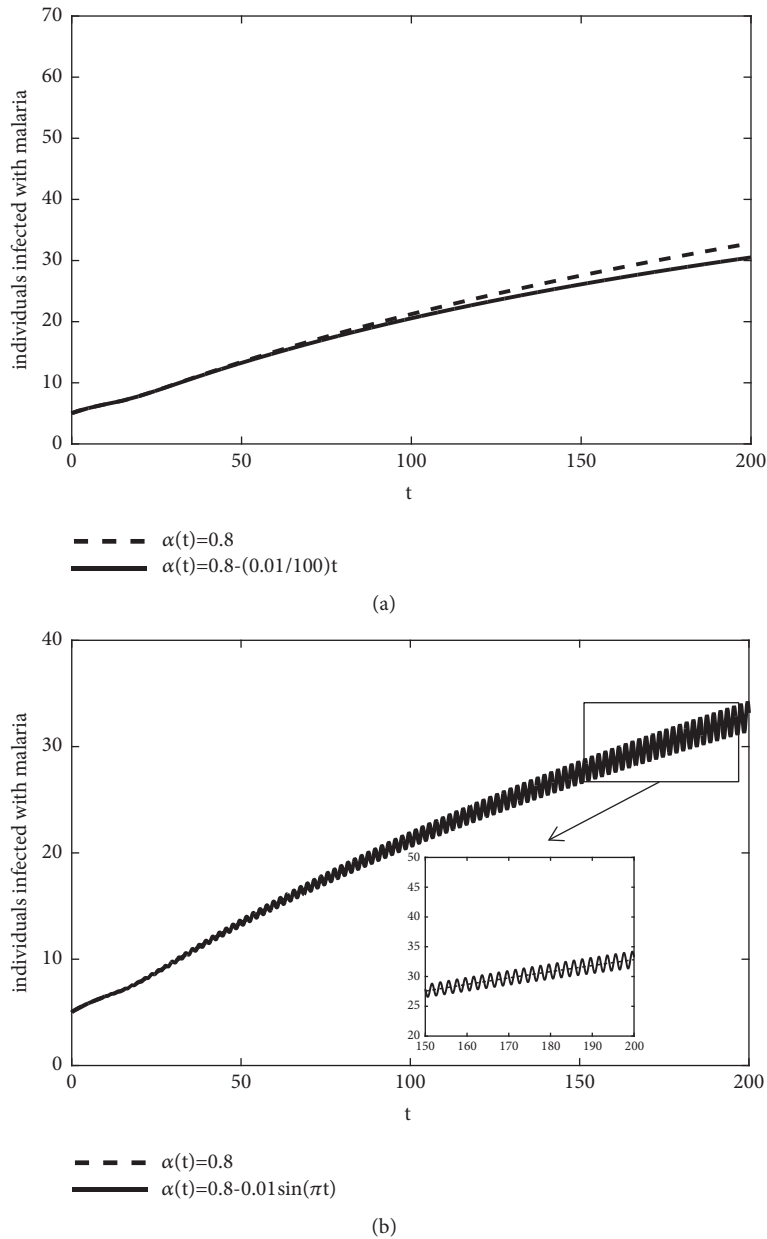
FIGURE 6: Individuals infected with malaria with $\psi = 3$. Parameters values are in Table 1 with $\beta_h = 0.05$. (a) $\alpha(t) = 0.8$ comparing with $\alpha(t) = 0.8 - (0.01/100)t$; (b) $\alpha(t) = 0.8$ comparing with $\alpha(t) = 0.8 - 0.01\sin(\pi t)$.

in the model is described by a decreasing function so the model behavior is slower with time as in Figures 2 and 3.

In Figure 4, we show the effect of the parameter ψ which is HIV mortality due to the coinfection with malaria. It is shown that when ψ increases; it leads to decreasing of new cases of malaria. Besides, when we use the variable fractional-order $\alpha(t) = 0.8 - 0.01\sin(\pi t)$ means the memory of the model is described as a periodic function; hence the behavior of the model is also periodic. Also, when we use the variable fractional-order $\alpha(t) = 0.8 - (0.01/100)t$ means the memory in the model is described by a decreasing function so the model behavior is slower with time as in Figures 5 and 6.

The presented numerical results indicate that the proposed delay variable fractional-order model is a generalization of the constant fractional-order model with a time delay which has been presented in [32].

7. Conclusion

A delay variable fractional-order model for the coinfection of HIV/AIDS and malaria which includes malaria vaccination and personal protection strategies is proposed in this paper. Also, the basic reproduction number and stability of the disease-free equilibrium have been studied. The numerical results showed the impact of changing the parameters values

Table 1: The values of parameters used in the numerical results.

Parameter	Value	Reference
A_h	0.05	[32]
p	0.4	[37]
σ	0.009	[37]
η_{HM}	1.5030	[32]
c	0.5	[38]
A_m	6	[37]
ϕ_2	0.002	[39]
ϕ_3	0.0005	[39]
b	0.3	[32]
z	0.9	[32]
r_h	0.005	[37]
a_{h1}	0.0004	[32]
a_{h2}	0.004	[32]
β_m	0.83	[40]
ε_2	0.8	[32]
δ_H	0.000913	[39]
μ_h	0.000039	[41]
γ	0.64	[37]
ε	0.86	[37]
τ_h	14	[37]
τ_m	12	[42]
μ_m	0.04	[37]
τ	1.001	[39]
ψ	1.002	[39]
θ_1	4.1	[37]
θ_2	0.06	[37]
v_1	1.002	[39]
v_2	1.5	[39]
η_A	1.4	[39]
a_m	0.01	[37]
ζ	1.002	[39]
β_H	0.001	[39]

such as v_2 and ψ on the number of the infected individuals with malaria/HIV, coinfected individuals, and infectious mosquitoes as well. The variable fractional-order derivative in the proposed model is used to distinguish the effect of the memory that changes over time on the disease progression of distinct patients. In Our future work, comparisons between the numerical results and real data will be held in order to examine the numerical simulation results at different variable fractional-order $\alpha(t)$.

Data Availability

No data were used to support this study.

Conflicts of Interest

The authors declare that there are no conflicts of interest regarding the publication of this paper.

References

[1] S. Hochman and K. Kim, "The impact of HIV and malaria coinfection: what is known and suggested venues for further study," *Interdisciplinary Perspectives on Infectious Diseases*, vol. 2009, Article ID 617954, 8 pages, 2009.

[2] World Health Organization: HIV/AIDS, 2017, http://www.who.int/mediacentre/factsheets/fs360/en/.

[3] World Health Organization: Malaria, 2017, http://www.who.int/mediacentre/factsheets/fs094/en/.

[4] About HIV/AIDS, https://www.cdc.gov/hiv/basics/whatishiv.html.

[5] R. Idro, K. Marsh, C. C. John, and C. R. J. Newton, "Cerebral malaria: mechanisms of brain injury and strategies for improved neurocognitive outcome," *Pediatric Research*, vol. 68, no. 4, pp. 267–274, 2010.

[6] World Health Organization: Malaria in HIV/AIDS patients, http://www.who.int/malaria/areas/high_risk_groups/hiv_aids_patients/en/.

[7] S. C. K. Tay, K. Badu, and A. A. Mensah, "The prevalence of malaria among HIV seropositive individuals and the impact of the co- infection on their hemoglobin levels," *Annals of Clinical Microbiology and Antimicrobials*, vol. 14, no. 1, p. 10, 2015.

[8] A. Baradaji, B. Sigauquw, S. Sanz et al., "Impact of malaria at the end of pregnancy on infant mortality and morbidity," *The Journal of Infectious Diseases*, vol. 203, no. 5, pp. 691–699, 2011.

[9] G. V. Brown, "Progress in the development of malaria vaccines: context and constraints," *Parassitologia*, vol. 41, no. 1-3, pp. 429–432, 1999.

[10] L. H. Miller, P. H. David, T. J. Hadley, and R. R. Freeman, "Perspectives for malaria vaccination," *Philosophical Transactions of the Royal Society B: Biological Sciences*, vol. 84, no. 2, pp. 99–115, 1984.

[11] D. Kazmin, H. I. Nakaya, E. K. Lee et al., "Systems analysis of protective immune responses to RTS,S malaria vaccination in humans," *Proceedings of the National Academy of Sciences of the United States of America*, vol. 114, no. 9, pp. 2425–2430, 2017.

[12] A. A. M. Arafa, S. Z. Rida, and M. Khalil, "A fractional-order model of HIV infection: numerical solution and comparisons with data of patients," *International Journal of Biomathematics*, vol. 7, no. 4, article 1450036, 2014.

[13] A. A. Arafa, S. Z. Rida, and M. Khalil, "A fractional-order model of HIV infection with drug therapy effect," *Journal of the Egyptian Mathematical Society*, vol. 22, no. 3, pp. 538–543, 2014.

[14] A. A. Arafa, S. Z. Rida, and M. Khalil, "The effect of anti-viral drug treatment of human immunodeficiency," *Applied Mathematical Modelling*, vol. 37, pp. 2189–2196, 2013.

[15] A. A. M. Arafa, S. Z. Rida, and M. Khalil, "Fractional modeling dynamics of HIV and CD4+ T-cells during primary infection," *Nonlinear Biomedical Physics*, vol. 6, pp. 1–7, 2012.

[16] A. R. Carvalho, C. M. Pinto, and D. Baleanu, "HIV/HCV coinfection model: a fractional-order perspective for the effect of the HIV viral load," *Advances in Difference Equations*, vol. 2018, no. 1, p. 2, 2018.

[17] C. M. A. Pinto and A. R. Carvalho, "A latency fractional order model for HIV dynamics," *Journal of Computational and Applied Mathematics*, vol. 312, pp. 240–256, 2017.

[18] C. M. A. Pinto and J. A. T. Machado, "Fractional model for malaria transmission under control strategies," *Computers & Mathematics with Applications*, vol. 66, no. 5, pp. 908–916, 2013.

[19] Z. U. A. Zafar, K. Rehan, and M. Mushtaq, "Fractional-order scheme for bovine babesiosis disease and tick populations," *Advances in Difference Equations*, vol. 2017, no. 1, 86 pages, 2017.

[20] Z. U. A. Zafar, K. Rehan, and M. Mushtaq, "HIV/AIDS epidemic fractional-order model," *Journal of Difference Equations and Applications*, vol. 23, no. 7, pp. 1298–1315, 2017.

[21] Z. U. A. Zafar, K. Rehan, M. Mushtaq, and M. Rafiq, "Numerical treatment for nonlinear Brusselator chemical model," *Journal of Difference Equations and Applications*, vol. 23, no. 3, pp. 521–538, 2017.

[22] Z. U. A. Zafar, M. Mushtaq, and K. Rehan, "A non-integer order dengue internal transmission model," *Advances in Difference Equations*, vol. 2018, no. 1, 23 pages, 2018.

[23] A. V. Chechkin, R. Gorenflo, and I. M. Sokolov, "Fractional diffusion in inhomogeneous media," *Journal of Physics A: Mathematical and General*, vol. 38, no. 42, pp. L679–L684, 2005.

[24] A. V. Chechkin, V. Y. Gonchar, R. Gorenflo, N. Korabel, and I. M. Sokolov, "Generalized fractional diffusion equations for accelerating subdiffusion and truncated Levy flights," *Physical Review E: Statistical, Nonlinear, and Soft Matter Physics*, vol. 78, no. 2, article 021111, 2008.

[25] L. M. Petrovic, D. T. Spasic, and T. M. Atanackovic, "On a mathematical model of a human root dentin," *Dental Materials*, vol. 21, no. 2, pp. 125–128, 2005.

[26] H. G. Sun, W. Chen, H. Wei, and Y. Q. Chen, "A comparative study of constant-order and variable-order fractional models in characterizing memory property of systems," *The European Physical Journal Special Topics*, vol. 193, no. 1, pp. 185–192, 2011.

[27] Y. Xu and Z. He, "Existence and uniqueness results for Cauchy problem of variable-order fractional differential equations," *Applied Mathematics and Computation*, vol. 43, no. 1-2, pp. 295–306, 2013.

[28] U. Saeed and M. U. Rehman, "Hermite wavelet method for fractional delay differential equations," *Journal of Differential Equations*, vol. 2014, Article ID 359093, pp. 1–8, 2014.

[29] B. P. Moghaddam and Z. S. Mostaghim, "A Matrix scheme based on fractional finite difference method for solving fractional delay differential equations with boundary condition," *New Trends in Mathematical Sciences*, vol. 3, no. 2, pp. 13–23, 2015.

[30] V. Daftardar-Gejji, Y. Sukale, and S. Bhalekar, "Solving fractional delay differential equations: a new approach," *Fractional Calculus and Applied Analysis*, vol. 18, no. 2, pp. 400–418, 2015.

[31] B. P. Moghaddam, S. Yaghoobi, and J. T. Machado, "An extended predictor–corrector algorithm for variable-order fractional delay differential equations," *Journal of Computational and Nonlinear Dynamics*, vol. 11, no. 6, article 061001, 2016.

[32] A. R. Carvalho and C. M. A. Pinto, "A delay fractional order model for the co-infection of malaria and HIV/AIDS," *International Journal of Dynamics and Control*, vol. 5, no. 1, pp. 168–186, 2017.

[33] E. Ahmed and A. S. Elgazzar, "On fractional order differential equations model for nonlocal epidemics," *Physica A: Statistical Mechanics and Its Applications*, vol. 379, no. 2, pp. 607–614, 2007.

[34] A. M. A. El-Sayed, "On the existence and stability of positive solution for a nonlinear fractional-order differential equation and some applications," *Alexandria Journal of Mathematics*, vol. 1, no. 1, pp. 1–10, 2010.

[35] R. M. Murray, *A Mathematical Introduction to Robotic Manipulation*, CRC Press, 2017.

[36] F. M. Asl and A. G. Ulsoy, "Analysis of a system of linear delay differential equations," *Journal of Dynamic Systems, Measurement, and Control*, vol. 125, no. 2, pp. 215–223, 2003.

[37] C. Chiyaka, J. M. Tchuenche, W. Garira, and S. Dube, "A mathematical analysis of the effects of control strategies on the transmission dynamics of malaria," *Applied Mathematics and Computation*, vol. 195, no. 2, article 20080, pp. 641–662, 2008.

[38] K. Dietz, L. Molineaux, and A. Thomas, "A malaria model tested in the African Savannah," *Bulletin of the World Health Organization*, vol. 50, no. 3-4, pp. 347–357, 1974.

[39] Z. Mukandavire, A. B. Gumel, W. Garira, and J. M. Tchuenche, "Mathematical analysis of a model for HIV-malaria co-infection," *Mathematical Biosciences and Engineering*, vol. 6, no. 2, pp. 333–362, 2009.

[40] N. Chitnis, J. M. Cushing, and J. M. Hyman, "Bifurcation analysis of a mathematical model for malaria transmission," *SIAM Journal on Applied Mathematics*, vol. 67, no. 1, pp. 24–45, 2006.

[41] C. Bowman, A. B. Gumel, P. van den Driessche, J. Wu, and H. Zhu, "Amathematical model for assessing control strategies against West Nile virus," *Bulletin of Mathematical Biology*, vol. 67, no. 5, pp. 1107–1133, 2005.

[42] T. S. Detinova, *Age Grouping Methods in Diptera of Medical Importance, with Special Reference to Some Vectors of Malaria*, vol. 48 of *Monographs Series, no.47*, 1962.

[43] C. Wu and Z. Jiang, "Global stability for the disease free equilibrium of a delayed model for malaria transmission," *International Journal of Mathematical Analysis*, vol. 6, no. 37-40, pp. 1877–1881, 2012.

Research Article

Assessment of Diabetic Autonomic Nervous Dysfunction with a Novel Percussion Entropy Approach

Hai-Cheng Wei,[1] Ming-Xia Xiao,[1,2] Na Ta,[1] Hsien-Tsai Wu,[3] and Cheuk-Kwan Sun [ID][4]

[1] *School of Electrical and Information Engineering, North Minzu University, No. 204 North – Wenchang St., Xixia District, Yinchuan, Ningxia 750021, China*
[2] *School of Computer and Information, Hefei University of Technology, No. 193, Tunxi Rd., Hefei, Anhui 230009, China*
[3] *Department of Electrical Engineering, National Dong Hwa University, No. 1, Sec. 2, Da Hsueh Rd., Shoufeng, Hualien 97401, Taiwan*
[4] *Department of Emergency Medicine, E-Da Hospital, I-Shou University School of Medicine for International Students, No. 1, Yida Road, Jiaosu Village, Yanchao District, Kaohsiung City 82445, Taiwan*

Correspondence should be addressed to Cheuk-Kwan Sun; lawrence.c.k.sun@gmail.com

This study investigated the validity of a novel parameter, percussion entropy index (PEI), for assessing baroreflex sensitivity. PEI was acquired through comparing the similarity in tendency of change between the amplitudes of successive digital volume pulse (DVP) signals and changes in R-R intervals (RRI) of successive cardiac cycles. Totally 108 upper middle-aged volunteers were divided into three groups: healthy subjects (Group 1, age 41–80, n=41), those with well-controlled type 2 diabetes mellitus (T2DM) (Group 2, age 41–82, n=36, glycated hemoglobin (HbA1c)<6.5%), and patients with poorly controlled T2DM (Group 3, age 44–77, n=31, HbA1c≧6.5%). Percussion entropy index (PEI) was computed from DVP signals acquired through photoplethysmography (PPG) and RRI from electrocardiogram in 1000 successive cardiac cycles for each subject. Autonomic function was also assessed by Poincaré index (SD1/SD2 ratio, SSR), low- to high-frequency power ratio (LFP/HFP, LHR), and small-scale multiscale entropy index (MEI$_{SS}$) for comparison. Demographic, anthropometric, hemodynamic, and serum biochemical parameters of all testing subjects were obtained for investigating the significance of associations with the three parameters. The results showed that MEI$_{SS}$ and PEI successfully discriminated among the three groups ($p<0.017$). However, only PEI showed significant associations with indicators of both acute (i.e., fasting blood sugar concentration, $p<0.017$) and chronic (i.e., HbA1c level, $p<0.001$) blood sugar control. Multivariate analysis also showed significant associations of PEI with fasting blood sugar and HbA1c levels in all subjects. The interpreting effect of the two independent variables, HbA1c level and fasting blood sugar concentration, on PEI was 71.4% and 12.3%, respectively. In conclusion, the results demonstrated that additional information on diabetic autonomic dysfunction can be obtained through comparing two simultaneously acquired physiological time series. The significant associations of percussion entropy index with indicators of blood sugar control also highlight its possible role in early screening of the disease.

1. Introduction

Diabetes mellitus (DM) is a dominant metabolic disease worldwide with an estimated prevalence of 108 million in 1980, which soared by almost four times to 422 million in 2014 and is still on the increase [1]. Patients with type 2 DM are at increased risk of developing autonomic nervous dysfunction [2], atherosclerosis [3, 4], and even cancers [5]. Therefore, early diagnosis and treatment are of vital importance. Clinically, retinopathy [6], nephropathy [7], and neuropathy [8] are the three hallmarks of the disease [9]. Although the

former two can be diagnosed through physical examination and laboratory study, respectively, the latter cannot be easily assessed objectively. The adverse impact of diabetes-associated neurological damage cannot be overemphasized. In addition to diabetic sensory and motor neuropathy [8], a number of studies have shown significant associations between compromised autonomic nervous function and an increased risk of cardiovascular morbidity and mortality [10–12]. Besides, depressed autonomic function has been found to be a predictor of rapid progression of atherosclerosis [13].

Baroreflex is a physiological phenomenon in which an increase in blood pressure would lead to a prolongation of the R-R interval (RRI). Accordingly, a decrease in blood pressure would shorten the RRI [14]. It is a physiological compensatory mechanism to maintain hemodynamic stability of an individual [15]. Baroreflex sensitivity, which refers quantitatively to the degree of matching between a change in blood pressure and a change in interbeat intervals (i.e., RRI) of the heart [14, 16], has been found to be impaired in patients with systemic diseases such as diabetes [2, 11, 17]. Previous studies have demonstrated the successful application of noninvasive approaches to assessing autonomic function. For instance, frequency domain analysis of heart rate variability (HRV) based on R-R intervals (RRI) from electrocardiograph (EKG) is an assessment method for autonomic nervous activity and baroreflex sensitivity [14]. The parameter of low- to high-frequency power ratio (LFP/HFP, LHR) thus obtained is considered to reflect the relative activities of the sympathetic and parasympathetic nervous systems [17–19]. However, such a frequency domain parameter has its limitations because of the nonstationary and nonlinear nature of the physiological signals to be analyzed [20–22]. In an attempt to tackle this problem, the Poincaré index (SD1/SD2 ratio, SSR) was introduced to assess autonomic nervous activities and baroreflex sensitivity using a nonlinear approach to analyzing HRV [20, 23]. Nevertheless, both frequency (i.e., LHR) and time (i.e., SSR) domain analyses assess autonomic activities (i.e., HRV) merely based on a one-dimensional time series (i.e., RRI) without taking into account other simultaneous physiological changes.

Multiscale entropy (MSE), which was first proposed by Costa et al. [24], is a method for analyzing the complexity of nonlinear and nonstationary signals in finite length time series. It was used to analyze the complexity of a single time series (i.e., RRI) to differentiate between healthy and diseased subjects [24]. The present study attempted to apply a novel parameter of "percussion entropy index (PEI)" to assess baroreflex sensitivity by comparing the degree of matching between the changes of two autonomic function-related time series (i.e., amplitude of digital volume pulse and RRI) during successive cardiac cycles to more accurately investigate an individual's autonomic functions. The concept of percussion entropy index (PEI) in the present study is based on that of MSE index (MEI). The difference between small-scale multiscale entropy index (MEI_{SS}) and PEI is that the former evaluates the degree of fluctuations of a parameter within a defined region in a time series, whereas the latter is a simple means to assess the similarity in the pattern of changes (i.e., increase or decrease) of two related time series to evaluate the adaptive capacity of a physiological system.

Although baroreflex sensitivity (BRS) has been shown to be a good indicator of autonomic activity [15], assessment of BRS requires the simultaneous acquisition of information on real-time blood pressure and HRV. Previous studies have demonstrated that the sensitivity of BRS assessment by noninvasive means is comparable to that acquired through invasive measurement [14, 25]. Digital volume pulse (DVP) signals acquired noninvasively through photoplethysmography (PPG) have been found to correlate well with changes in blood pressure [26–28]. Besides, the current study was designed based on the finding that baroreceptor sensitivity was impaired in subjects with chronic systemic diseases, particularly those that affect the cardiovascular system (e.g., diabetes) [2, 11, 17]. Using percussion entropy index (PEI), the present study is aimed at investigating the validity of a two-dimensional approach to the assessment of diabetes-associated changes in autonomic activities using two noninvasively acquired time series, including waveform amplitudes of DVP signals from finger and RRI. Results of autonomic function assessment from data on RRI using time (i.e., Poincaré index: SD1/SD2 ratio, SSR) and frequency (i.e., low- to high-frequency power ratio: LFP/HFP, LHR) domain analyses as well as MEI_{SS} were also obtained for comparison.

The rest of this paper is organized as follows: Section 2 comprises study population (i.e., study period, criteria for subject recruitment, and grouping), study protocol (i.e., comparison of the computational parameters with the demographic, anthropometric, hemodynamic, and serum biochemical parameters of the three groups of testing subjects), details on data acquisition and analysis including calculation of unilateral fingertip PPG amplitude sequence and RRI sequence (i.e., Amp and RRI), and computation of multiscale small-scale entropy index (MEI_{SS}) and percussion entropy index (PEI) as well as statistical analysis. In Section 3, the choice of shift number for percussion entropy index computation was first justified, followed by the comparison of the four computational parameters for autonomic function assessment. In Sections 4 and 5, discussion and conclusions derived from this study are summarized with several suggestions for future work.

2. Methods

2.1. Study Population. Between July 2009 and Feb. 2012, 114 volunteers were recruited for the present study. All diabetic patients were enrolled from the diabetes outpatient clinic of the Hualien Hospital, while healthy controls were recruited from a physical check-up program at the same hospital. Of the 114 volunteers, 6 were excluded due to incomplete or unstable waveform data acquisition. The remaining 108 subjects were then divided into three groups, namely, healthy upper middle-aged subjects (Group 1, age range: 41-80, number = 41), upper middle-aged subjects diagnosed as having type 2 DM with satisfactory blood sugar control (Group 2, age range: 41-82, number = 36, glycated hemoglobin (HbA1c) < 6.5%), and type 2 diabetic patients with poor blood sugar control (Group 3, age range: 44-77, number = 31, HbA1c ≧ 6.5%) (Table 1). All healthy subjects had no personal or family history of cardiovascular diseases. Type 2 diabetes was diagnosed by either a fasting blood sugar concentration ≧ 126 mg/dL or HbA1c ≧ 6.5% [29]. All diabetic patients underwent regular treatment and follow-up in outpatient clinic for at least two years. Each subject was required to refrain from theophylline-containing medications and caffeine-containing beverages for at least 8 hours before acquisition of data. Before taking the tests, all subjects were requested to sign informed consent and complete questionnaires on demographics and medical histories as well as

TABLE 1: Demographic, anthropometric, hemodynamic, and serum biochemical parameters of the testing subjects.

Parameters	Group 1 (number: 41)	Group 2 (number: 36)	Group 3 (number: 31)
Female/male	24/17	16/20	11/20
Age (year)	56.75 ± 3.88	59.16 ± 8.40	56.08 ± 11.38
Body height (cm)	163.49 ± 8.30	162.59 ± 7.95	163.39 ± 5.20
Body weight (kg)	65.01 ± 13.78	71.59 ± 11.89	79.69 ± 16.35
WC (cm)	81.74 ± 11.81	94.25 ± 9.72**	100.69 ± 13.51[†]
BMI (kg/m^2)	24.17 ± 4.12	26.96 ± 2.87*	29.87 ± 6.05
SBP (mmHg)	116.41 ± 15.63	125.71 ± 18.06	126.69 ± 10.29
DBP (mmHg)	73.70 ± 9.70	74.06 ± 12.41	76.38 ± 4.23
PP (mmHg)	42.41 ± 10.73	51.65 ± 11.94	50.31 ± 12.07
HDL (mg/dL)	53.22 ± 20.81	44.07 ± 9.89	40.50 ± 9.68
LDL (mg/dL)	122.34 ± 29.49	94.36 ± 21.93	118.10 ± 29.91
Cholesterol (mg/dL)	192.46 ± 40.01	170.80 ± 31.00	199.09 ± 34.63[†]
Triglyceride (mg/dL)	98.05 ± 85.35	112.93 ± 39.92	185.91 ± 74.89[†]
HbA1c (%)	5.68 ± 0.38	6.95 ± 0.39**	9.25 ± 1.63[††]
Fasting blood sugar (mg/dL)	93.98 ± 10.67	127.47 ± 25.70**	176.91 ± 68.71[†]

Group 1: healthy subjects; Group 2: diabetic subjects with satisfactory blood sugar control; Group 3: diabetic subjects with poor blood sugar control. Values are expressed as mean ± SD; WC: waist circumference; BMI: body mass index; SBP: systolic blood pressure; DBP: diastolic blood pressure; PP: pulse pressure; HbA1c: glycated hemoglobin. *$p < 0.017$: Group 1 vs. Group 2; **$p < 0.001$: Group 1 vs. Group 2; [†]$p < 0.017$: Group 2 vs. Group 3, and [††]$p < 0.001$: Group 2 vs. Group 3.

receive blood sampling for serum biochemical analysis. The study was approved by the Institutional Review Board (IRB) of Hualien Hospital.

2.2. Study Protocol. One waveform parameter (i.e., amplitude, Amp) and one parameter of cardiac electricalactivity (i.e., RRI) were acquired from all subjects. Autonomic function analysis was performed on the acquired data of RRI from the frequency [17–19] and time [20, 23] domains to obtain the low- to high-frequency power ratio (LFP/HFP, LHR) and Poincaré index (SD1/SD2 ratio, SSR), respectively. Percussion entropy index (PEI) was computed from the synchronized Amp and RRI time series for each testing subject. The associations of the computational parameters thus obtained (i.e., PEI, MEI$_{SS}$, LHR, SSR) with the demographic (i.e., age), anthropometric (i.e., body height, body weight, waist circumference, body-mass index), hemodynamic (i.e., systolic and diastolic blood pressures), and serum biochemical (i.e., high- and low-density lipoprotein cholesterol, total cholesterol, and triglyceride) parameters of the three groups of testing subjects were then analyzed and compared.

2.3. Data Acquisition and Analysis. All participants were required to rest supinely in a quiet, temperature-controlled room at 25 ± 1°C for 4 minutes before 30 minutes of measurement. Using an automated oscillometric device (BP3AG1, Microlife, Taiwan) with an inflatable cuff of appropriate size, blood pressure was obtained once over left arm in supine position. Data on left index finger waveform were collected with a six-channel EKG-photoplethysmography (PPG) system as described previously [30, 31]. The digitized signals (both PPG and ECG) were processed through an analog-to-digital converter (USB-6009 DAQ, National Instruments,

Austin, TX) using a sampling frequency of 500 Hz before being stored in a computer for later analysis. The digital volume pulses (DVPs) were acquired through PPG as previously reported [30]. In the present study, DVPs from the fingertip were used for waveform contour analysis. The systolic peak and foot point were identified from the contour of the DVP. The amplitude of each waveform (Amp) was defined as that between the foot point and the systolic peak of a pulse wave [32] (Figure 1).

2.3.1. Calculation of Unilateral Fingertip PPG Amplitude Sequence and RRI Sequence (i.e., Amp and RRI). Time series of DVP waveform amplitude, {Amp(j)} = {Amp(1), Amp(2),..., Amp(n)}, and that of RRI, {RRI(i)} = {RRI(1), RRI(2),..., RRI(n)}, were simultaneously acquired from n successive and stable cardiac cycles with photoplethysmography (PPG) and EKG, respectively, for each testing subject [33]:

$$\{Amp\} = \{Amp(1), Amp(2), Amp(3), \ldots, Amp(n)\} \quad (1)$$

$$\{RRI\} = \{RRI(1), RRI(2), RRI(3), \ldots, RRI(n)\}. \quad (2)$$

2.3.2. Computation of Multiscale Small-Scale Entropy Index (MEI$_{SS}$). Multiscale entropy (MSE) was first proposed by Costa et al. [21] as a method for analyzing the complexity of time series of nonlinear signals in 2002 using the RRI time series as mentioned in (2) above. MSE consists of two main procedures, including coarse-graining and computation of sample entropy for each coarse-grained time series as detailed below.

(1) Coarse-Graining. Coarse-graining is the process of creating new time series of different lengths through averaging
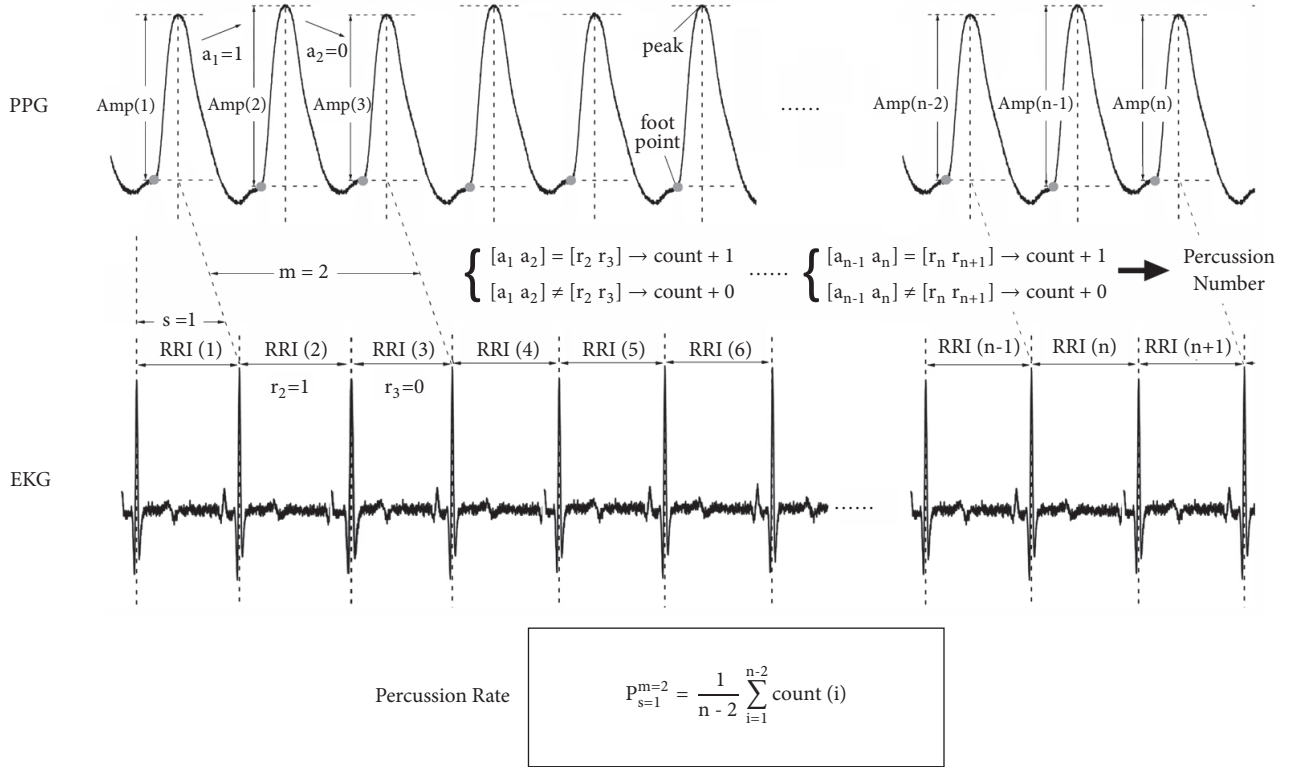
FIGURE 1: Computation of percussion rate by matching changes in the amplitudes (Amp, defined as the height of a waveform from foot point to peak) of n successive photoplethysmography (PPG)-acquired digital volume pulse (DVP) waveforms with changes in R-R intervals (RRI) using a shift number (s) of 1 and the dimension of vector pattern (m) (i.e., impact points) of 2. Note that n = 1000 for the present study. PPG: photoplethysmography; EKG: electrocardiogram; Amp(n): amplitude of DVP waveform during n^{th} cardiac cycle; RRI(n): R-R interval during n^{th} cardiac cycle; a: binary code denoting increase (i.e., 1) or decrease (i.e., 0) in amplitude when compared with the previous waveform; r: binary code denoting increase (i.e., 1) or decrease (i.e., 0) in RRI when compared with the previous cardiac cycle.

successive points in the original series according to a scale factor, τ, which is the number of points to be included:

$$RRI(a)^\tau = \frac{1}{\tau} \sum_{i=(a-1)\tau+1}^{a\tau} RRI(i),$$

$$1 \le a \le \frac{n}{\tau}, \ a \text{ is positive integer number.}$$

(3)

Here n is the number of points in the original {RRI} time series (i.e., n = 1000 in the present study). RRI(i) refers to the duration of RRI of the ith cardiac cycle (2). RRI($a)^\tau$ is the value of RRI during the ath cardiac cycle in the new time series created according to τ ($\tau = 1, 2, \ldots, 10$ in the present study).

For instance, coarse-graining (i.e., (3)) can transform a time series {RRI} with 1000 points to a new series with 500 points when $\tau = 2$ and to another time series with 333 points when $\tau = 3$. Following the same pattern of computation, a time series with 100 points can be obtained when $\tau = 10$. In other words, through coarse-graining, the original {RRI} time series can be transformed into 10 series of different lengths (i.e., number of points). For the purpose of the present study, the sample entropy for each of the 10 series was computed for analysis.

(2) Sample Entropy. Sample entropy was first introduced in the year 2000 for the assessment of complexity in physiological time series [34]. The computation of sample entropy involves three parameters, namely, m, r, and n. While m is the dimension of vector pattern (i.e., impact points), r is the range of acceptable fluctuation within the comparable time segments and n is the number of points in the time series (i.e., length of the series). The process of computation is described as follows:

(1) R-R intervals (RRI) of different time scales were grouped into n-m+1 vectors with dimension m:

$$u_m(i)$$
$$= [RRI(j) \ RRI(j+1) \ RRI(j+2) \ \cdots \ RRI(j+m-1)], \quad (4)$$
$$1 \le j \le n-m+1.$$

For instance, to analyze the changes in RRI among three cardiac cycles, m is set at 2 (Figure 1). Accordingly, to discern the fluctuations among four cardiac cycles, m is set at 3. For the purpose of the present study that analyzed 1000 cardiac cycles, m was set at 2 and 3 for the assessment of complexity of signals acquired from each testing subject.

(2) Define $d[u_m(i), u_m(j)]$ as the maximum value:

$$d\left[u_m(i), u_m(j)\right]$$
$$= \max\left\{\left|RRI(i+k) - RRI(j+k)\right| : 0 \le k \le m-1\right\}, \quad (5)$$
$$(i \ne j).$$

Two time segments were considered comparable when the absolute value of the difference between their respective components was less than the range of acceptable fluctuation, r (i.e., $d[u_m(i), u_m(j)] \le r$ in (5)). The acceptable range, r, was defined as 0.15 × SD (where SD is the standard deviation of the original time series) according to a previous study [35].

(3) Count the number of $d[u_m(i), u_m(j)]$ within r distance, and let $no_m(r)$ represent the number of vectors $u_m(j)$ within r distance of $u_m(i)$. Therefore, $C^m(r)$ in (6) represents the probability that any vectors $u_m(j)$ exist within r distance of $u_m(i)$.

$$C^m(r) = \frac{no_m(r)}{(n-m+1)} \quad (6)$$

(4) The mean of the probability of similarity of n-m+1 sets of data is denoted by $\Phi^m(r)$.

$$\Phi^m(r) = \frac{1}{n-m+1} \sum_{j=1}^{N-m+1} C^m(r) \quad (7)$$

(5) Similarly, repeating step (1) to step (4) above with m+1 gives $\Phi^{m+1}(r)$. The sample entropy of the RRI time series at a particular time scale can then be obtained.

$$\text{Sample entropy} (S_E) = \ln\left(\Phi^m(r)\right) - \ln\left(\Phi^{m+1}(r)\right)$$
$$= \ln \frac{\Phi^m(r)}{\Phi^{m+1}(r)} \quad (8)$$

After acquisition of 10 time series from (3) using different time scales (i.e., τ from 1 to 10), the corresponding sample entropy for each time series was computed using (8). Each sample entropy value provides information on an aspect of complexity. Previous studies have reported that small-scale entropy index (MEI_{SS}) and large-scale entropy index (MEI_{LS}) obtained by taking the average of sample entropy values from 1 to 5 and from 6 to 10, respectively, can reflect the complexity of different physiological systems. While MEI_{SS} represents the complexity of signals from the autonomic nervous system, MEI_{LS} reflects signal complexity of the vascular system [35, 36]. Accordingly, since the present study is aimed at investigating autonomic nervous function, MEI_{SS} of the testing subjects was acquired for comparison.

$$MEI_{SS} = \frac{1}{5} \sum_{\tau=1}^{5} (S_E) \quad (9)$$
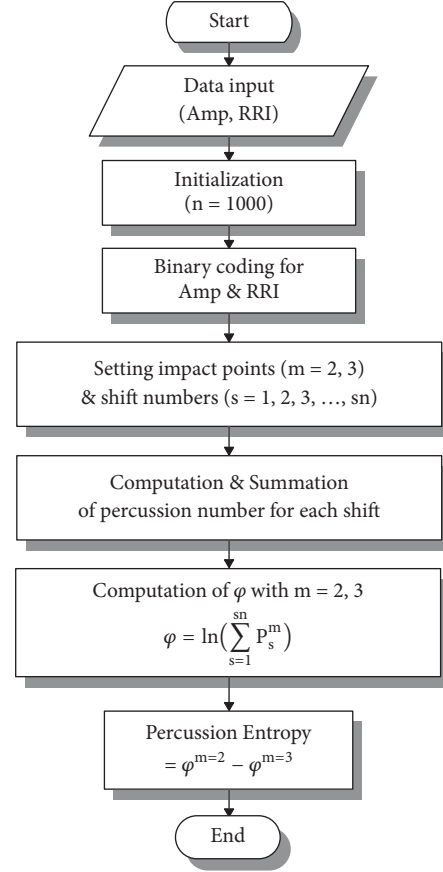
Figure 2: Flow chart of percussion entropy computation. Amp: amplitude; RRI: R-R interval.

2.3.3. Computation of Percussion Entropy Index (PEI).
The computation of percussion entropy index (PEI) comprises the following (Figure 2).

Step 1. Binary sequence transformation for {Amp} and {RRI}

$$B_{Amp} = \left\{a_1 \quad a_2 \quad a_3 \quad \cdots \quad a_n\right\},$$

$$a_i = \begin{cases} 0, & Amp(i+1) \le Amp(i) \\ 1, & Amp(i+1) > Amp(i) \end{cases} \quad (10)$$

$$B_{RRI} = \left\{r_1 \quad r_2 \quad r_3 \quad \cdots \quad r_n\right\},$$

$$r_i = \begin{cases} 0, & RRI(i+1) \le RRI(i) \\ 1, & RRI(i+1) > RRI(i) \end{cases} \quad (11)$$

Based on the previous finding that the change in amplitudes of DVP waveforms reflects the fluctuation in blood pressure [26–28] that gives rise to a corresponding compensatory change in RRI because of baroreflex, the fluctuations among successive DVP waveform amplitudes and RRIs undergo binary transformation to give two binary sequences (i.e., B_{Amp} and B_{RRI}, respectively).

Step 2. Define the series B_{Amp} and B_{RRI} with length n as well as the two parameters of m and sn [where m is the impact points (i.e., embedded dimension of vectors); sn is the shift number of B_{RRI}].

Step 3. Define n − m + 1 vectors of sample pattern, each of size m, composed as follows:

$$B_{Amp}(i) = \{a_i, a_{i+1}, \ldots, a_{i+m-1}\}, \quad 1 \leq i \leq n-m+1. \quad (12)$$

Step 4. For s = 1 to sn (i.e., shift numbers) for the series B_{RRI}

$$B_{RRI}(i+s) = \{r_{i+s}, r_{i+s+1}, \ldots, r_{i+s+m-1}\},$$
$$1 \leq i \leq n-m+1, \ s = 1 \text{ to sn.} \quad (13)$$

Although an increase in blood pressure would cause a prolongation of RRI in the next cardiac cycle in healthy young subjects, this baroreflex response may be delayed in the elderly or those with systemic diseases [2, 11, 17]. Therefore, we assumed that variations in baroreflex sensitivity would cause corresponding delays (counted as number of cardiac cycles, i.e., 1, 2, 3. . . sn) in the effects of blood pressure changes (i.e., reflected in DVP amplitudes) on RRI.

Step 5. Count the match number for $B_{Amp}(i)$ and $B_{RRI}(i + s)$ with given m.

In addition, calculate the total match number of $B_{Amp}(i)$ and $B_{RRI}(i+s)$ with the same pattern (i.e., percussion number) and divide by the total number of vectors of pattern (n-m-s+1) to obtain the percussion rate, which is defined as

$$P_s^m = \frac{1}{(n - m - s + 1)} \sum_{i=1}^{n-m-s+1} \text{count}(i). \quad (14)$$

For example (Figure 1), $P_{s=1}^{m=2} = (1/(n - 2)) \sum_{i=1}^{n-2} \text{count}(i)$ is a binary amplitude series (B_{Amp}) to be compared to a binary RRI series (B_{RRI}) with a left shift of one cardiac cycle (s=1) in the same testing subject. Comparing the amplitudes of three consecutive waveforms gives two binary codes [a_1 a_2] denoting increase (i.e., 1) or decrease (i.e., 0). Similarly, [r_2 r_3] are binary codes representing increase or decrease in RRI of three successive cardiac cycles with a shift number of 1 (i.e., s = 1) shown on EKG.

Matching the two binary codes from changes in waveform amplitudes and the two binary codes of changes in RRI from EKG with left shift of one cardiac cycle gives a number 1 or 0.

$$[a_1 \ a_2] = [r_2 \ r_3] \longrightarrow \text{count} + 1$$
$$[a_1 \ a_2] \neq [r_2 \ r_3] \longrightarrow \text{count} + 0 \quad (15)$$

Similarly, the process continues till the amplitude of the nth waveform.

$$[a_{n-1} \ a_n] = [r_n \ r_{n+1}] \longrightarrow \text{count} + 1$$
$$[a_{n-1} \ a_n] \neq [r_n \ r_{n+1}] \longrightarrow \text{count} + 0 \quad (16)$$

Summation of all the numbers of matches (i.e., percussion number) is thus obtained and divided by the total number

of vectors of pattern gives the "percussion rate" (14). For instance, if the number of impact points (m) is 2 with a delay of one cardiac cycle [i.e., shift number (s) = 1] (Figure 1), then

$$P_{s=1}^{m=2} = \frac{1}{n - 2} \sum_{i=1}^{n-2} \text{count}(i). \quad (17)$$

Step 6. Because diabetes is known to delay the reaction time of baroreflex due to impaired sensitivity [2, 11, 17], we assume that there would be a delay in cardiac cycle from one to sn. Taking logarithm of the sum of percussion rates (P_s^m) from shift number 1 to sn (i.e., s = 1, 2, . . . , sn) gives

$$\varphi^m(n) = \ln\left(\sum_{s=1}^{sn} P_s^m\right),$$
$$\text{ln: natural logarithmic operation.} \quad (18)$$

For the present study, $\varphi^{m=2}(n)$ was used to assess baroreflex sensitivity.

Step 7. Increase impact points (i.e., the embedded dimension) to (m+1) and repeat Steps 2–6 to get

$$P_s^{m+1} = \frac{1}{(n - m - s + 2)} \sum_{i=1}^{n-m-s+2} \text{count}(i), \quad (19)$$

$$\varphi^{m+1}(n) = \ln\left(\sum_{s=1}^{sn} P_s^{m+1}\right). \quad (20)$$

In the current study, $\varphi^{m=3}(n)$ indicated the complexity of a biological system. The higher the value of $\varphi^{m=3}(n)$, the lower the complexity of the biological system.

Step 8. Therefore, percussion entropy index (PEI) can be defined from (18) and (20):

$$\text{PEI}(m, s, n) = \varphi^m(n) - \varphi^{m+1}(n), \quad (21)$$

$$= \ln\left[\frac{\sum_{s=1}^{sn} P_s^m}{\sum_{s=1}^{sn} P_s^{m+1}}\right]. \quad (22)$$

In (21) and (22), m represents the chosen impact points (i.e., vector dimension), s represents a shift number for B_{RRI}, and n is the data length.

In other words, the degree of similarity between the changes in the binary series of digital volume pulse (DVP) waveform amplitudes (B_{Amp}) and the corresponding fluctuations in the binary series of RRI (B_{RRI}) on electrocardiogram over n cardiac cycles were first compared using a vector dimension of m, taking into account the possible delay in baroreflex from one cardiac cycle to sn cardiac cycles. The computation was then repeated with a vector dimension of m+1 over the same set of data points. Subtraction of the latter from the former gave the percussion entropy index (PEI) as in (21). The present study adopted an embedded vector dimension number of 2 (i.e., impact points, m = 2) to compute the value of percussion entropy, $\varphi^{m=2}(n)$.

Similarly, using m = 3, the percussion entropy value, $\varphi^{m=3}(n)$, was obtained. PEI was then obtained through subtracting $\varphi^{m=3}(n)$ from $\varphi^{m=2}(n)$. Physiologically, $\varphi^{m=2}(n)$ represents baroreflex sensitivity, while $\varphi^{m=3}(n)$ reflects the complexity of a biological system. The higher the former, the more sensitive the baroreflex. By contrast, an elevated value of the latter denotes decreased complexity of the acquired signals that implicates an impaired physiological status. Therefore, the optimal physiological condition would be $\varphi^{m=2}(n) \gg \varphi^{m=3}(n)$ (i.e., a high PEI value) when both baroreflex sensitivity and physiological complexity are high.

2.4. Statistical Analysis. Average values are expressed as mean ± SD. One sample Kolmogorov-Smirnov test was used for testing the normality of distribution, while the Statistical Package for the Social Science (SPSS, version 14.0 for Windows, SPSS Inc. Chicago, II) was adopted for verifying the homoscedasticity of variables. The significance of difference in anthropometric, hemodynamic, and computational parameters (i.e., PEI, MEI$_{SS}$, LHR, SSR) among different groups was determined using independent sample t-test with Bonferroni correction. The correlation between parameters and risk factors for different groups was compared using Pearson correlation test with Bonferroni correction. For significant parameters acquired through univariate analysis, multivariate regression analysis was used for further verification of the statistical significance. SPSS was used for all statistical analyses.

In statistical hypothesis testing, the probability value (i.e., p-value) or asymptotic significance is the probability for a given statistical model that, when the null hypothesis is true, the statistical summary (e.g., the sample mean difference between two compared groups) would be greater than or equal to the actual observed results. Although the level of significance is commonly set to 0.05, the p-values may need to be corrected for multiple test comparison. For the purpose of the present study, a corrected p-value of 0.017 was used because of comparison among three groups (i.e., 0.05 divided by three). Pearson's correlation coefficient, also referred to as Pearson's r, is a measure of the linear correlation between two variables X and Y. It has a value between +1 and −1. While 1 stands for total positive linear correlation, 0 means no linear correlation, and −1 signifies total negative linear correlation.

3. Results

3.1. Choice of Shift Number for Percussion Entropy Index Computation. The changes in percussion entropy index with shift number in all testing subjects are shown in Figure 3. Successful discrimination among the three groups was noted at shift number 5. Therefore, shift number 5 was used for percussion entropy index computation to ensure adequate coverage of possible delays due to impaired baroreflex sensitivity; the parameters of this study were set at m = 2, n = 1000, and s = 1 to 5.

3.2. Comparison of Computational Parameters for Autonomic Function Assessment. The results of comparing the two
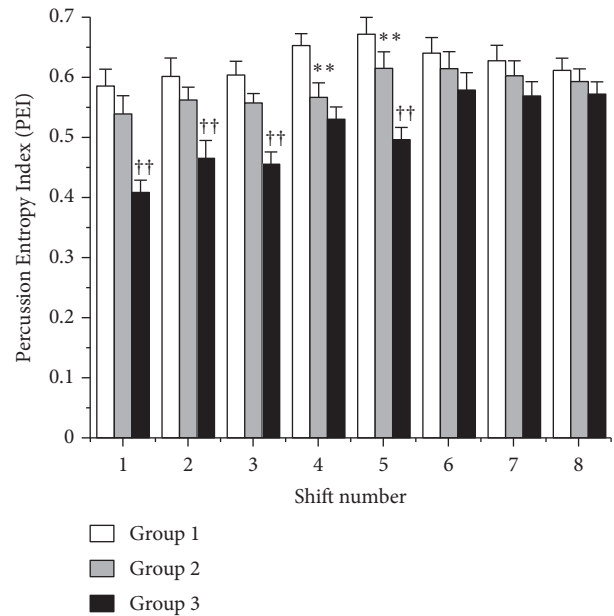
FIGURE 3: Changes in percussion entropy index of the three groups of testing subjects from shift number (s) of 1 to 8; $^{**}p < 0.001$: Group 1 vs. Group 2; $^{\dagger\dagger}p < 0.001$: Group 2 vs. Group 3; Group 1: healthy subjects; Group 2: diabetic subjects with satisfactory blood sugar control; Group 3: diabetic subjects with poor blood sugar control. Values are expressed as mean ± SD.

one-dimensional HRV-based computational parameters (i.e., LHR and SSR) with percussion entropy index (PEI) for autonomic function assessment among the three groups of testing subjects are shown in Table 2. Although SSR was significantly higher in Group 2 than that in Group 1 ($p < 0.017$), there was no notable difference in LHR among the three groups. On the other hand, both MEI$_{SS}$ and PEI successfully discriminated among the three groups (all $p < 0.017$), although the discrimination between Group 1 and Group 2 was more significant with PEI ($p < 0.001$) compared to that with MEI$_{SS}$ ($p < 0.017$).

3.3. Correlations of Demographic, Anthropometric, Hemodynamic, and Serum Biochemical Data with Computational Parameters for Autonomic Function Assessment in All Testing Subjects. Significant associations were noted between LHR and serum triglyceride concentration as well as between SSR and fasting blood sugar concentration (both $p < 0.017$) (Table 3). MEI$_{SS}$ showed a significant positive association with glycated hemoglobin level ($p < 0.005$), which is an index of chronic diabetes control, but not with fasting blood sugar concentration, an indicator of acute diabetes control. On the other hand, percussion entropy was significantly related to fasting blood sugar concentration ($p < 0.017$) and highly significantly associated with glycated hemoglobin level ($p < 0.001$).

3.4. Multivariate Analysis for PEI, MEI$_{SS}$, SSR, and LHR. The demographic, anthropometric, hemodynamic, and serum biochemical parameters of the testing subjects found to be

TABLE 2: Comparison of computational parameters for autonomic function assessment in three groups of testing subjects.

Parameters	Group 1 (n = 41)	Group 2 (n = 36)	Group 3 (n = 31)
LHR	1.62 ± 1.03	1.59 ± 1.54	2.48 ± 2.43
SSR	0.47 ± 0.22	0.61 ± 0.27*	0.61 ± 0.31
MEI_{SS}	0.56 ± 0.08	0.54 ± 0.02*	0.44 ± 0.13††
PEI	0.73 ± 0.04	0.63 ± 0.05**	0.56 ± 0.06††

Group 1: healthy subjects; Group 2: diabetic subjects with satisfactory blood sugar control; Group 3: diabetic subjects with poor blood sugar control. Values are expressed as mean ± SD. LHR: low- to high-frequency power ratio; SSR: Poincaré index (SD1/SD2 ratio); MEI_{SS}: small-scale multiscale entropy index (mean value of sample entropy from time scale from 1 to 5); PEI: percussion entropy index; *$p < 0.017$: Group 1 vs. Group 2; **$p < 0.001$: Group 1 vs. Group 2; ††$p < 0.001$ Group 2 vs. Group 3.

TABLE 3: Associations of demographic, anthropometric, hemodynamic, and serum biochemical data with computational parameters for autonomic function assessment in all testing subjects.

	PEI r	PEI p	MEI_{SS} r	MEI_{SS} p	SSR r	SSR p	LHR r	LHR p
Age (years)	0.10	0.562	0.06	0.662	0.02	0.832	0.09	0.398
BH (cm)	0.14	0.251	0.13	0.351	-0.02	0.887	0.17	0.142
BW (kg)	-0.10	0.397	-0.12	0.417	-0.07	0.580	0.14	0.244
WC (cm)	0.55	0.241	0.65	0.351	0.05	0.861	0.20	0.074
BMI (kg/m^2)	-0.16	0.173	0.03	0.573	-0.04	0.742	0.07	0.543
SBP (mmHg)	-0.06	0.641	-0.01	0.741	0.10	0.421	-0.02	0.870
DBP (mmHg)	0.06	0.620	0.07	0.650	0.10	0.409	0.10	0.419
PP (mmHg)	-0.15	0.189	-0.10	0.428	0.06	0.632	-0.10	0.436
HDL (mg/dL)	0.01	0.942	0.05	0.963	-0.01	0.946	-0.08	0.548
LDL (mg/dL)	-0.01	0.934	-0.06	0.534	-0.04	0.749	-0.10	0.449
Cholesterol (mg/dL)	-0.10	0.439	-0.09	0.539	-0.01	0.920	0.02	0.899
Triglyceride (mg/dL)	-0.09	0.468	-0.10	0.439	0.21	0.079	0.30	*0.012*
HbA1c (%)	0.16	*0.001*	0.14	*0.005*	0.11	0.371	0.01	0.946
FBS (mg/dL)	0.13	*0.012*	0.13	0.018	0.03	*0.014*	0.07	0.587

BH: body height; BW: body weight; WC: waist circumference; BMI: body mass index, SBP: systolic blood pressure; DBP: diastolic blood pressure; PP: pulse pressure; HbA1c: glycated hemoglobin; HDL: high-density lipoprotein cholesterol; LDL low-density lipoprotein cholesterol; FBS: fasting blood sugar. LHR: low- to high-frequency power ratio; SSR: Poincaré index (SD1/SD2 ratio); MEI_{SS}: small-scale multiscale entropy index (mean value of sample entropy from time scale from 1 to 5); PEI: percussion entropy index; $|r| \leqq 0.3$: correlation of low significance; $0.3 \leqq |r| \leqq 0.7$: correlation of moderate significance; $0.7 \leqq |r| \leqq 1$: highly significant correlation. *$p < 0.017$; **$p < 0.001$. Significance of correlations determined with Pearson correlation.

TABLE 4: Multivariate linear regression analysis for percussion entropy index (PEI), LHR, and SSR for all subjects (n = 108).

	PEI B-Coef	PEI β	PEI p	MEI_{SS} B-Coef	MEI_{SS} β	MEI_{SS} p	SSR B-Coef	SSR β	SSR p	LHR B-Coef	LHR β	LHR p
Variable												
FBS (mg/dL)	0.824	0.123	0.012	0.825	0.053	0.032	0.841	0.096	0.022	0.826	0.042	0.853
HbA1c (%)	0.654	0.714	<0.001	0.702	0.156	<0.001	0.734	0.037	0.041	0.724	0.129	0.566
Constant	0.894	-	<0.001	0.507	-	0.003	1.750	-	0.010	0.409	-	0.008

B-Coef: regression coefficient; β: standardized coefficient; FBS: fasting blood sugar; HbA1c: glycated hemoglobin; PEI: percussion entropy index; MEI_{SS}: small-scale multiscale entropy index (mean value of sample entropy from time scale from 1 to 5); SSR: Poincaré index (SD1/SD2 ratio); LHR: low- to high-frequency power ratio.

significantly associated with PEI in this study using Pearson correlation test were fasting blood sugar concentration and glycated hemoglobin level for which multivariate analysis was performed (Table 4). The results showed significant associations of PEI with fasting blood sugar and glycated hemoglobin levels in all subjects as a whole without focusing on the effects of age and diabetes (all $p < 0.05$). In addition, the interpreting effects [37] of the two independent variables, glycated hemoglobin level and fasting blood sugar concentration, on dependent variable PEI were 71.4% and 12.3%, respectively. In other words, with multiple linear regression, the results of the present study demonstrated an 83.7% accuracy when the two independent variables (i.e., glycated hemoglobin level and fasting blood sugar

concentration) were used to describe the dependent variable (i.e., PEI). In contrast, the interpreting effects of glycated hemoglobin level and fasting blood sugar concentration (i.e., independent variables) on the dependent variable MEI_{SS} were comparatively low at 15.6% and 5.3%, respectively.

4. Discussion

Diabetes is a common metabolic disease characterized by vasculopathy commonly involving the eyes [6] and kidneys [7]. Neuropathy is another well-known diabetes-associated complication [8]. Using the method of multiscale cross-approximate entropy, we previously investigated the feasibility of adopting a multiscale cross-approximate entropy index in detecting diabetes-related arterial stiffness as reflected by the crest time (CT) of the study subjects [38]. The results of that study indicated that although multiscale cross-approximate entropy could identify diabetes-associated subtle changes in vascular functional integrity, it failed to demonstrate the impact of diabetes on autonomic nervous function [38]. Therefore, focusing on diabetes-associated autonomic neuropathy, the present study proposed a new approach to the assessment of baroreflex impairment through comparing the tendency of changes between the primary time series (i.e., Amp that reflects fluctuations in blood pressure) and the secondary time series (i.e., RRI that indicates corresponding baroreflex-triggered heart rate alterations) among three successive cardiac cycles. Meanwhile, taking into account the healthy physiological complexity of human body, lack of variation in the tendency of changes among four successive cardiac cycles is regarded as unhealthy and was used as a negative contributor to computation of the percussion entropy index. The results of the current study indicated that, through taking into account the physiology of baroreflex [14–16], this novel approach could give additional information on diabetic autonomic dysfunction through comparing the pattern of changes between two simultaneously acquired physiological time series (i.e., digital volume pulse amplitude and R-R interval).

The present study, which attempted to assess the impact of diabetes and its control on autonomic nervous function by comparing the tendency of changes of two simultaneous physiological time series (i.e., DVP amplitude and RRI) in subjects with and without the disease, has several interesting implications. First, among the three one-dimensional approaches to HRV analysis [i.e., frequency (i.e., LHR) and time (i.e., SSR) domain as well as multiscale (i.e., MEI_{SS})], only MEI_{SS} successfully discriminated among nondiabetic subjects as well as those with diabetes with and without satisfactory blood sugar control. Besides, the two-dimensional percussion entropy index (PEI) showed better ability to differentiate between healthy subjects and those with well-controlled diabetes than that of MEI_{SS}. Second, PEI was the only parameter with significant correlations with both acute (i.e., fasting blood sugar concentration) and chronic (i.e., glycated hemoglobin level) blood sugar control indicators. Third, strong interpreting effects from the two independent sugar control variables were noted only for PEI but not MEI_{SS}, LHR, and SSR. The results, therefore, highlight its notable

sensitivity in detecting diabetes-associated autonomic dysfunction.

Previous studies have demonstrated that diabetes is associated with suppressed autonomic activities and blunted baroreflex [19, 39]. Previous studies have demonstrated the use of frequency domain [17–19] and time domain [20, 23] parameters in noninvasively assessing autonomic nervous function in diabetic patients but their sensitivities remain unclear. Taking into account the fact that baroreflex sensitivity is an indicator of autonomic function [15] as well as previous findings showing a good correlation between DVP signals and real-time changes in blood pressure [26–28], the current study investigated the possibility of assessing autonomic sensitivity through quantifying the matches between the two time series of DVP and RRI with a shift number of 1 to 5 based on the finding of a previous report that showed a delay of BRS between one to five heartbeats [16]. The finding of our study was consistent with that study [16] that using a shift number of 5 provided the best discriminating ability for PEI (Figure 3).

While considering the integrity of baroreflex by choosing a dimension of vector pattern (i.e., impact point, m) of 2, the physiological health of an individual as reflected in the complexity of signals was taken into account through adding a dimension of vector pattern of 3 into the computation of percussion entropy index (PEI). The major difference between multiscale entropy (MSE) and PEI is that the former evaluates changes in actual sample values within a defined range over time, whereas the latter simply compares the pattern of fluctuation between two related time series. In addition to utilizing the concept of MSE, PEI also encompasses the assessment of baroreflex sensitivity (BRS) (i.e., m = 2; higher value in (8) stands for higher BRS) and complexity (i.e., m =3; higher value in (10) represents lower complexity).

The present study has its limitations. First, the number of testing subjects in each group was relatively small. Nevertheless, highly significant associations between percussion entropy and indices of blood sugar control were still noted. Second, direct assessment of baroreflex sensitivity with either invasive or noninvasive means was not performed for comparison with the results of the current study.

5. Conclusions

This study demonstrated the validity of gaining additional information on diabetic autonomic dysfunction through comparing two simultaneously acquired physiological time series (i.e., digital volume pulse amplitude and R-R interval). The significant associations of percussion entropy with the indices of blood sugar control also highlight its possible role in early screening of the disease. The successful identification of the markers for diabetes by comparing the nonlinear coupling behavior of two synchronized time series of different natures raises the possibility of identifying the risk factors for diseases of other organs through analyzing the complexity of synchronized physiological signals related to the respective organ systems.

Data Availability

No data were used to support this study.

Conflicts of Interest

The authors declare that there are no conflicts of interest regarding the publication of this paper.

Authors' Contributions

Hsien-Tsai Wu has equal contribution compared with the corresponding author.

Acknowledgments

References

[1] World Health Organization, "Global report on diabetes," 2016.

[2] M. Debono and E. Cachia, "The impact of Cardiovascular Autonomic Neuropathy in diabetes: is it associated with left ventricular dysfunction?" *Autonomic Neuroscience: Basic and Clinical*, vol. 132, no. 1-2, pp. 1–7, 2007.

[3] P. O. Bonetti, L. O. Lerman, and A. Lerman, "Endothelial dysfunction: a marker of atherosclerotic risk," *Arteriosclerosis, Thrombosis, and Vascular Biology*, vol. 23, no. 2, pp. 168–175, 2003.

[4] F. Grover-Páez and A. B. Zavalza-Gómez, "Endothelial dysfunction and cardiovascular risk factors," *Diabetes Research and Clinical Practice*, vol. 84, no. 1, pp. 1–10, 2009.

[5] J. Pearson-Stuttard, B. Zhou, V. Kontis, J. Bentham, M. J. Gunter, and M. Ezzati, "Worldwide burden of cancer attributable to diabetes and high body-mass index: a comparative risk assessment," *The Lancet Diabetes & Endocrinology*, vol. 6, no. 6, pp. e6–e15, 2018.

[6] D. A. Antonetti, R. Klein, and T. W. Gardner, "Diabetic retinopathy," *The New England Journal of Medicine*, vol. 366, no. 13, pp. 1227–1239, 2012.

[7] G. Remuzzi, A. Schieppati, and P. Ruggenenti, "Clinical practice. Nephropathy in patients with type 2 diabetes," *The New England Journal of Medicine*, vol. 346, no. 15, pp. 1145–1151, 2002.

[8] A. I. Vinik, "Clinical practice. Diabetic sensory and motor neuropathy," *The New England Journal of Medicine*, vol. 374, no. 15, pp. 1455–1464, 2016.

[9] J.-P. Le Floch, J. Doucet, B. Bauduceau, and C. Verny, "Retinopathy, nephropathy, peripheral neuropathy and geriatric scale scores in elderly people with type 2 diabetes," *Diabetic Medicine*, vol. 31, no. 1, pp. 107–111, 2014.

[10] S. Lankhorst, S. W. M. Keet, C. S. E. Bulte, and C. Boer, "The impact of autonomic dysfunction on peri-operative cardiovascular complications," *Anaesthesia*, vol. 70, no. 3, pp. 336–343, 2015.

[11] J. D. Lefrandt, A. J. Smit, C. J. Zeebregts, R. O. Gans, and K. H. Hoogenberg, "Autonomic dysfunction in diabetes: a consequence of cardiovascular damage," *Current Diabetes Reviews*, vol. 6, no. 6, pp. 348–358, 2010.

[12] V. Spallone, D. Ziegler, R. Freeman et al., "Cardiovascular autonomic neuropathy in diabetes: clinical impact, assessment, diagnosis, and management," *Diabetes/Metabolism Research and Reviews*, vol. 27, no. 7, pp. 639–653, 2011.

[13] H. V. Huikuri, V. Jokinen, M. Syvänne et al., "Heart rate variability and progression of coronary atherosclerosis," *Arteriosclerosis, Thrombosis, and Vascular Biology*, vol. 19, no. 8, pp. 1979–1985, 1999.

[14] G. D. Pinna, M. T. La Rovere, R. Maestri, A. Mortara, J. T. Bigger, and P. J. Schwartz, "Comparison between invasive and noninvasive measurements of baroreflex sensitivity: implications for studies on risk stratification after a myocardial infarction," *European Heart Journal*, vol. 21, no. 18, pp. 1522–1529, 2000.

[15] N. Wada, W. Singer, T. L. Gehrking, D. M. Sletten, J. D. Schmelzer, and P. A. Low, "Comparison of baroreflex sensitivity with a fall and rise in blood pressure induced by the valsalva manoeuvre," *Clinical Science (London)*, vol. 127, no. 5, pp. 307–313, 2014.

[16] P. Martínez-García, C. Lerma, and O. Infante, "Baroreflex sensitivity estimation by the sequence method with delayed signals," *Clinical Autonomic Research*, vol. 22, no. 6, pp. 289–297, 2012.

[17] R. Dalla Pozza, S. Bechtold, W. Bonfig et al., "Impaired short-term blood pressure regulation and autonomic dysbalance in children with type 1 diabetes mellitus," *Diabetologia*, vol. 50, no. 12, pp. 2417–2423, 2007.

[18] C. Li, Q. Chang, J. Zhang, and W. Chai, "Effects of slow breathing rate on heart rate variability and arterial baroreflex sensitivity in essential hypertension," *Medicine (Baltimore)*, vol. 97, no. 18, article e0639, 2018.

[19] M. Rosengård-Bärlund, L. Bernardi, J. Holmqvist et al., "Deep breathing improves blunted baroreflex sensitivity even after 30 years of type 1 diabetes," *Diabetologia*, vol. 54, no. 7, pp. 1862–1870, 2011.

[20] A. M. Climent, M. D. L. S. Guillem, D. Husser, F. Castells, J. Millet, and A. Bollmann, "Poincaré surface profiles of RR intervals: a novel noninvasive method for the evaluation of preferential AV nodal conduction during atrial fibrillation," *IEEE Transactions on Biomedical Engineering*, vol. 56, no. 2, pp. 433–442, 2009.

[21] V. Spallone and G. Menzinger, "Diagnosis of cardiovascular autonomic neuropathy in diabetes," *Diabetes*, vol. 46, no. 2, pp. S67–S76, 1997.

[22] G. Merati, M. Di Rienzo, G. Parati, A. Veicsteinas, and P. Castiglioni, "Assessment of the autonomic control of heart rate variability in healthy and spinal-cord injured subjects: contribution of different complexity-based estimators," *IEEE Transactions on Biomedical Engineering*, vol. 53, no. 1, pp. 43–52, 2006.

[23] C. Lerma, O. Infante, H. Pérez-Grovas, and M. V. José, "Poincare plot indexes of heart rate variability capture dynamic adaptations after haemodialysis in chronic renal failure patients," *Clinical Physiology and Functional Imaging*, vol. 23, no. 2, pp. 72–80, 2003.

[24] M. Costa, A. L. Goldberger, and C.-K. Peng, "Multiscale entropy analysis of complex physiologic time series," *Physical Review Letters*, vol. 89, no. 6, Article ID 068102, 2002.

[25] N. Takahashi, M. Nakagawa, T. Saikawa et al., "Noninvasive assessment of the cardiac baroreflex: Response to downward tilting and comparison with the phenylephrine method," *Journal of the American College of Cardiology*, vol. 34, no. 1, pp. 211–215, 1999.

[26] I. Jeong, S. Jun, D. Um, J. Oh, and H. Yoon, "Non-invasive estimation of systolic blood pressure and diastolic blood pressure using photoplethysmograph components," *Yonsei Medical Journal*, vol. 51, no. 3, pp. 345–353, 2010.

[27] H. Shin and S. D. Min, "Feasibility study for the non-invasive blood pressure estimation based on ppg morphology: normotensive subject study," *Biomedical Engineering Online*, vol. 16, no. 1, p. 10, 2017.

[28] X. Xing and M. Sun, "Optical blood pressure estimation with photoplethysmography and fft-based neural networks," *Biomedical Optics Express*, vol. 7, no. 8, pp. 3007–3020, 2016.

[29] American Diabetes Association, "Diagnosis and classification of diabetes mellitus," *Diabetes Care*, vol. 37, supplement 1, pp. S81–S90, 2014.

[30] H. T. Wu, P. C. Hsu, C. F. Lin et al., "Multiscale entropy analysis of pulse wave velocity for assessing atherosclerosis in the aged and diabetic," *IEEE Transactions on Biomedical Engineering*, vol. 58, no. 10, pp. 2978–2981, 2011.

[31] H. T. Wu, K. W. Lee, W. Y. Pan, A. B. Liu, and C. K. Sun, "Difference in bilateral digital volume pulse as a novel non-invasive approach to assessing arteriosclerosis in aged and diabetic subjects: a preliminary study," *Diabetes & Vascular Disease Research*, vol. 14, no. 3, pp. 254–257, 2017.

[32] P.-C. Hsu, H.-T. Wu, and C.-K. Sun, "Assessment of subtle changes in diabetes-associated arteriosclerosis using photoplethysmographic pulse wave from index finger," *Journal of Medical Systems*, vol. 42, no. 3, p. 43, 2018.

[33] A.-B. Liu, P.-C. Hsu, Z.-L. Chen, and H.-T. Wu, "Measuring pulse wave velocity using ECG and photoplethysmography," *Journal of Medical Systems*, vol. 35, no. 5, pp. 771–777, 2011.

[34] J. S. Richman and J. R. Moorman, "Physiological time-series analysis using approximate entropy and sample entropy," *American Journal of Physiology-Heart and Circulatory Physiology*, vol. 278, no. 6, pp. H2039–H2049, 2000.

[35] M. Costa, A. L. Goldberger, and C. K. Peng, "Multiscale entropy analysis of biological signals," *Physical Review E: Statistical, Nonlinear, and Soft Matter Physics*, vol. 71, no. 2, Article ID 021906, pp. 1–18, 2005.

[36] W.-Y. Pan, M.-C. Su, H.-T. Wu, T.-J. Su, M.-C. Lin, and C.-K. Sun, "Multiscale entropic assessment of autonomic dysfunction in patients with obstructive sleep apnea and therapeutic impact of continuous positive airway pressure treatment," *Sleep Medicine*, vol. 20, pp. 12–17, 2016.

[37] F. E. Harrell Jr., "Describing, resampling, validating, and simplifying the model," in *Regression Modeling Strategies with Applications to Linear Models, Logistic and Ordinal Regression, and Survival Analysis*, F. E. Harrell Jr., Ed., Springer Series in Statistics, pp. 103–126, Springer, Switzerland, 2015.

[38] M.-X. Xiao, H.-C. Wei, Y.-J. Xu, H.-T. Wu, and C.-K. Sun, "Combination of R-R interval and crest time in assessing complexity using multiscale cross-approximate entropy in normal and diabetic subjects," *Entropy*, vol. 20, no. 7, pp. 1–15, 2018.

[39] A. N. Syamsunder, P. Pal, G. K. Pal et al., "Decreased baroreflex sensitivity is linked to the atherogenic index, retrograde inflammation, and oxidative stress in subclinical hypothyroidism," *Endocrine Research*, vol. 42, no. 1, pp. 49–58, 2017.

Research Article

A Parameter-Free Model Comparison Test Using Differential Algebra

Heather A. Harrington [ID],[1] Kenneth L. Ho,[2] and Nicolette Meshkat[3]

[1]*Mathematical Institute, University of Oxford, Oxford OX2 6GG, UK*
[2]*Department of Mathematics, Stanford University, Stanford, CA 94305, USA*
[3]*Department of Mathematics and Computer Science, 500 El Camino Real, Santa Clara University, Santa Clara, CA 95053, USA*

Correspondence should be addressed to Heather A. Harrington; harrington@maths.ox.ac.uk

We present a method for rejecting competing models from noisy time-course data that does not rely on parameter inference. First we characterize ordinary differential equation models in only measurable variables using differential-algebra elimination. This procedure gives input-output equations, which serve as invariants for time series data. We develop a model comparison test using linear algebra and statistics to reject incorrect models from their invariants. This algorithm exploits the dynamic properties that are encoded in the structure of the model equations without recourse to parameter values, and, in this sense, the approach is parameter-free. We demonstrate this method by discriminating between different models from mathematical biology.

1. Introduction

Given competing mathematical models to describe a process, we wish to know whether our data are compatible with the candidate models. Often comparing models requires optimization and fitting time-course data to estimate parameter values and then apply an information criterion to select a "best" model [1]. However sometimes it is not feasible to estimate the value of these unknown parameters (e.g., large parameter space, nonlinear objective function, nonidentifiability, etc.). In this paper, we compare candidate models with time-course data while avoiding the parameter estimation problem by considering a "parameter-free" approach.

The parameter problem has motivated the growth of fields that embrace a parameter-free flavor such as chemical reaction network theory and stoichiometric theory [2–4]. However many of these approaches are limited to comparing the behavior of models at steady-state [5–7]. Inspired by techniques commonly used in applied algebraic geometry [8] and algebraic statistics [9], methods for discriminating between possible models without estimating parameters have been developed for steady-state data [10, 11]. These approaches characterize a model in only observable variables—called

a *steady-state invariant* [5]—using techniques from computational algebraic geometry and determine whether the noisy steady-state data are compatible with this steady-state invariant via a statistical test. However, unlike other Bayesian and parameter estimation approaches, it does not select models; it can only rule them out. Notably the method does not require parameter estimation, hence there is the term parameter-free.

Extending the method developed in [10], we present a method for comparing models using time-course data instead of steady-state data. In this approach we compute input-output equations, which we refer to as input-output invariants for time series data. We consider state-space ordinary differential equations (ODE) models of the form $\dot{\mathbf{x}}(\mathbf{t}) = \mathbf{f}(\mathbf{x}(\mathbf{t}), \mathbf{u}(\mathbf{t}), \mathbf{p})$ and $\mathbf{y}(t) = \mathbf{g}(\mathbf{x}(t), \mathbf{p})$ where $x_k(t)$ are species variables, $k = 1, \ldots, N$, $u_i(t)$ is a known input into the system, $i = 1, \ldots, L$, $y_j(t)$ is a known output (measurement) from the system, $j = 1, \ldots, M$, $\mathbf{p}$ is the unknown R–dimensional parameter vector, and the functions $\mathbf{f}, \mathbf{g}$ are rational functions of their arguments. The dynamics of the model can be observed in terms of a time series where $\mathbf{u}(t)$ is the input at discrete points and $\mathbf{y}(t)$ is the output.

In this setting, we aim to characterize our ODE models by eliminating variables that we cannot measure using differential elimination from differential algebra [12]. From the elimination, we obtain a system of equations in 0, 1, and higher order derivatives forming the *input-output invariants*: $F_j(\mathbf{u}, \dot{\mathbf{u}}, \ddot{\mathbf{u}}, \dddot{\mathbf{u}}, \ldots, \mathbf{y}, \dot{\mathbf{y}}, \ddot{\mathbf{y}}, \dddot{\mathbf{y}}, \ldots) = \mathbf{0}$, $j = 1, \ldots, M$. Importantly, the coefficients of these equations are rational functions of the parameters. We will see shortly that, in the linear case, F_j is a linear differential equation. For nonlinear models, F_j is nonlinear. Computing input-output invariants is described in Section 2.

In order to test model compatibility, we substitute the data into the input-output invariant, which is given in the form of $\mathbf{u}, \dot{\mathbf{u}}, \ddot{\mathbf{u}}, \dddot{\mathbf{u}}, \ldots, \mathbf{y}, \dot{\mathbf{y}}, \ddot{\mathbf{y}}, \ldots$ evaluated at given time points. This results in a linear system of equations, $A\kappa = b$, where each row of A and b corresponds to the input-output invariant evaluated at a different time point. The components of κ are the coefficient functions of the parameters in the input-output invariants. The set-up of the model compatibility test is given in Section 3.

Then we ask: does there exist a κ such that $A\kappa = b$. If $b = 0$, of course we are guaranteed a zero trivial solution and the nontrivial solution can be determined via a rank test (e.g., singular value decomposition, or SVD). Since data may be imperfect, we can perform the statistical criterion developed in [10] with the bound improved in [11] to determine whether or not to reject the model. One of the key differences in adapting this method to time-course data is considering $A\kappa = b$ when $b \neq 0$. For $A\kappa = b$, there may be no solutions. Thus, we must check if the linear system of equations $A\kappa = b$ is consistent, i.e., has one or infinitely many solutions. We present a rank test, based on the SVD, for determining the compatibility of the data with input-output invariants from various (potentially incorrect) models. The linear solvability test is described in Section 4. We assume our data have Gaussian measurement noise. In Section 5, we derive a statistical cut-off for when the model is incompatible with the data.

Another key difference in this approach than previous parameter-free model discrimination methods is the occurrence of higher order derivatives of the input and output variables in the input-output invariants, requiring them to be known at various time instances. Often one does not have data points for the higher order derivatives, then these need to be estimated. Unlike numerical estimation or splines, which assume a specific functional form, one can use Gaussian Process Regression (GPR) to estimate the higher order derivatives from time-course data. In Section 6, we present such a method, which has previously been done for first and second derivatives of biological data [13]. Bounding error of derivative estimates is a difficult problem, which requires us to remove certain data points; however, the advantage of GPR is that one can consider a family of functions, which [13] points out to be able to capture many more temporal trends in the data than any one equation. This enables us to substitute the newly estimated derivative data into the input-output invariant and test model compatibility using the solvability test with the statistical cut-off that we present in Sections 4 and 5.

In Sections 4 and 7, we showcase our method with examples from linear and nonlinear models. Finally we discuss special cases and other related topics in Section 8, before concluding in Section 9.

2. Differential Elimination

We now give some background on differential algebra since a crucial step in our algorithm is to perform differential elimination to obtain equations purely in terms of input variables, output variables, and parameters. For this reason, we will only give background on the ideas from differential algebra required to understand the differential elimination process. For a more detailed description of differential algebra and the algorithms listed below, see [12, 14, 15]. In what follows, we assume the reader is familiar with concepts such as *rings* and *ideals*, which are covered in great detail in [8].

Definition 1. A ring S is said to be a *differential ring* if there is a derivative defined on S and S is closed under differentiation. A *differential ideal* is an ideal which is closed under differentiation.

Let our differential ideal be equipped with a *ranking*, i.e., a total ordering, denoted $<$, among the variables and their derivatives. Let $z_i^{(\mu)}$ and $z_j^{(\nu)}$ be arbitrary derivatives. Then the ranking should be such that, for arbitrary positive integer k:

$$z_i^{(\nu)} < z_i^{(\nu+k)},$$
$$z_i^{(\mu)} < z_j^{(\nu)} \implies \qquad (1)$$
$$z_i^{(\mu+k)} < z_j^{(\nu+k)}$$

Let u_j be the leader of a polynomial A_j, which is the highest ranking derivative of the variables appearing in that polynomial. A polynomial A_i is said to be of *lower rank* than A_j if the order of u_i is less than the order of u_j or, whenever $u_i = u_j$, the highest algebraic degree of any term containing the leader of A_i is less than the highest algebraic degree of any term containing the leader of A_j. A polynomial A_i is *reduced with respect to a polynomial A_j* if A_i contains neither the leader of A_j with equal or greater algebraic degree, nor its derivatives. If A_i is not reduced with respect to A_j, it can be reduced by using the pseudodivision algorithm in Section 2.1. A set of differential polynomials $A = \{A_1, A_2, \ldots, A_r\}$ that are all reduced with respect to each other is called an *auto-reduced set*.

Two auto-reduced sets, $A = \{A_1, A_2, \ldots, A_r\}$ and $B = \{B_1, B_2, \ldots, B_s\}$ ordered in increasing rank so that $A_1 < A_2 < \ldots < A_r, B_1 < B_2 < \ldots < B_s$, are ranked according to the following principle: if there is an integer k, $k \leq \min(s, r)$ such that rank A_i = rank B_i, $i = 1, \ldots, k-1$, rank $A_k <$ rank B_k, then A is said to be lower rank than B. If $r < s$ and rank A_i = rank B_i, $i = 1, \ldots, r$, then A is also said to be of lower rank than B.

A useful description of a differential ideal is called a *differential characteristic set*, which is a finite description of

a possibly infinite set of differential polynomials. We give the technical definition from [12].

Definition 2. Let Σ be a set of differential polynomials, not necessarily finite. If $A \subset \Sigma$ is an auto-reduced set, such that no lower ranked auto-reduced set can be formed in Σ, then A is called a *differential characteristic set*.

A well-known fact in differential algebra is that differential ideals need not be finitely generated [12, 15]. However, a radical differential ideal is finitely generated by the *Ritt-Raudenbush basis theorem* [16]. This result gives rise to Ritt's pseudodivision algorithm (see below), allowing us to compute the differential characteristic set of a radical differential ideal. We now describe various methods to find a differential characteristic set and other related notions, and we describe why they are relevant to our problem; namely, they can be used to find the *input-output equations*.

In what follows, we will be considering the differential ring $\mathbf{R}(\mathbf{p})[\mathbf{u}, \mathbf{y}, \mathbf{x}]$, where $\mathbf{R}(\mathbf{p})$ is the field of rational functions in the parameter vector $\mathbf{p}$. The variables in this differential ring are the states, the inputs, the outputs, and possibly their derivatives.

Consider an ODE system of the form $\dot{\mathbf{x}}(\mathbf{t}) = \mathbf{f}(\mathbf{x}(\mathbf{t}), \mathbf{p}, \mathbf{u}(\mathbf{t}))$ and $y_j(t) = g_j(\mathbf{x}(t), \mathbf{p})$ for $j = 1, \ldots, M$ with $\mathbf{f}$ and $\mathbf{g}$ rational functions of their arguments. Let our differential ideal be generated by the differential polynomials obtained by subtracting the right-hand-side from the ODE system to obtain $\dot{\mathbf{x}}(\mathbf{t}) - \mathbf{f}(\mathbf{x}(\mathbf{t}), \mathbf{p}, \mathbf{u}(\mathbf{t}))$ and $y_j(t) - g_j(\mathbf{x}(t), \mathbf{p})$ for $j = 1, \ldots, M$. In what follows, we use the ranking in [17], which is given by

$$\mathbf{u} < \dot{\mathbf{u}} < \ddot{\mathbf{u}} < \cdots < \mathbf{y} < \dot{\mathbf{y}} < \ddot{\mathbf{y}} < \cdots$$
$$< x_1 < x_2 < \cdots < \dot{x}_1 < \dot{x}_2 < \cdots \tag{2}$$

Note that the notation reflects the fact that the ordering among the components of $\mathbf{u}$ and $\mathbf{y}$ is immaterial, since these are known variables, whereas different ordering of the components of $\mathbf{x}$ may lead to different characteristic sets [17]. With respect to this ordering, a differential characteristic set is of the form [17]:

$$A_1(\mathbf{u}, \mathbf{y}), \ldots, A_M(\mathbf{u}, \mathbf{y})$$
$$A_{M+1}(\mathbf{u}, \mathbf{y}, x_1)$$
$$A_{M+2}(\mathbf{u}, \mathbf{y}, x_1, x_2)$$
$$\vdots \tag{3}$$
$$A_{M+N}(\mathbf{u}, \mathbf{y}, x_1, \ldots, x_N)$$

where A_i are differential polynomials. Note that the resulting system is not necessarily auto-reduced in $\mathbf{R}(\mathbf{p})[\mathbf{u}, \mathbf{y}, \mathbf{x}]$, namely, $A_1(u, y), \ldots, A_M(u, y)$ may not be auto-reduced. The first M terms of the differential characteristic set, $A_1(\mathbf{u}, \mathbf{y}), \ldots, A_M(\mathbf{u}, \mathbf{y})$, are those terms independent of the state variables and when set to zero form the *input-output equations*:

$$\mathbf{F}(\mathbf{u}, \dot{\mathbf{u}}, \ddot{\mathbf{u}}, \dddot{\mathbf{u}}, \ldots, \mathbf{y}, \dot{\mathbf{y}}, \ddot{\mathbf{y}}, \dddot{\mathbf{y}}, \ldots) = \mathbf{0}. \tag{4}$$

Specifically, the M input-output equations $\mathbf{F}(\mathbf{u}, \dot{\mathbf{u}}, \ddot{\mathbf{u}}, \dddot{\mathbf{u}}, \ldots, \mathbf{y}, \dot{\mathbf{y}}, \ddot{\mathbf{y}}, \dddot{\mathbf{y}}, \ldots) = \mathbf{0}$ are polynomial equations in the variables $\mathbf{u}, \dot{\mathbf{u}}, \ddot{\mathbf{u}}, \dddot{\mathbf{u}}, \ldots, \mathbf{y}, \dot{\mathbf{y}}, \ddot{\mathbf{y}}, \dddot{\mathbf{y}}, \ldots$ with rational coefficients in the parameter vector $\mathbf{p}$. Note that the differential characteristic set is in general non-unique, but the coefficients of the input-output equations can be fixed uniquely by normalizing the equations to make them monic.

We now discuss several methods to find the input-output equations. The first method (Ritt's pseudodivision algorithm) can be used to find a differential characteristic set for a radical differential ideal. The second method (RosenfeldGroebner) gives a representation of the radical of the differential ideal as an intersection of regular differential ideals and can also be used to find a differential characteristic set under certain conditions [18, 19]. Finally, we discuss Gröbner basis methods to find the *input-output equations*.

2.1. Ritt's Pseudodivision Algorithm.

An algorithm to find a differential characteristic set of a radical (in particular, prime) differential ideal generated by a finite set of differential polynomals is called Ritt's pseudodivision algorithm. We describe the process in detail below, which comes from the description in [17]. Note that our differential ideal as described above is a prime differential ideal [12, 20]. Let A_i and A_j be differential polynomials.

(1) If A_i contains the kth derivative $u_j^{(k)}$ of the leader of A_j, A_j is differentiated k times so its leader becomes $u_j^{(k)}$.

(2) Multiply the polynomial A_i by the coefficient of the highest power of $u_j^{(k)}$; let R be the remainder of the division of this new polynomial by $A_j^{(k)}$ with respect to the variable $u_j^{(k)}$. Then R is reduced with respect to $A_j^{(k)}$. The polynomial R is called the *pseudoremainder* of the pseudodivision.

(3) The polynomial A_i is replaced by the pseudoremainder R and the process is iterated using $A_j^{(k-1)}$ in place of $A_j^{(k)}$ and so on, until the pseudoremainder is reduced with respect to A_j.

This algorithm is applied to a set of differential polynomials, such that each polynomial is reduced with respect to each other, to form an auto-reduced set. The result is a differential characteristic set. Note that the multiplication mentioned in Step (2) above may yield a nonequivalent system if that coefficient happens to belong to the ideal. However, in practice, this does not occur for the ODE systems studied [17].

2.2. RosenfeldGroebner.

Using the `DifferentialAlgebra` package in Maple, one can find a representation of the radical of a differential ideal generated by some equations, as an intersection of radical differential ideals with respect to a given ranking [21]. Specifically, the `RosenfeldGroebner` command in Maple takes two arguments: `sys` and `R`, where `sys` is a list of set of differential equations or inequations

which are all rational in the independent and dependent variables and their derivatives and R is a differential polynomial ring built by the command `DifferentialRing` specifying the independent and dependent variables and a ranking for them [21]. Then `RosenfeldGroebner` returns a representation of the radical of the differential ideal generated by `sys`, as an intersection of radical differential ideals saturated by the multiplicative family generated by the inequations found in `sys`. This representation consists of a list of regular differential chains with respect to the ranking of R. Note that `RosenfeldGroebner` returns a differential characteristic set if the differential ideal is prime [18].

2.3. Gröbner Basis Methods. Finally, both algebraic and differential Gröbner bases can be employed to find the input-output equations. To use an algebraic Gröbner basis, one can take a sufficient number of derivatives of the model equations and then treat the derivatives of the variables as indeterminates in the polynomial ring in $\mathbf{x}$, $\dot{\mathbf{x}}$, $\ddot{\mathbf{x}}$,..., $\mathbf{u}$, $\dot{\mathbf{u}}$, $\ddot{\mathbf{u}}$,..., $\mathbf{y}$, $\dot{\mathbf{y}}$, $\ddot{\mathbf{y}}$,..., etc. Then a Gröbner basis of the ideal generated by this full system of (differential) equations with an elimination ordering where the state variables and their derivatives are eliminated first can be found. Details of this approach can be found in [22]. Differential Gröbner bases have been developed by Carrà Ferro [23], Ollivier [24], and Mansfield [25], but currently there are no implementations in computer algebra systems [14].

3. Model Rejection Using Input-Output Invariants

We now discuss how to use the input-output invariants obtained from differential elimination (using Ritt's pseudo-division, differential Gröbner bases, or some other method) for model selection/rejection.

We can write our input-output relations in (4), or input-output invariants, in the form:

$$\sum_i c_i(\mathbf{p})\,\psi_i(\mathbf{u}, \mathbf{y}) = 0 \tag{5}$$

The functions $\psi_i(\mathbf{u}, \mathbf{y})$ are differential monomials, i.e., monomials in the input/output variables $\mathbf{u}$, $\dot{\mathbf{u}}$, $\ddot{\mathbf{u}}$, $\dddot{\mathbf{u}}$, ..., $\mathbf{y}$, $\dot{\mathbf{y}}$, $\ddot{\mathbf{y}}$, $\dddot{\mathbf{y}}$, ..., etc., and the functions $c_i(\mathbf{p})$ are rational functions in the unknown parameter vector $\mathbf{p}$. In order to uniquely fix the rational coefficients $c_i(\mathbf{p})$ to the differential monomials $\psi_i(\mathbf{u}, \mathbf{y})$, we normalize each input/output equation to make it monic. In other words, we can rewrite our input-output relations as

$$\sum_i \widetilde{c}_i(\mathbf{p})\,\psi_i(\mathbf{u}, \mathbf{y}) = \xi(\mathbf{u}, \mathbf{y}) \tag{6}$$

Here $\xi(\mathbf{u}, \mathbf{y})$ is a differential monomial in the input/output variables $\mathbf{u}$, $\dot{\mathbf{u}}$, $\ddot{\mathbf{u}}$, $\dddot{\mathbf{u}}$, ..., $\mathbf{y}$, $\dot{\mathbf{y}}$, $\ddot{\mathbf{y}}$, $\dddot{\mathbf{y}}$, ..., etc. If the values of $\mathbf{u}$, $\dot{\mathbf{u}}$, $\ddot{\mathbf{u}}$, $\dddot{\mathbf{u}}$..., $\mathbf{y}$, $\dot{\mathbf{y}}$, $\ddot{\mathbf{y}}$, $\dddot{\mathbf{y}}$, ..., etc., were known at a sufficient number of time instances $t_1, t_2, \ldots, t_m$, then one could substitute in values of $\psi_i(\mathbf{u}, \mathbf{y})$ and $\xi(\mathbf{u}, \mathbf{y})$ at each of these time instances to obtain a linear system of equations in the variables $\widetilde{c}_i(\mathbf{p})$.

First consider the case of a single input-output equation. If there are n unknown coefficients $\widetilde{c}_i(\mathbf{p})$, we obtain the system:

$$\widetilde{c}_1(\mathbf{p})\,\psi_1(\mathbf{u}(t_1), \mathbf{y}(t_1)) + \cdots$$
$$+ \widetilde{c}_n(\mathbf{p})\,\psi_n(\mathbf{u}(t_1), \mathbf{y}(t_1)) = \xi(\mathbf{u}(t_1), \mathbf{y}(t_1))$$
$$\vdots \tag{7}$$
$$\widetilde{c}_1(\mathbf{p})\,\psi_1(\mathbf{u}(t_m), \mathbf{y}(t_m)) + \cdots$$
$$+ \widetilde{c}_n(\mathbf{p})\,\psi_n(\mathbf{u}(t_m), \mathbf{y}(t_m)) = \xi(\mathbf{u}(t_m), \mathbf{y}(t_m))$$

We write this linear system as $A\kappa = b$, where A is an m by n matrix of the form:

$$\begin{pmatrix} \psi_1(\mathbf{u}(t_1), \mathbf{y}(t_1)) & \cdots & \psi_n(\mathbf{u}(t_1), \mathbf{y}(t_1)) \\ \vdots & \vdots & \vdots \\ \psi_1(\mathbf{u}(t_m), \mathbf{y}(t_m)) & \cdots & \psi_n(\mathbf{u}(t_m), \mathbf{y}(t_m)) \end{pmatrix} \tag{8}$$

κ is the vector of unknown coefficients $[\widetilde{c}_1(\mathbf{p}), \ldots, \widetilde{c}_n(\mathbf{p})]^T$, and b is of the form $[\xi(\mathbf{u}(t_1), \mathbf{y}(t_1)), \ldots, \xi(\mathbf{u}(t_m), \mathbf{y}(t_m))]^T$.

For the case of multiple input-output equations, we get the following block diagonal system of equations $A\kappa = b$:

$$\begin{pmatrix} A_1 & 0 & 0 & \ldots & 0 \\ 0 & A_2 & 0 & \ldots & 0 \\ \vdots & \vdots & \ddots & \vdots & \vdots \\ 0 & 0 & 0 & \ldots & A_M \end{pmatrix} \begin{pmatrix} \kappa_1 \\ \kappa_2 \\ \vdots \\ \kappa_M \end{pmatrix} = \begin{pmatrix} b_1 \\ b_2 \\ \vdots \\ b_M \end{pmatrix} \tag{9}$$

where A is a $m = m_1 + \cdots + m_M$ by $n = n_1 + \cdots + n_M$ matrix.

In the symbolic setting, given a general input function $\mathbf{u}$ and generic initial conditions and parameters, this system $A\kappa = b$ should have a unique solution for κ, due to the persistence of excitation conditions [26]. In other words, we assume that the vectors of differential monomials $\psi_1, \ldots, \psi_n$ at various time points are linearly independent. This means the coefficients $\widetilde{c}_i(\mathbf{p})$ of the input-output equations can be uniquely determined in the generic setting [26]. Note that we have assumed that the parameters are all unknown and we have not taken any possible algebraic dependencies among the coefficients into account.

The main idea of this paper is to translate the symbolic setting to the numerical setting and can be described as follows. Assume we have perfect data; i.e., we know values of $\mathbf{u}$, $\dot{\mathbf{u}}$, $\ddot{\mathbf{u}}$, $\dddot{\mathbf{u}}$, ..., $\mathbf{y}$, $\dot{\mathbf{y}}$, $\ddot{\mathbf{y}}$, $\dddot{\mathbf{y}}$, ..., etc., at many time instances $t_1, \ldots, t_m$, perfectly. Given a set of candidate models, we find their associated input-output invariants and then substitute in our values of $\mathbf{u}$, $\dot{\mathbf{u}}$, $\ddot{\mathbf{u}}$, $\dddot{\mathbf{u}}$, ..., $\mathbf{y}$, $\dot{\mathbf{y}}$, $\ddot{\mathbf{y}}$, $\dddot{\mathbf{y}}$, ..., etc., at time instances $t_1, \ldots, t_m$, thus setting up the linear system $A\kappa = b$ for each model. With perfect data and assuming the persistence of excitation conditions mentioned above, the solution to $A\kappa = b$ should be unique for the correct model, but there should, in theory, be no solution for each of the incorrect models. Thus under ideal circumstances, one should be able to select the correct model since the input/output data corresponding to that model should satisfy

its input-output invariant. Likewise, one should be able to reject the incorrect models since the input/output data should not satisfy their input-output invariants.

However, with imperfect data, there could be no solution to $A\kappa = b$ even for the correct model, and likewise there may or may not be a solution to $A\kappa = b$ for an incorrect model. Thus, with imperfect data, one may be unable to select the correct model. On the other hand, if there is no solution to $A\kappa = b$ for each of the candidate models, then the goal is to determine how "badly" each of the models fails and rejects models accordingly.

A subtle point regarding this approach is that this model rejection technique works best if the models under consideration are in the simplest possible form. This means that, ideally, redundant parameters have been eliminated from the model so that the input-output equations are as reduced as possible; i.e., there are not extra columns in A when considering the linear system $A\kappa = b$. Extra columns generically mean more possible solutions, which can make it harder for our algorithm to reject incorrect models. However, redundant parameters, and the related notion of parameter unidentifiability, do not necessarily yield more coefficients in the input-output equations, as can be seen from the structure of input-output equations for linear compartment models as discussed in Section 8.

A related question to model compatibility is that of structural indistinguishability. Two models are structurally indistinguishable if for any choice of parameters in the first model there is a choice of parameters in the second model that will yield the same dynamics in both models, and vice versa [27]. One way to test for structural indistinguishability of two models is to find the associated input-output equations and then equate their coefficient functions and attempt to solve for one set of parameters in terms of the other set of parameters, and vice versa [27]. A necessary condition for models to be structurally indistinguishable is to have input-output equations with the same differential monomial terms. Since our approach only considers the structure of the input-output equations and not the specific coefficient functions, it is possible to have several different models, all with the same structure of their input-output equations, to be compatible using our model compatibility test. Thus, if a given model is found to be compatible, then any model that is structurally indistinguishable from that model is also compatible and thus our approach and structural indistinguishability testing can be applied in parallel. For more on structural indistinguishability, see [28–30]. The specific form of the coefficients of the input-output equations is considered in Section 8.

We now describe criteria to reject models.

4. Linear Solvability

Let $A \in \mathbb{R}^{m \times n}$ and consider the linear system

$$A\kappa = b. \tag{10}$$

Here, we study the solvability of (10) under noisy perturbation of both A and b. Let $\widetilde{A}$ and $\widetilde{b}$ denote the perturbed versions of A and b, respectively, and assume that $\widetilde{A} - A$ and $\widetilde{b} - b$ depend

only on $\widetilde{A}$ and $\widetilde{b}$, respectively (see Section 5). Our goal is to infer the *unsolvability* of the unperturbed system (10) from observation of $\widetilde{A}$ and $\widetilde{b}$ only.

Our method is based on detecting the rank of an augmented matrix, but first let us introduce some notation. The singular values of a matrix $A \in \mathbb{R}^{m \times n}$ will be denoted by

$$\sigma_1(A) \geq \cdots \geq \sigma_\ell(A) \geq \sigma_{\ell+1}(A) = \cdots = \sigma_n(A) = 0, \tag{11}$$
$$\ell = \min(m, n).$$

(Note that we have trivially extended the number of singular values of A from ℓ to n.) The rank of A is written rank(A). The range of A is denoted $\mathscr{R}(A)$. Throughout, $\|\cdot\|$ refers to the Euclidean norm.

The basic strategy will be to assume as a null hypothesis that (10) has a solution, i.e., $b \in \mathscr{R}(A)$, and then to derive its consequences in terms of $\widetilde{A}$ and $\widetilde{b}$. If these consequences are not met, then we conclude by contradiction that (10) is unsolvable. In other words, we will provide *sufficient but not necessary* conditions for (10) to have no solution; i.e., we can only reject (but not confirm) the null hypothesis. We will refer to this procedure as *testing* the null hypothesis.

4.1. Preliminaries. We first collect some useful results.

Theorem 3 (Weyl's inequality). *Let $A, \widetilde{A} \in \mathbb{R}^{m \times n}$. Then*

$$\left| \sigma_k(\widetilde{A}) - \sigma_k(A) \right| \leq \|\widetilde{A} - A\|, \quad k = 1, \ldots, n. \tag{12}$$

Corollary 4. *Let $A, \widetilde{A} \in \mathbb{R}^{m \times n}$ and assume that rank(A) < k. Then*

$$\sigma_k(\widetilde{A}) \leq \|\widetilde{A} - A\|. \tag{13}$$

Therefore, if (13) is not satisfied, then rank(A) $\geq k$.

4.2. Augmented Matrix. Assume the null hypothesis. Then $b \in \mathscr{R}(A)$, so rank($[A, b]$) = rank(A) $\leq$ min(m, n). Therefore, $\sigma_{n+1}([A, b]) = 0$. But we do not have access to $[A, b]$ and so must consider instead the perturbed augmented matrix $[\widetilde{A}, \widetilde{b}]$.

Theorem 5. *Under the null hypothesis,*

$$\sigma_{n+1}\left(\left[\widetilde{A}, \widetilde{b}\right]\right) \leq \left\|\left[\widetilde{A} - A, \widetilde{b} - b\right]\right\|$$
$$\leq \|\widetilde{A} - A\| + \|\widetilde{b} - b\|. \tag{14}$$

Proof. Apply Corollary 4. □

In other words, if (14) does not hold, then (10) has no solution.

Remark 6. This approach can fail to correctly reject the null hypothesis if A is (numerically) low-rank.

Remark 7. In principle, we should test directly the assertion that rank($[A, b]$) = rank(A). However, we can only establish lower bounds on the matrix rank (we can only tell if a

singular value is "too large"), so this is not feasible in practice. An alternative approach is to consider only *numerical* ranks obtained by thresholding. How to choose such a threshold, however, is not at all clear and can be a very delicate matter especially if the data have high dynamic range.

Remark 8. The theorem is uninformative if $m \leq n$ since then $\sigma_{n+1}([A, b]) = \sigma_{n+1}([\widetilde{A}, \widetilde{b}]) = 0$ trivially. However, this is not a significant disadvantage beyond that described above since if A is full-rank, then it must be true that (10) is solvable.

4.3. Example: Perfect Data. As a proof of principle, we first apply Theorem 5 to a simple linear model. We start by taking perfect input and output data and then add a specific amount of noise to the output data and attempt to reject the incorrect model. In the subsequent sections, we will see how to interpret Theorem 5 statistically under a particular "noise" model for the perturbations.

Here, we take data from a linear 3-compartment model, add noise, and try to reject the general form of the linear 2-compartment model with the same input/output compartments. Linear compartment models are defined in Section 8. In practice, one would like to compare models with the same input and output compartments, as the number of compartments involved may not be known, but the injection and measurement compartments would be known. Thus, in this particular example, we are assuming the linear 3-compartment model is the "true model" and want to reject a competing model, but as our method concerns model rejection and not model selection, this notion of a "true model" is not a requirement for our method to work.

Example 9. Let our model be a 3-compartment model of the following form:

$$\begin{pmatrix} \dot{x}_1 \\ \dot{x}_2 \\ \dot{x}_3 \end{pmatrix} = \begin{pmatrix} -2 & 1 & 0 \\ 1 & -3 & 1 \\ 0 & 1 & -2 \end{pmatrix} \begin{pmatrix} x_1 \\ x_2 \\ x_3 \end{pmatrix}$$
$$+ \begin{pmatrix} 2e^{-3t} + 12e^{-5t} \\ 0 \\ 0 \end{pmatrix},$$
$$y = x_1$$
$$x_1(0) = 1,$$
$$x_2(0) = 7,$$
$$x_3(0) = 9 \tag{15}$$

Here we have an input to the first compartment of the form $u_1 = 2e^{-3t} + 12e^{-5t}$ and the first compartment is measured, so that $y = x_1$ represents the output. Note that we have chosen a smooth, persistently exciting input function [26] so that derivatives can be taken and the coefficients of the input-output equation can be uniquely determined, as required. The

solution to this system of ODEs can be easily found of the form:

$$\begin{pmatrix} x_1 \\ x_2 \\ x_3 \end{pmatrix} = 7 \begin{pmatrix} 1 \\ 1 \\ 1 \end{pmatrix} e^{-t} + \begin{pmatrix} -1 \\ 0 \\ 1 \end{pmatrix} e^{-2t} + \begin{pmatrix} 1 \\ -2 \\ 1 \end{pmatrix} e^{-4t}$$
$$+ \begin{pmatrix} -1 \\ -1 \\ 1 \end{pmatrix} e^{-3t} + \begin{pmatrix} -5 \\ 3 \\ -1 \end{pmatrix} e^{-5t} \tag{16}$$

so that $y = 7e^{-t} - e^{-2t} + e^{-4t} - e^{-3t} - 5e^{-5t}$.

The input-output equation for a 3-compartment model with a single input/output to the first compartment has the form:

$$\dddot{y} + c_1 \ddot{y} + c_2 \dot{y} + c_3 y = \ddot{u}_1 + c_4 \dot{u}_1 + c_5 u_1 \tag{17}$$

where c_1, c_2, c_3 are the coefficients of the characteristic polynomial of the matrix A and c_4, c_5 are the coefficients of the characteristic polynomial of the matrix A_1 which has the first row and first column of A removed [31].

We now substitute values of $u_1, \dot{u}_1, \ddot{u}_1, y, \dot{y}, \ddot{y}, \dddot{y}$ at time instances $t = 0, 0.2, 0.4, 0.6, 0.8, 1$ into our input-output equation and solve the resulting linear system of equations for c_1, c_2, c_3, c_4, c_5. We get that $c_1 = 7, c_2 = 14, c_3 = 8, c_4 = 5, c_5 = 5$, which agrees with the coefficients of the characteristic polynomials of A and A_1.

We now attempt to reject the 2-compartment model using 3-compartment model data. We find the input-output equations for a 2-compartment model with a single input/output to the first compartment, which has the form:

$$\ddot{y} + C_1 \dot{y} + C_2 y = \dot{u}_1 + C_3 u_1 \tag{18}$$

where again C_1, C_2 are the coefficients of the characteristic polynomial of the matrix A and C_3 is the coefficient of the characteristic polynomial of the matrix A_1 which has the first row and first column of A removed.

We substitute values of $u_1, \dot{u}_1, y, \dot{y}, \ddot{y}$ at time instances $t = 0, 0.2, 0.4, 0.6, 0.8, 1$ into our input-output equation and attempt to solve the resulting linear system of equations for C_1, C_2, C_3.

The singular values for the matrix A with the substituted values of $u_1, y, \dot{y}$ at time instances $t = 0, 0.2, 0.4, 0.6, 0.8, 1$ are

$$24.8133, 7.64917, 0.0626589 \tag{19}$$

The singular values of the matrix $[A, b]$ with the substituted values of $u_1, \dot{u}_1, y, \dot{y}, \ddot{y}$ at time instances $t = 0, 0.2, 0.4, 0.6, 0.8, 1$ are

$$57.174, 7.69381, 0.326204, 0.00596031 \tag{20}$$

Since the smallest singular value is greater than zero (or order machine precision), it is evident that the 2-compartment model can be rejected.

We now add noise to our matrix A in the following way. To each entry $\dot{y}$, and y, we add ϵk_{ij} where k_{ij} is a random

real number between 0 and 1, and $\epsilon = 0.001$. Then the noisy matrix $\widetilde{A}$ has the following singular values:

$$24.8134, 7.64949, 0.0627827 \tag{21}$$

We add noise to our vector b in a similar way. To each entry $\dot{u}_1 - \ddot{y}$, we add ϵk_{ij} where k_{ij} is again a random real number between 0 and 1. Then the noisy matrix $[\widetilde{A}, \widetilde{b}]$ has the following singular values:

$$57.1747, 7.69409, 0.326141, 0.00579117 \tag{22}$$

To determine whether the noisy data are compatible, we need to compute $\|[\widetilde{A} - A, \widetilde{b} - b]\|$. Due to the specific noise model chosen, this can be bounded independently of the true unobservable data $[A, b]$ as $\epsilon \|\mathbf{1}\| = 0.00489898$, where $\mathbf{1}$ is a matrix of all ones of the appropriate size (the actual norm is 0.00207018). Since this norm is *less than* the smallest singular value 0.00579117, we can reject this model. Thus, using noisy 3-compartment model data, we are able to reject the 2-compartment model.

5. Statistical Inference

We now consider the statistical inference of the solvability of (10). First, we need a noise model.

5.1. Noise Model. If the perturbations $\|\widetilde{A} - A\|$ and $\|\widetilde{b} - b\|$ are bounded, e.g., $\|\widetilde{A} - A\| \le \epsilon \|\widetilde{A}\|$ and $\|\widetilde{b} - b\| \le \epsilon \|\widetilde{b}\|$ for some $\epsilon > 0$ (representing a relative accuracy of ϵ in the "measurements" $\widetilde{A}$ and $\widetilde{b}$), then Theorem 5 can be used at once. However, it is customary to model such perturbations as normal random variables, which are not bounded. Here, we will assume a noise model of the form

$$\begin{aligned} \widetilde{A} - A &= C_{\widetilde{A}} \circ Z, \\ \widetilde{b} - b &= C_{\widetilde{b}} \circ Z, \end{aligned} \tag{23}$$

where $C_{\widetilde{A}}$ is a (computable) matrix that depends only on $\widetilde{A}$ and similarly with $C_{\widetilde{b}}$, $A \circ B$ denotes the Hadamard (entrywise) matrix product $(A \circ B)_{ij} = A_{ij} B_{ij}$, and Z is a matrix-valued random variable whose entries $Z_{ij} \sim \mathcal{N}(0, 1)$ are independent standard normals.

In our application of interest, the entries of $C_{\widetilde{A}}$ depend on those of $\widetilde{A}$ as follows. Let $A_{ij} = \phi_{ij}(v)$ for some input vector v, but suppose that we can only observe the "noisy" vector $\widetilde{v} = (1 + \epsilon Z) \circ v$. Then the corresponding perturbed matrix entries are

$$\begin{aligned} \widetilde{A}_{ij} &= \phi_{ij}(\widetilde{v}) \\ &= \phi_{ij}(v) + \epsilon \sum_k \left(\nabla \phi_{ij}(v) \right)_k v_k Z_k + O(\epsilon^2), \end{aligned} \tag{24}$$

$$Z_k \sim \mathcal{N}(0, 1).$$

By the additivity formula

$$\sum_k a_k Z_k = \sqrt{\sum_k a_k^2} Z = \|a\| Z \tag{25}$$

for standard Gaussians,

$$\begin{aligned} \sum_k \left(\nabla \phi_{ij}(v) \right)_k v_k Z_k &= \sum_k \left(\nabla \phi_{ij}(v) \circ v \right)_k Z_k \\ &= \left\| \nabla \phi_{ij}(v) \circ v \right\| Z. \end{aligned} \tag{26}$$

Therefore,

$$\begin{aligned} \widetilde{A}_{ij} &= A_{ij} + \epsilon \left\| \nabla \phi_{ij}(v) \circ v \right\| Z + O(\epsilon^2) \\ &= A_{ij} + \epsilon \left\| \nabla \phi_{ij}(\widetilde{v}) \circ \widetilde{v} \right\| Z + O(\epsilon^2), \end{aligned} \tag{27}$$

so, to first order in ϵ,

$$\left(C_{\widetilde{A}} \right)_{ij} = \epsilon \left\| \nabla \phi_{ij}(\widetilde{v}) \circ \widetilde{v} \right\|. \tag{28}$$

An analogous derivation holds for $C_{\widetilde{b}}$.

The basic strategy is now as follows. Let τ be a test statistic, i.e., $\sigma_{n+1}([\widetilde{A}, \widetilde{b}])$ in Section 4.2. Then since

$$\tau_\omega \le \left(\|C_{\widetilde{A}} \circ Z\| + \|C_{\widetilde{b}} \circ Z\| \right)_\omega, \tag{29}$$

where we have made explicit the dependence of both sides on the same underlying random mechanism ω, the (cumulative) distribution function of τ must dominate that of $\|C_{\widetilde{A}} \circ Z\| + \|C_{\widetilde{b}} \circ Z\|$, i.e.,

$$\Pr(\tau \le v) \ge \Pr\left(\|C_{\widetilde{A}} \circ Z\| + \|C_{\widetilde{b}} \circ Z\| \le v \right). \tag{30}$$

Thus,

$$\Pr(\tau \ge v) \le \Pr\left(\|C_{\widetilde{A}} \circ Z\| + \|C_{\widetilde{b}} \circ Z\| \ge v \right) \tag{31a}$$

$$= \int_0^\infty \Pr\left(\|C_{\widetilde{A}} \circ Z\| = t \right) \Pr\left(\|C_{\widetilde{b}} \circ Z\| \ge v - t \right) dt \tag{31b}$$

$$\begin{aligned} &= \int_0^v \Pr\left(\|C_{\widetilde{A}} \circ Z\| = t \right) \Pr\left(\|C_{\widetilde{b}} \circ Z\| \ge v - t \right) dt \\ &\quad + \int_v^\infty \Pr\left(\|C_{\widetilde{A}} \circ Z\| = t \right) dt \end{aligned} \tag{31c}$$

$$\begin{aligned} &\le \int_0^v \Pr\left(\|C_{\widetilde{A}} \circ Z\| \ge t \right) \Pr\left(\|C_{\widetilde{b}} \circ Z\| \ge v - t \right) dt \\ &\quad + \Pr\left(\|C_{\widetilde{A}} \circ Z\| \ge v \right). \end{aligned} \tag{31d}$$

Using (31a)–(31d), we can associate a p-value to any given realization of τ by referencing upper tail bounds for quantities of the form $\|C \circ Z\|$. Recall that $\tau = 0$ under the null hypothesis. In a classical statistical hypothesis testing framework, we may therefore reject the null hypothesis if (31d) is at most α, where α is the desired significance level (e.g., $\alpha = 0.05$).

5.2. Hadamard Tail Bounds. We now turn to bounding $\Pr(\|C \circ Z\| \ge v)$, where we will assume that $C, Z \in \mathbb{R}^{m \times n}$. This can be done in several ways.

One easy way is to recognize that

$$\|C \circ Z\| \le \|C \circ Z\|_F \le \|C\|_F \|Z\|_F, \tag{32}$$

where $\| \cdot \|_F$ is the Frobenius norm, so

$$
\begin{aligned}
\Pr \left(\| C \circ Z \| \geq v \right) &\leq \Pr \left(\| C \circ Z \|_F \geq v \right) \\
&\leq \Pr \left(\| Z \|_F \geq \frac{v}{\| C \|_F} \right).
\end{aligned}
\tag{33}
$$

But $\| Z \|_F \sim \chi_{mn}$ has a chi distribution with mn degrees of freedom. Therefore,

$$
\Pr \left(\| Z \|_F \geq \frac{v}{\| C \|_F} \right) = \Pr \left(V \geq \frac{v}{\| C \|_F} \right), \quad V \sim \chi_{mn}.
\tag{34}
$$

However, each inequality in (32) can be quite loose; a slightly better approach is to use the inequality [32]

$$
\| C \circ Z \| \leq \| \min \left(\max_i \| C_{i,:} \|, \max_j \| C_{:,j} \| \right) \| Z \|,
\tag{35}
$$

where $C_{i,:}$ and $C_{:,j}$ denote the ith row and jth column, respectively, of C. The $\| Z \|$ term can then be handled using a chi distribution via $\| Z \| \leq \| Z \|_F$ as above or directly using a concentration bound (see below). Variations on this undoubtedly exist.

Here, we will appeal to a result by Tropp [33]. The following is from Section 4.3 in [33].

Theorem 10. *Let* $C, Z \in \mathbb{R}^{m \times n}$, *where each* $Z_{ij} \sim \mathcal{N}(0, 1)$. *Then for any* $v \geq 0$,

$$
\Pr \left(\| C \circ Z \| \geq v \right) \leq (m + n) \exp \left(-\frac{v^2}{2\sigma^2} \right),
\tag{36}
$$

$$
\sigma^2 = \max \left(\max_i \| C_{i,:} \|^2, \max_j \| C_{:,j} \|^2 \right).
$$

5.3. Test Statistic Tail Bounds. The bound (31d) for $\Pr(\tau \geq v)$ can then be computed as follows. Let

$$
\begin{aligned}
&P_1(v) \\
&= \int_0^v \Pr \left(\| C_{\bar{A}} \circ Z \| \geq t \right) \Pr \left(\| C_{\bar{b}} \circ Z \| \geq v - t \right) dt,
\end{aligned}
\tag{37}
$$

$$
P_2(v) = \Pr \left(\| C_{\bar{A}} \circ Z \| \geq v \right)
$$

so that $\Pr(\tau \geq v) \leq P_1(v) + P_2(v)$. Then by Theorem 10,

$$
\begin{aligned}
&P_1(v) \\
&\leq m(m+n) \int_0^v \exp \left[-\frac{1}{2} \left(\frac{t^2}{\sigma_A^2} + \frac{(v-t)^2}{\sigma_b^2} \right) \right] dt,
\end{aligned}
\tag{38}
$$

where σ_A^2 and σ_b^2 are the "variance" parameters in the theorem for $C_{\bar{A}}$ and $C_{\bar{b}}$, respectively. This simplifies to

$$
\begin{aligned}
P_1(v) &\leq m(m+n) \exp \left[-\frac{1}{2} \left(\frac{v^2}{\sigma_A^2 + \sigma_b^2} \right) \right] \\
&\cdot \int_0^v \exp \left[-\frac{1}{2} \left(\frac{\sigma_A^2 + \sigma_b^2}{\sigma_A^2 \sigma_b^2} \right) \left(t - \frac{\sigma_A^2}{\sigma_A^2 + \sigma_b^2} v \right)^2 \right] dt
\end{aligned}
\tag{39}
$$

on completing the square. Now set

$$
\begin{aligned}
\sigma^2 &= \frac{\sigma_A^2 \sigma_b^2}{\sigma_A^2 + \sigma_b^2}, \\
\alpha &= \frac{\sigma_A^2}{\sigma_A^2 + \sigma_b^2}
\end{aligned}
\tag{40}
$$

so that the integral becomes

$$
\begin{aligned}
&\int_0^v \exp \left[-\frac{1}{2} \left(\frac{\sigma_A^2 + \sigma_b^2}{\sigma_A^2 \sigma_b^2} \right) \left(t - \frac{\sigma_A^2}{\sigma_A^2 + \sigma_b^2} v \right)^2 \right] dt \\
&= \int_0^v \exp \left[-\frac{(t - \alpha v)^2}{2\sigma^2} \right] dt.
\end{aligned}
\tag{41}
$$

The variable substitution $u = (t - \alpha v)/\sigma$ then gives

$$
\begin{aligned}
\int_0^v \exp \left[-\frac{(t - \alpha v)^2}{2\sigma^2} \right] dt &= \sigma \int_{-\alpha v/\sigma}^{(1-\alpha)v/\sigma} e^{-u^2/2} du \\
&= \sqrt{2\pi} \sigma \left[\Phi \left(\frac{(1 - \alpha) v}{\sigma} \right) - \Phi \left(-\frac{\alpha v}{\sigma} \right) \right],
\end{aligned}
\tag{42}
$$

where

$$
\Phi(v) = \frac{1}{\sqrt{2\pi}} \int_{-\infty}^v e^{-t^2/2} dt
\tag{43}
$$

is the standard normal distribution function. Thus,

$$
\begin{aligned}
P_1(v) &\leq \sqrt{2\pi} \sigma m(m+n) \\
&\cdot \left[\Phi \left(\frac{(1-\alpha) v}{\sigma} \right) - \Phi \left(-\frac{\alpha v}{\sigma} \right) \right] \\
&\cdot \exp \left[-\frac{1}{2} \left(\frac{v^2}{\sigma_A^2 + \sigma_B^2} \right) \right].
\end{aligned}
\tag{44}
$$

A similar analysis yields

$$
P_2(v) \leq (m+n) \exp \left(-\frac{v^2}{2\sigma_A^2} \right).
\tag{45}
$$

Equations (44) and (45) together comprise the probability bound on the null hypothesis that we will use hereafter.

6. Gaussian Processes to Estimate Derivatives

We next present a method for estimating higher order derivatives and the estimation error using Gaussian Process Regression and then apply the input-output invariant method to both linear and nonlinear models in the subsequent sections.

A Gaussian process (GP) is a stochastic process $W(t) \sim \mathcal{N}(\mu(t), \Sigma(t, t'))$, where $\mu(t)$ is a mean function and $\Sigma(t, t')$ a covariance function. GPs are often used for regression/prediction as follows.

Suppose that there is an underlying deterministic function $w(t)$ that we can only observe with some measurement

noise as $\widehat{w}(t) = w(t) + \epsilon(t)$, where $\epsilon(t) \sim \mathcal{N}(0, \sigma^2(t)\delta(t, t'))$ for

$$\delta\left(t, t'\right) = \begin{cases} 1 & \text{if } t = t' \\ 0 & \text{if } t \neq t' \end{cases} \tag{46}$$

the Dirac delta. We consider the problem of finding $w(t)$ in a Bayesian setting by assuming it to be a GP with prior mean and covariance functions μ_{prior} and Σ_{prior}, respectively. Then the joint distribution of $\widehat{w}(\mathbf{t}) = [\widehat{w}(t_1), \ldots, \widehat{w}(t_p)]^\top$ at the observation points $\mathbf{t} = [t_1, \ldots, t_p]^\top$ and $w(\mathbf{s}) = [w(s_1), \ldots, w(s_q)]^\top$ at the prediction points $\mathbf{s} = [s_1, \ldots, s_q]^\top$ is

$$\begin{bmatrix} \widehat{w}(\mathbf{t}) \\ w(\mathbf{s}) \end{bmatrix} \sim \mathcal{N}\left(\begin{bmatrix} \mu_{\text{prior}}(\mathbf{t}) \\ \mu_{\text{prior}}(\mathbf{s}) \end{bmatrix}, \right.$$
$$\left. \begin{bmatrix} \Sigma_{\text{prior}}(\mathbf{t}, \mathbf{t}) + \sigma^2(\mathbf{t}) I & \Sigma_{\text{prior}}^\top(\mathbf{s}, \mathbf{t}) \\ \Sigma_{\text{prior}}(\mathbf{s}, \mathbf{t}) & \Sigma_{\text{prior}}(\mathbf{s}, \mathbf{s}) \end{bmatrix} \right) \tag{47}$$

The conditional distribution of $w(\mathbf{s})$ given $w(\mathbf{t}) = \widehat{w}(\mathbf{t})$ is also Gaussian:

$$w(\mathbf{s}) \mid (w(\mathbf{t}) = \widehat{w}(\mathbf{t})) \sim \mathcal{N}(\mu_{\text{post}}, \Sigma_{\text{post}}), \tag{48}$$

$$\begin{bmatrix} \widehat{w}(\mathbf{t}) \\ \hline w(\mathbf{s}) \\ w'(\mathbf{s}) \\ \vdots \\ w^{(n)}(\mathbf{s}) \end{bmatrix} \sim \mathcal{N}\left(\begin{bmatrix} \mu_{\text{prior}}(\mathbf{t}) \\ \hline \mu_{\text{prior}}(\mathbf{s}) \\ \mu_{\text{prior}}^{(1)}(\mathbf{s}) \\ \vdots \\ \mu_{\text{prior}}^{(n)}(\mathbf{s}) \end{bmatrix}, \begin{bmatrix} \Sigma_{\text{prior}}(\mathbf{t}, \mathbf{t}) + \sigma^2(\mathbf{t}) I & \Sigma_{\text{prior}}^\top(\mathbf{s}, \mathbf{t}) & \Sigma_{\text{prior}}^{(1,0),\top}(\mathbf{s}, \mathbf{t}) & \cdots & \Sigma_{\text{prior}}^{(n,0),\top}(\mathbf{s}, \mathbf{t}) \\ \hline \Sigma_{\text{prior}}(\mathbf{s}, \mathbf{t}) & \Sigma_{\text{prior}}(\mathbf{s}, \mathbf{s}) & \Sigma_{\text{prior}}^{(1,0),\top}(\mathbf{s}, \mathbf{s}) & \cdots & \Sigma_{\text{prior}}^{(n,0),\top}(\mathbf{s}, \mathbf{s}) \\ \Sigma_{\text{prior}}^{(1,0)}(\mathbf{s}, \mathbf{t}) & \Sigma_{\text{prior}}^{(1,0)}(\mathbf{s}, \mathbf{s}) & \Sigma_{\text{prior}}^{(1,1)}(\mathbf{s}, \mathbf{s}) & \cdots & \Sigma_{\text{prior}}^{(n,1),\top}(\mathbf{s}, \mathbf{s}) \\ \vdots & \vdots & \vdots & \ddots & \vdots \\ \Sigma_{\text{prior}}^{(n,0)}(\mathbf{s}, \mathbf{t}) & \Sigma_{\text{prior}}^{(n,0)}(\mathbf{s}, \mathbf{s}) & \Sigma_{\text{prior}}^{(n,1)}(\mathbf{s}, \mathbf{s}) & \cdots & \Sigma_{(n,n)}(\mathbf{s}, \mathbf{s}) \end{bmatrix} \right), \tag{50}$$

where $\mu_{\text{prior}}^{(i)}(t)$ is the prior mean for $w^{(i)}(t)$ and $\Sigma_{\text{prior}}^{(i,j)}(t, t') = \partial_t^i \partial_{t'}^j \Sigma_{\text{prior}}(t, t')$. This joint distribution is exactly of the form (47). An analogous application of (48) then yields the posterior estimate of $w^{(i)}(\mathbf{s}) \mid (w(\mathbf{t}) = \widehat{w}(\mathbf{t}))$ for all $i = 0, 1, \ldots, n$.

Alternatively, if we are interested only in the posterior variances of each $w^{(i)}(\mathbf{s})$, then it suffices to consider each 2×2 block independently:

$$\begin{bmatrix} \widehat{w}(\mathbf{t}) \\ w^{(i)}(\mathbf{s}) \end{bmatrix} \sim \mathcal{N}\left(\begin{bmatrix} \mu_{\text{prior}}(\mathbf{t}) \\ \mu_{\text{prior}}^{(i)}(\mathbf{s}) \end{bmatrix}, \right.$$
$$\left. \begin{bmatrix} \Sigma_{\text{prior}}(\mathbf{t}, \mathbf{t}) + \sigma^2(\mathbf{t}) I & \Sigma_{\text{prior}}^{(i,0),\top}(\mathbf{s}, \mathbf{t}) \\ \Sigma_{\text{prior}}^{(i,0)}(\mathbf{s}, \mathbf{t}) & \Sigma_{\text{prior}}^{(i,i)}(\mathbf{s}, \mathbf{s}) \end{bmatrix} \right). \tag{51}$$

The cost of computing $(\Sigma_{\text{prior}}(\mathbf{t}, \mathbf{t}) + \sigma^2(\mathbf{t}) I)^{-1}$ can clearly be amortized over all i.

where

$$\mu_{\text{post}} = \mu_{\text{prior}}(\mathbf{s}) + \Sigma_{\text{prior}}(\mathbf{s}, \mathbf{t})\left(\Sigma_{\text{prior}}(\mathbf{t}, \mathbf{t}) + \sigma^2(\mathbf{t}) I\right)^{-1}$$
$$\cdot \left(\widehat{w}(\mathbf{t}) - \mu_{\text{prior}}(\mathbf{t})\right),$$
$$\Sigma_{\text{post}} = \Sigma_{\text{prior}}(\mathbf{s}, \mathbf{s}) - \Sigma_{\text{prior}}(\mathbf{s}, \mathbf{t}) \tag{49}$$
$$\cdot \left(\Sigma_{\text{prior}}(\mathbf{t}, \mathbf{t}) + \sigma^2(\mathbf{t}) I\right)^{-1}) \Sigma_{\text{prior}}^\top(\mathbf{s}, \mathbf{t})$$

are the posterior mean and covariance, respectively. This allows us to infer $w(\mathbf{s})$ on the basis of observing $\widehat{w}(\mathbf{t})$. The diagonal entries of Σ_{post} are the posterior variances and quantify the uncertainty associated with this inference procedure. In particular, the square roots of these variances give us estimates on the ϵw term in the assumed noise model $\widehat{w} = (1 + \epsilon Z) \circ w$ in Section 5.

6.1. Estimating Derivatives. Equation (48) provides an estimate for the function values $w(\mathbf{s})$. What if we want to estimate its derivatives? Let $\text{cov}(w(t), w(t')) = k(t, t')$ for some covariance function k. Then $\text{cov}(w^{(m)}(t), w^{(n)}(t')) = \partial_t^m \partial_{t'}^n k(t, t')$ by linearity of differentiation. Thus,

6.2. Formulae for Squared Exponential Covariance Functions. We now consider the specific case of the squared exponential (SE) covariance function

$$k\left(t, t'\right) = \theta^2 \exp\left[-\frac{\left(t - t'\right)^2}{2\ell^2}\right], \tag{52}$$

where θ^2 is the signal variance and ℓ is a length scale. The SE function is one of the most widely used covariance functions in practice. Its derivatives can be expressed in terms of the (probabilists') Hermite polynomials

$$H_n(w) = (-1)^n e^{w^2/2} \frac{d^n}{dw^n} e^{-w^2/2} \tag{53}$$

(these are also sometimes denoted $He_n(w)$). The first few Hermite polynomials are $H_0(w) = 1$, $H_1(w) = w$, and $H_2(w) = w^2 - 1$.

We need to compute the derivatives $\partial_t^m \partial_{t'}^n k(t, t')$. Let $v = (t - t')/\ell$ so that $k(t, t') = k(v) = \theta^2 e^{-v^2/2}$. Then $\partial_t^m f(v) = (1/\ell)^m f^{(m)}(v)$ and $\partial_{t'}^n f(v) = (-1/\ell)^n f^{(n)}(v)$. Therefore,

$$
\begin{aligned}
\frac{\partial^m}{\partial t^m} \frac{\partial^n}{\partial t'^n} k\left(t, t'\right) &= \frac{(-1)^n}{\ell^{m+n}} k^{(m+n)}(v) \\
&= \frac{(-1)^m}{\ell^{m+n}} H_{m+n}(v) k(v) \\
&= \frac{(-1)^m}{\ell^{m+n}} H_{m+n}\left(\frac{t - t'}{\ell}\right) k\left(t, t'\right).
\end{aligned}
\tag{54}
$$

The GP regression requires us to have the values of the hyperparameters σ^2, θ^2, and ℓ. In practice, however, these are hardly ever known. In the examples below, we deal with this by estimating the hyperparameters from the data by maximizing the likelihood. We do this by using a nonlinear conjugate gradient algorithm, which can be quite sensitive to the initial starting point, so we initialize multiple runs over a small grid in hyperparameter space and return the best estimate found. This increases the quality of the estimated hyperparameters but can still sometimes fail.

7. Results

We showcase our method on competing models: linear compartment models (2 and 3 species), Lotka-Volterra models (2 and 3 species) and Lorenz. We compute the input-output invariants of the Lotka-Volterra and Lorenz using `RosenfeldGroebner`. The method to compute the linear compartment input-output invariants is presented in the following section. We simulate each of these models to generate time-course data, add varying levels of noise, and estimate the necessary higher order derivatives using GP regression. Using the estimated GP regression data, we test each of the models using the input-output invariant method on other models.

Example 11. The two species Lotka-Volterra model is

$$
\begin{aligned}
\dot{x}_1 &= p_1 x_1 - p_2 x_1 x_2, \\
\dot{x}_2 &= -p_3 x_2 + p_4 x_1 x_2,
\end{aligned}
\tag{55}
$$

where x_1 and x_2 are variables and p_1, p_2, p_3, p_4 are parameters. We assume only x_1 is observable and perform differential elimination and obtain our input-output invariant in terms of only $y = x_1(t)$:

$$
p_4 \dot{y} y^2 - p_3 \dot{y} y - p_1 p_4 y^3 + p_1 p_3 y^2 = \ddot{y} y - \dot{y}^2.
\tag{56}
$$

Example 12. By including an additional variable z, the three species Lotka-Volterra model is

$$
\begin{aligned}
\dot{x}_1 &= p_1 x_1 - p_2 x_1 x_2, \\
\dot{x}_2 &= -p_3 x_2 + p_4 x_1 x_2 - p_5 x_2 x_3, \\
\dot{x}_3 &= -p_6 x_3 + p_7 x_2 x_3,
\end{aligned}
\tag{57}
$$

assuming only $y = x_1$ is observable. After differential elimination, the input-output invariant is

$$
\begin{aligned}
&\left(p_1^2 p_4 p_6 - \frac{p_1^3 p_4 p_7}{p_2}\right) y^5 + \left(\frac{p_1^3 p_3 p_7}{p_2} - p_1^2 p_3 p_6\right) y^4 \\
&\quad + \left(\frac{3 p_1^2 p_4 p_7}{p_2} + p_1^2 p_4 + 2 p_1 p_4 p_6\right) \dot{y} y^4 \\
&\quad + \left(2 p_1 p_3 p_6 - \frac{3 p_1^2 p_3 p_7}{p_2}\right) \dot{y} y^3 \\
&\quad + \left(p_4 p_6 - 2 p_1 p_4 - \frac{3 p_1 p_4 p_7}{p_2}\right) \dot{y}^2 y^3 \\
&\quad + \left(\frac{p_1^2 p_7 + 3 p_1 p_3 p_7}{p_2} - p_3 p_6 - p_1 p_6\right) \dot{y}^2 y^2 \\
&\quad + \left(\frac{p_4 p_7}{p_2} + p_4\right) \dot{y}^3 y^2 \\
&\quad + \left(2 p_1 + p_6 - \frac{2 p_1 p_7 + p_3 p_7}{p_2}\right) \dot{y}^3 y + \frac{p_7}{p_2} \dot{y}^4 \\
&\quad + \left(p_1 p_6 - \frac{p_1^2 p_7}{p_2}\right) \ddot{y} y^3 \\
&\quad + \left(\frac{2 p_1 p_7}{p_2} - 3 p_1 - p_6\right) \ddot{y} \dot{y} y^2 - \frac{p_7}{p_2} \ddot{y} \dot{y}^2 y \\
&\quad + p_1 \ddot{y} y^3 = -\ddot{y}^2 y^2 + \ddot{y} \dot{y} y^2 - \ddot{y} \dot{y}^2 y + \dot{y}^4.
\end{aligned}
\tag{58}
$$

Example 13. Another three species model, the Lorenz model, is described by the system of equations:

$$
\begin{aligned}
\dot{x}_1 &= p_1 (x_2 - x_1), \\
\dot{x}_2 &= x_1 (p_2 - x_3) - x_2, \\
\dot{x}_3 &= x_1 x_2 - p_3 x_3,
\end{aligned}
\tag{59}
$$

We assume only $y = x_1$ is observable, perform differential elimination, and obtain the following invariant:

$$
\begin{aligned}
&-(p_1 + p_3) \ddot{y} y + p_1 \dot{y}^2 - (p_1 p_3 + p_3) \dot{y} y - p_1 y^4 \\
&\quad + (p_1 p_2 p_3 - p_1 p_3) y^2 \\
&= \ddot{y} y - \ddot{y} \dot{y} + \ddot{y} y - \dot{y}^2 + \dot{y} y^3.
\end{aligned}
\tag{60}
$$

Example 14. A linear 2-compartment model without input can be written as

$$
\begin{aligned}
\dot{x}_1 &= p_{11} x_1 + p_{12} x_2, \\
\dot{x}_2 &= p_{21} x_1 + p_{22} x_2,
\end{aligned}
\tag{61}
$$

where x_1 and x_2 are variables and $p_{11}, p_{12}, p_{21}, p_{22}$ are parameters. We assume only x_1 is observable and perform differential elimination and obtain our input-output invariant in terms of only $y = x_1(t)$:

$$
\ddot{y} - (p_{11} + p_{22}) \dot{y} + (p_{11} p_{22} - p_{12} p_{21}) y = 0
\tag{62}
$$

Example 15. A linear 3-compartment model without input is

$$\dot{x}_1 = p_{11}x_1 + p_{12}x_2 + p_{13}x_3,$$
$$\dot{x}_2 = p_{21}x_1 + p_{22}x_2 + p_{23}x_3, \qquad (63)$$
$$\dot{x}_3 = p_{31}x_1 + p_{32}x_2 + p_{33}x_3,$$

where x_1, x_2, x_3 are variables and $p_{11}, p_{12}, p_{13}, p_{21}, p_{22}, p_{23}, p_{31}, p_{32}, p_{33}$ are parameters. We assume only x_1 is observable and perform differential elimination and obtain our input-output invariant in terms of only $y = x_1(t)$:

$$\dddot{y} - (p_{11} + p_{22} + p_{33})\,\ddot{y} + (p_{12}p_{21} - p_{11}p_{22} + p_{13}p_{31}$$
$$+ p_{23}p_{32} - p_{11}p_{33} - p_{22}p_{33})\,\ddot{y} - (-p_{13}p_{22}p_{31}$$
$$+ p_{12}p_{23}p_{31} + p_{13}p_{21}p_{32} - p_{11}p_{23}p_{32} - p_{12}p_{21}p_{33} \qquad (64)$$
$$+ p_{11}p_{22}p_{33})\,y = 0$$

By assuming $y = x_1$ in Examples 6.1–6.5 representing the same observable variable, we apply our method to data simulated from each model and perform model comparison. The models are simulated and 100 time points are obtained for the variable x in each model. We add different levels of Gaussian noise to the simulated data and then estimate the higher order derivatives from the data. Accurate estimation of the derivatives was not always possible. For example, during our study we found that for some parameters of the Lotka-Volterra three species model, e.g., $p_1, p_2, p_3, p_4, p_5, p_6, p_7 = [1.24; 1.68; 3.26; 0.38; 1.50; 0.15; 1.14]$, the data could not adequately fit with a GP, as indicated by a small likelihood. Furthermore, even when a good fit is achieved, the derivative estimates themselves could be poor as reflected in high posterior variances. This is a notoriously difficult problem and we offer only some pragmatic guidance here. In particular, we err on the side of being overly conservative by keeping only "good" time points defined as follows. Let $\sigma_{post}^k(t)$ be the posterior standard deviation of the estimate of $y^{(k)}(t)$. Then a time point t_i is considered good only if

$$\sigma_{post}^k(t_i) \le \mathrm{mean}\left\{\sigma_{post}^k(t_j)\right\} + \mathrm{std}\left\{\sigma_{post}^k(t_j)\right\} \qquad (65)$$

for all k, where mean(·) and std(·) give the mean and standard deviations, respectively, of a set. In this way, we adaptively filter out potentially problematic inputs to the ensuing model rejection framework. Note that filtering out data is equivalent to removing constraints so that we can only decrease the discriminatory power, i.e., models that are flagged as incompatible after data filtering would have been incompatible as well without filtering.

Once the data are obtained and derivative data are estimated through the GP regression, each model data set is tested against the other input-output invariants. Results are shown in Figure 1, which gives a probability bound that the data are compatible with a given model (i.e., ∼ 0 means model rejected) at a variety of noise levels. We find that we can reject the three species Lotka-Volterra model and Lorenz model for data simulated from the Lotka-Volterra two species; however, both linear compartment models are compatible.

For data from the three species Lotka-Volterra model, the linear compartment models and two species Lotka-Volterra can be rejected until the noise increases and then the method can no longer reject any models. Finally data generated from the Lorenz model can only reject the two species linear compartment and two species Lotka-Volterra model.

8. Other Considerations: Known Parameter Values and Algebraic Dependencies

We have demonstrated our model discrimination algorithm on various models. In this section, we consider some other theoretical points regarding input-output invariants.

As mentioned earlier, we have assumed that the parameters are all unknown and we have not taken any possible algebraic dependencies among the coefficients into account. This latter point is another reason our algorithm only concerns model rejection and not model selection. Thus, each unknown coefficient is essentially treated as an independent unknown variable in our linear system of equations. However, there may be instances where we would like to consider incorporating this additional information.

To analyze the effects of incorporating known parameter values and algebraic dependencies, we will examine a particularly nice class of models, linear compartment models, whose input-output equations can be found using linear algebra techniques [31]; i.e., computation of the input-output equations does not rely on more computationally intensive approaches such as RosenfeldGroebner and Gröbner bases. Since we will now be considering the explicit form of the coefficients of the input-output equations, we describe the set-up of linear compartment models below.

Let $G = (V, E)$ be a directed graph with vertex set V and set of directed edges E. Each vertex $i \in V$ corresponds to a compartment in our model and each edge $j \longrightarrow i$ corresponds to a direct flow of material from the jth compartment to the ith compartment. Let $In, Out, Leak \subseteq V$ be three sets of compartments: the set of input compartments, output compartments, and leak compartments, respectively. To each edge $j \longrightarrow i$ we associate an independent parameter p_{ij}, the rate of flow from compartment j to compartment i. To each leak node $i \in Leak$, we associate an independent parameter p_{0i}, the rate of flow from compartment i leaving the system.

To such a graph G and set of leaks $Leak$ we associate the matrix A in the following way:

$$A_{ij}$$

$$= \begin{cases} -p_{0i} - \sum\limits_{k:i\longrightarrow k \in E} p_{ki} & \text{if } i = j \text{ and } i \in Leak \\ -\sum\limits_{k:i\longrightarrow k \in E} p_{ki} & \text{if } i = j \text{ and } i \notin Leak \\ p_{ij} & \text{if } j \longrightarrow i \text{ is an edge of } G \\ 0 & \text{otherwise} \end{cases} \qquad (66)$$

Then we construct a system of linear ODEs with inputs and outputs associated with the quadruple $(G, In, Out, Leak)$ as follows:

(a) Data from Lotka-Volterra two species

(b) Data from Lotka-Volterra three species

(c) Data from Lorenz model
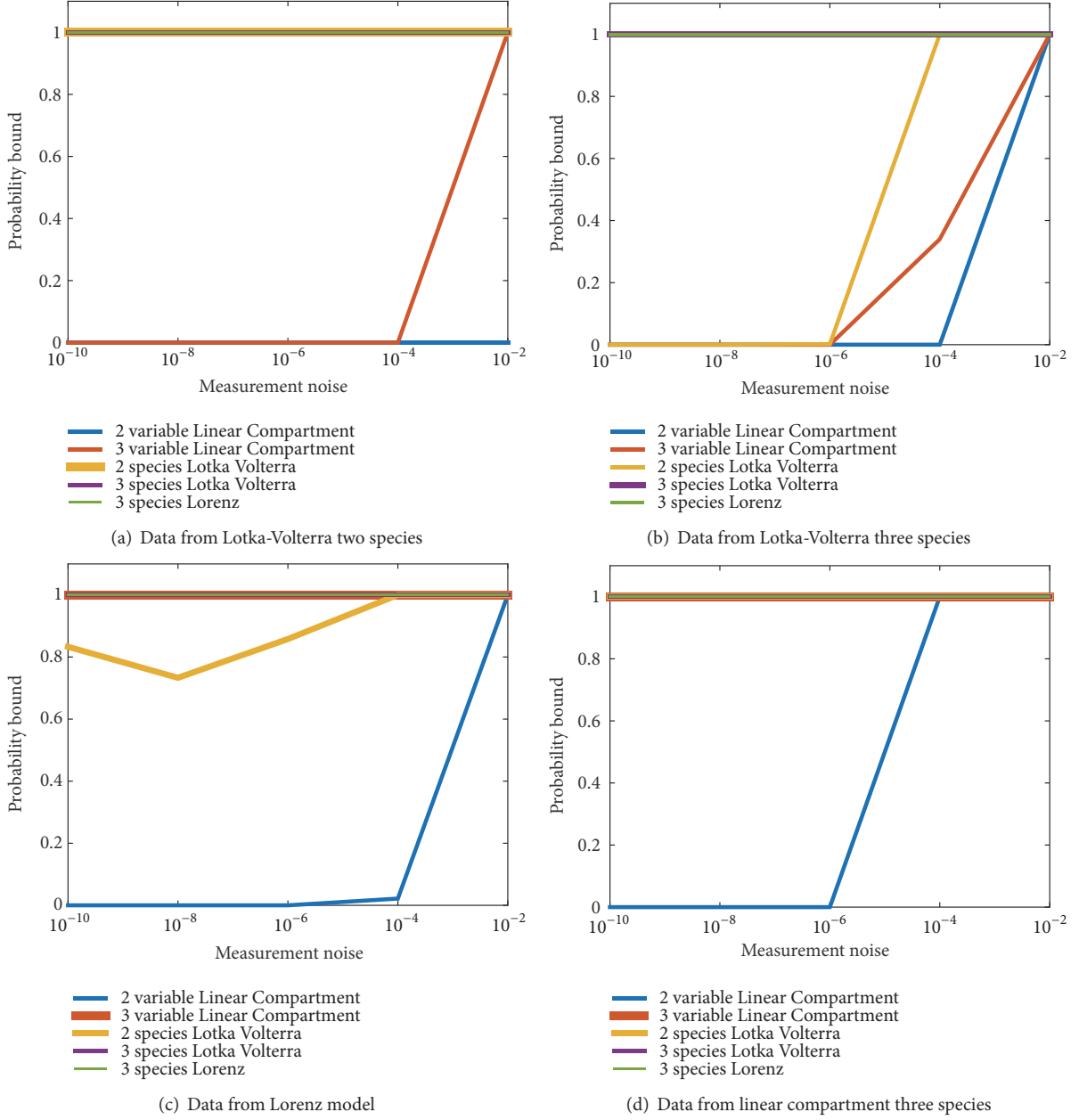
(d) Data from linear compartment three species

FIGURE 1: Data simulated from model specified and differential algebraic statistics model rejection applied to five model invariants. Gaussian noise is added to data in factors of 10 at levels shown in the figure. (a) Data simulated from two species Lotka-Volterra model with parameter values $p_1, p_2, p_3, p_4 = [1.24; 1.68; 3.26; 0.38]$ and initial condition $[10, 1]$. (b) Data simulated from three species Lotka-Volterra model with parameter values $p_1, p_2, p_3, p_4, p_5, p_6, p_7 = [0.178; 0.12; 0.99; 0.17; 0.03; 0.56; 0.88]$ and initial condition $[2, 1, 1]$. (c) Data simulated from the Lorenz model with parameter values $p_1, p_2, p_3 = [3.5, .3, 2.8]$ and initial condition $[2, 1, 1]$. (d) Data simulated from the linear compartment three species model with parameter values $p_{11}, p_{12}, p_{13}, p_{21}, p_{22}, p_{23}, p_{31}, p_{32}, p_{33} = [-2, 1, 0, 1, -3, 1, 0, 1, -2]$ and initial condition $[3, 1, 5]$.

$$\dot{x}(t) = Ax(t) + u(t)$$
$$y_i(t) = x_i(t) \quad \text{for } i \in Out \tag{67}$$

where $u_i(t) \equiv 0$ for $i \notin In$. The coordinate functions $x_i(t)$ are the state variables, the functions $y_i(t)$ are the output variables, and the nonzero functions $u_i(t)$ are the inputs. The resulting model is called a *linear compartment model*.

In [31], an explicit formula for the input-output equations for linear models was derived. In particular, it was shown that

all linear n-compartment models corresponding to strongly connected graphs with at least one leak and having the same input and output compartments will have the same differential polynomial form of the input-output equations. For example, a linear 2-compartment model with a single input and output in the same compartment and corresponding to a strongly connected graph with at least one leak has the form:

$$\ddot{y} + c_1\dot{y} + c_2 y = \dot{u} + c_3 u \tag{68}$$

Thus, our model discrimination method would not work for two distinct linear 2-compartment models with the above-mentioned form. In order to discriminate between two such models, we need to take other information into account, e.g., known parameter values.

Example 16. Consider the following two linear 2-compartment models:

$$\begin{pmatrix} \dot{x}_1 \\ \dot{x}_2 \end{pmatrix} = \begin{pmatrix} -p_{01} - p_{21} & p_{12} \\ p_{21} & -p_{12} \end{pmatrix} \begin{pmatrix} x_1 \\ x_2 \end{pmatrix} + \begin{pmatrix} u \\ 0 \end{pmatrix},$$
$$y = x_1$$
$$\begin{pmatrix} \dot{x}_1 \\ \dot{x}_2 \end{pmatrix} = \begin{pmatrix} -p_{21} & p_{12} \\ p_{21} & -p_{02} - p_{12} \end{pmatrix} \begin{pmatrix} x_1 \\ x_2 \end{pmatrix} + \begin{pmatrix} u \\ 0 \end{pmatrix},$$
$$y = x_1$$
(69)

whose corresponding input-output equations are of the form:

$$\ddot{y} + \left(p_{01} + p_{21} + p_{12}\right) \dot{y} + p_{01} p_{12} y = \dot{u} + p_{12} u$$
$$\ddot{y} + \left(p_{21} + p_{12} + p_{02}\right) \dot{y} + p_{02} p_{21} y$$
$$= \dot{u} + \left(p_{02} + p_{12}\right) u$$
(70)

Notice that both of these equations are of the above-mentioned form, i.e., both 2-compartment models have a single input and output in the same compartment and correspond to strongly connected graphs with at least one leak. In the first model, there is a leak from the first compartment and an exchange between compartments 1 and 2. In the second model, there is a leak from the second compartment and an exchange between compartments 1 and 2. Assume that the parameter p_{12} is known. In the first model, this changes our invariant to

$$\left(p_{01} + p_{21}\right) \dot{y} + p_{01} \left(p_{12} y\right) = \dot{u} + p_{12} u - \ddot{y} - p_{12} \dot{y}$$
$$\text{or, } c_1 \dot{y} + c_2 \left(p_{12} y\right) = \dot{u} + p_{12} u - \ddot{y} - p_{12} \dot{y}$$
(71)

In the second model, our invariant is

$$\left(p_{21} + p_{02}\right) \dot{y} + p_{02} p_{21} y - p_{02} u$$
$$= \dot{u} + p_{12} u - \ddot{y} - p_{12} \dot{y}$$
$$\text{or, } c_1 \dot{y} + c_2 y + c_3 u = \dot{u} + p_{12} u - \ddot{y} - p_{12} \dot{y}$$
(72)

In this case, the right-hand sides of the two equations are the same, but the first equation has two variables (coefficients) while the second equation has three variables (coefficients). Thus, if we had data from the second model, we could try to reject the first model (much like the 3-compartment versus 2-compartment model discrimination in the examples above). In other words, a vector in the span of $\dot{y}$, y, and u for t_1, t_2, t_3 may not be in the span of $\dot{y}$ and y only.

We next consider the effect of incorporating coefficient dependency relationships. While we cannot incorporate the polynomial algebraic dependency relationships among the coefficients in our linear algebraic approach to model rejection, we can include certain dependency conditions, such as certain coefficients becoming known constants. We have already seen one way in which this can happen in the previous example (from known nonzero parameter values). We now explore the case where certain coefficients go to zero. From the explicit formula for input-output equations from [31], we get that a linear model without any leaks has a zero term for the coefficient of y. Thus a linear 2-compartment model with a single input and output in the same compartment and corresponding to a strongly connected graph without any leaks has the form:

$$\ddot{y} + c_1 \dot{y} = \dot{u} + c_2 u$$
(73)

Thus to discriminate between two distinct linear 2-compartment models, one with leaks and one without any leaks, we should incorporate this zero coefficient into our invariant.

Example 17. Consider the following two linear 2-compartment models:

$$\begin{pmatrix} \dot{x}_1 \\ \dot{x}_2 \end{pmatrix} = \begin{pmatrix} -p_{01} - p_{21} & p_{12} \\ p_{21} & -p_{12} \end{pmatrix} \begin{pmatrix} x_1 \\ x_2 \end{pmatrix} + \begin{pmatrix} u \\ 0 \end{pmatrix}, \quad y = x_1$$
$$\begin{pmatrix} \dot{x}_1 \\ \dot{x}_2 \end{pmatrix} = \begin{pmatrix} -p_{21} & p_{12} \\ p_{21} & -p_{12} \end{pmatrix} \begin{pmatrix} x_1 \\ x_2 \end{pmatrix} + \begin{pmatrix} u \\ 0 \end{pmatrix}, \quad y = x_1$$
(74)

whose corresponding input-output equations are of the form:

$$\ddot{y} + \left(p_{01} + p_{21} + p_{12}\right) \dot{y} + p_{01} p_{12} y = \dot{u} + p_{12} u$$
$$\ddot{y} + \left(p_{21} + p_{12}\right) \dot{y} = \dot{u} + p_{12} u$$
(75)

In the first model, there is a leak from the first compartment and an exchange between compartments 1 and 2. In the second model, there is an exchange between compartments 1 and 2 and no leaks. Thus, our invariants can be written as

$$c_1 \dot{y} + c_2 y + c_3 u = \dot{u} - \ddot{y}$$
$$c_1 \dot{y} + c_2 u = \dot{u} - \ddot{y}$$
(76)

Again, the right-hand sides of the two equations are the same, but the first equation has three variables (coefficients) while the second equation has two variables (coefficients). Thus, if we had data from the first model, we could try to reject the second model. In other words, a vector in the span of $\dot{y}$, y, and u for t_1, t_2, t_3 may not be in the span of $\dot{y}$ and u only.

9. Conclusion

After performing this differential algebraic and statistical model rejection, one has already obtained the input-output equations and thus can test structural identifiability [17, 26, 34]. In a sense, our method extends the current spectrum of potential approaches for comparing models with time-course

data, in that one can first reject incompatible models, then test structural identifiability of compatible models using input-output equations obtained from the differential elimination, infer parameter values of the admissible models, and apply an information criterion model selection method to assert the best model.

Notably the presented differential algebraic and statistical method does not penalize for model complexity, unlike traditional model selection techniques. Rather, we reject when a model cannot, for any parameter values, be compatible with the given data. We found that simpler models, such as the linear 2-compartment model, could be rejected when data were generated from a more complex model, such as the three species Lotka-Volterra model, which elicits a wider range of behavior. On the other hand, more complex models, such as the Lorenz model, were often not rejected, from data simulated from less complex models. In the future it would be helpful to better understand the relationship between input-output invariants and dynamics. It would be useful to develop numerical algorithms in differential algebra (similar to that in numerical algebraic geometry); a natural extension, if such algorithms were available, would be to analyze models with data, although not parameter-free, similar to that done in [35, 36]. Another future direction is creating an algorithm that takes a probabilistic or randomized approach for eliminating variables of larger differential-algebra models [37].

We believe there is large scope for additional parameter-free coplanarity model comparison methods. It would be beneficial to explore whether algorithms for differential elimination can handle larger systems and whether this area could be extended.

Data Availability

The data used to support the findings of this study are available from the corresponding author upon request. All methods for data generation and analysis are described throughout the paper. Detailed research materials supporting this publication can be accessed by contacting HA Harrington.

Disclosure

Current address of Kenneth L. Ho: TSMC Technology, Inc., San Jose, CA 95134, USA.

Conflicts of Interest

The authors declare that there are no conflicts of interest regarding the publication of this paper.

Acknowledgments

References

[1] H. Akaike, "A new look at the statistical model identification," *IEEE Transactions on Automatic Control*, vol. 19, pp. 716–723, 1974.

[2] M. Feinberg, "Chemical reaction network structure and the stability of complex isothermal reactors—I. The deficiency zero and deficiency one theorems," *Chemical Engineering Science*, vol. 42, p. 2229, 1987.

[3] M. Feinberg, "Chemical reaction network structure and the stability of complex isothermal reactors-II. Multiple steady states for networks of deficiency one," *Chemical Engineering Science*, vol. 43, no. 1, pp. 1–25, 1988.

[4] B. L. Clarke, "Stoichiometric network analysis," *Cell Biophysics*, vol. 12, no. 1, pp. 237–253, 1988.

[5] J. Gunawardena, "Distributivity and processivity in multisite phosphorylation can be distinguished through steady-state invariants," *Biophysical Journal*, vol. 93, no. 11, pp. 3828–3834, 2007.

[6] A. K. Manrai and J. Gunawardena, "The geometry of multisite phosphorylation," *Biophysical Journal*, vol. 95, no. 12, pp. 5533–5543, 2008.

[7] C. Conradi, J. Saez-Rodriguez, E.-D. Gilles, and J. Raisch, "Using chemical reaction network theory to discard a kinetic mechanism hypothesis," *IEE Proceedings—Systems Biology*, vol. 152, no. 4, pp. 243–248, 2005.

[8] D. Cox, J. Little, and D. O'Shea, *Ideals, Varieties, and Algorithms*, Springer, New York, NY, USA, 2007.

[9] M. Drton, B. Sturmfels, and S. Sullivant, *Lectures on algebraic statistics*, vol. 39 of *Oberwolfach Seminars*, Springer, Basel, Switzerland, 2009.

[10] H. A. Harrington, K. L. Ho, T. Thorne, and M. P. Stumpf, "Parameter-free model discrimination criterion based on steady-state coplanarity," *Proceedings of the National Acadamy of Sciences of the United States of America*, vol. 109, no. 39, pp. 15746–15751, 2012.

[11] A. L. MacLean, Z. Rosen, H. M. Byrne, and H. A. Harrington, "Parameter-free methods distinguish Wnt pathway models and guide design of experiments," *Proceedings of the National Acadamy of Sciences of the United States of America*, vol. 112, no. 9, pp. 2652–2657, 2015.

[12] J. F. Ritt, *Differential Algebra*, Dover, 1950.

[13] P. S. Swain, K. Stevenson, A. Leary et al., "Inferring time derivatives including cell growth rates using Gaussian processes," *Nature Communications*, vol. 7, p. 13766, 2016.

[14] C. Aistleitner, *Relations between Gröbner bases, differential Gröbner bases, and differential characteristic sets, [M.S., thesis]*, Johannes Kepler Universität, 2010.

[15] E. R. Kolchin, *Differential Algebra and Algebraic Groups*, vol. 54 of *Pure and Applied Mathematics*, Academic Press, New York, NY, USA, 1973.

[16] I. Kaplansky, *An introduction to differential algebra*, Hermann, Paris, France, 1957.

[17] M. P. Saccomani, S. Audoly, and L. D'Angiò, "Parameter identifiability of nonlinear systems: The role of initial conditions," *Automatica*, vol. 39, no. 4, pp. 619–632, 2003.

[18] F. Boulier, F. Ollivier, D. Lazard, and M. Petitot, "Representation for the radical of a finitely generated differential ideal," in *Proceedings of the 1995 International Symposium on Symbolic and Algebraic Computation*, pp. 158–166, ACM Press, July 1995.

[19] O. Golubitsky, M. Kondratieva, M. Moreno Maza, and A. Ovchinnikov, "A bound for the Rosenfeld-Gröbner algorithm," *Journal of Symbolic Computation*, vol. 43, no. 8, pp. 582–610, 2008.

[20] S. Diop, "Differential-algebraic decision methods and some applications to system theory," *Theoretical Computer Science*, vol. 98, no. 1, pp. 137–161, 1992.

[21] "Maple documentation," 2016, http://www.maplesoft.com/support/help/maple/view.aspx?path=DifferentialAlgebra.

[22] N. Meshkat, C. Anderson, and I. DiStefano III, "Alternative to Ritt's pseudodivision for finding the input-output equations of multi-output models," *Mathematical Biosciences*, vol. 239, no. 1, pp. 117–123, 2012.

[23] G. Carrà Ferro, "em Gröbner bases and differential algebra," in *Proceedings of the 5th International Symposium on Applied Algebra, Algebraic Algorithms and Error-Correcting Codes*, L. Huguet and A. Poli, Eds., vol. 356 of *Lecture Notes in Computer Science*, pp. 131–140, Springer, 1987.

[24] F. Ollivier, "Standard bases of differential ideals," in *Proceedings of the 8th ternational Symposium on Applied Algebra, Algorithms, and Error-Correcting Codes*, S. Sakata, Ed., vol. 508 of *Lecture Notes in Computer Science*, pp. 304–321, Springer, 1991.

[25] E. Mansfield, *Differential Gröbner bases, [Ph.D. thesis]*, University of Sydney, 1991.

[26] L. Ljung and T. Glad, "On global identifiability for arbitrary model parametrizations," *Automatica*, vol. 30, no. 2, pp. 265–276, 1994.

[27] L. Q. Zhang, J. C. Collins, and P. H. King, "Indistinguishability and identifiability analysis of linear compartmental models," *Mathematical Biosciences*, vol. 103, no. 1, pp. 77–95, 1991.

[28] M. J. Chapman and K. R. Godfrey, "Nonlinear compartmental model indistinguishability," *Automatica*, vol. 32, no. 3, pp. 419–422, 1996.

[29] N. D. Evans, M. J. Chappell, M. J. Chapman, and K. R. Godfrey, "Structural indistinguishability between uncontrolled (autonomous) nonlinear analytic systems," *Automatica*, vol. 40, no. 11, pp. 1947–1953, 2004.

[30] K. R. Godfrey and M. J. Chapman, "Identifiability and indistinguishability of linear compartmental models," *Mathematics and Computers in Simulation*, vol. 32, no. 3, pp. 273–295, 1990.

[31] N. Meshkat, S. Sullivant, and M. Eisenberg, "Identifiability results for several classes of linear compartment models," *Bulletin of Mathematical Biology*, vol. 77, no. 8, pp. 1620–1651, 2015.

[32] X. Zhan, "Inequalities for the singular values of Hadamard products," *SIAM Journal on Matrix Analysis and Applications*, vol. 18, no. 4, pp. 1093–1095, 1997.

[33] J. A. Tropp, "User-friendly tail bounds for sums of random matrices," *Foundations of Computational Mathematics*, vol. 12, no. 4, pp. 389–434, 2012.

[34] F. Ollivier, *Le probleme de lidentifiabilite structurelle globale: etude theoretique, methodes effectives et bornes de complexite, [Ph.D. thesis]*, Ecole Polytechnique, 1990.

[35] E. Gross, H. A. Harrington, Z. Rosen, and B. Sturmfels, "Algebraic systems biology: a case study for the Wnt pathway," *Bulletin of Mathematical Biology*, vol. 78, no. 1, pp. 21–51, 2016.

[36] E. Gross, B. Davis, K. L. Ho, D. J. Bates, and H. A. Harrington, "Numerical algebraic geometry for model selection and its application to the life sciences," *Journal of the Royal Society Interface*, vol. 13, no. 123, Article ID 20160256, 2016.

[37] A. Ovchinnikov, G. Pogudin, and N. T. Vo, "Bounds for elimination of unknowns in systems of differential-algebraic equations," https://arxiv.org/abs/1610.04022.

Research Article

Dynamic Modeling of the Angiogenic Switch and Its Inhibition by Bevacizumab

Dávid Csercsik [1,2] **and Levente Kovács** [1]

[1]*Physiological Controls Research Center, University Research, Innovation and Service Center, Óbuda University, Budapest, Hungary*
[2]*Pázmány Péter Catholic University, Faculty of Information Technology and Bionics, P.O. Box 278, 1444 Budapest, Hungary*

Correspondence should be addressed to Dávid Csercsik; csercsik@itk.ppke.hu

We formulate a dynamic model of vascular tumor growth, in which the interdependence of vascular dynamics with tumor volume is considered. The model describes the angiogenic switch; thus the inhibition of the vascularization process by antiangiogenic drugs may be taken into account explicitly. We validate the model against volume measurement data originating from experiments on mice and analyze the model behavior assuming different inputs corresponding to different therapies. Furthermore, we show that a simple extension of the model is capable of considering cytotoxic and antiangiogenic drugs as inputs simultaneously in qualitatively different ways.

1. Introduction

Neovascularization means the formation of new blood vessels. Angiogenesis, an important form of neovascularization, is characterized by hypoxia-driven sprouting of new capillaries from postcapillary venules. This mechanism plays an important role in many physiological (e.g., wound healing [1]) and pathological (e.g., macular degeneration [2]) processes. In the development of tumors, angiogenesis plays an exceptionally important role [3, 4]. In the beginning, when the tumorous cells form a small plaque, the tumor cells are well supported with metabolites by diffusion from the environment. However, as the size of the tumor increases, cells in the inside become insufficiently supported. Tumor-induced angiogenesis is the process of blood vessel formation, in which new vasculature is formed in order to support these insufficiently supported tumor cells.

Lately, much has been revealed about the details of tumor-induced angiogenesis and the underlying biochemical and biomechanical regulatory processes. These studies served as basis for the development of targeted molecular therapies [5]. The aim of these therapies is to inhibit tumor-related angiogenesis, thus cutting the tumor from metabolic support.

Bevacizumab (Avastin) is a pharmacotherapeutic antiangiogenic agent developed to withhold pathological angiogenesis [6] via the inhibition of the tumor angiogenic factor VEGF (vascular endothelial growth factor) [7]. VEGF may be considered as a representative member of the family of biochemical agents promoting angiogenesis, called tumor angiogenic factors (TAFs).

In [8], two different dosage protocols of bevacizumab were compared. In the case of the first protocol, experimental animals (mice) received one high dose according to the generally accepted medical principle, while in the case of the second protocol (quasi-continuous therapy), a much lower dose was delivered every day of the therapy. Results have shown that the quasi-continuous protocol was more effective, while the total injected amount of the drug was significantly less. As antiangiogenic agents are expensive, the total used drug amount is an important aspect to consider in therapeutic design. In addition, reduction of therapeutic doses is also desirable to minimize drug side effects. The result described in [8] underlines the importance of therapy optimization in the case of the application of antiangiogenic drugs and shows that computational methods may help to exploit the potentials of this approach.

On the other hand, based on the new data and paradigms brought to light in biological studies on angiogenesis, computational modeling of tumor-related vasculature development has became popular in the last decades, producing numerous computational models describing tumor growth and tumor-induced angiogenesis under different physiological circumstances (for a review on mathematical modeling of angiogenesis, see [9–12], while for a biological viewpoint on the mechanisms of physiological and tumor-related/pathological angiogenesis, one may refer to [13]). An important aspect of these modeling studies is to predict the effect of possible therapeutic approaches in cancer treatment [14–16].

A large part of the aforementioned models exhibit a quite high level of complexity, which implies that while they may be potentially appropriate for the comparison of different therapeutic approaches under the assumption of a given parameter set, it can be challenging to fit them to single patients. Furthermore, exact therapy optimization may be computationally infeasible if one relies on complex and spatially detailed models as [17, 18].

Feedback control [19, 20] may be an alternative to offline therapy optimization approaches. One benefit of closed-loop methods is that, assuming appropriate physiological signals, they may provide performance guarantees also in the presence of parametric uncertainties [21]. Other potential benefits of closed-loop treatments over protocol-based cancer therapies are discussed in [22]. In the case of diabetes, a similar biological control problem, such approaches have been successfully applied [23–27]. Control theoretic methods require, however, concentrated parameter models and ordinary differential (or difference) equation models with moderate complexity to perform well.

Recently, a simple dynamical model of tumor growth and the effect of the antiangiogenic drug bevacizumab has been published [28]. This model contains very few parameters and state variables and thus it is ideal for parameter estimation and controller design purposes. This model is based on three state variables, namely, the proliferating tumor volume, the necrotic tumor volume, and the concentration of the angiogenic inhibitor. Although this model provides a good fit for certain experimental data (see the data later in Section 2.2), it holds some flaws.

First, as it does not include the description of vasculature dynamics, its drawback is that it is unable to interpret advanced measurement data corresponding to tumor and vasculature evolution dynamics, potentially available in the foreseeable future. Recently, several imaging techniques have been described, which allow the reconstruction of vascular microstructures: Doppler optical frequency domain imaging [29] and functional photoacoustic microscopy [30] are used today already in *in vivo* setups to map vascular networks, while diffusible iodine-based contrast-enhanced computed tomography [31] may be used in terminal experimental animals. These methods could provide valuable data about vasculature dynamics in the near future, which may be used for the identification of the details of the angiogenic processes.

Second, minimal models not including vasculature dynamics as [28] are lacking the potential to describe the phenomenon of the angiogenic switch [32]. This hypothesis, formulated by Folkman, assumes that angiogenesis begins only at a certain stage of tumor development, more precisely at the time when the limited diffusion distance (which is about 0.1 mm [33]) makes the support of tumor cells inside the tumor with oxygen and metabolites no longer possible. According to the prediction of the minimal model [28], antiangiogenic drugs significantly affect the tumor growth also in the initial period. This contradicts with the consideration based on Folkman's hypothesis that implies that in the initial period no insufficiently supported tumor cells are present, so no TAF synthesis is present; thus its effect can not be inhibited. In addition to the fact that minimal models like [28, 34] do not explicitly consider angiogenesis, the model [28] assumes a very simple constant rate of drug-independent necrosis, in which the proliferating cells turn into necrotic cells. In contrast, the process of necrosis strongly depends on the metabolic support and thus on the vascularization state of the tumor.

Third, paper [28] is based on the comparison of simulation results to measurement data originating from two scenarios. In these two scenarios, the antiangiogenic drug Bevacizumab was administered to experimental animals according to different protocols. In the first protocol, one 200 μg bevacizumab dose was used for an 18-day therapy, while in the second (quasi-continuous) protocol one-tenth of the 200 μg (20 μg) dose was spread over 18 days; that is, 1.11 μg bevacizumab was administered every day to the animals. Paper [8] is also based on results corresponding to these 2 administration protocols but also discusses results corresponding to therapy/drug-free case; namely, it states that mice that were treated with protocol 1 (one 200 μg bevacizumab dose) did not have significantly smaller tumor volume than mice that did not receive therapy at all. In contrast to this result, if we compare the final tumor volumes resulting from the simulation of the model [28] in the case of protocol 1 and in the no-therapy case, we find that, in the case of protocol 1, the model prediction for the final tumor volume is 4741 mm^3 (which is in good agreement with the experimental results), while in the no-therapy case, the model prediction for the final tumor volume is 37628 mm^3. This means that, according to the prediction of this model, the no-therapy final tumor size is almost 8 times larger than the protocol 1 case, making the validity of the model questionable in the no-therapy case, based on the results of [8]. We would underline that this does not question the validity of the model [28] in the case of Bevacizumab protocols and feedbacks similar to the ones discussed therein.

Another paper that aimed to formulate a control-oriented dynamical model was also recently published [35]. This model, which uses a bicompartmental approach, does describe the dynamics of vasculature but results in a 7-dimensional state space and 23 parameters, which is quite challenging size for control design. In addition, the model described in [35] was fit only to data corresponding to the first protocol in [8] (not both, like [28]).

According to the above preliminary results and considerations, our aim in this paper is as follows. We formulate

a dynamic model, which includes the dynamics of the vasculature volume and describes the interplay between the tumor and vasculature volumes. To achieve this, we also include the dynamics of TAF in the model, which is produced by unsupported tumor and initiates the formation of new blood vessels from existing ones. This way our model will be capable of the interpretation of measurement corresponding to tumor and vasculature evolution dynamics. Furthermore, we aim to formulate a model, the predictions of which are also more acceptable in the therapy-free case.

2. Model Synthesis

In the following, we introduce the state-space variables of the model and interpret the state equations with the discussion of the model assumptions. Afterwards, the model parameters, their estimation, and the contextualization of the resulting parameters are described.

2.1. State Variables and Equations. The state-space variables of the model are summarized in Table 1 and their dynamics are described by the following equations:

$$\frac{dV}{dt} = c_g \gamma V - c_n V_u \tag{1}$$

$$\frac{dN}{dt} = c_n V_u \tag{2}$$

$$\frac{dB}{dt} = c_{ev}\dot{V}_{tot} + c_v TB \tag{3}$$

$$\frac{dT}{dt} = c_T \frac{V_u}{V} - q_T T - c_h \frac{TI}{ED_{50} + I} \tag{4}$$

$$\frac{dI}{dt} = u - q_I \frac{I}{k_I + I} - k_V c_h \frac{TI}{ED_{50} + I} \tag{5}$$

V_{tot} is the total volume of the tumor, the sum of the proliferating (living) volume and the necrotic volume: $V_{tot} = V + N$; thus $\dot{V}_{tot} = c_g \gamma V$. Furthermore, V_u denotes the unsupported living tumor volume $V_u = (1-\gamma)V$; thus $V_u/V = (1-\gamma)$. u denotes the input, the injection of the antiangiogenic drug.

We assume a simple spherical tumor. This simplifying assumption (one-dimensional growth in other words) is widely used in the tumor modeling literature (see, e.g., [36–42]).

The auxiliary variable γ in the above equation is a key element of the model: it describes the actual ratio of the well-supported tumor cells in the tumor. γ is the function of the actual total volume V_{tot} and the vascularization ratio of the tumor (r_v). r_v can be computed as

$$r_v = 1 - \frac{[B]^{id} - [B]}{[B]^{id}} \tag{6}$$

where $[B]^{id}$ denotes the ideal density of vasculature in the tumor (notations with square brackets always refer to densities). This ideal density corresponds to the vasculature

TABLE 1: State variables of the model.

Notation	Variable	Dimension
V	Proliferating tumor volume	mm^3
N	Necrotic tumor volume	mm^3
B	Vasculature volume in the tumor	mm^3
T	Concentration of TAF in the tumor	mg/ml
I	Inhibitor serum level	mg/ml

density, when all tumor cells are sufficiently supported; in other words, $r_v = 1$. In accordance with biological results [43–45], we assume that the vasculature is present in the living part of the tumor; thus the vasculature density is interpreted as density of blood vessels in the living (nonnecrotic) part of the tumor and is calculated as $[B] = B/V$. Regarding the validity range of the model, we assume that the inequality $[B] < [B]^{id}$ holds at all times (in other words, we assume that the tumor is never fully vascularized).

The supported ratio of the tumor (γ) is computed as

$$\gamma = (1 - r_v) f_P (V_{tot}) + r_v \tag{7}$$

which may be viewed as a linear homotopy in $r_v \in [0, 1]$ between the constant 1 function and the function $f_P(V_{tot})$, which is also between zero and one. Thus $\gamma \in [0, 1]$ also holds. The interpretation is that $f_P(V_{tot})$ denotes a function that describes the ratio of tumor cells on the periphery of the tumor, which receive nutrients from outside of the tumor, so they are well supported. Naturally, this ratio depends on the actual total tumor volume V_{tot}. More precisely, in our terms, the periphery of the tumor is the outer shell of the sphere of our model, composed by tumor cells, which are closer to the surface of the tumor than the diffusion distance. According to [33], we assume the diffusion distance to be 150 μm. The ratio of periphery cells depends upon the radius of the tumor, which can be expressed from the tumor volume V, according to the following simple derivation. Based on the tumor volume, we may derive the tumor radius (in mm) as

$$V_{tot} = \frac{4}{3}\pi r^3$$
$$r = \sqrt[3]{\frac{3V_{tot}}{4\pi}}. \tag{8}$$

If $r \le 0.15$, there is no tumor core. Assuming $r > 0.15$, the volume of the tumor core is

$$V_C = \frac{4}{3}\pi (r - 0.15)^3, \tag{9}$$

And thus the volume of the periphery is

$$V_P = V_{tot} - V_C, \tag{10}$$

and finally the function $f_P(V_{tot})$ is derived as

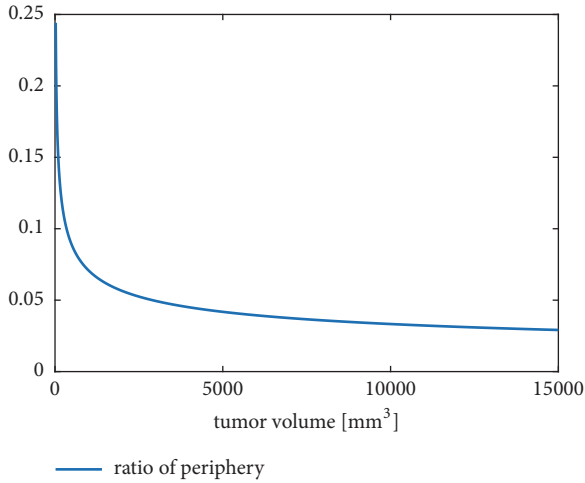$$f_P (V_{tot}) = \frac{V_P}{V_{tot}}. \tag{11}$$

FIGURE 1: The function $f_P(V_{tot})$ describing the ratio of periphery cells in the range of 20-15000 mm^3 tumor volume.

If the tumor radius is below the diffusion distance, all cells are considered as periphery cells. The function $f_P(V_{tot})$ describing the ratio of periphery cells in the range of 20-15000 mm^3 is depicted in Figure 1 (according to [8], in the time of the first measurement, the volume of the tumors is about 50-60 mm^3).

Now let us return our focus to the auxiliary variable γ. The consideration behind the form of function (7) is that we assume two possible ways by which a tumor cell may get nutrient support. On one hand, if it is at the periphery of the tumor, it gets nutrients from the environment of the tumor via diffusion. On the other hand, if it is inside the tumor near a blood vessel, it also receives nutrient supply. The properties of function (7) reflect these considerations. We may see that if the tumor is composed only (or because of the approximation mostly) periphery cells or is almost fully vascularized ($r_v \simeq$ 1), the value of γ is approximately 1. In addition, at a fixed value of r_v, it increases as the value of $f_P(V_{tot})$ is increased, and at a fixed vale of $f_P(V_{tot})$, the value of γ is increased as r_v increases (to put it simple, it is monotonically increasing in both variables).

Now, as we have discussed the interpretation of the auxiliary variables and the corresponding assumptions, we may return to the state equations. Equation (1) describes the tumor growth. The formula originates from the assumption that the well-supported part of the tumor volume (γV) proliferates at the rate c_g, while the unsupported volume V_u necrotizes at the rate c_n.

Equation (3) formalizes the dynamics of the vasculature, which may increase by two ways. On one hand, the term $c_{ev}\dot{V}_{tot}$ describes the internalization of new vasculature from the environment as the tumor grows, and on the other hand the term $c_v TB$ describes the formation of new blood vessels from existing ones in response to the TAF.

Equation (2) corresponds to necrotic volume. The importance of formally describing the process of necrosis lies in the fact that necrotized cells neither proliferate nor contribute to TAF production, so they must be distinguished from the general tumor volume.

Equations (4) and (5) describe the dynamics of TAF and the inhibitor concentration, respectively. The terms

$$c_T \frac{V_u}{V} - q_T T \tag{12}$$

of (4) describe that the production of TAF is proportional to the ratio of unsupported cells V_u/V and takes place at rate c_T, while it is cleared at the rate q_T from the tumor. In the case of the inhibitor, the source is the injection (the input) u, while based on [28], we assume that its clearance takes place according to Michaelis-Menten kinetics. The terms

$$c_h \frac{TI}{ED_{50} + I} \tag{13}$$

and

$$k_V c_h \frac{TI}{ED_{50} + I} \tag{14}$$

in (4) and (5), respectively, correspond to the reaction in which the inhibitor binds the TAF molecule. Also, based on [28], the dynamics of the inhibition are considered assuming Michaelis-Menten kinetics with Michaelis-Menten constant ED_{50} (effective median dose).

The variable k_V corresponds to the consideration that the concentrations of TAF (T) and the inhibitor (I) are not interpreted in the same volume (the compartment in the former case is the tumor; the volume in the latter case is the plasma). k_V is the ratio of these volumes and can be computed as

$$k_V = \frac{V_{tot}}{1460} \tag{15}$$

where the value 1460 stands for the average blood volume of a mice in μm^3, in which the concentration of the inhibitor is interpreted [46].

2.2. Model Parameters. Some parameters of the model were taken from the literature (see Table 2), while the remaining parameters were estimated using experimental data originating from mice. Sápi et al. [8] carried out experiments, where C57Bl/6 mice with C38 colon adenocarcinoma were treated with bevacizumab using two different therapies.

(i) Therapy 1 (protocol-based treatment): five mice (mice C1-C5) were injected with 0.171 mg/ml bevacizumab at day 3 of the treatment (day 0 is considered as the day of the tumor implantation) (see Figure 2(a)).

(ii) Therapy 2 (daily, quasi-continuous small amount administration): nine mice (mice E1-E9) received $9.5 \cdot 10^{-4}$ mg/ml injection of bevacizumab each day for 18 days from day 3 (see Figure 2(b)).

The nominal parameter set of the model was determined using the average of measurements as reference and minimizing the mean square error of the deviance between the
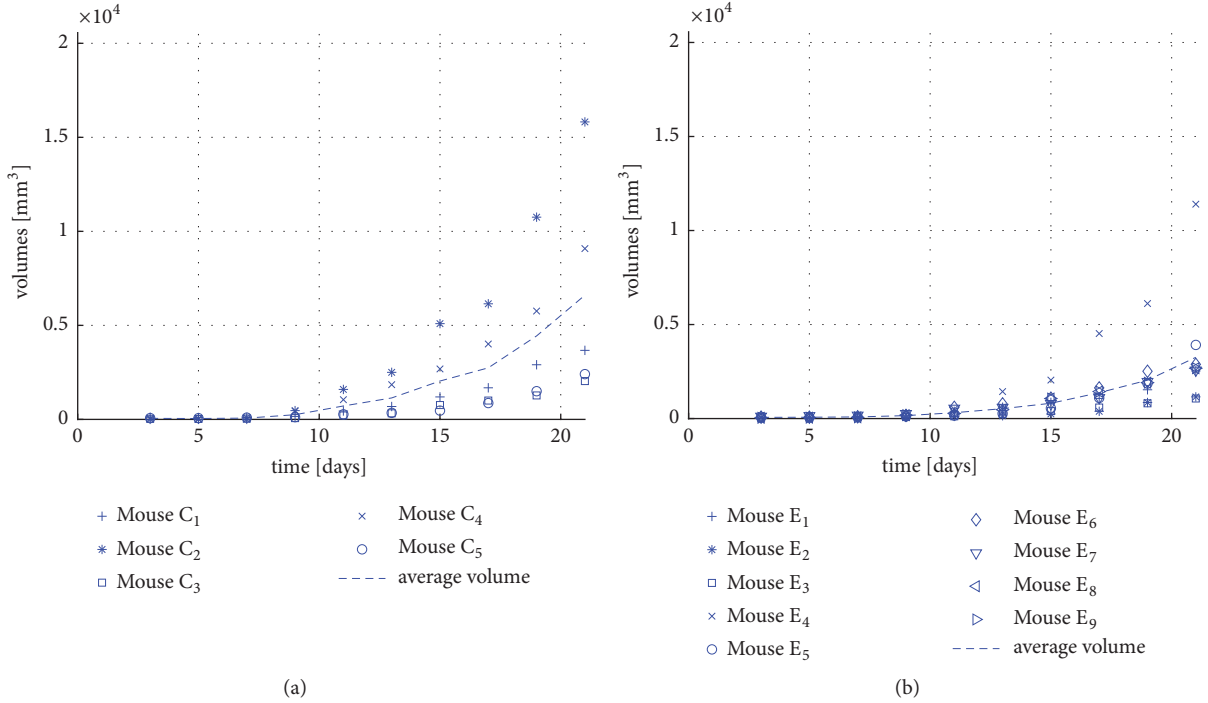
Figure 2: (a) The measured tumor volumes for mice C1-C5 that received therapy 1 and their average. (b) The measured tumor volumes for mice E1-E9 that received therapy 2 and their average.

simulated and measured total volumes using the combination of particle swarm global optimization method [47] and the "nlinfit" function of MATLAB. During the simulations, the initial volume of the tumor was assumed to be equal to 5 mm³, while the initial values of all other state variables were assumed to be 0. To capture the qualitatively different response of tumor growth to the two different protocols, both average curves (corresponding to protocols 1 and 2) were used simultaneously for the purpose of parameter estimation. While initial guess of the parameters was determined by the particle swarm global search method, the final values of the parameters were obtained using the "nlinfit" function. From the results of this function, the 95% confidence intervals (CI_{95}) were determined using the function "nlparci."

In order to potentially achieve a global optimum with the resulting parameter set, the estimation procedure was started from several initial coordinates in the parameter space. During parameter estimation, the average measurement results of both protocols were used to capture the qualitatively different response of the system to different inputs. Table 2 summarizes the model parameters. These parameters are to be referenced as nominal parameters in the further discussion and are denoted as θ_{nom}.

In addition, to quantify parameter variance in the context of single trajectories, the model was fitted also for single growth curves as described in the Appendix.

Most estimated parameters of the model are hard to measure individually (in fact some of them are only interpreted inside the framework of this model) and no data are available on them which could serve as basis for comparison.

3. Results and Discussion

3.1. Fitting the Model to Measurement Data. In this subsection, we compare the model behavior and parameter values to measurement data. Figure 3 shows the fit of the model simulation output (total volume) to the experimental data sets that were used for the parameter estimation (therapy 1 and therapy 2). As it can be seen in the figures, the model sufficiently reproduces the measured growth trajectories, and the better fit is achieved in the case of therapy 2. For the sake of clarity, we note that since the average curve of measurement results was used for parameter estimation, the number of mice used in the experiments did not influence the objective function (in other words, this is not the reason for better fit in the case of therapy 2). To quantify the fit, we introduce the normalized squared deviation (NSD) as

$$NSD = \frac{\sum_{t_S} \left(V_{tot}\left(t_S\right) - V_{tot}^M\left(t_S\right) \right)^2}{|t_s|} \qquad (16)$$

where V_{tot} is the simulated total volume ($V_{tot} = V + N$) and V_{tot}^M is the measured total volume. t_S stands for the set of sample times, corresponding to days 3, 5, 7, 9, 11, 13, 15, 17, 19, and 21 in this case, while $|t_S|$ denotes the number of sample days. Normalization by the number of days is required, because we will use this measure later as well in the case of experimental data, where the number of sample points is lower. According to this measure, the representative values are $NSD_{T1} = 5.5614 \cdot 10^5$ and $NSD_{T2} = 6.0609 \cdot 10^4\ mm^6$ in the case of therapy 1 and therapy 2, respectively.

TABLE 2: Nominal model parameters (θ_{nom}) and their dimension, source, and 95% confidence interval (CI_{95}). PE stands for parameter estimation.

| Notation	Dimension	Value	Source	CI_{95}
c_g	$\dfrac{1}{day}$	1.4353	PE	$\begin{bmatrix} 1.4252 & 1.4455 \end{bmatrix}$
$[B]^{id}$	-	0.0388	PE	$\begin{bmatrix} 0.0383 & 0.0393 \end{bmatrix}$
c_{ev}	-	$1.1586 \cdot 10^{-3}$	PE	$\begin{bmatrix} 1.1548 & 1.1624 \end{bmatrix} \cdot 10^{-3}$
c_n	$\dfrac{1}{day}$	0.0941	PE	$\begin{bmatrix} 0.0934 & 0.0947 \end{bmatrix}$
c_v	$\dfrac{ml}{mg\,s}$	11.6690	PE	$\begin{bmatrix} 11.6060 & 11.7320 \end{bmatrix}$
c_T	$\dfrac{mg}{ml\,s}$	$1.1377 \cdot 10^{-2}$	PE	$\begin{bmatrix} 1.1330 & 1.1423 \end{bmatrix} \cdot 10^{-2}$
q_T	$\dfrac{1}{day}$	0.2473	PE	$\begin{bmatrix} 0.2466 & 0.2480 \end{bmatrix}$
c_h	$\dfrac{mg}{ml\,mm^3\,s}$	0.1633	PE	$\begin{bmatrix} 0.1628 & 0.1637 \end{bmatrix}$
ED_{50}	$\dfrac{mg}{ml}$	$5 \cdot 10^{-5}$	[48]	-
q_I	$\dfrac{1}{day}$	0.5776	[49]	-
k_I	$\dfrac{mg}{ml}$	0.4409	[28]	-

(a)

(b)
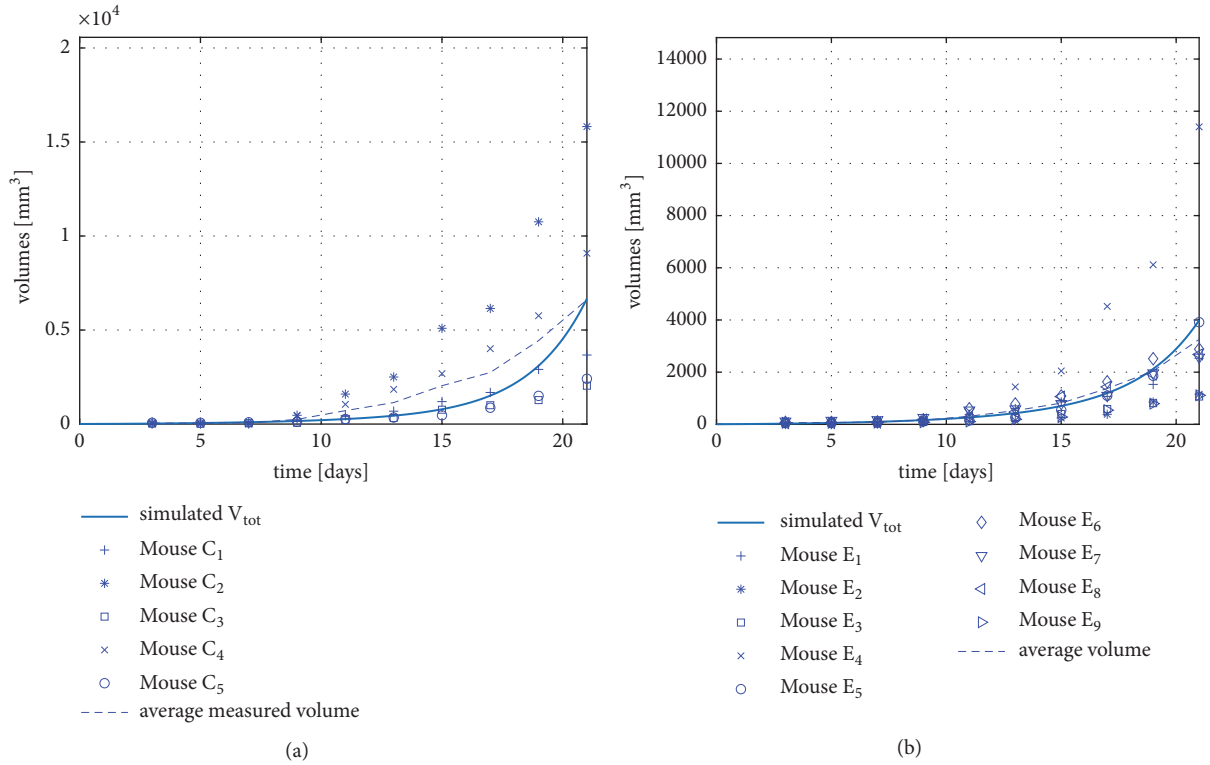
FIGURE 3: Measured and simulated tumor volumes in the case of therapy 1 (a) and therapy 2 (b).

The possible reason for the better fit in the case of the quasi-continuous therapy may be that the average of the measurements provides a more smooth, exponential-like curve in this case, which was possibly more easy to be achieved by the model.

The final volume of the tumor according to simulation results is 6670 mm^3 in the case of therapy 1 and 3993 mm^3 in the case of therapy 2. Considering the data described in Section 2.2, the final average measured volumes (corresponding to day 21) were 6604 and 3257 mm^3 in the cases of therapy 1 and therapy 2, respectively.

3.2. Model Validation

3.2.1. Qualitative Validation. In this subsection, we analyze and compare the dynamic behavior of key model variables in the cases of no therapy, therapy 1, and therapy 2 defined in Section 2.2.

Figure 4 depicts the trajectory of γ and r_v in the various cases.

In general, it can be said that, in the beginning, when the tumor is small, due to the high ratio of periphery cells, γ (i.e., the ratio of the well-supported tumor cells) is high. However, as the tumor grows, the ratio of peripherial cells and so γ also decrease. The trajectories of the various cases differ only after day 6. The reason for this is that the process of angiogenesis becomes significant only if a large part of unsupported cells and TAF is already present, and the inhibition of the process becomes important only in this period. This is also shown in Figure 4(b), where it can be seen that the various cases regarding the vascularization ratio (r_v) differ only after day 6. Furthermore, it can be seen in Figure 4 that both γ and r_v remain in the range $[0, 1]$ as assumed during the model formulation. Figure 5 depicts the inhibitor concentration in the cases of therapy 1 and therapy 2 (in the case of no therapy, the inhibitor concentration is constant zero during the simulation). It can be seen in the figure that, in the case of therapy 1, the concentration is several orders of magnitude higher compared to therapy 2.

Figure 6 depicts the concentration of TAF (T) and the term $c_v TB$ of (3) (corresponding ot TAF-dependent vascularization) in response to the various levels of the inhibitor in the case of different therapies.

In this figure (Figure 6(a)), it can be seen that the concentration of TAF (T) around days 3-8 is almost the same in the case of therapy 1 and therapy 2, although the concentration of the inhibitor (I) differs on the orders of magnitude. The explanation for this is the effective median dose (ED_{50}) of the inhibitor, which defines the inhibitor level at which the effect of the drug saturates. We have to note that this parameter was not subject to estimation but it was taken from the article [48]. Figure 6(b) depicts that from the time when the large bolus has been cleared in the case of therapy 1 (around day 13), the TAF-dependent vascularization (TdV) becomes significantly different in the case of the two therapies.

Since the volume trajectories of the model follow an exponential-like fashion in all cases, they are maybe not so

Table 3: Simulated and measured average total volumes on day 21 (mm^3).

Therapy	$V_{tot}(21)$	$V_{tot}^M(21)$
No therapy	$1.03 \cdot 10^4$	No data
Therapy 1	$6.67 \cdot 10^3$	$6.60 \cdot 10^3$
Therapy 2	$3.99 \cdot 10^3$	$3.26 \cdot 10^3$

Table 4: Simulated and measured average total volumes on day 19 (mm^3).

Therapy	$V_{tot}(19)$	$V_{tot}^M(19)$
No therapy	$4.68 \cdot 10^3$	$6.15 \cdot 10^3$
Therapy 1	$3.10 \cdot 10^3$	$4.44 \cdot 10^3$
Therapy 2	$2.13 \cdot 10^3$	$2.03 \cdot 10^3$

informative as, for example, the plot of γ, but for the sake of completeness, they are depicted in Figure 7.

3.2.2. Validation against Measurement Data with No Therapy. In phase I of the experiments described in [8], the experimental animals received no treatment. In this case, the length of the experiment was only 19 days (compared to 21 days in all other experiments discussed before and depicted in Figure 2). The measurement data originating from this experiment was used to validate the model. Figure 8 shows the results of the model validation.

The measure of the fit introduced in (16) gives a value of $NSD_{NT} = 1.5451 \cdot 10^6$ mm^6 in this case (the lower index corresponds to "no therapy"). If one compares this value to the NSD values corresponding to the experimental data to which the model was fitted (see Section 3.1), or examines the figures, it can be seen that the error of the fit is one order of magnitude higher in this case (since the no-therapy case was not considered during parameter estimation). On the other hand, taking into account the significant variation among experimental animals as well, the the model output in the case of no therapy provides an acceptable fit with measurement data.

3.2.3. Validation regarding Final Tumor Volume Values in Various Cases. As in control applications, for which the current model is primary proposed, the usual aim is to minimize the final volume of the tumor (under, e.g., constraints corresponding to the total applied drug quantity); it is important to compare the final tumor sizes. As the final day of the experiments was different in the no-therapy case and therapies 1 and 2, Tables 3 and 4 summarize the simulated and measured tumor volumes on days 19 and 21.

For the sake of comparison to previous literature results, let us note that the simulated volume on day 19 assuming no therapy is $1.85 \cdot 10^4$ in the case of the model described in [28] (this value has been obtained by the reproduction of the model described in [28]). Comparing the differences of the values, we may say that the validity of the proposed model compared to [28] is significantly better regarding the final volume in the no-therapy case.

(a)   (b)
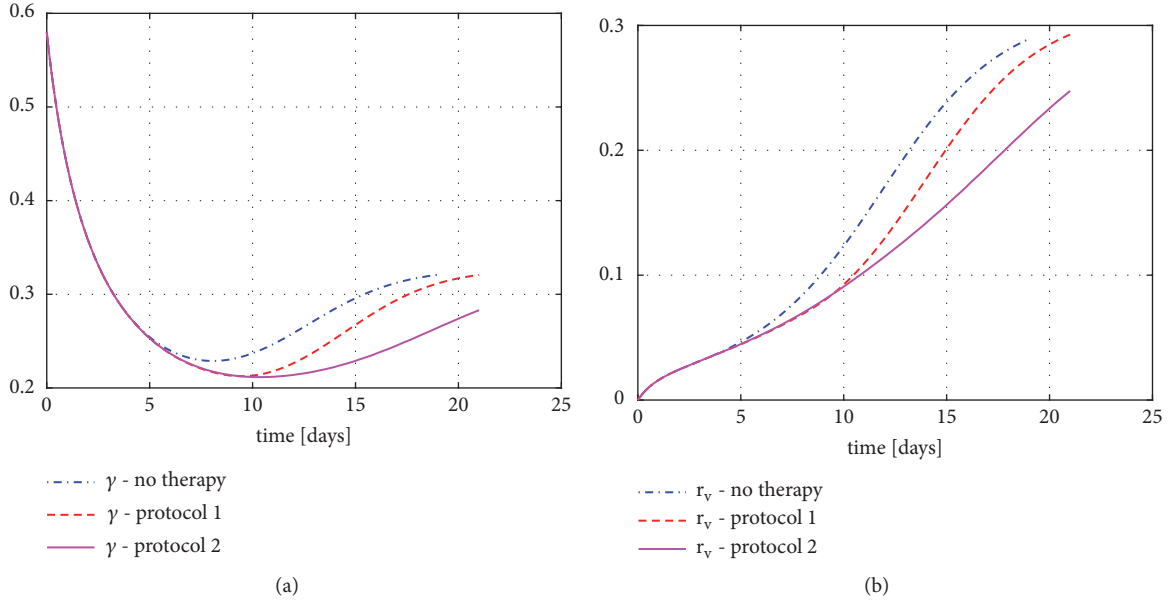
FIGURE 4: (a) Ratio of the well-supported tumor cells (γ) in the case of various therapies; (b) vascularization ratio (r_v) in the case of various therapies.
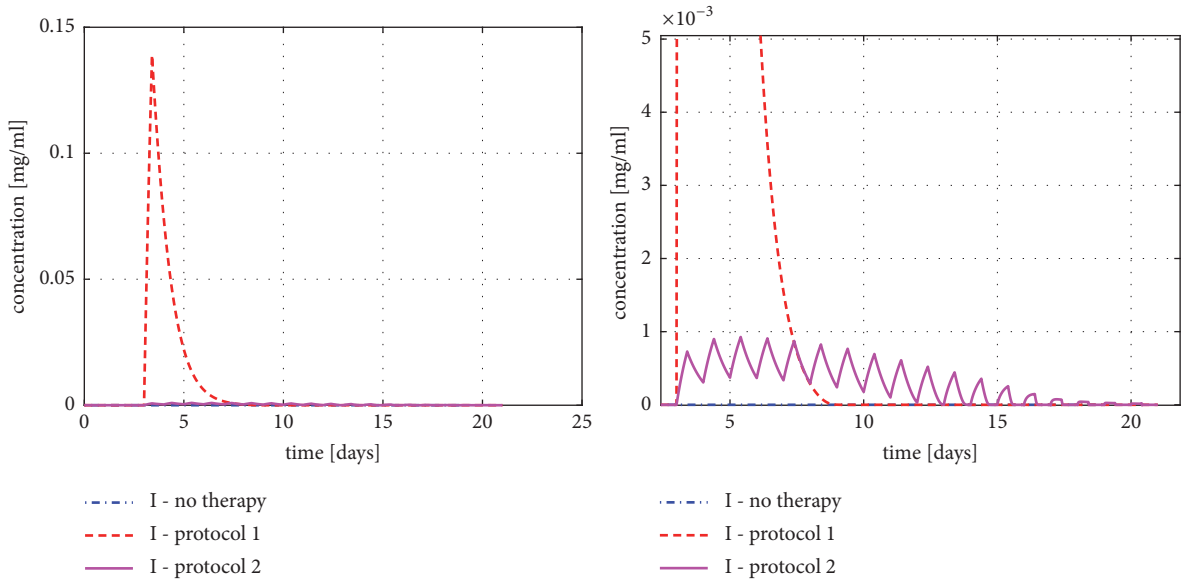
FIGURE 5: Concentration of the inhibitor (I) in the case of various therapies on two different scales.

3.3. Model Identifiability.
In the following two subsections, we present some results related to the parameter sensitivity and structural identifiability of the proposed model.

3.3.1. Parameter Sensitivity of the Model.
In this subsection, we analyze the parameter sensitivity of the model for the estimated parameters. The sensitivity analysis is an important tool to characterize how the model parameters affect the simulation output. The presence of very large differences in the sensitivities of parameters may point to identifiability problems.

In order to formalize this analysis, we define the sensitivity measure detailed in the following equation:

$$S\left(\widehat{\theta}\right) = \int_0^T \frac{\left(V_{tot}\left(t, \theta_{nom}\right) - \widehat{V}_{tot}\left(t, \widehat{\theta}\right)\right)^2}{T} dt \qquad (17)$$

In (17), θ_{nom} denotes the nominal parameter vector detailed in Table 2, while $\widehat{\theta}$ denotes a perturbed parameter vector. $V_{tot}(\tau, \theta_{nom})$ and $\widehat{V}_{tot}(\tau, \widehat{\theta})$ stand for the nominal output ($V_{tot}(t)$) of the model and for the output in the case of the perturbed parameter vector, respectively.

FIGURE 6: (a) Concentration of TAF (T) in the case of various therapies; (b) TAF-dependent vascularization (TdV) in the case of different therapies.

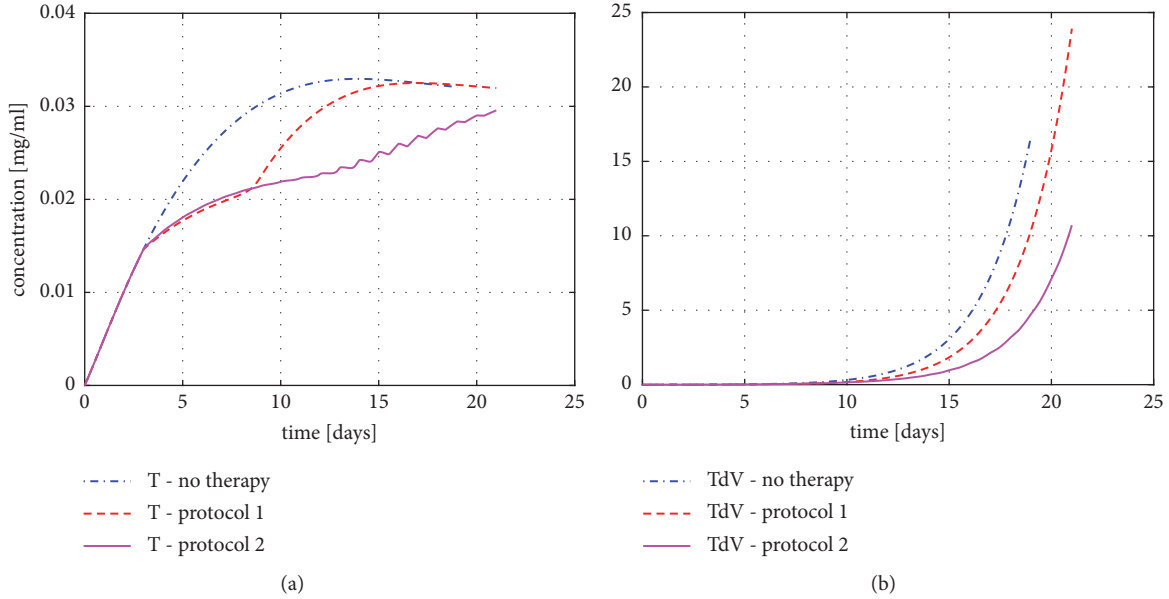*No-Therapy Case.* Table 5 summarizes the results in the no-therapy case. Each row of this table corresponds to a $\hat{\theta}$ perturbed parameter vector, in which only one element differs from the nominal θ vector (by 20, 10, or 5%).

First, it is conspicuous that the sensitivity to the parameter c_h is zero in this case. The explanation for this is that this parameter corresponds to the effect of the angiogenic inhibitor (I), the concentration of which is constantly 0 in this case. In other words, there is no drug effect in this case, the dynamics of which are affected by this parameter.

Second, we can see in Table 5 that the sensitivity for c_v is equal to the sensitivity of c_T in the no-therapy case. The reason for this is that while c_T corresponds to the synthesis rate of TAF, c_v corresponds to the rate of TAF-dependent vascularization. If no inhibitor is present, there is no difference between an increase in the TAF concentration and a more efficient TAF-driven vascularization (see (3) and (4)). Let us note that if the inhibitor is present, not the whole portion of the synthetized TAF takes part in the blood vessel formation process (since some molecules are binding to the inhibitor); thus the situation is different if input (thus nonzero drug concentration) is also present.

Third, the model is the most sensitive to the parameter c_g. This is not surprising, as c_g directly affects the dynamics of V (see (1)) as a proportional term, so its effect in V, which is directly present in the output, is exponential. Apart form c_h, q_I, and k_V, the model shows the least sensitivity to c_n, the rate of necrosis.

Therapy 1. Table 6 shows that the model sensitivity for c_h, the parameter corresponding to the effect of the inhibitor, is relatively low.

Table 7 shows that, in the case of therapy 2, an extreme high sensitivity is experienced in the case of the increase of

parameter c_g. Moreover, the sensitivity to q_I is also significantly decreased. As the injections and thus the concentrations of the inhibitor (I) are by 2 orders of magnitude lower compared to therapy one (see Figure 5), it is plausible that the exact value of its clearance parameter (q_I) has a significantly less effect on the dynamics of the model compared to therapy 1, where a large dose is applied.

Apart from this, the results are similar to the case of therapy 1.

Altogether, based on the results of the sensitivity analysis, it can be said that further experiments focusing solely on pharmacokinetics of the applied drugs are desirable to estimate the parameter c_h decoupled from other model parameters.

3.3.2. Structural Identifiability. Structural identifiability properties of a system describe whether there is a theoretical possibility for the unique determination of system parameters from appropriate input-output measurements or not. It is important to emphasize that identifiability is a property of the model structure. Basic early references for studying identifiability of dynamical systems are [50, 51]. Since the introduction of this concept, multiple approaches have been proposed for the analysis of structural identifiability of various nonlinear system classes, for example, polynomial systems [52] or rational function state-space models [53]. A critical comparison of methods for identifiability analysis is described in [54].

First, let us note that as our model uses the variable $[B] = B/V$ describing vasculature density, our model falls into the class of rational function state-space models.

Second, let us consider the factors that make the structural identifiability analysis challenging in our case. Structural identifiability methods usually rely on iterative
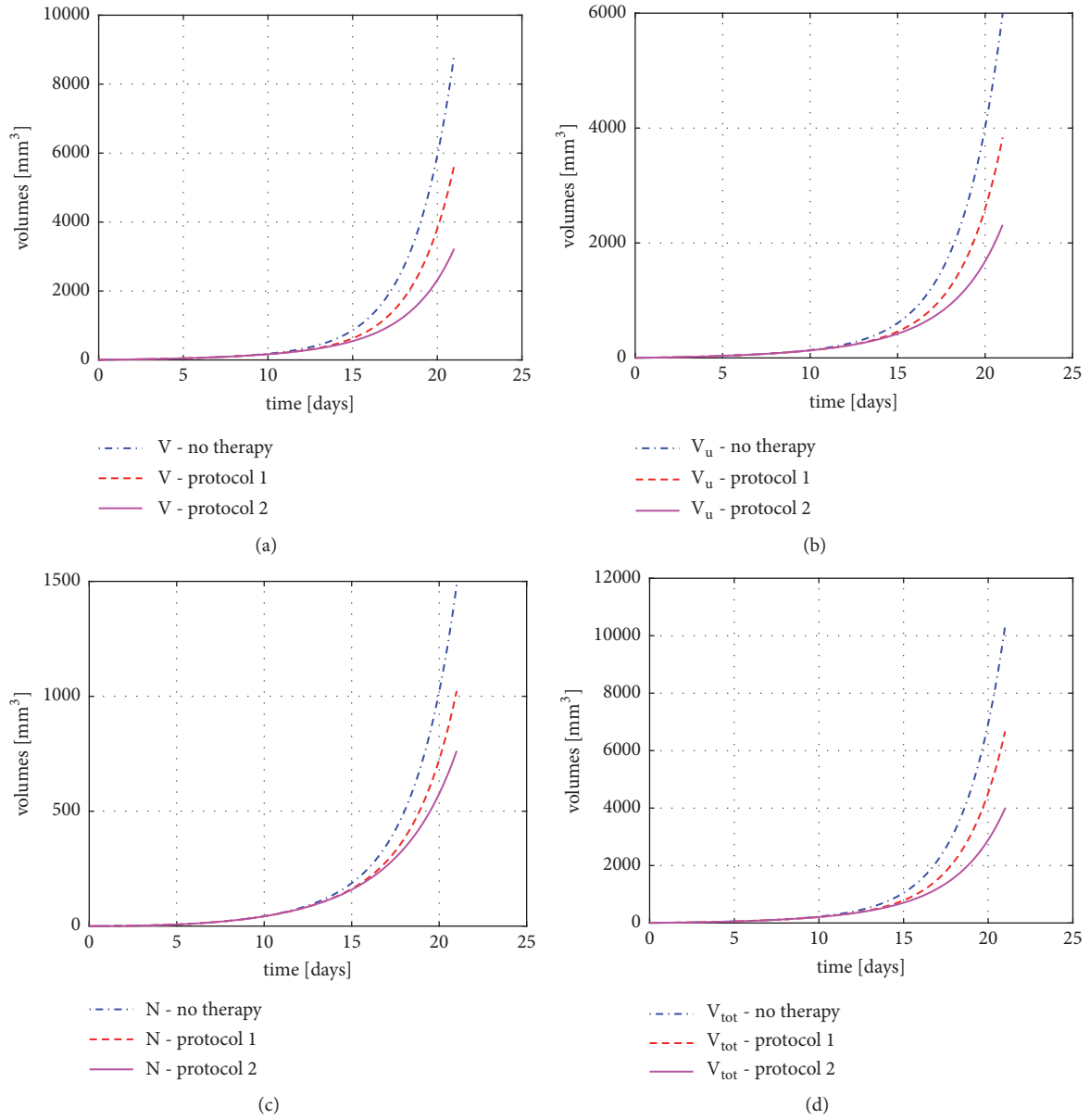
FIGURE 7: Volume trajectories of the model (living volume V, unsupported volume V_u, necrotic volume N, and total volume V_{tot}, corresponding to subfigures (a), (b), (c), and (d), resp.) in the case of various therapies.

TABLE 5: Sensitivities (S) of the model to the changes of parameters $[B]^{id}$, c_g, c_{ev}, c_n, c_v, c_T, q_T, c_h, q_I, and k_V in the no-therapy case. One unit is 10^6 mm^3.

	-20%	-10%	-5%	+5%	+10%	+20%
$[B]^{id}$	0.1321	0.0240	0.0052	0.0040	0.0143	0.0462
c_g	0.4715	0.1601	0.0467	0.0640	0.2996	1.6456
c_{ev}	0.0653	0.0173	0.0044	0.0047	0.0193	0.0821
c_n	0.0072	0.0017	0.0004	0.0004	0.0016	0.0061
c_v	0.2287	0.0769	0.0224	0.0309	0.1454	0.8147
c_T	0.2287	0.0769	0.0224	0.0309	0.1454	0.8148
q_T	0.5561	0.0868	0.0176	0.0120	0.0405	0.1185
c_h	0	0	0	0	0	0

Table 6: Sensitivities (S) of the model to the changes of parameters $[B]^{id}$, c_g, c_{ev}, c_n, c_v, c_T, q_T, c_h, q_I, and k_V in the case of therapy 1. One unit is 10^6 mm^3.

	-20%	-10%	-5%	+5%	+10%	+20%
$[B]^{id}$	0.2926	0.0525	0.0114	0.0086	0.0305	0.0975
c_g	0.9383	0.3259	0.0962	0.1353	0.6422	3.6265
c_{ev}	0.1375	0.0368	0.0095	0.0102	0.0420	0.1807
c_n	0.0181	0.0043	0.0011	0.0010	0.0039	0.0149
c_v	0.4498	0.1518	0.0442	0.0611	0.2889	1.6242
c_T	0.4594	0.1559	0.0456	0.0634	0.3011	1.7086
q_T	0.9364	0.1493	0.0305	0.0213	0.0720	0.2128
c_h	0.0100	0.0023	0.0005	0.0005	0.0019	0.0069

Table 7: Sensitivities (S) of the model to the changes of parameters $[B]^{id}$, c_g, c_{ev}, c_n, c_v, c_T, q_T, c_h, q_I, and k_V in the case of therapy 2. One unit is 10^7 mm^3.

	-20%	-10%	-5%	+5%	+10%	+20%
$[B]^{id}$	0.1304	0.0230	0.0050	0.0038	0.0131	0.0415
c_g	0.4012	0.1422	0.0427	0.0620	0.3015	1.7891
c_{ev}	0.0582	0.0157	0.0041	0.0044	0.0185	0.0798
c_n	0.0090	0.0021	0.0005	0.0005	0.0019	0.0072
c_v	0.1232	0.0402	0.0116	0.0155	0.0722	0.3971
c_T	0.1332	0.0448	0.0131	0.0179	0.0859	0.4902
q_T	0.1690	0.0288	0.0061	0.0045	0.0154	0.0473
c_h	0.0135	0.0030	0.0007	0.0006	0.0023	0.0081

computation of (Lie-) derivatives of the output (see, e.g., [55], on which the software used later is based).

For identifiability analysis, let us consider a reduced version of the proposed model, which assumes no input (no antiangiogenic drug is present). The simplified form of the model is described by (18)-(21). As we will see, this submodel already poses a challenge regarding identifiability due to the complexity of the resulting equations.

$$\frac{dV}{dt} = c_g \gamma V - c_n (1 - \gamma) V \tag{18}$$

$$\frac{dN}{dt} = c_n (1 - \gamma) V \tag{19}$$

$$\frac{dB}{dt} = c_{ev} c_g \gamma V + c_v T B \tag{20}$$

$$\frac{dT}{dt} = c_T (1 - \gamma) - q_T T \tag{21}$$

In this case, if only the total volume may be measured (as in the case of our measurements used for the parameter estimation),

$$y = V_{tot} = V + N$$
$$\dot{y} = \dot{V} + \dot{N} = c_g \gamma V \tag{22}$$

If we consider further derivatives,

$$\ddot{y} = c_g \left(\dot{\gamma} V + \dot{V} \gamma \right) \tag{23}$$

where

$$\gamma = (1 - r_v) f_P (V_{tot}) + r_v = (1 - r_v) f_P (V_{tot}) + r_v \tag{24}$$

$$\left(\frac{[B]^{id} - [B]}{[B]^{id}} \right) f_P (V_{tot}) + \left(1 - \frac{[B]^{id} - [B]}{[B]^{id}} \right) \tag{25}$$

It is easy to se that, in $\dot{\gamma}$, on one hand, the derivative of the function $f_P(V_{tot})$ appears, and, on the other hand, the derivative of $[B] = B/V$ is also present. These are long and complicated expressions, the higher-order derivatives of which are needed in the further steps.

Based on the above considerations, for the structural identifiability analysis, we use the freely available GenSSI [56, 57] software, which is able to handle complex expressions with the help of computer-algebra methods. GenSSI implements iteratively the generating series method, as presented in [58], with the help of identifiability tableaus, as described in [55].

According to the results of this software, the parameter c_g of the model is structurally globally identifiable, but neither positive (structural global/local identifiability) nor negative (structural nonidentifiability) results are obtained for other parameters. This result is based on 7th-order Lie-derivatives, which has been proven to be the computational limit in our case.

Nevertheless, let us discuss this topic a bit further from the point of view of possible future measurements with regard to the proposed model. In the recent years, multiple imaging techniques have been developed, which
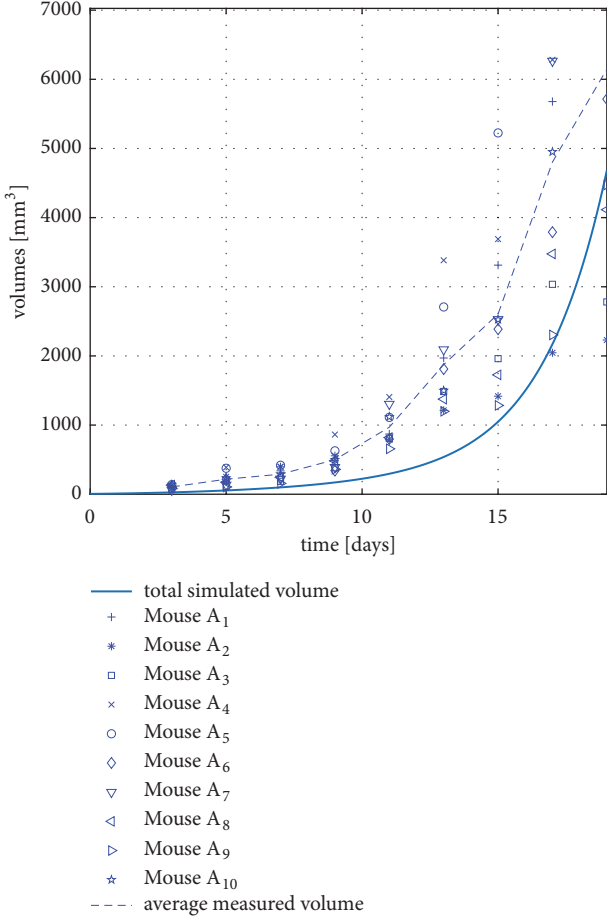
FIGURE 8: Measured and simulated tumor volumes in the case of no therapy.

allow the 3D reconstruction of vascular microstructures: Doppler optical frequency domain imaging [29] and functional photoacoustic microscopy [30] are used today already in *in vivo* setups to map vascular networks, while diffusible iodine-based contrast-enhanced computed tomography [31] may be used in terminal experimental animals.

If these methods will be applicable in the case of animals used in the experiments, total tumor volume V_{tot} will be accessible during measurements together with the total vasculature volume B. Interpreted for our case, this will mean that we will have two observables $y_1 = V_{tot}$ and $y_2 = B$. If we rerun the structural identifiability analysis with this new model output, we get the result that c_g, c_{ev}, $[B]^{id}$, and c_n are structurally globally identifiable (and no result is obtained for other parameters, similar to the previous case, so they might be or might be not identifiable). In this case, the maximum order of the Lie-derivatives, for which the computation was feasible, was the 6th order.

The complete identifiability tableaus of the reduced model are depicted in Figure 9. For the interpretation of these tableaus, see [55] or the GenSSI UserGuide [56].

Based on the above, it may be suspected that the model will have beneficial properties shall it be fitted for measurements planned to be carried out in the foreseeable future.

3.4. Extension of the Model in order to Account for Combined Therapy.

In the clinical practice, antiangiogenic drugs are often used together with conventional cytotoxic substances. In this setup, while the cytotoxic agent enhances the degeneration/necrosis of tumor cells, the antiangiogenic drugs are resposible for cutting the tumor from metabolic support via the inhibition of angiogenesis. Several results have been published recently corresponding to these combined therapies [59, 60].

Models with predictive power regarding the efficiency of combined therapies and model-based optimization of such treatments are not prevalent in literature. Some initial results on the optimization of combined therapies are described in [61], using the model of [35].

As the proposed model is taking into account vasculature and tumor cell dynamics in a differentiated way, it is able to distinguish between qualitatively different inputs related to different therapeutic agents. As a consequence, the proposed model may be easily extended to consider not only angiogenic drugs but also cytotoxic drugs. Let us consider the following modified state-space model described in the following equations:

$$\frac{dV}{dt} = c_g \gamma V - c_n V_u - \frac{c_c C V}{K_C + V} \tag{26}$$

$$\frac{dN}{dt} = c_n V_u + \frac{c_c C V}{K_C + V} \tag{27}$$

$$\frac{dB}{dt} = c_{ev} \dot{V}_{tot} + c_v T B \tag{28}$$

$$\frac{dT}{dt} = c_T \frac{V_u}{V} - q_T T - c_h \frac{TI}{ED_{50} + I} \tag{29}$$

$$\frac{dI}{dt} = u_1 - q_I \frac{I}{k_I + I} - k_V c_h \frac{TI}{ED_{50} + I} \tag{30}$$

$$\frac{dC}{dt} = u_2 - q_C C \tag{31}$$

First, the new equation (31) describes the time evolution of the cytotoxic drug, the injection of which is described by the term u_2. To clarify notations, the injection of the angiogenic inhibitor is denoted by u_1 in this case. The term $q_C C$ describes the clearance of the cytotoxic drug; the parameter q_C denotes its clearance rate. In this case, we assume a simple clearance (no saturation dynamics). The reason for this is on one hand that this approach requires less parameters, and on the other hand as long as the exact identity of the cytotoxic drug is unknown, the dynamical features of its clearance can not be precisely determined (of course the clearance dynamics may be later refined).

The effect of the cytotoxic drug is modeled in this case as an enzymatic reaction, in which the cytotoxic drug acts as an
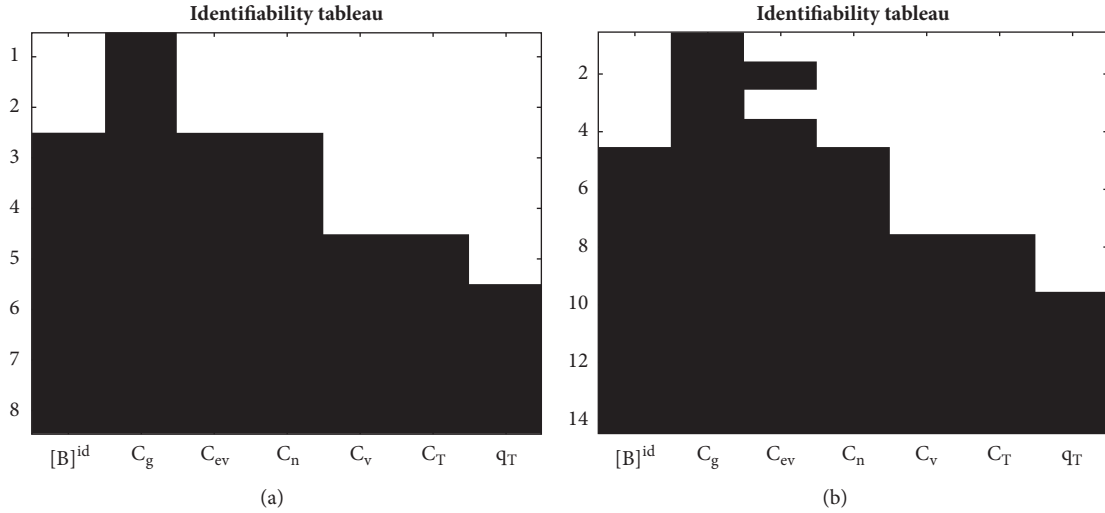
FIGURE 9: Complete identifiability tableaus of the reduced model in the case when the output is V_{tot} (a) and in the case when the output is $[V_{tot}, B]$ (b).

enzyme, turning living cells to necrotic cells. This mechanism is described by the term

$$-\frac{c_c CV}{K_C + V} \qquad (32)$$

in (26) and by the complementary term

$$\frac{c_c CV}{K_C + V} \qquad (33)$$

in (27). c_c and K_C are new parameters describing the efficiency of the cytotoxic drug in enzymatic context assuming Michaelis-Menten kinetics.

This way the effects of the two drugs are considered in qualitatively different ways in the model. While the antiangiogenic drug acts explicitly on the formation of new blood vessels by binding to TAF and thus inhibiting angiogenesis, the cytotoxic drug acts as an enzyme, driving living tumor cells to necrosis, independent of the actual vascular state of the tumor.

4. Conclusions and Future Work

In this article, we formulated a dynamic model of vascular tumor growth, which accounts for the vasculature and TAF concentration development of the tumor and thus is able to reproduce the phenomenon of the angiogenic switch. We validated the model against volume measurement data originating from experiments on mice and found that the model provides a good fit for tumor volume data in both cases of the two analyzed therapies. The extension of the model described in Section 3.4 makes the model capable of accounting for qualitatively different effect of antiangiogenic and cytotoxic drugs.

When comparing the proposed model to literature results, we may state the following. Regarding the model in

[28] (considering the extended model described therein), the proposed approach uses more state variables (5 vs 3) and holds more parameters (12 versus 8) but describes vasculature dynamics as well. This feature will allow us to fit the model to dynamical vasculature data, hopefully available in the foreseeable future, and thus get a more precise dynamical representation of angiogenesis-dependent tumor growth and its inhibition. Furthermore, the validity of the proposed model compared to [28] seems better regarding the no-therapy case.

Comparing the model described in the current article to [35], we see that although the model described in [35] accounts for vasculature dynamics as well, it uses more state variables (7 versus 5) and significantly more parameters (22 versus 12). Furthermore, the model in [35] was fitted only for measurement data originating from protocol 1, while the proposed model has been validated against both protocol 1 and protocol 2. Similar to the model described in [35], the model proposed in the current article also allows for the analysis of combined therapies, as done in the article in [61].

Regarding future work, in the framework of the project Tamed Cancer (ERC grant agreement number 679681), animal experiments (mice) aiming to characterize the vasculature development during tumor growth are planned in the near future. These experiments will provide reference data for both vasculature volumes and tumor volumes, so we will be able to fit the model in either dimension against experimental data. This will allow further validation, refinement, or recalibration of the model.

Experiments regarding the efficiency of various combined therapies are also expected in the future, which will serve as reference scenarios regarding the identification of the extended model described in Section 3.4.

Once the model is identified and validated from multiple aspects, studies on therapy optimization in open-loop and closed-loop setup will take place.
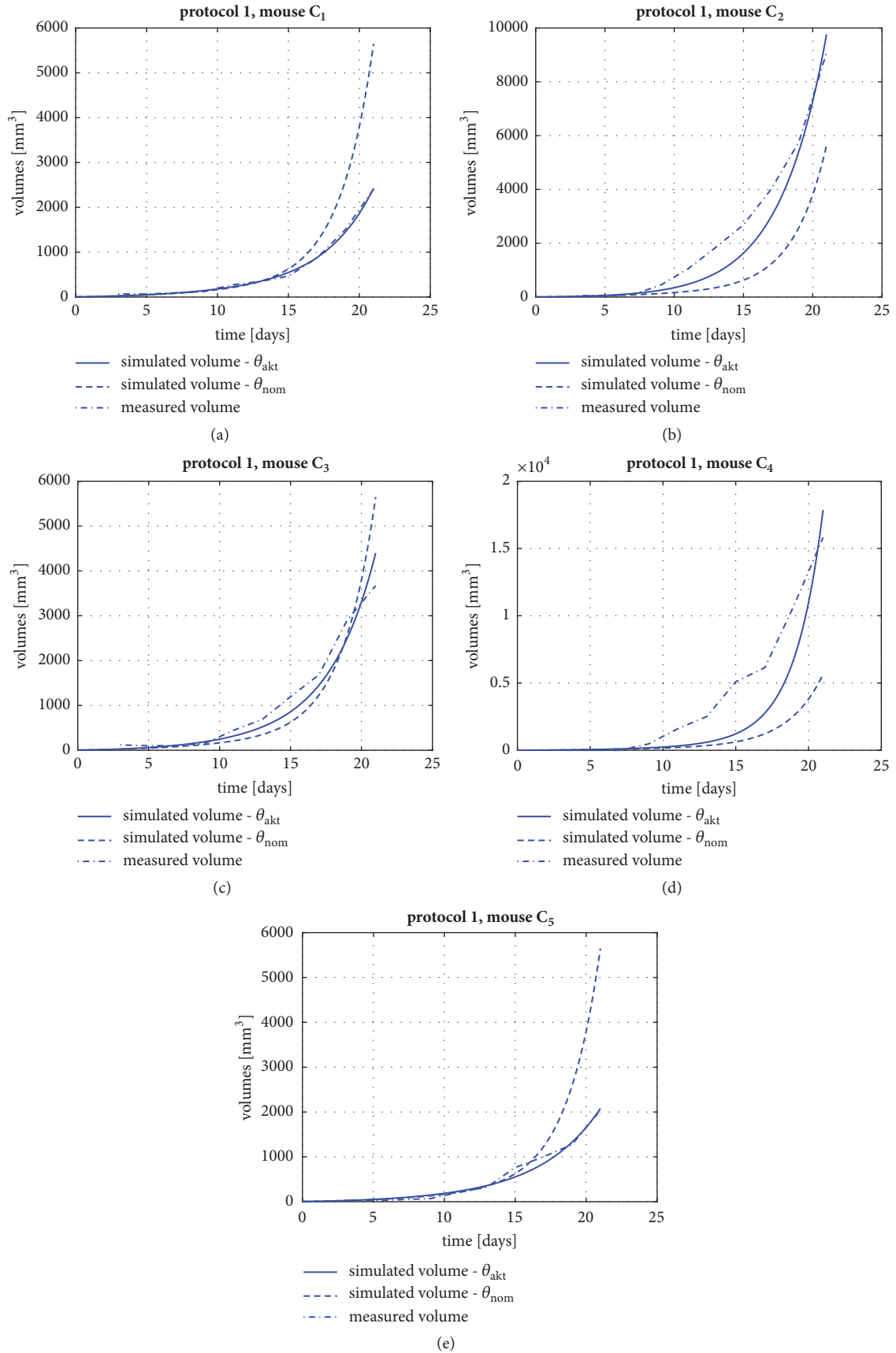
FIGURE 10: Fitting the model to individual trajectories in the case of therapy 1: simulated output (with the parameters obtained from fitting the model to the specific trajectory (θ_{akt}), simulated output with nominal parameters (θ_{nom}), and measured output.)
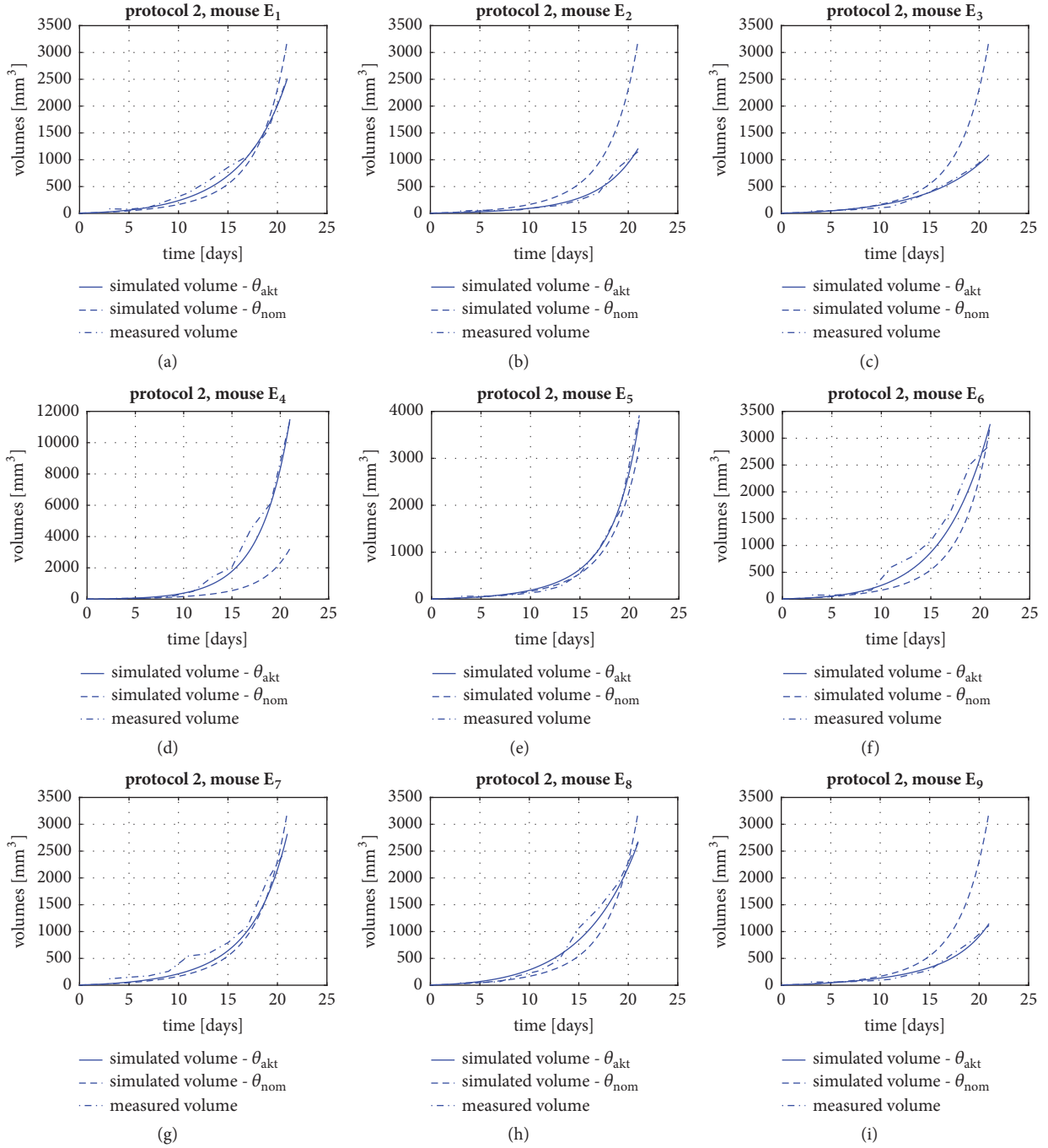
FIGURE 11: Fitting the model to individual trajectories in the case of therapy 2: simulated output (with the parameters obtained from fitting the model to the specific trajectory (θ_{akt}), simulated output with nominal parameters (θ_{nom}), and measured output.)

Appendix

In this appendix, we detail the fitting of the model to the individual trajectories corresponding to single mice in the case of either therapy 1 or therapy 2. $V_0 = 5$ was assumed in all cases. Figures 10(a)–10(e) depict the fit of the model output (V_{tot}) to the individual measured growth trajectories in the case of therapy 1, while Figures 11(a)–11(i) depict the fit of the

model output to the individual measured growth trajectories in the case of therapy 2.

In every case, the simulated output assuming the nominal parameters detailed in Table 2 is also depicted to serve as basis of comparison. Tables 8 and 9 summarize the parameter values resulting in the case of fitting to individual trajectories in the case of therapy 1 and therapy 2, respectively.

Table 8: Model parameter values resulting from fitting to individual trajectories in the case of therapy 1 (mice C_1-C_5).

Parameter	C_1	C_2	C_3	C_4	C_5	Scale
$[B]^{id}$	0.0336	0.0127	0.0289	0.0374	0.0246	
c_g	1.4336	1.4454	1.55	1.435	1.4154	
c_{ev}	1.4403	1.9642	1.4604	2.2084	1.2167	10^{-3}
c_n	0.0838	0.1684	0.0737	0.0739	0.0791	
c_v	4.4337	5.5455	10.2252	4.4032	4.4909	
c_T	1.8021	0.5612	0.7111	1.9291	1.4795	10^{-2}
q_T	0.2762	0.3917	0.2517	0.1173	0.3162	
c_h	0.1995	0.1637	0.1701	0.2114	0.1369	

Table 9: Model parameter values resulting from fitting to individual trajectories in the case of therapy 2 (mice E_1-E_9).

Par.	E_1	E_2	E_3	E_4	E_5	E_6	E_7	E_8	E_9	Scale
$[B]^{id}$	0.0322	0.0393	0.0331	0.0184	0.039	0.0179	0.0422	0.0223	0.0331	
c_g	1.622	0.9568	1.436	1.433	1.408	1.442	1.634	1.609	1.432	
c_{ev}	1.463	2.01	1.373	2.026	1.195	2.004	1.173	0.9805	0.6332	10^{-3}
c_n	0.0933	0.0552	0.1056	0.0567	0.0618	0.1236	0.0933	0.0425	0.1056	
c_v	17.34	18.67	18.08	18.66	18.66	18.08	18.08	18.65	18.08	
c_T	0.444	0.6039	0.4612	0.4512	0.923	0.1138	0.6959	0.335	0.9693	10^{-2}
q_T	0.2834	0.2657	0.4071	0.3201	0.3063	0.4105	0.3123	0.3311	0.4066	
c_h	0.2449	0.1011	0.2605	0.2546	0.259	0.2496	0.1749	0.2643	0.2603	

Table 10: Standard deviation (STD) of the estimated parameters, regarding fitting to individual trajectories compared to their nominal value in %.

Parameter	STD (%)
c_g	10.96
$[B]^{id}$	23.40
c_{ev}	39.60
c_n	33.33
c_v	52.64
c_T	47.20
q_T	31.40
c_h	32.57

Table 10 holds the standard deviation (STD) values of the estimated parameters obtained by fitting the model to individual trajectories. Let us emphasize that, in the case of these estimates, only one of the protocols was considered for the fitting, namely, the one from which the actual trajectory originates. Naturally, it is a significantly harder task to find a parameter set for the model which describes the response to both protocols simultaneously (as in Table 2). Parameters obtained by fitting to single volume trajectories are potentially unable to appropriately describe the response to the two protocols at the same time. The relatively high STD values are not surprising in the light of the significant differences among individual tumor growth trajectories.

Data Availability

The data used to support the findings of this study are available from the corresponding author upon request.

Conflicts of Interest

The authors declare that there are no conflicts of interest regarding the publication of this paper.

Acknowledgments

Supplementary Materials

simulate_MMAGS.m is the file that performs the simulation of the model in MATLAB; it uses the following files: inj_fnc_prot_1_discrete.m, description of the injection function in the case of therapy 1; inj_fnc_prot_2_discrete.m, description of the injection function in the case of therapy 2; f_gamma.m, implementation of the function \gamma detailed in the article (see (7)). sim_tumor_dynamics_MMAGS_2_discrete.m is one central file that calls simulate_MMAGS.m; it has two important input parameters, flag_plot_details, may be 0 or 1, if it is one, more figures are generated, protocol - can be 0, 1 or 2 depending

on the actual simulated protocol (therapy); it depicts the simulation results and compares them with experimental data (Figure 3 in the manuscript). Experimental data is defined inside the file. Corresponding to protocol 1, the variable "adatsor" holds the vector of the experimental data. Corresponding to protocol 2, the variable "adatsor_2" holds the vector of the experimental data. In both cases, the data corresponding to various mice are integrated in one vector (see its decomposition later in the file. In the case of protocol 1, the variable sote_data holds the decomposed version; in the case of protocol 2, the variables "Eger1" and so forth hold the decomposed data). sim_compare_discrete_1.m performs the simulations in the case of no therapy, protocol 1, and protocol 2 and depicts the results corresponding to the 3 different cases in figures (Figures 4–7 in the manuscript). *(Supplementary Materials)*

References

[1] P. C. Lee, A. N. Salyapongse, G. A. Bragdon et al., "Impaired wound healing and angiogenesis in eNOS-deficient mice," *American Journal of Physiology-Heart and Circulatory Physiology*, vol. 277, no. 4, pp. H1600–H1608, 1999.

[2] E. W. M. Ng and A. P. Adamis, "Targeting angiogenesis, the underlying disorder in neovascular age-related macular degeneration," *Canadian Journal of Ophthalmology*, vol. 40, no. 3, pp. 352–368, 2005.

[3] J. Folkman, "The role of angiogenesis in tumor growth," *Seminars in Cancer Biology*, vol. 3, no. 2, pp. 65–71, 1992.

[4] J. Folkman, "Role of angiogenesis in tumor growth and metastasis," *Seminars in Oncology*, vol. 29, 6, supplement 6, pp. 15–18, 2002.

[5] T. A. Baudino, "Targeted cancer therapy: the next generation of cancer treatment," *Current Drug Discovery Technologies*, vol. 12, no. 1, pp. 3–20, 2015.

[6] N. Ferrara, K. J. Hillan, and W. Novotny, "Bevacizumab (Avastin), a humanized anti-VEGF monoclonal antibody for cancer therapy," *Biochemical and Biophysical Research Communications*, vol. 333, no. 2, pp. 328–335, 2005.

[7] N. Ferrara, H. Gerber, and J. LeCouter, "The biology of VEGF and its receptors," *Nature Medicine*, vol. 9, no. 6, pp. 669–676, 2003.

[8] J. Sápi, L. Kovács, D. A. Drexler, P. Kocsis, D. Gajári, and Z. Sápi, "Tumor volume estimation and quasi- continuous administration for most effective bevacizumab therapy," *PLoS ONE*, vol. 10, no. 11, Article ID e0142190, pp. 1–20, 2015.

[9] M. A. J. Chaplain, S. R. McDougall, and A. R. A. Anderson, "Mathematical modeling of tumor-induced angiogenesis," *Annual Review of Biomedical Engineering*, vol. 8, pp. 233–257, 2006.

[10] S. M. Peirce, "Computational and mathematical modeling of angiogenesis," *Microcirculation*, vol. 15, no. 8, pp. 739–751, 2008.

[11] M. Scianna, C. G. Bell, and L. Preziosi, "A review of mathematical models for the formation of vascular networks," *Journal of Theoretical Biology*, vol. 333, pp. 174–209, 2013.

[12] H. Rieger and M. Welter, "Integrative models of vascular remodeling during tumor growth," *Wiley Interdisciplinary Reviews: Systems Biology and Medicine*, vol. 7, no. 3, pp. 113–129, 2015.

[13] M. Papetti and I. M. Herman, "Mechanisms of normal and tumor-derived angiogenesis," *American Journal of Physiology-Cell Physiology*, vol. 282, no. 5, pp. C947–C970, 2002.

[14] H. A. Levine, B. D. Sleeman, and M. Nilsen-Hamilton, "A mathematical model for the roles of pericytes and macrophages in the initiation of angiogenesis. I. The role of protease inhibitors in preventing angiogenesis," *Mathematical Biosciences*, vol. 168, no. 1, pp. 77–115, 2000.

[15] L. Arakelyan, V. Vainstein, and Z. Agur, "A computer algorithm describing the process of vessel formation and maturation, and its use for predicting the effects of anti-angiogenic and anti-maturation therapy on vascular tumor growth," *Angiogenesis*, vol. 5, no. 3, pp. 203–214, 2002.

[16] J. Poleszczuk, P. Hahnfeldt, and H. Enderling, "Therapeutic implications from sensitivity analysis of tumor angiogenesis models," *PLoS ONE*, vol. 10, no. 3, 2015.

[17] A. L. Bauer, T. L. Jackson, and Y. Jiang, "A cell-based model exhibiting branching and anastomosis during tumor-induced angiogenesis," *Biophysical Journal*, vol. 92, no. 9, pp. 3105–3121, 2007.

[18] J. L. Gevertz and S. Torquato, "Modeling the effects of vasculature evolution on early brain tumor growth," *Journal of Theoretical Biology*, vol. 243, no. 4, pp. 517–531, 2006.

[19] G. F. Franklin, D. J. Powell, and A. Emami-Naeini, *Feedback control of dynamic systems*, vol. 3, Addison-Wesley, Reading, MA, USA, 1994.

[20] J. C. Doyle, B. A. Francis, and A. R. Tannenbaum, *Feedback control theory*, Courier Corporation, 2013.

[21] Z. Kemin and J. C. Doyle, *Essentials of Robust Control*, vol. 104, Prentice Hall, Upper Saddle River, NJ, USA, 1998.

[22] J. Sápi, D. A. Drexler, and L. Kovács, "Potential benefits of discrete-time controller-based treatments over protocol-based cancer therapies," *Acta Polytechnica Hungarica*, vol. 14, no. 1, pp. 11–23, 2017.

[23] J. Bondia, S. Romero-Vivo, B. Ricarte, and J. L. Diez, "Insulin estimation and prediction: a review of the estimation and prediction of subcutaneous insulin pharmacokinetics in closed-loop glucose control," *IEEE Control Systems Magazine*, vol. 38, no. 1, pp. 47–66, 2018.

[24] F. J. Doyle, L. M. Huyett, J. B. Lee, H. C. Zisser, and E. Dassau, "Closed-loop artificial pancreas systems: Engineering the algorithms," *Diabetes Care*, vol. 37, no. 5, pp. 1191–1197, 2014.

[25] R. A. Harvey, E. Dassau, W. C. Bevier et al., "Clinical evaluation of an automated artificial pancreas using zone-model predictive control and health monitoring system," *Diabetes Technology & Therapeutics*, vol. 16, no. 6, pp. 348–357, 2014.

[26] L. Kovács, "Linear parameter varying (LPV) based robust control of type-I diabetes driven for real patient data," *Knowledge-Based Systems*, vol. 122, pp. 199–213, 2017.

[27] P. H. Colmegna, R. S. Sanchez-Pena, R. Gondhalekar, E. Dassau, and F. J. Doyle, "Switched LPV Glucose Control in Type 1 Diabetes," *IEEE Transactions on Biomedical Engineering*, vol. 63, no. 6, pp. 1192–1200, 2016.

[28] D. A. Drexler, J. Sápi, and L. Kovács, "Modeling of Tumor Growth Incorporating the Effects of Necrosis and the Effect of Bevacizumab," *Complexity*, vol. 2017, Article ID 5985031, 10 pages, 2017.

[29] B. J. Vakoc, R. M. Lanning, J. A. Tyrrell et al., "Three-dimensional microscopy of the tumor microenvironment in vivo using optical frequency domain imaging," *Nature Medicine*, vol. 15, no. 10, pp. 1219–1223, 2009.

[30] H. F. Zhang, K. Maslov, G. Stoica, and L. V. Wang, "Functional photoacoustic microscopy for high-resolution and noninvasive in vivo imaging," *Nature Biotechnology*, vol. 24, no. 7, pp. 848–851, 2006.

[31] P. M. Gignac, N. J. Kley, J. A. Clarke et al., "Diffusible iodine-based contrast-enhanced computed tomography (diceCT): An emerging tool for rapid, high-resolution, 3-D imaging of metazoan soft tissues," *Journal of Anatomy*, vol. 228, no. 6, pp. 889–909, 2016.

[32] D. Hanahan and J. Folkman, "Patterns and emerging mechanisms of the angiogenic switch during tumorigenesis," *Cell*, vol. 86, no. 3, pp. 353–364, 1996.

[33] S. Redline and N. A. Berger, *Impact of Sleep and Sleep Disturbances on Obesity and Cancer*, Springer, New York, NY, USA, 2014.

[34] D. A. Drexler, J. Sápi, and L. Kovács, "A minimal model of tumor growth with angiogenic inhibition using bevacizumab," in *Proceedings of the 15th IEEE International Symposium on Applied Machine Intelligence and Informatics, SAMI 2017*, pp. 185–190, Slovakia, January 2017.

[35] D. Csercsik, J. Sapi, T. Gonczy, and L. Kovacs, "Bi-compartmental modelling of tumor and supporting vasculature growth dynamics for cancer treatment optimization purpose," in *Proceedings of the 2017 IEEE 56th Annual Conference on Decision and Control (CDC)*, pp. 4698–4702, Melbourne, VIC, December 2017.

[36] J. Landry, J. P. Freyer, and R. M. Sutherland, "A model for the growth of multicellular spheroids," *Cell Proliferation*, vol. 15, no. 6, pp. 585–594, 1982.

[37] S. A. Maggelakis and J. A. Adam, "Mathematical model of prevascular growth of a spherical carcinoma," *Mathematical and Computer Modelling*, vol. 13, no. 5, pp. 23–38, 1990.

[38] G. W. Swan, "The diffusion of an inhibitor in a spherical tumor," *Mathematical Biosciences*, vol. 108, no. 1, pp. 75–79, 1992.

[39] M. A. J. Chaplain, D. L. Benson, and P. K. Maini, "Nonlinear diffusion of a growth inhibitory factor in multicell spheroids," *Mathematical Biosciences*, vol. 121, no. 1, pp. 1–13, 1994.

[40] M. A. J. Chaplain, "Avascular growth, angiogenesis and vascular growth in solid tumours: The mathematical modelling of the stages of tumour development," *Mathematical and Computer Modelling*, vol. 23, no. 6, pp. 47–87, 1996.

[41] S. A. Maggelakis, "The effects of tumor angiogenesis factor (TAF) and tumor inhibitor factors (TIFs) on tumor vascularization: A mathematical model," *Mathematical and Computer Modelling*, vol. 23, no. 6, pp. 121–133, 1996.

[42] H. M. Byrne, J. R. King, D. L. McElwain, and L. Preziosi, "A two-phase model of solid tumour growth," *Applied Mathematics Letters*, vol. 16, no. 4, pp. 567–573, 2003.

[43] R. H. Thomlinson and L. H. Gray, "The histological structure of some human lung cancers and the possible implications for radiotherapy," *British Journal of Cancer*, vol. 9, no. 4, pp. 539–549, 1955.

[44] K. I. E. M. Wÿffels, J. H. A. M. Kaanders, P. F. J. W. Rijken et al., "Vascular architecture and hypoxic profiles in human head and neck squamous cell carcinomas," *British Journal of Cancer*, vol. 83, no. 5, pp. 674–683, 2000.

[45] J. Forster, W. Harriss-Phillips, M. Douglass, and E. Bezak, "A review of the development of tumor vasculature and its effects on the tumor microenvironment," *Hypoxia*, vol. Volume 5, pp. 21–32, 2017.

[46] J. J. Heatley, "Cardiovascular Anatomy, Physiology, and Disease of Rodents and Small Exotic Mammals," *Veterinary Clinics of North America - Exotic Animal Practice*, vol. 12, no. 1, pp. 99–113, 2009.

[47] A. I. Vaz and L. N. Vicente, "A particle swarm pattern search method for bound constrained global optimization," *Journal of Global Optimization*, vol. 39, no. 2, pp. 197–219, 2007.

[48] H.-P. Gerber and N. Ferrara, "Pharmacology and pharmacodynamics of bevacizumab as monotherapy or in combination with cytotoxic therapy in preclinical studies," *Cancer Research*, vol. 65, no. 3, pp. 671–680, 2005.

[49] European Medicines Agency. Scientific discussion. 2005. http://www.ema.europa.eu/docs/en_GB/document_library/ EPAR_-_Scientific_Discussion/human/000582/WC500029262 .pdf.

[50] E. Walter, *Identifiability of state space models*, Springer, Berlin, Germany, 1982.

[51] E. Walter, *Identifiability of Parametric Models*, Elsevier, 2014.

[52] S. Vajda, "Identifiability of polynomial systems: structural and numerical aspects," *Identifiability of Parametric Models*, vol. 4, pp. 42–49, 1987.

[53] G. Margaria, E. Riccomagno, M. . Chappell, and H. P. Wynn, "Differential algebra methods for the study of the structural identifiability of rational function state-space models in the biosciences," *Mathematical Biosciences*, vol. 174, no. 1, pp. 1–26, 2001.

[54] O.-T. Chis, J. R. Banga, and E. Balsa-Canto, "Structural identifiability of systems biology models: A critical comparison of methods," *PLoS ONE*, vol. 6, no. 11, p. e27755, 2011.

[55] E. Balsa-Canto, A. Antonio Alonso, and R. Julio Banga, "An iterative identification procedure for dynamic modeling of biochemical networks," *BMC systems Biology*, vol. 4, no. 1, p. 11, 2010.

[56] O. Chiş, J. R. Banga, and E. Balsa-Canto, "GenSSI: A software toolbox for structural identifiability analysis of biological models," *Bioinformatics*, vol. 27, no. 18, Article ID btr431, pp. 2610-2611, 2011.

[57] T. S. Ligon, F. Fröhlich, O. T. Chiş et al., "GenSSI 2.0: multi-experiment structural identifiability analysis of SBML models," *Bioinformatics*, vol. 34, no. 8, pp. 1421–1423, 2018.

[58] E. Walter and Y. Lecourtier, "Unidentifiable compartmental models: what to do?" *Mathematical Biosciences*, vol. 56, no. 1-2, pp. 1–25, 1981.

[59] M. Scalerandi, B. C. Sansone, and C. A. Condat, "Diffusion with evolving sources and competing sinks: development of angiogenesis," *Physical review. E, Statistical, nonlinear, and soft matter physics*, vol. 65, no. 1, Article ID 011902, p. 011902, 2002.

[60] R. K. Jain, "Normalizing tumor vasculature with anti-angiogenic therapy: A new paradigm for combination therapy," *Nature Medicine*, vol. 7, no. 9, pp. 987–989, 2001.

[61] D. Csercsik, J. Sapi, and L. Kovacs, "Model-Based Simulation and Comparison of Open-Loop and Closed-Loop Combined Therapies for Tumor Treatment," in *Proceedings of the 2018 IEEE Conference on Control Technology and Applications (CCTA)*, pp. 1383–1388, Copenhagen, August 2018.

Review Article

Observability and Structural Identifiability of Nonlinear Biological Systems

Alejandro F. Villaverde iD

Bioprocess Engineering Group, IIM-CSIC, Vigo 36208, Galicia, Spain

Correspondence should be addressed to Alejandro F. Villaverde; afvillaverde@iim.csic.es

Observability is a modelling property that describes the possibility of inferring the internal state of a system from observations of its output. A related property, structural identifiability, refers to the theoretical possibility of determining the parameter values from the output. In fact, structural identifiability becomes a particular case of observability if the parameters are considered as constant state variables. It is possible to simultaneously analyse the observability and structural identifiability of a model using the conceptual tools of differential geometry. Many complex biological processes can be described by systems of nonlinear ordinary differential equations and can therefore be analysed with this approach. The purpose of this review article is threefold: (I) to serve as a tutorial on observability and structural identifiability of nonlinear systems, using the differential geometry approach for their analysis; (II) to review recent advances in the field; and (III) to identify open problems and suggest new avenues for research in this area.

1. Introduction

A model is observable if it is theoretically possible to infer its internal state by observing its output. Model parameters can be considered as constant state variables. The particular case of parameter observability is called structural identifiability. Both concepts are *structural* in the sense that they depend only on the model equations; that is, they are completely determined by the system dynamics and output definition. They are not affected by limitations related to the frequency or accuracy of the experimental measurements, in contrast to the related concept of *practical* identifiability or estimability.

The concept of observability was introduced by Kalman in 1960 for linear time-invariant systems [1, 2]. Conditions for checking observability of nonlinear systems were soon developed by several authors [3–7]. At the same time, the interest in parametric identifiability was growing among researchers using biological models, especially in biomedical applications. As a result, the concept of structural identifiability was introduced in 1970, when Bellman and Åström coined the term and presented the Laplace transform method for its study in the context of (linear) compartmental models [8].

Both concepts, observability and structural identifiability, are applicable to dynamic models of any kind: electrical, chemical, mechanical, biological, etc. Observability analysis, as well as the related question of observer design, has been and continues to be frequently investigated by systems and control theorists. In turn, researchers working in biological modelling (e.g., in mathematical biology and, more recently, in the systems biology community) have more often addressed structural identifiability issues. This is due to the fact that biological applications typically have more experimental limitations than engineering ones in terms of which measurements are feasible, making parameter identification a more challenging problem and calling for a deeper study of parametric identifiability issues and methods.

Observability and structural identifiability play a central role in system identification. There are a number of classic books on the subject, such as the ones by Walter and Pronzato [9] and Ljung [10]. In the context of biological modelling a very complete and recent reference is the book by DiStefano [11], which covers thoroughly the topic of identifiability, both from structural and practical points of view. The interested reader is also referred to [12], which reviews the different

types of identifiability and related concepts, and to [13, 14], which deal specifically with structural identifiability. In a different context, Chatzis and coworkers have reviewed the observability and structural identifiability of nonlinear mechanical systems [15].

The present paper reviews observability and structural identifiability concepts and tools, with the aim of facilitating their application to biological models. Instead of attempting to discuss all the existing methodologies, it focuses on methods that adopt a differential geometry approach [16–18]. These properties may also be analysed with other symbolic approaches, such as power series [19–21], differential algebra [22–26], or others [27–29], to name just a few, as well as with seminumerical [30, 31] or numerical approaches [32, 33]. A comparison or discussion of the aforementioned methods is out of the scope of the present paper; the interested reader is again referred to [12–14, 34].

This manuscript begins by motivating the study in Section 2, illustrating the possible consequences of unobservability and unidentifiability. In Section 3 these concepts are analysed with the differential geometry approach, which provides a unified view of observability and structural identifiability and can be applied to a very general class of nonlinear systems. Section 4 reports recent developments in this area, and Section 5 concludes by suggesting some open problems as possible research directions.

2. Motivation: Implications of Unobservability and Unidentifiability in Biological Models

The importance of structural identifiability analysis has been recently stressed in different areas of biological modelling, such as animal science [36], pharmacodynamics [37], epidemiology [38], environmental modelling [39], physiology [40], neuroscience [41], oncology [42], and many more. On the other hand, assessing observability and structural identifiability can be difficult even for relatively small systems and becomes increasingly complicated as the model complexity increases. Furthermore, the theoretical foundations of the analyses have some aspects that are not fully studied yet. These reasons help explain why some modellers are reluctant to analyse these properties of their models [11], which might be understandable taking into account the fact that even the need of determining parameter values has been questioned in the context of biological modelling [43]. However, such analysis is worth the effort, since lack of identifiability and/or observability can compromise the ability of a model to provide biological insight [36, 37, 44–46]. For example, one of the possible purposes of a model is for inferring the values of certain parameters of interest; in such case, identifiability is obviously desirable *per se*. Alternatively, the main purpose of the model may be to predict the dynamic behaviour of unmeasured states; in this case one is more interested in state observability than in parameter identifiability (although issues with the latter property may compromise the former).

As an example, consider the model of a possible glucose homeostasis mechanism depicted in Figure 1, which was presented in [35] and analysed in [46]. This so-called βIG model

describes the regulation of plasma glucose concentration (G) by means of insulin (I), which is secreted by pancreatic β cells. The model consists of three state variables (β,I,G) whose time courses are defined by nonlinear ordinary differential equations (ODEs) with five parameters ($c, s_i, p, \alpha, \gamma$). For the sake of the exercise, let us assume that glucose and β-cell mass are the measured outputs. In this case, if the model parameters are unknown, p and s_i are structurally unidentifiable. Figure 1 illustrates this fact by showing that changes in the model outputs (i.e., glucose concentration and β-cell mass) resulting from halving the value of s_i can be compensated by doubling the value of p. Therefore, it is not possible to distinguish between two parameter vectors of the form (s_i, p) and ($s_i/2, 2 \cdot p$). This also entails that insulin is an unobservable state, since the impossibility of determining the true parameter vector leads to the impossibility of determining which of the time courses shown in the lower left plot of Figure 1 is the true one. Therefore, the model cannot be used for inferring insulin concentration from measurements of the other variables. This limitation can be overcome if the value of p or of s_i is known.

Such lack of structural identifiability can have important consequences. A nice illustration is given in a recent work [45], where Procopio et al. presented a model of the release of a cardiac damage biomarker, cardiac troponin T, with the purpose of diagnosing acute myocardial infarction in a clinical setting. After the authors realized that the first version of the model was structurally unidentifiable, which could potentially lead to wrong conclusions, they removed the redundancies in their model and obtained an equivalent one that was structurally identifiable.

Structural unidentifiability is related to unobservability, as shown in the βIG model example, in which the inability to estimate p leads to wrong predictions of I. However, unidentifiability does not always entail unobservability. As a trivial example, consider the case in which the value of p is known. Then the βIG model becomes structurally identifiable and observable. If we now modify the model by replacing parameter c with the sum of two new parameters ($c \longrightarrow c_1 + c_2$), the two new parameters would obviously be structurally unidentifiable, but the unmeasured state I would remain observable. Therefore, it is desirable to analyse both the structural identifiability and observability of a model to decrease the possibility of drawing false conclusions from it.

Before concluding this section, it should be noted that a structurally identifiable model may nevertheless be practically unidentifiable, that is, the numerical estimates of its parameters may contain large errors due to insufficient or bad quality data. A recent example of this scenario is given in [44], where different models of cancer chemotherapy were analysed. The results showed that, although the models were structurally identifiable, they were not practically identifiable. This deficiency could lead to infer incorrect cell cycle distributions and, as a result, to the choice of suboptimal therapies. It is thus reasonable to ask: if a model can be structurally identifiable and yet unidentifiable in practice, why should we care about analysing its structural identifiability in the first place? The answer is that practical and structural unidentifiability have different causes and also different remedies. Practical unidentifiability may be
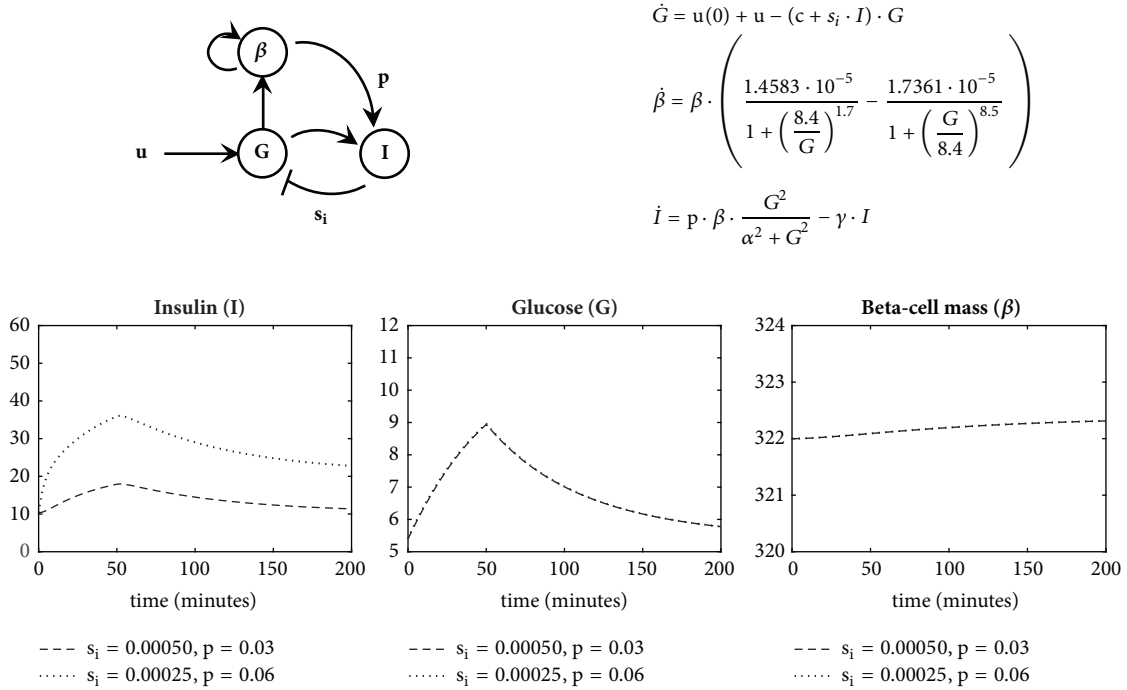
$$\dot{G} = u(0) + u - (c + s_i \cdot I) \cdot G$$

$$\dot{\beta} = \beta \cdot \left(\frac{1.4583 \cdot 10^{-5}}{1 + \left(\frac{8.4}{G}\right)^{1.7}} - \frac{1.7361 \cdot 10^{-5}}{1 + \left(\frac{G}{8.4}\right)^{8.5}} \right)$$

$$\dot{I} = p \cdot \beta \cdot \frac{G^2}{\alpha^2 + G^2} - \gamma \cdot I$$

--- $s_i = 0.00050, p = 0.03$
······ $s_i = 0.00025, p = 0.06$

--- $s_i = 0.00050, p = 0.03$
······ $s_i = 0.00025, p = 0.06$

--- $s_i = 0.00050, p = 0.03$
······ $s_i = 0.00025, p = 0.06$

FIGURE 1: Illustration of observability and structural identifiability issues. Top: diagram and equations of the 'βIG model' of the glucose-insulin system [35]. If glucose concentration (G) and β-cell mass are measured, the parameters p and s_i are structurally unidentifiable: the bottom plots show that different combinations of p and s_i values yield identical curves of G and β, so it is not possible to distinguish between them as long as the product $p \cdot s_i$, which is structurally identifiable, remains constant. Likewise, in this case insulin concentration (I) is an unobservable state: it is not possible to determine which of the two time courses of I shown in the lower left plot is the true one.

surmounted by using more informative data for calibration, but structural unidentifiabilities cannot be removed in this way (unless the new data involves modifying the output of the model, which strictly speaking entails modifying the model structure). Any attempt to remove a structural unidentifiability by incorporating more experimental data to the calibration (e.g., by sampling more densely or for a longer time) is doomed to fail, leading to a loss of resources and time. Practical identifiability analysis is not covered in this review; the interested reader is referred to [9, 11, 12].

In summary, it is advisable to analyse the observability and structural identifiability of a model before attempting to obtain insights from it. If this analysis reveals deficiencies, actions must be taken depending on the intended application of the model.

For example, if the intended application is for determining the value of a parameter that turns out to be structurally unidentifiable, it is necessary to eliminate this structural identifiability. There are several ways of achieving this. Sometimes it may be possible to determine the unidentifiable parameter by direct measurements, either of the parameter of interest or of the parameter(s) that are correlated with it. However, direct measurements of parameters are seldom possible. It is often more practical to measure additional state variables, which may make the model (or at least the parameter of interest) structurally identifiable; this possibility should be analysed before performing the experiments. Finally, if the experimental setup cannot be modified, or if it is not practical to obtain new experimental data, one can try to modify

the model structure by reducing the number of parameters. This can be achieved by fixing some parameters to values taken from the literature or by merging several unidentifiable parameters into an identifiable one.

If the intended application of the model is for determining the system states, as opposed to the parameters, a structurally unidentifiable model may still be useful—as mentioned previously—as long as the states of interest are observable. In this case, lack of observability may be remedied in a similar way as structural identifiability.

3. Background: Observability and Structural Identifiability

To define observability it is necessary to introduce the notion of distinguishable states.

Definition 1. Let M be a model with internal state x and measurable output y. Let $y_{x_0}(t)$ denote the time evolution of the model output when started from an initial state x_0 at t_0. Two states x_1 and x_2 are *indistinguishable* if $y_{x_1}(t) = y_{x_2}(t)$ for all $t \geq t_0$. The set of states that are indistinguishable from x_1 is denoted by $I(x_1)$.

A model is observable if it is possible to distinguish its internal state from any other state, that is as follows.

Definition 2. A model M is *observable* at x_0 if $I(x_0) = x_0$.

Observability describes the possibility of determining the current state from present and future measurements. A similar concept, reconstructability, refers to determining the current state from present and past measurements.

3.1. Observability of Linear Systems.
For illustration purposes, this subsection presents the special case of linear time-invariant (LTI) systems, whose equations can be written as

$$M_L : \begin{cases} \dot{x}(t) = A(\theta) \cdot x(t) + B(\theta) \cdot u(t), \\ y(t) = C(\theta) \cdot x(t), \\ x_0 = x(t_0, \theta) \end{cases} \quad (1)$$

where $\theta \in \mathbb{R}^q$ is the parameter vector, $u(t) \in \mathbb{R}^r$ the input vector, $x(t) \in \mathbb{R}^n$ the state variable vector, and $y(t) \in \mathbb{R}^m$ the output vector. $A(\theta)$, $B(\theta)$, and $C(\theta)$ are constant matrices of dimensions $n \times n$, $n \times r$, and $m \times n$, respectively. The dependence on θ may be dropped for ease of notation.

Assessing the observability of M_L amounts to determining whether it is possible to infer its internal state, x, by observing its output, y. An intuitive way of obtaining a condition for checking observability is the following. The available knowledge consists of the output and its derivatives; that is,

$$y = C \cdot x$$

$$\dot{y} = C \cdot \dot{x} = C \cdot A \cdot x + C \cdot B \cdot u$$

$$\ddot{y} = C \cdot A \cdot \dot{x} + C \cdot B \cdot \dot{u} == C \cdot A^2 \cdot x + C \cdot A \cdot B \cdot u$$

$$+ C \cdot B \cdot \dot{u} \quad (2)$$

$$\vdots$$

$$\frac{d^i y}{dt^i} = C \cdot A^i \cdot x + h\left(A, B, C, u, \dot{u}, \ddot{u}, \ldots, \frac{d^{i-1}u}{dt^{i-1}}\right)$$

where h is a known matrix function. Setting $i = n$ and writing the above equations in matrix form leads to

$$\begin{pmatrix} y \\ \dot{y} \\ \ddot{y} \\ \vdots \\ \frac{d^{(n-1)}y}{dt^{(n-1)}} \end{pmatrix} = \begin{pmatrix} C \\ C \cdot A \\ C \cdot A^2 \\ \vdots \\ C \cdot A^{n-1} \end{pmatrix} \cdot x + \cdots$$

$$+ h\left(A, B, C, u, \dot{u}, \ddot{u}, \ldots, \frac{d^{n-2}u}{dt^{n-2}}\right) \quad (3)$$

$$== \mathcal{O}^L \cdot x$$

$$+ h\left(A, B, C, u, \dot{u}, \ddot{u}, \ldots, \frac{d^{n-2}u}{dt^{n-2}}\right)$$

where the linear observability matrix has been introduced, $\mathcal{O}^L = (C|C \cdot A|C \cdot A^2| \ldots |C \cdot A^{n-1})^T$. If $\mathcal{O}^L$ is invertible,

one can uniquely obtain x from the knowledge of y and its derivatives, as long as rank($\mathcal{O}^L$) $= n$. This is known as the linear observability rank condition.

Theorem 3. *Linear Observability Rank Condition. Given a linear time-invariant model M_L as defined in (1), a necessary and sufficient condition for complete observability is that* rank($\mathcal{O}^L$) $= n$, where $\mathcal{O}^L = (C|C \cdot A|C \cdot A^2| \ldots |C \cdot A^{n-1})^T$ [2].

"Complete" observability means that all the model states can be inferred from observations of the output.

3.2. Observability of Nonlinear Systems.
Let us now consider nonlinear ODE models. In their most general form they can be written as

$$M_{NL} : \begin{cases} \dot{x}(t) = f(x(t), u(t), \theta), \\ y(t) = g(x(t), \theta), \\ x_0 = x(t_0, \theta) \end{cases} \quad (4)$$

where f and g are analytic vector functions. A special case of (4) is that of nonlinear affine-in-the-input systems:

$$M_{\text{aff}} : \begin{cases} \dot{x}(t) = f_1(x(t), \theta) + f_2(x(t), \theta) \cdot u(t), \\ y(t) = g(x(t), \theta), \\ x_0 = x(t_0, \theta) \end{cases} \quad (5)$$

Shortly after Kalman's introduction of the concept of observability [1, 2], several researchers worked on its application to nonlinear systems of the type defined in (4) and (5). As a result, sufficient and/or necessary conditions for nonlinear observability were obtained [3–6], allowing to extend the observability rank condition in this context. For nonlinear models, unlike for LTI models like (1), the derivatives of the output cannot be expressed in terms of the A, B, C arrays. It is therefore necessary to define a nonlinear version of the observability matrix, $\mathcal{O}^{NL}$; to this end Lie derivatives are used.

Definition 4. The *Lie derivative* of $g(x)$ with respect to $f(x)$ is defined by

$$L_f g(x) = \frac{\partial g(x)}{\partial x} f(x). \quad (6)$$

Higher order Lie derivatives can be recursively calculated as

$$L_f^2 g(x) = \frac{\partial L_f g(x)}{\partial x} f(x),$$

$$\vdots \quad (7)$$

$$L_f^i g(x) = \frac{\partial L_f^{i-1} g(x)}{\partial x} f(x).$$

It can be noticed from (3) that the linear observability matrix, $\mathcal{O}^L$, is the partial derivative of the derivatives of the output with respect to the states; that is,

$$\mathcal{O}^L = \begin{pmatrix} C \\ C \cdot A \\ C \cdot A^2 \\ \vdots \\ C \cdot A^{n-1} \end{pmatrix} = \frac{\partial}{\partial x} \begin{pmatrix} y \\ \dot{y} \\ \ddot{y} \\ \vdots \\ y^{(n-1)} \end{pmatrix} \tag{8}$$

In a nonlinear model such as (4) with constant input, $u(t) = u$, the ith Lie derivative of the output function $g(x)$ coincides with the ith time derivative of $y(t)$, i.e., $y^{(i)}(t) = L_f^i g(x)$. Thus, Lie derivatives can be used to calculate $\mathcal{O}^{NL}$ for nonlinear models with constant inputs as follows:

$$\mathcal{O}^{NL}(x) = \begin{pmatrix} \dfrac{\partial}{\partial x} y(t) \\ \dfrac{\partial}{\partial x} \dot{y}(t) \\ \dfrac{\partial}{\partial x} \ddot{y}(t) \\ \vdots \\ \dfrac{\partial}{\partial x} y^{(n-1)}(t) \end{pmatrix}$$

$$= \begin{pmatrix} \dfrac{\partial}{\partial x} g(x) \\ \dfrac{\partial}{\partial x} \left(L_f g(x)\right) \\ \dfrac{\partial}{\partial x} \left(L_f^2 g(x)\right) \\ \vdots \\ \dfrac{\partial}{\partial x} \left(L_f^{n-1} g(x)\right) \end{pmatrix} \tag{9}$$

The nonlinear version of the observability rank condition can be stated as follows.

Theorem 5. *Nonlinear Observability Rank Condition. If the model M_{NL} given by (4) with constant input u satisfies* rank$(\mathcal{O}^{NL}(x_0)) = n$, *where $\mathcal{O}^{NL}$ is defined by (9), then it is (locally) observable around x_0 [4, 18].*

Two remarks are in order. First, it should be noted that the nonlinear observability rank condition (ORC) is a *sufficient*, but not strictly necessary, condition for nonlinear observability (unlike the linear case, in which the ORC is both sufficient and necessary). In the nonlinear case, the ORC is "almost necessary" in the sense that, if M_{NL} is locally observable around x_0, then rank$(\mathcal{O}^{NL}(x_0)) = n$ for an open dense subset of the state space [18]. This is a rather technical distinction, and in practice a failure to comply with the ORC is often considered as a very strong indication of unobservability. Second, it should also be noted that the ORC determines *local*

observability: if a model satisfies the ORC, it is possible to distinguish between two adjacent states, but there may still be distant states that are indistinguishable. A locally observable model is often—although not always—globally observable too.

3.3. Structural Local Identifiability as Observability. In this paper structural identifiability is considered as a particular case of observability. As noted in the preceding Section 3.2, nonlinear observability is a local concept, which means we will study structural *local* identifiability. The analysis of structural *global* identifiability requires other approaches [12–14]. Note however that the definitions provided here do not prevent a locally identifiable model to be also globally identifiable, and this will actually be the case in many practical applications.

Definition 6. A parameter θ_i in a model M_{NL} given by (4) is *structurally locally identifiable* (s.l.i.) if for almost any parameter vector $\theta^* \in \mathbb{R}^q$ there is a neighbourhood $\mathcal{N}(\theta^*)$ such that the following property holds:

$$\widehat{\theta} \in \mathcal{N}(\theta^*)$$
$$\text{and } g(x, \widehat{\theta}) = g(x, \theta^*) \implies \tag{10}$$
$$\widehat{\theta}_i = \theta_i^*$$

Definition 7. A parameter θ_i is *structurally unidentifiable* (s.u.) if (10) does not hold in any neighbourhood of θ^*.

Definition 8. A model M_{NL} is s.l.i. if all its parameters are s.l.i.

Definition 9. A model M_{NL} is s.u. if at least one of its parameters is s.u.

Structural identifiability can be considered as a particular case of observability by considering the parameters as state variables with zero dynamics [31, 47–50]. The augmented state variable vector is

$$\widetilde{x} = \begin{bmatrix} x \\ \theta \end{bmatrix} \tag{11}$$

Similar to the nonlinear observability matrix of (9), it is possible to define an augmented nonlinear observability-identifiability matrix, $\mathcal{O}_I^{NL}(\widetilde{x})$, as

$$\mathcal{O}_I^{NL}(\widetilde{x}) = \begin{pmatrix} \dfrac{\partial}{\partial \widetilde{x}} g(\widetilde{x}) \\ \dfrac{\partial}{\partial \widetilde{x}} \left(L_f g(\widetilde{x})\right) \\ \dfrac{\partial}{\partial \widetilde{x}} \left(L_f^2 g(\widetilde{x})\right) \\ \vdots \\ \dfrac{\partial}{\partial \widetilde{x}} \left(L_f^{n+q-1} g(\widetilde{x})\right) \end{pmatrix} \tag{12}$$

Theorem 10. *Nonlinear Observability-Identifiability Condition (OIC). If a model M_{NL} given by (4) satisfies*

$\text{rank}(\mathcal{O}_I^{NL}(\widetilde{x}_0)) = n + q$, with $\mathcal{O}_I^{NL}(\widetilde{x}_0)$ given by (12), then it is (locally) observable and identifiable in a neighbourhood $\mathcal{N}(\widetilde{x}_0)$ of $\widetilde{x}_0$.

Remark 11. Identifiability of individual parameters: if the OIC condition is fulfilled, all the parameters of M_{NL} are s.l.i. If the OIC does not hold, M_{NL} is s.u. and at least some parameter(s) are s.u. (and/or some states are unobservable). Since each column in $\mathcal{O}_I^{NL}$ corresponds to the partial derivative with respect to a state or parameter, it is possible to determine which parameters (states) are structurally unidentifiable (unobservable) by removing the corresponding column and recalculating $\text{rank}(\mathcal{O}_I^{NL})$. If deleting the ith column does not change $\text{rank}(\mathcal{O}_I^{NL})$, then the ith parameter (state) is structurally unidentifiable (unobservable) [47]. We can thus define a Structural Identifiability Condition for a parameter as follows:

Theorem 12. *Structural Identifiability Condition (SIC). Given a model M_{NL} defined by (4), its ith parameter θ_i is structurally locally identifiable in a neighbourhood $\mathcal{N}(\widetilde{x}_0)$ of $\widetilde{x}_0$ if $\text{rank}(\mathcal{O}_I^{i*}(\widetilde{x}_0)) < \text{rank}(\mathcal{O}_I(\widetilde{x}_0))$, where $\mathcal{O}_I(\widetilde{x}_0)$ is the $\mathcal{O}_I^{NL}(\widetilde{x}_0)$ defined in (12), and $\mathcal{O}_I^{i*}(\widetilde{x}_0)$ is the array that results from removing the column corresponding to $\partial/\partial\theta_i$ from $\mathcal{O}_I(\widetilde{x}_0)$.*

3.4. Example: Observability and Structural Identifiability Analysis of a Nonlinear Model. The approach described in Section 3.3 is demonstrated here by applying it to the nonlinear model used as motivating example in Section 2. This case study was briefly described in Section 2 and Figure 1, which shows its dynamic equations. It consists of $n = 3$ states, $x = [G, \beta, I]$, $m = 2$ outputs, $y = [G, \beta]$, $q = 5$ parameters, $\theta = [p, s_i, \gamma, c, \alpha]$, and $r = 1$ input, u. The augmented vector consisting of the states and parameters is $\widetilde{x} = [G, \beta, I, p, s_i, \gamma, c, \alpha]$.

The observability and structural identifiability of this system can be analysed with the observability-identifiability condition (OIC) of Theorem 10. To this end one must build the $\mathcal{O}_I^{NL}$ matrix defined in (12). The first two rows in $\mathcal{O}_I^{NL}$ correspond to the partial derivatives of the output function with respect to the states and parameters; since the output is $y = g(\widetilde{x}) = [G, \beta]$, the first two rows of $\mathcal{O}_I^{NL}$ are

$$\frac{\partial G}{\partial \widetilde{x}} = [1, 0, 0, 0, 0, 0, 0]$$
$$\frac{\partial \beta}{\partial \widetilde{x}} = [0, 1, 0, 0, 0, 0, 0]$$

(13)

The matrix made up of the two rows above has rank equal to two. Subsequent rows are calculated with Lie derivatives as defined in (6) and (7). In principle, $n + q - 1 = 7$ Lie derivatives must be symbolically calculated. However, in practice it may be possible to stop the calculation earlier: if the rank of the matrix does not increase after the addition of a new derivative, it is not necessary to calculate higher order derivatives since they will not modify the rank.

The first Lie derivative is obtained as

$$L_f g(\widetilde{x}) = \frac{\partial g(\widetilde{x})}{\partial \widetilde{x}} f(\widetilde{x})$$

$$= \begin{pmatrix} u + u_0 - x_1 \cdot (p_4 + p_2 \cdot x_3) \\ x_2 \cdot \left(\dfrac{1.4583 \cdot 10^{-5}}{(8.4/x_1)^{1.7} + 1} - \dfrac{1.7361 \cdot 10^{-5}}{(x_1/4.8)^{8.5} + 1} \right) \end{pmatrix}$$

(14)

Thus, the third and fourth rows of $\mathcal{O}_I^{NL}$ are

$$\frac{\partial}{\partial \widetilde{x}}\left(L_f g(\widetilde{x})\right)$$
$$= \begin{pmatrix} \mathcal{O}_{3,1} & 0 & \mathcal{O}_{3,3} & 0 & \mathcal{O}_{3,5} & 0 & \mathcal{O}_{3,7} & 0 \\ \mathcal{O}_{4,1} & \mathcal{O}_{4,2} & 0 & 0 & 0 & 0 & 0 & 0 \end{pmatrix}$$

(15)

where

$$\mathcal{O}_{3,1} = -c - s_i \cdot x_3$$
$$\mathcal{O}_{3,3} = -s_i \cdot x_1$$
$$\mathcal{O}_{3,5} = -x_1 \cdot x_3$$
$$\mathcal{O}_{3,7} = -x_1$$
$$\mathcal{O}_{4,1} = \frac{3.0743 \cdot 10^{-5} \cdot x_2 \cdot (x_1/4.8)^{7.5}}{\left((x_1/4.8)^{8.5} + 1\right)^2}$$
$$\quad - \frac{0.0052 \cdot (8.4/x_1)^{0.7}}{\left(25 \cdot x_1^2 \cdot (8.4/x_1)^{1.7} + 1\right)^2}$$
$$\mathcal{O}_{4,2} = \frac{1.4583 \cdot 10^{-5}}{(8.4/x_1)^{1.7} + 1} - \frac{1.7361 \cdot 10^{-5}}{(x_1/4.8)^{8.5} + 1}$$

(16)

By adding the two rows corresponding to $(\partial/\partial\widetilde{x})(L_f g(\widetilde{x}))$, the rank of $\mathcal{O}_I^{NL}$ increases from two to three. Proceeding in the same manner, the rank of the matrix increases with every additional Lie derivative until it stops: it is equal to 7 when $\mathcal{O}_I^{NL}$ is built with both 5 and 6 Lie derivatives. Thus with 6 derivatives we know that the model has some observability/identifiability issues, since its matrix does not have full rank.

At this point we can determine the observability of each state and the structural identifiability of each parameter using the procedure described in Remark 11. This yields that the unmeasured state I is not observable, and that there are two s.u. parameters (p, s_i) and three s.l.i. parameters (γ, c, α). It can be noticed that multiplying by s_i the dynamic equation of I shown in Figure 1 leads to a modified model in which the third state is $(s_i \cdot I)$ instead of I, and parameter p only appears in the equations as part of the product $s_i \cdot p$. This model formulation highlights the fact that only the products $s_i \cdot p$ and $s_i \cdot I$ are observable (identifiable).

4. Recent Developments

4.1. Computational Implementations of the Rank Conditions. The conditions described in Section 3 involve building observability ($\mathcal{O}^{NL}$) or observability-identifiability matrices

$(\mathcal{O}_I^{NL})$ and calculating their rank. Building these arrays involves symbolic calculations, which can be performed in environments such as Mathematica (Wolfram Research, Champaign, IL, USA), MATLAB (MathWorks, Natick, MA, USA), or MAPLE (Maplesoft, Waterloo, ON, Canada). Some software tools provide advanced implementations of these calculations.

August and Papachristodoulou [49] used semidefinite programming to evaluate the OIC (Theorem 10). They used SOSTOOLS [51], a free MATLAB toolbox that performs a sum of squares decomposition. This technique allows assessing identifiability for all parameter values within an interval; however, the computational cost of the rank calculation quickly becomes high as the problem size increases, which hinders the applicability of this method to medium-to-large models.

Another MATLAB tool is the STRIKE-GOLDD toolbox [52], publicly available software that analyses structural identifiability and observability using the OIC. It includes options such as performing partial analyses and decomposing the models, which can be helpful for analysing large models.

For rational systems, the Exact Arithmetic Rank (EAR) method is a numerical alternative for calculating the rank. It is based on an algorithm originally presented by Sedoglavic [31], which was extended and implemented in Mathematica by Jirstrand and coworkers [30].

4.2. Accessibility and the Role of Initial Conditions. The rank conditions of Theorems 5 and 10 provide results that are valid for "almost all" values of the variables (state and parameter vectors), that is, for all possible values except for a set of measure zero (a "thin set"). Consequently, for specific values there may be loss of identifiability. This was pointed out by Saccomani et al. [53, 54], who analysed this phenomenon with a differential algebra approach, tracing its cause to a loss of accessibility from certain initial conditions. Accessibility, also called reachability, is a property that describes the ability to move a system to any state in a neighbourhood of the initial one. Saccomani and coworkers noted that a loss of accessibility from specific initial conditions could lead to loss of structural identifiability.

This matter has been recently approached from the differential geometry viewpoint. In [55] it was remarked that loss of accessibility is not the only possible cause of loss of structural identifiability from specific initial conditions: this phenomenon can take place even for models that are not accessible from generic initial conditions. Furthermore, it was also noted that a decrease in rank($\mathcal{O}_I^{NL}$) at a specific initial condition $x(0)$ does not necessarily result in a loss of structural identifiability, even if the system is started at that initial condition. In [55] a method for finding potentially problematic vectors was also suggested, although it scales up poorly with system size.

4.3. The Role of Inputs. The methodology presented in Section 3 assumes that the input vector u is *known and constant*. Obviously, the same formulation can account for the case of *unknown constant* inputs simply by considering

them as additional parameters, which are unknown and constant by definition. For *known, time-varying* inputs that are differentiable functions of time, a differential algebra approach would still be valid. However, the differential geometry procedure described in Section 3 needs to be extended in order to cope with this case. To this end it has recently been suggested to use extended Lie derivatives [56], which are defined as follows:

Definition 13. The *extended Lie derivative* is [30]

$$L_f g(\tilde{x}) = \frac{\partial g(\tilde{x})}{\partial \tilde{x}} f(\tilde{x}, u) + \sum_{j=0}^{j=\infty} \frac{\partial g(\tilde{x})}{\partial u^{(j)}} u^{(j+1)} \qquad (17)$$

where $u^{(j)}$ is the jth derivative of the input u. Higher order extended Lie derivatives are recursively calculated as:

$$L_f^i g(\tilde{x}) = \frac{\partial L_f^{i-1} g(\tilde{x})}{\partial \tilde{x}} f(\tilde{x}, u) + \sum_{j=0}^{j=\infty} \frac{\partial L_f^{i-1} g(\tilde{x})}{\partial u^{(j)}} u^{(j+1)} \quad (18)$$

(Note that this definition considers a time-dependent input vector $u(t)$, which is simply written as u for ease of notation.) Unlike the previously defined Lie derivatives of ((6), (7)), the extended Lie derivatives are equal to the output derivatives for time-varying inputs, $y^{(i)}(t) = L_f^i g(x)$. Evaluating the OIC with a $\mathcal{O}_I^{NL}$ built with extended Lie derivatives correctly determines the observability and structural identifiability of a model. Some models may require time-varying inputs in order to be identifiable. In [56] it was shown how the extended Lie derivatives can be used for experimental design, by determining the number of nonzero derivatives of the input that are required for structural identifiability.

The identifiability of the βIG model used in Sections 2 and 3.4 does not depend on the input derivatives. Hence in this section this situation will be illustrated with a different example, the following two-compartment model [56]:

$$\dot{x}_1 = -(k_{1e} + k_{12}) \cdot x_1 + k_{21} \cdot x_2 + b \cdot u,$$
$$\dot{x}_2 = k_{12} \cdot x_1 - k_{21} \cdot x_2, \qquad (19)$$
$$y = x_1$$

Compartmental models of this type are commonly used to describe physiological processes. Note that, although the model given by (19) is linear in the states, if the state vector is augmented with the parameters (as needed for structural identifiability analysis) the model becomes nonlinear.

This model is structurally unidentifiable from an experiment with a constant input, but becomes structurally identifiable with a continuous time-varying input such as a ramp [56]. This is illustrated in Figure 2. The constant input result can be obtained by applying the procedure described in Section 3.3 as shown in Section 3.4. Since this model has $n = 2$ states and $q = 4$ parameters, it would require rank($\mathcal{O}_I^{NL}$) = $n + q = 6$ to be observable and s.l.i. However, the aforementioned procedure yields rank($\mathcal{O}_I^{NL}$) = 5, and the procedure
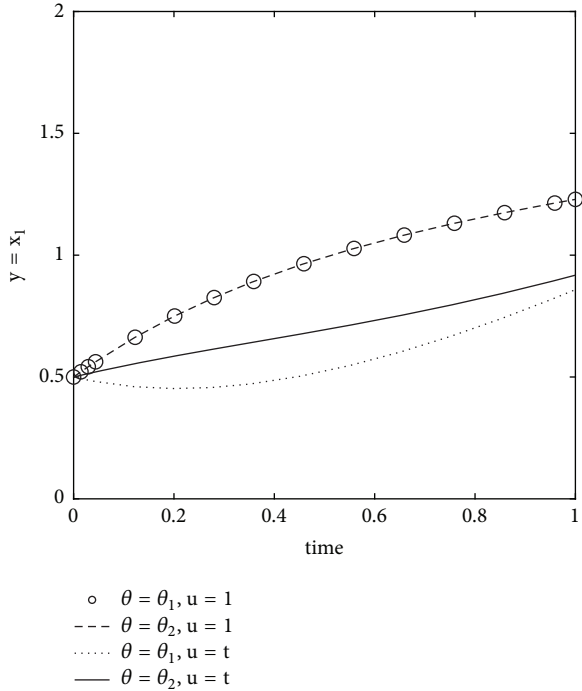
FIGURE 2: Output of the two-compartment model of (19) for two different parameter vectors (θ_1 given by $k_{1e} = 1, k_{12} = 3, k_{21} = 1, b = 1$, and θ_2 given by $k_{1e} = 2, k_{12} = 2.5, k_{21} = 0.5, b = 2$), and two different inputs, $u = 1$ and $u = t$ (where t stands for time). With a constant input $u = 1$ both parameter vectors are indistinguishable from the model output (there is actually an infinite number of pairs of indistinguishable parameter vectors), and the parameters are structurally unidentifiable. However, with a ramp input $u = t$ two different parameter vectors yield two different model outputs; in this case the parameters are structurally identifiable.

in Remark 11 determines that x_2 is observable but all the parameters are s.u. The time-varying input result is obtained by building $\mathcal{O}_I^{NL}$ with the extended Lie derivatives defined in ((6), (7)); in the corresponding symbolic derivations $\dot{u}$ is set to a constant value and higher order derivatives, $\ddot{u}, \dddot{u}, \ldots$ are set to zero. This yields $\text{rank}(\mathcal{O}_I^{NL}) = 6$ with 5 derivatives, and the model is observable and s.l.i. These calculations can be performed with STRIKE-GOLDD2 [56] and take less than one second in a standard computer. The difference in the results with $\dot{u} = 0$ and $\dot{u} \neq 0$ is due to the presence of terms containing $\dot{u}$ in some entries of $\mathcal{O}_I^{NL}$, whose contribution is needed for a full rank. Setting $\dot{u} = 0$ removes these terms and decreases the matrix rank, leading to a loss of identifiability.

It should be noted that this model can also be analysed with a differential algebra approach; for example, the COM-BOS application [57] obtains the same result in comparable time. Compared to the differential geometry approach, the advantages of this method are the ability to distinguish between local and global identifiability and to find identifiable combinations. Its disadvantages are that in principle it cannot consider specific derivatives being zero (e.g., $\dot{u} \neq 0$ but $\ddot{u} = 0$) and that it typically has worse computational scale-up for models with large nonlinearities.

A different problem arises when the inputs are *time-varying* and *unknown*. Such inputs can be viewed as external disturbances, of which there are neither measurements nor information about their dependence on time. Martinelli [58] extended the ORC to account for this situation for the case of nonlinear systems that are affine with respect to the inputs, which must be differentiable but may be known and/or unknown. To this end, the model defined by (5) is augmented in order to include an unknown input vector w as follows:

$$\dot{x} = f_1(x, \theta) + f_2(x, \theta) \cdot u + f_3(x, \theta) \cdot w,$$
$$y = g(x, \theta), \tag{20}$$

In [58] it was proposed to extend this model by augmenting the original state x to ${}^k x$, which includes the input and its derivatives up to order k, that is ${}^k x = [x, \theta, \dot{w}, \ddot{w}, \ldots, w^{(k)}]$. An extended observability rank condition (EORC) was then presented, allowing checking the observability of systems with unknown inputs, although not of the inputs themselves, at least in its published form. Although in [58, 59] the structural identifiability problem was not explicitly considered, it is of course possible to apply this idea to a joint observability and structural identifiability analysis.

4.4. Model Symmetries and Identifiable Combinations. If a set of parameters are found to be structurally unidentifiable, a question naturally arises: it is possible to reformulate the model by combining such parameters in an identifiable quantity? The answer to this question entails characterizing the form in which the structurally unidentifiable parameters are correlated. Many methods for structural identifiability analysis are capable of addressing this problem to a certain extent; however, no generally applicable and automatic procedure exists.

One of the first examples, the "exhaustive modelling" method for finding the set of models that are output indistinguishable from a given one, was presented in [60]. This procedure, also known as the similarity transformation approach, can be used to obtain structurally identifiable versions of linear compartmental models. An extension to controlled nonlinear models, which requires testing controllability and observability conditions, was presented in [28], and the case of uncontrolled systems was considered in [61, 62].

Differential algebra is a classic approach for the study of observability [63] and structural identifiability [25]. The equivalence between the observability definitions from the algebraic and differential geometric viewpoints was established in [64] for a class of rational systems. DAISY is a software that adopts the differential algebra approach to assess global structural identifiability and observability [65], and COMBOS [57] is a tool specifically developed for finding identifiable parameter combinations using differential algebra concepts such as Gröbner bases [26, 66].

Other approaches to this problem use Lie transformations. A method based on the generation of Lie algebras that represent the symmetries of the model equations was presented in [67]. This procedure uses random numerical specializations and is valid for autonomous, rational systems.

Instead of using random specializations, another method described in [68] finds Lie symmetries by transforming rational terms into linear terms. Finally, the aforementioned toolbox STRIKE-GOLDD [52], which uses Lie derivatives to calculate the observability-identifiability matrix $\mathscr{O}_I^{NL}$, includes a procedure for finding identifiable parameter combinations that is based on ideas from [47, 69, 70]. Briefly, it removes from $\mathscr{O}_I^{NL}$ the columns corresponding to identifiable parameters and calculates a basis for the null space of the resulting matrix. The coefficients of this basis define a set of partial differential equations, whose solutions yield the identifiable combinations.

4.5. Sloppiness, Dynamical Compensation, and Structural Identifiability. A structurally unidentifiable model can yield the same output for different parameter values. This situation might be interpreted as a sign of robustness of the system to changes in parameter values. However, while lack of identifiability is usually considered an undesirable model property, in certain contexts robustness is seen as a desirable property. This apparent contradiction highlights the subtle character of the relationship between identifiability and robustness. As an illustration of this relationship, this subsection discusses two concepts developed in recent years – sloppiness and dynamical compensation – that are related but not equivalent to unidentifiability.

The first concept, sloppiness or sloppy models, was introduced in [71] to refer to the situation in which the model output is sensitive to changes in so-called stiff parameters, but largely insensitive to changes in sloppy parameters. Sloppiness was defined as the existence of a clear gap between the eigenvalues of the system's Fisher information matrix (FIM), with large eigenvalues corresponding to stiff parameters and small eigenvalues corresponding to sloppy parameters. It was claimed that sloppiness is a universal feature of systems biology models [43], which would make it impossible to estimate all parameters accurately. More recent publications have provided new insights about sloppiness, as reviewed in [72]. The concept of sloppiness, which has been linked to information theory, highlights the fact that a model's output behaviour may still be tightly constrained despite the parameter values being only loosely constrained. Sloppiness provides a viewpoint for studying how distinguishable models are, and how they can be reduced. Several papers have clarified the relation between sloppiness and identifiability [73–76]. It is now understood that sloppiness is related to *practical* rather than *structural* identifiability, and that it is not equivalent to unidentifiability of any kind, meaning that sloppy models can indeed be identifiable.

The second concept, dynamical compensation (DC for short), was introduced in [35] as a property found in certain physiological circuits. Originally DC was defined simply as the invariance of the model output with respect to changes in a parameter value. It was immediately noted that according to this definition DC amounted to structural unidentifiability [77, 78]. (Note that the glucose homeostasis mechanism discussed in the Introduction was proposed in [35] as a possible mechanism for achieving DC; depending

on its formulation—i.e., on which states are measured and which parameters are known—this model can be structurally unidentifiable). This equivalence between structural unidentifiability and the original definition of DC was not discussed in [35] and was potentially problematic, since the purpose of DC was to describe a phenomenon different to structural unidentifiability. More precisely, DC referred to the capability of a physiological circuit to maintain its dynamic behaviour unchanged after a change in the value of a model parameter, following a transition period. An alternative definition of DC that provided a more detailed description of the phenomenon and that took into account the relationship with structural identifiability was proposed in [46].

5. Open Problems and Future Directions

The differential geometry approach adopted in this review has been used to analyse observability and structural identifiability of nonlinear systems for more than forty years. The theoretical and computational advances made in the last decades have increased its applicability. However, there are still many challenges that call for more research in this area.

For example, an intrinsic limitation of the approach is that it yields only *local* results. Other methods, such as differential algebra, are capable of providing global structural identifiability results. They could possibly serve as an inspiration for extending (hybridizing?) the differential geometry techniques to perform global analyses.

Other desirable developments would consist of advanced implementations to alleviate the computational burden of the analyses. Such improvements, which may benefit from the use of parallelization and high performance computing techniques, would facilitate the application of these methods to the increasingly large models being built in the biological modelling community.

Another possible direction concerns the role of inputs in observability and identifiability analysis. Despite recent advances, there are still several open questions regarding this matter. It has been noted that certain models that are structurally unidentifiable from a single constant input experiment can become identifiable if a continuously time-varying input is used [56]. In some cases the same improvement can be obtained with multiple constant input experiments [56, 79], or, equivalently, with a single experiment with a piecewise constant input. However, the question of when a time-varying input and multiple constant inputs are equivalent for the purpose of structural identifiability has not been answered yet. Likewise, the problem of analysing observability and structural identifiability in presence of unmeasured inputs has not been fully solved yet.

Finally, an important open question is the relationship between observability/identifiability and model predictions. On the one hand, it is known that lack of the former can lead to errors in the latter. On the other hand, it is true that this is not necessarily the case. Therefore, further insights into the requisites for accurate predictive modelling would be a valuable contribution.

Conflicts of Interest

The author declares that he has no conflicts of interest.

Acknowledgments

References

[1] R. E. Kalman, "Contributions to the theory of optimal control," *Boletín de la Sociedad Matemática Mexicana*, vol. 5, pp. 102–119, 1960.

[2] R. Kalman, "On the general theory of control systems," *IFAC Proceedings Volumes*, vol. 1, no. 1, pp. 491–502, 1960.

[3] E. W. Griffith and K. S. Kumar, "On the observability of nonlinear systems: I," *Journal of Mathematical Analysis and Applications*, vol. 35, pp. 135–147, 1971.

[4] R. Hermann and A. J. Krener, "Nonlinear controllability and observability," *IEEE Transactions on Automatic Control*, vol. 22, no. 5, pp. 728–740, 1977.

[5] Y. M. Kostyukovskii, "Simple conditions of observability of nonlinear controlled systems," *Avtomat. i Telemeh.*, no. 10, pp. 32–41, 1968.

[6] S. R. Kou, D. L. Elliott, and T. J. Tarn, "Observability of nonlinear systems," *Information and Control*, vol. 22, no. 1, pp. 89–99, 1973.

[7] H. J. Sussmann and V. Jurdjevic, "Controllability of nonlinear systems," *Journal of Differential Equations*, vol. 12, pp. 95–116, 1972.

[8] R. Bellman and K. J. Åström, "On structural identifiability," *Mathematical Biosciences*, vol. 7, no. 3-4, pp. 329–339, 1970.

[9] E. Walter and L. Pronzato, "Identification of parametric models from experimental data," in *Communications and Control Engineering Series*, Springer, London, UK, 1997.

[10] L. Ljung, *System identification: theory for the user*, Prentice Hall, Upper Saddle River, NJ, USA, 1999.

[11] J. III. DiStefano, *Dynamic systems biology modeling and simulation*, Academic Press, 2015.

[12] A. F. Villaverde and A. Barreiro, "Identifiability of large nonlinear biochemical networks," *MATCH - Communications in Mathematical and in Computer Chemistry*, vol. 76, no. 2, pp. 259–296, 2016.

[13] O.-T. Chis, J. R. Banga, and E. Balsa-Canto, "Structural identifiability of systems biology models: A critical comparison of methods," *PLoS ONE*, vol. 6, no. 11, 2011.

[14] H. Miao, X. Xia, A. S. Perelson, and H. Wu, "On identifiability of nonlinear ODE models and applications in viral dynamics," *SIAM Review*, vol. 53, no. 1, pp. 3–39, 2011.

[15] M. N. Chatzis, E. N. Chatzi, and A. W. Smyth, "On the observability and identifiability of nonlinear structural and mechanical systems," *Structural Control and Health Monitoring*, vol. 22, no. 3, pp. 574–593, 2015.

[16] A. Isidori, *Nonlinear control systems*, Springer Science & Business Media, 1995.

[17] E. D. Sontag, *Mathematical Control Theory: Deterministic Finite Dimensional Systems*, vol. 6, Springer Science & Business Media, 2013.

[18] M. Vidyasagar, *Nonlinear Systems Analysis*, Prentice Hall, Englewood Cliffs, NJ, USA, 1993.

[19] O. Chis, J. R. Banga, and E. Balsa-Canto, "GenSSI: A software toolbox for structural identifiability analysis of biological models," *Bioinformatics*, vol. 27, no. 18, Article ID btr431, pp. 2610-2611, 2011.

[20] H. Pohjanpalo, "System identifiability based on the power series expansion of the solution," *Mathematical Biosciences*, vol. 41, no. 1-2, pp. 21–33, 1978.

[21] E. Walter and Y. Lecourtier, "Global approaches to identifiability testing for linear and nonlinear state space models," *Mathematics and Computers in Simulation*, vol. 24, no. 6, pp. 472–482, 1982.

[22] S. Audoly, G. Bellu, L. D'angiò, M. P. Saccomani, and C. Cobelli, "Global identifiability of nonlinear models of biological systems," *IEEE Transactions on Biomedical Engineering*, vol. 48, no. 1, pp. 55–65, 2001.

[23] S. Diop and M. Fliess, "Nonlinear observability, identifiability, and persistent trajectories," in *Proceedings of the 30th IEEE Conference on Decision and Control*, pp. 714–719, Brighton, UK, December 1991.

[24] H. Hong, A. Ovchinnikov, G. Pogudin, and C. Yap, "Global identifiability of differential models," 2018, https://arxiv.org/abs/1801.08112.

[25] L. Ljung and T. Glad, "On global identifiability for arbitrary model parametrizations," *Automatica*, vol. 30, no. 2, pp. 265–276, 1994.

[26] N. Meshkat, M. Eisenberg, and I. DiStefano, "An algorithm for finding globally identifiable parameter combinations of nonlinear ODE models using Gröbner bases," *Mathematical Biosciences*, vol. 222, no. 2, pp. 61–72, 2009.

[27] L. Denis-Vidal, G. Joly-Blanchard, and C. Noiret, "Some effective approaches to check the identifiability of uncontrolled nonlinear systems," *Mathematics and Computers in Simulation*, vol. 57, no. 1-2, pp. 35–44, 2001.

[28] S. Vajda, K. R. Godfrey, and H. Rabitz, "Similarity transformation approach to identifiability analysis of nonlinear compartmental models," *Mathematical Biosciences*, vol. 93, no. 2, pp. 217–248, 1989.

[29] X. Xia and C. H. Moog, "Identifiability of nonlinear systems with application to HIV/AIDS models," *IEEE Transactions on Automatic Control*, vol. 48, no. 2, pp. 330–336, 2003.

[30] J. Karlsson, M. Anguelova, and M. Jirstrand, "An efficient method for structural identiability analysis of large dynamic systems," in *Proceedings of the 16th IFAC Symposium on System Identification*, vol. 16, pp. 941–946, 2012.

[31] A. Sedoglavic, "A probabilistic algorithm to test local algebraic observability in polynomial time," *Journal of Symbolic Computation*, vol. 33, no. 5, pp. 735–755, 2002.

[32] A. Raue, C. Kreutz, T. Maiwald et al., "Structural and practical identifiability analysis of partially observed dynamical models by exploiting the profile likelihood," *Bioinformatics*, vol. 25, no. 15, pp. 1923–1929, 2009.

[33] J. D. Stigter and J. Molenaar, "A fast algorithm to assess local structural identifiability," *Automatica*, vol. 58, pp. 118–124, 2015.

[34] A. Raue, J. Karlsson, M. P. Saccomani, M. Jirstrand, and J. Timmer, "Comparison of approaches for parameter identifiability analysis of biological systems," *Bioinformatics*, vol. 30, no. 10, pp. 1440–1448, 2014.

[35] O. Karin, A. Swisa, B. Glaser, Y. Dor, and U. Alon, "Dynamical compensation in physiological circuits," *Molecular Systems Biology*, vol. 12, no. 11, article no. 886, 2016.

[36] R. Muñoz-Tamayo, L. Puillet, J. B. Daniel et al., "Review: To be or not to be an identifiable model. Is this a relevant question in animal science modelling?" *Animal*, vol. 12, no. 4, pp. 701–712, 2018.

[37] D. L. I. Janzén, L. Bergenholm, M. Jirstrand et al., "Parameter identifiability of fundamental pharmacodynamic models," *Frontiers in Physiology*, vol. 7, 2016.

[38] N. Tuncer, M. Marctheva, B. LaBarre, and S. Payoute, "Structural and practical identifiability analysis of Zika epidemiological models," *Bulletin of Mathematical Biology*, vol. 80, no. 8, pp. 2209–2241, 2018.

[39] J. D. Stigter, M. B. Beck, and J. Molenaar, "Assessing local structural identifiability for environmental models," *Environmental Modeling and Software*, vol. 93, pp. 398–408, 2017.

[40] T. R. Middendorf and R. W. Aldrich, "Structural identifiability of equilibrium ligand-binding parameters," *The Journal of General Physiology*, vol. 149, no. 1, pp. 105–119, 2017.

[41] O. J. Walch and M. C. Eisenberg, "Parameter identifiability and identifiable combinations in generalized Hodgkin-Huxley models," *Neurocomputing*, vol. 199, pp. 137–143, 2016.

[42] M. P. Saccomani and K. Thomaseth, "The Union between Structural and Practical Identifiability Makes Strength in Reducing Oncological Model Complexity: A Case Study," *Complexity*, vol. 2018, Article ID 2380650, 10 pages, 2018.

[43] R. N. Gutenkunst, J. J. Waterfall, F. P. Casey, K. S. Brown, C. R. Myers, and J. P. Sethna, "Universally sloppy parameter sensitivities in systems biology models," *PLoS Computational Biology*, vol. 3, no. 10, pp. 1871–1878, 2007.

[44] M. C. Eisenberg and H. V. Jain, "A confidence building exercise in data and identifiability: Modeling cancer chemotherapy as a case study," *Journal of Theoretical Biology*, vol. 431, pp. 63–78, 2017.

[45] A. Procopio, S. De Rosa, C. Covello et al., "A model of cardiac troponin T release in patient with acute myocardial infarction," in *Proceedings of the 2017 IEEE 56th Annual Conference on Decision and Control (CDC)*, pp. 435–440, Melbourne, VIC, December 2017.

[46] A. F. Villaverde and J. R. Banga, "Dynamical compensation and structural identifiability of biological models: Analysis, implications, and reconciliation," *PLoS Computational Biology*, vol. 13, no. 11, p. e1005878, 2017.

[47] M. Anguelova, *Nonlinear observability and identifiability: General theory and a case study of a kinetic model for S. cerevisiae [Master's thesis]*, Chalmers University of Technology and Göteborg University, 2004.

[48] M. Anguelova, *Observability and identifiability of nonlinear systems with applications in biology [PhD thesis]*, Chalmers University of Technology, 2007.

[49] E. August and A. Papachristodoulou, "A new computational tool for establishing model parameter identifiability," *Journal of Computational Biology*, vol. 16, no. 6, pp. 875–884, 2009.

[50] E. T. Tunali and T. J. Tarn, "New results for identifiability of nonlinear systems," *IEEE Transactions on Automatic Control*, vol. 32, no. 2, pp. 146–154, 1987.

[51] S. Prajna, A. Papachristodoulou, and P. A. Parrilo, "Introducing SOSTOOLS: A general purpose sum of squares programming solver," in *Proceedings of the 41st IEEE Conference on Decision and Control*, pp. 741–746, December 2002.

[52] A. F. Villaverde, A. Barreiro, and A. Papachristodoulou, "Structural Identifiability of Dynamic Systems Biology Models," *PLoS Computational Biology*, vol. 12, no. 10, p. e1005153, 2016.

[53] L. D'Angiò, M. P. Saccomani, S. Audoly, and G. Bellu, "Identifiability of nonaccessible nonlinear systems," in *Positive systems*, R. Bru and Romero-Vivó, Eds., vol. 389, pp. 269–277, Springer, Berlin, Germany, 2009.

[54] M. P. Saccomani, S. Audoly, and L. D'Angiò, "Parameter identifiability of nonlinear systems: The role of initial conditions," *Automatica*, vol. 39, no. 4, pp. 619–632, 2003.

[55] A. F. Villaverde and J. R. Banga, "Structural properties of dynamic systems biology models: Identifiability, reachability, and initial conditions," *Processes*, vol. 5, no. 2, 2017.

[56] A. F. Villaverde, N. D. Evans, M. J. Chappell, and J. R. Banga, "Input-Dependent Structural Identifiability of Nonlinear Systems," *IEEE Control Systems Letters*, vol. 3, no. 2, pp. 272–277, 2019.

[57] N. Meshkat, C. Er-zhen Kuo, and J. DiStefano, "On finding and using identifiable parameter combinations in nonlinear dynamic systems biology models and combos: a novel web implementation," *PLoS ONE*, vol. 9, no. 10, Article ID e110261, 2014.

[58] A. Martinelli, "Extension of the observability rank condition to nonlinear systems driven by unknown inputs," in *Proceedings of the 23rd Mediterranean Conference on Control and Automation, MED 2015*, pp. 589–595, Spain, June 2015.

[59] A. Martinelli, "Nonlinear Unknown Input Observability: Extension of the Observability Rank Condition," *IEEE Transactions on Automatic Control*, vol. 64, no. 1, pp. 222–237, 2019.

[60] E. Walter and Y. Lecourtier, "Unidentifiable compartmental models: what to do?" *Mathematical Biosciences*, vol. 56, no. 1-2, pp. 1–25, 1981.

[61] N. D. Evans, M. J. Chapman, M. J. Chappell, and K. R. Godfrey, "Identifiability of uncontrolled nonlinear rational systems," *Automatica*, vol. 38, no. 10, pp. 1799–1805, 2002.

[62] G. Joly-Blanchard and L. Denis-Vidal, "Some remarks about an identifiability result of nonlinear systems," *Automatica*, vol. 34, no. 9, pp. 1151-1152, 1998.

[63] S. Diop and M. Fliess, "On nonlinear observability," in *Proceedings of 1st European Control Conference*, pp. 152–157, 1991.

[64] S. Diop and Y. Wang, "Equivalence between algebraic observability and local generic observability," in *Proceedings of the 32nd IEEE Conference on Decision and Control. Part 3 (of 4)*, pp. 2864-2865, December 1993.

[65] G. Bellu, M. P. Saccomani, S. Audoly, and L. D'Angiò, "DAISY: a new software tool to test global identifiability of biological and physiological systems," *Computer Methods and Programs in Biomedicine*, vol. 88, no. 1, pp. 52–61, 2007.

[66] N. Meshkat, C. Anderson, and I. DiStefano, "Finding identifiable parameter combinations in nonlinear ODE models and the rational reparameterization of their input-output equations," *Mathematical Biosciences*, vol. 233, no. 1, pp. 19–31, 2011.

[67] J. W. Yates, N. D. Evans, and M. . Chappell, "Structural identifiability analysis via symmetries of differential equations," *Automatica*, vol. 45, no. 11, pp. 2585–2591, 2009.

[68] B. Merkt, J. Timmer, and D. Kaschek, "Higher-order Lie symmetries in identifiability and predictability analysis of dynamic models," *Physical Review E: Statistical, Nonlinear, and Soft Matter Physics*, vol. 92, no. 1, 012920, 9 pages, 2015.

[69] M. J. Chappell and R. N. Gunn, "A procedure for generating locally identifiable reparameterisations of unidentifiable nonlinear systems by the similarity transformation approach," *Mathematical Biosciences*, vol. 148, no. 1, pp. 21–41, 1998.

[70] N. D. Evans and M. J. Chappell, "Extensions to a procedure for generating locally identifiable reparameterisations of unidentifiable systems," *Mathematical Biosciences*, vol. 168, no. 2, pp. 137–159, 2000.

[71] K. S. Brown and J. P. Sethna, "Statistical mechanical approaches to models with many poorly known parameters," *Physical Review E: Statistical, Nonlinear, and Soft Matter Physics*, vol. 68, no. 2, p. 021904/9, 2003.

[72] M. K. Transtrum, B. B. Machta, K. S. Brown, B. C. Daniels, C. R. Myers, and J. P. Sethna, "Perspective: Sloppiness and emergent theories in physics, biology, and beyond," *The Journal of Chemical Physics*, vol. 143, no. 1, Article ID 010901, 2015.

[73] J. F. Apgar, D. K. Witmer, F. M. White, and B. Tidor, "Sloppy models, parameter uncertainty, and the role of experimental design," *Molecular BioSystems*, vol. 6, no. 10, pp. 1890–1900, 2010.

[74] O.-T. Chis, A. F. Villaverde, J. R. Banga, and E. Balsa-Canto, "On the relationship between sloppiness and identifiability," *Mathematical Biosciences*, vol. 282, pp. 147–161, 2016.

[75] D. V. Raman, J. Anderson, and A. Papachristodoulou, "Delineating parameter unidentifiabilities in complex models," *Physical Review E: Statistical, Nonlinear, and Soft Matter Physics*, vol. 95, no. 3, 2017.

[76] C. Tönsing, J. Timmer, and C. Kreutz, "Cause and cure of sloppiness in ordinary differential equation models," *Physical Review E: Statistical, Nonlinear, and Soft Matter Physics*, vol. 90, no. 2, 2014.

[77] E. D. Sontag, "Dynamic compensation, parameter identifiability, and equivariances," *PLoS Computational Biology*, vol. 13, no. 4, 2017.

[78] A. F. Villaverde and J. R. Banga, "Dynamical compensation in biological systems as a particular case of structural non-identifiability," 2017, https://arxiv.org/abs/1701.02562.

[79] T. S. Ligon, F. Fröhlich, O. T. Chiş et al., "GenSSI 2.0: multi-experiment structural identifiability analysis of SBML models," *Bioinformatics*, vol. 34, no. 8, pp. 1421–1423, 2018.